Universidad Católica de Valencia San Vicente Mártir

Study of the microRNA expression profile dysregulation by hydrogen peroxide on the retinal pigment epithelium cells: role of miR-205-5p

Maria Oltra Sanchis

Doctoral Thesis

Supervised by:
Dr. D. Jorge Miguel Barcia González
Dr. D. Francisco Javier Romero Gómez

Dr.D. Jorge Miguel Barcia González, Profesor Universidad, Universidad Católica de Valencia San Vicente Mártir

Dr.D. Francisco Javier Romero Gómez, Catedrático de Fisiología, Hospital Universitario de la Rivera.

CERTIFICAN:

Que la presente tesis doctoral titulada **Study of the microRNA expression profile dysregulation by Hydrogen peroxide on the retinal pigment epithelium cells: role of miR-205-5p** ha sido realizada por Dª Maria Oltra Sanchis bajo nuestra dirección, en el Programa de Doctorado Ciencias de la Vida y del Medio Natural para la obtención del título de Doctor por la Universidad Católica de Valencia San Vicente Mártir.

Para que así conste a los efectos legales oportunos, se presenta esta tesis doctoral y se extiende la presente certificación en Valencia a 27 de enero de 2021.

Fdo.: Jorge Miguel Barcia González Fdo.: Francisco Javier Romero Gómez

La presente tesis doctoral titulada “Study of the microRNA expression profile dysregulation by Hydrogen peroxide on the retinal pigment epithelium cells: role of miR-205-5p” ha sido realizada gracias a la financiación concedida por las siguientes instituciones: Generalitat Valenciana (PROMETEO/2016/094), Ayudas Internas Investigación de la Universidad Católica de Valencia San Vicente Mártir (2017-128-001 y 2018-128-001) Ayuda a Proyectos de Investigación San Alberto Magno de la Universidad Católica de Valencia San Vicente Mártir (2019-128-001).

“Un país sin investigación es un país sin desarrollo”

Margarita Salas

Agradecimientos

En primer lugar, agradecer a mi director de tesis el Dr. Barcia quien ha hecho posible esta tesis, pese a las dificultades. Gracias por confiar en mi, formarme y ayudarme a encaminar mi futuro. Gracias también al Dr. Sancho quien ha sido para mi como mi segundo director. Gracias por vuestro apoyo durante estos años y por luchar por el grupo RETOS. Durante todo este tiempo he aprendido mucho de los dos.

Gracias al Dr. Romero por darme la oportunidad de conocer al grupo RETOS y formar parte de él.

Gracias a mi fiel compañera Lorena, has sido un gran apoyo para mí. Gracias por tus charlas sinceras, consejos de vida y lecciones de ciencia.

A todos los compañeros RETOS Javi, Natalia, Rosa, Dani y Bea aunque el viaje fue corto muchas gracias por vuestro apoyo.

Gracias también a todos los compañeros del laboratorio de San Carlos: Teresa, Cristina, Rafa, Tamara, Eloy, Sandra, Jesús y Álvaro por amenizar el día a día en el laboratorio, apoyarme y acompañarme. Gracias por hacer que este camino sea más fácil.

Agradecer también a todos los LInCEs por haberme enseñado tanta ciencia, por vuestros consejos y por continuar ayudándome en todo lo que está en vuestras manos.

A totes les meues amigues, que encara que no entenen de ciència, han sigut el suport moral par a continuar en ella.

A vosaltres Papa i Mama sou el pilar fonamental. Gràcies per creure en mi, per estar orgullosos de tot el que faig i acompanyar-me allà on fora. No hi ha paraules per agrair-vos tot el que feu.

A Sara, la meua germana, amiga i companya de ciència. Tu entens totes les línies d'aquesta tesis. Gràcies per fer que esta tesis siga possible. Sobre tot, gràcies per animar-me a continuat endavant, per els teus consells de vida i per ajudar-me de forma incondicional.

Y a ti Lucas, gracias por seguirme en este camino que muchas veces no ha sido fácil.

Index

Agradecimientos ***- 19 -***

Index ***- 23 -***

Figure Index ***- 1 -***

Table Index ***- 3 -***

Annex Index ***- 5 -***

Abbreviations ***- 7 -***

Abstract ***- 11 -***

Resumen ***- 13 -***

Introduction ***- 17 -***

1. Ocular anatomy - 17 -
1.1. The retina - 18 -
1.2. The choroid - 20 -
1.3. The retinal pigment epithelium - 21 -

2. Retinal disorders - 30 -
2.1. Age related macular degeneration - 30 -

3. Angiogenesis - 32 -
3.1. Vascular endothelial growth factor family - 32 -
3.2. Vascular endothelial growth factor receptors family and signal transduction - 33 -
3.3. Vasculogenesis and retinal disorders - 37 -

4. Oxidative stress - 38 -
4.1. Reactive oxygen species - 39 -
4.2. Oxidative stress and retinal disorders - 41 -
4.3. Antioxidant defense of retinal pigment epithelium. - 42 -

5. microRNA - 43 -
5.1. microRNAs biogenesis - 43 -
5.2. microRNAs and eye disorders - 46 -

6. Extracellular vesicles - 52 -
6.1. Extracellular vesicles and composition - 52 -
6.2. Functions of extracellular vesicles - 55 -
6.3. Extracellular vesicles and eye disorders - 56 -
6.4. Extracellular vesicles, miRNAs and eye disorders - 58 -

Hypothesis ***- 63 -***

Objectives ..... *- 65 -*

Materials and Methods ..... *- 69 -*

1. Cell Culture and treatment ..... **- 69 -**

2. Determination of Cell viability ..... **- 70 -**

2.1. XTT Assay ..... - 70 -

2.2. Apoptosis detection ..... - 71 -

3. Determination of ROS levels ..... **- 71 -**

4. Transepithelial Resistance Measurement ..... **- 72 -**

5. sEVs isolation ..... **- 72 -**

6. SEVs Characterization ..... **- 73 -**

6.1. Nanoparticle tracking analysis ..... - 73 -

6.2. Electron microscopy ..... - 74 -

7. Protein isolation and quantification ..... **- 74 -**

7.1. Protein isolation from cells ..... - 74 -

7.2. Protein isolation from sEVs ..... - 75 -

7.3. Protein quantification ..... - 75 -

8. Western Blot Analysis ..... **- 76 -**

9. miRNA expression analysis using microarrays ..... **- 77 -**

9.1. RNA isolation from cells ..... - 77 -

9.2. sEVs isolation and RNA isolation from sEVs ..... - 78 -

9.3. Retro transcription (RT) ..... - 79 -

9.4. Quantitative Real Time Polimerase Chain Reaction (qRT-PCR) ..... - 80 -

9.5. Statistical data processing and analysis of miRNA expression ..... - 80 -

10. RNA isolation and quantification ..... **- 81 -**

10.1. RNA isolation from cells ..... - 81 -

10.2. RNA isolation from sEVs ..... - 81 -

10.3. RNA quantification ..... - 82 -

11. qRT-PCR ..... **- 83 -**

11.1. qRT-PCR for miRNAs ..... - 83 -

11.2. qRT-PCR for mRNAs ..... - 84 -

12. Analysis of miRNA target genes ..... **- 86 -**

13. Mimic and siRNA Cell transfection ..... **- 86 -**

14. Human Umbilical Vein Endothelial Cell (HUVEC) isolation and culture ..... **- 87 -**

15. Vasculogenesis Assays ..... - 87 -

16. Immunofluorescence ..... - 88 -

17. Statistical Analysis ..... - 89 -

Results ..... - 93 -

1. Effect of H_2O_2 in ARPE-19 cells ..... - 93 -

1.1. H_2O_2-induced oxidative stress in ARPE-19 cells ..... - 93 -

1.2. H_2O_2 reduced ARPE-19 viability ..... - 93 -

1.3. H_2O_2 increased sEVs release in ARPE-19 ..... - 96 -

2. miRNA expression in ARPE-19 cells and sEVs .. - 97 -

2.1. miRNA expression in ARPE-19 cells (Cell miRNA) . - 97 -

2.2. miRNA expression in ARPE-19 sEVs (SEV miRNA) - 102 -

3. Pathway enrichment analysis of miRNA regulated by oxidative stress ..... - 104 -

4. Microarray validation of miRNA expression in ARPE-19 cells. ..... - 109 -

5. Potential Targets of miRNAs ..... - 112 -

5.1. Potential Target of Cell miRNA ..... - 112 -

5.2. Potential Target of SEV miRNA ..... - 115 -

6. Oxidative stress down-regulates miR-205-5p ... - 117 -

7. miR-205-5p targets are related to vascular processes ..... - 119 -

8. VEGFA mRNA is a direct target of miR-205-5p - 122 -

9. VEGFA expression is regulated by miR-205-5p - 123 -

10. Vasculogenesis is affected by miR-205-5p deregulation via VEGFA ..... - 126 -

11. H_2O_2- sEVs and their influence in neighboring cells - 129 -

12. H_2O_2- sEVs increase angiogenesis ..... - 132 -

13. H_2O_2- sEVs increase VEGFA production ..... - 134 -

Discussion ..... - 137 -

1. Effect of H_2O_2 in ARPE-19 cells ..... - 137 -

2. miRNA expression profile in ARPE-19 cells and sEVs ..... - 139 -

2.1. miRNA expression profile in ARPE-19 cells ..... - 139 -
2.2. miRNA expression profile in sEVs from ARPE-19 cells .. - 141 -

3. miR-205-5p, oxidative stress, vasculogenesis . - 143 -

4. H_2O_2-sEVs influence ..... - 146 -

Conclusions ..... - 151 -

References ..... - 155 -

Annexes ..... - 183 -

Figure Index

Figure 1. Eye anatomy..... - 18 -
Figure 2. Retinal structure. ..... - 20 -
Figure 3. RPE structure. ..... - 22 -
Figure 4. The RPE functions. ..... - 23 -
Figure 5. Visual cycle biochemistry. ..... - 27 -
Figure 6. Structure of VEGF isoforms. ..... - 33 -
Figure 7. VEGF signaling pathway..... - 35 -
Figure 8. VEGF signaling pathway..... - 37 -
Figure 9. Biogenesis, function and miRNA transport..... - 46 -
Figure 10. Composition and structure of EVs. ..... - 53 -
Figure 11. EVs biogenesis process. ..... - 55 -
Figure 12. H_2O_2 induces oxidative stress in ARPE-19 cells. - 93 -
Figure 13. Effect of oxidative stress in ARPE-19 cells. ..... - 95 -
Figure 14. Effect of H_2O_2 600 μM in ARPE-19 cells..... - 96 -
Figure 15. Characterization of sEVs released by ARPE-19 cells. ..... - 97 -
Figure 16. Heatmap of miRNA expression profile from array assay of ARPE-19 cells. ..... - 98 -
Figure 17. miRNAs significantly regulated in ARPE-19 cells... - 102 -
Figure 18. Heatmap of miRNA expression profile from array assay of the sEVs released by ARPE-19 cells. ..... - 103 -
Figure 19. miRNAs significantly regulated in sEVs from ARPE-19 cells. ..... - 104 -
Figure 20. Cell miRNA related pathways after H_2O_2 exposure in ARPE-19 cells. ..... - 105 -
Figure 21. sEV miRNA related pathways after H_2O_2 exposure in ARPE-19 cells. ..... - 108 -
Figure 22. Cell miRNAs validation in ARPE-19 cells. .... - 110 -
Figure 23. Cell miRNAs in mature ARPE-19 cells. ..... - 111 -

Figure 24. sEVs miRNAs validation in ARPE-19 cells.... - 111 -
Figure 25. miR-205-5p protein target related pathways. .. - 113 -
Figure 26. miR-521 protein target related pathways..... - 114 -
Figure 27. miR-302c-3p protein target related pathways.. - 115 -
Figure 28. miR-302a-3p protein target related pathways.. - 116 -
Figure 29. miR-122-5p protein target related pathways. .. - 117 -
Figure 30. Oxidative stress regulates miR-205-5p expression. .. - 118 -
Figure 31. Oxidative stress regulates miR-205-5p expression in mature ARPE-19 cells. ..... - 119 -
Figure 32. miR-205-5p protein target related angiogenic pathways. ..... - 122 -
Figure 33. VEGFA and miR-205-5p. ..... - 123 -
Figure 34. VEGFA is predicted as a direct target of miR-205-5p..... - 123 -
Figure 35. ARPE-19 cell viability after mimic miR-205-5p transfection. ..... - 125 -
Figure 36. VEGFA expression is regulated by miR-205-5p. ..... - 126 -
Figure 37.VEGFA-mediated Vasculogenesis is regulated by miR-205-5p..... - 129 -
Figure 38. sEVs induce oxidative stress. ..... - 130 -
Figure 39. sEVs affect cell viability. ..... - 131 -
Figure 40. sEVs from H_2O_2 stressed ARPE-19 cells decrease barrier function.. ..... - 132 -

Table Index

Table 1. TaqMan® miRNA primer assays ..... - 84 -
Table 2. Primer sequences ..... - 85 -
Table 3. miRNAs significantly regulated in ARPE-19 cells under oxidative stress.. ..... - 99 -
Table 4. miRNAs significantly regulated in ARPE-19 cells. ..... - 101 -
Table 5. miRNAs significantly regulated in sEVs from ARPE-19 cells. ..... - 103 -
Table 6. Cell miRNA KEGG pathways deregulated in ARPE-19 cells after H_2O_2 exposure. ..... - 105 -
Table 7. sEVs miRNA KEGG pathways deregulated in ARPE-19 cells after H_2O_2 exposure..... - 108 -
Table8. mRNA targets of miR-205-5p related to vascular processes..... - 119 -
Table 9. Relevant miRNAs identified on eye-related disorders. - 139 -

Annex Index

Annex I. Cell miRNAs pathway enrichment analysis after H_2O_2 exposure in ARPE-19 cells..... - 183 -

Annex II. sEV miRNAs pathway enrichment analysis after H_2O_2 exposure in ARPE-19 cells..... - 190 -

Annex III. miR-205-5p predicted mRNA targets.. ..... - 194 -

Annex IV. miR-521 predicted mRNA targets. ..... - 197 -

Annex V. miR-302c-3p predicted mRNA targets. ..... - 201 -

Annex VI. miR-122-5p predicted mRNA targets. ..... - 205 -

Annex VII. miR-302a predicted mRNA targets. ..... - 208 -

Annex VIII. Related publications ..... - 212 -

Abbreviations

ADARs	Adenosine deaminases that act on RNA
AMD	Age-related macular degeneration
ARPE-19	Arising retinal pigment epithelium
ATCC	American Type Culture Collection
ATF-2	Activating transcription factor 2
BCA	Bicinchoninic acid
BSA	Bovine Serum Albumin
CAT	Catalase
CYP2E1	Cytochrome P450 2E1
DAS	Diallyl Sulfide
DGCR8	Di George Syndrome critical region gene 8
DHA	Docosahexaenoic acid
DHE	Dihydroethidium
ECM	Extracellular matrix
EGF	Epidermal growth factor
ELM	External limiting membrane
eNOS	Endothelial nitric oxide synthase
ERK1/2	Extracellular signal-regulated kinases 1/2
ESCRT	Endosomal sorting complex required for transport
EVs	Extracellular vesicles
FBS	Fetal Bovine Serum
FC	Fold change
FGF	Fibroblast growth factor
GCL	Ganglion cell layer
GSH-Px	Glutathione peroxidase
HIF	Hypoxia Inducible Factor
HUVEC	Human Umbilical Vein Cells

ILM	Internal limiting membrane
ILV	Intraluminal vesicles
INL	Inner nuclear layer
IPL	Inner plexiform layer
IS	Inner segments
MAPK	Mitogen-activated protein kinase
miRNA	microRNA
miRNoma	miRNA transcriptoma
MMPs	Matrix Metalloproteinase
mtDNA	Mitochondrial DNA
MVBs	Multivesicular bodies
NAC	N-acetylcysteine
NFKB	Nuclear factor KB
NFL	Nerve fiber layer
OS	Oxidative stress
ONL	Outer nuclear layer
PBS	Phosphate-Buffered Saline
PDGF	Platelet derived growth factor
PEDF	Pigment epithelium-derived factor
PFA	Paraformaldehyde
PIGF	Phosphatidylinositol-glycan biosynthesis class F
PI3K	Phosphoinositide-3-kinae
PKC	Protein kinase C
PLCγ1	Phospholipase Cγ1
POS	Photoreceptors outer segments
PRDX2	Peroxiredoxin 2
pre-miRNA	Precursor-miRNA
pri-miRNA	Primary-miRNA

PS	Phospholipid phosphatidylserine
PUFAS	Polyunsaturated fatty acids
PVDF	Polyvinylidene difluoride
qRT-PCR	quantitative Real Time- Polymerase Chane Reaction
RISC	RNA-induced silencing complex
ROS	Reactive oxygen species
RP	Retinitis pigmentosa
RPE	Retinal pigment epithelial
RT	Retro transcription
SOD	Superoxide dismutase
SDS	Sodium dodecyl sulphate
sEVs	Small Extracellular Vesicles
TEM	Transmission electron microscopy
TER	Transepithelial resistance
TIMPs	Tissue inhibitor of matrix metalloproteinase
TRBP	Transactivation-responsive RNA-binding protein
TTBS	Tris-buffered saline with Tween 20
UTR	Untranslated regions
VEGFA	Vascular endothelial growth factor
ZO-1	Zona occludens protein 1
4-HNE	4-hydroxinonenal

Abstract

Age related macular degeneration (ADM) and diabetic retinopathy (DR) are common retina-related diseases leading to blindness. The retinal pigment epithelium (RPE) is essential for the vision, in fact is well documented that oxidative stress (OS) generated in RPE and choroid neovascularization are related to the origin of these disorders. The study of circulating miRNAs, small non-codding RNA, is opening new possibilities in terms of diagnosis and therapeutics. miRNAs can travel inside small Extracellular Vesicles (sEVs) playing an important role in intracellular communication. Concretely, miR-205-5p is involved in VEGF-related angiogenesis and seems to regulate associated cell signaling pathways.

One of the aims of the present work is to establish a miRNA expression profile of ARPE-19 cells and sEVs released from ARPE-19 cells under oxidative conditions (H_2O_2). Moreover, we want to evaluate the role of the identified miRNAs and sEVs in the progression of pathological processes related to retinal disorders.

The miRNA expression profile was carried out using SeraMir Profiler that includes 384 miRNAs whose expression was analyzed in ARPE-19 cells and sEVs released by ARPE-19 cells, both in control conditions and treated with 600 μM H_2O_2 for 24 hours. Additionally, the role of miRNAs and sEVs in angiogenic processes was studied using matrigel assays with HUVEC cells.

We identify a different miRNA expression profile between oxidative stressed and control ARPE-19 cells (Cell miRNAs) and the sEVs (sEV miRNAs) released by them. As a result, 306 out of 384 Cell

miRNAs were detected by the array and 7 were significantly over-expressed in H_2O_2-treated cells. Moreover, 218 miRNAs could be detected in control and H_2O_2-induced sEVs and only 2 of them were significantly under-expressed in H_2O_2-induced sEVs. Among the dysregulated Cell miRNAs we found the miR-205-5p. Our results indicate that miR-205-5p is modulated by OS and regulates VEGFA-angiogenesis. We also found the role of 600 μM H_2O_2-sEVs on oxidative stress induction, cell death increasing and angiogenesis stimulation in healthy ARPE-19 cells.

The miRNA dysregulation observed suggest their implication in retinal disorders after oxidative challenge. Among the dysregulated miRNAs, miR-205-5p is proposed as a candidate against eye-related proliferative diseases. Therefore, results herein suggest the influence of sEV in neighboring cells and the possible utility of sEV miRNAs as biomarkers.

KEYWORDS: Retinal pigment epithelium; microRNAs; extracellular vesicles; oxidative stress; angiogenesis.

Resumen

La degeneración macular asociada con la edad (AMD) y la retinopatía diabética (RD) son alteraciones de la retina que llevan a la perdida de la visión. El epitelio pigmentario de la retina (RPE) es esencial para la visión, de hecho está bien documentado que el estrés oxidativo (OS) generado en el RPE y la neovascularización de la coroides están relacionados con el origen de estas alteraciones. El estudio de los microRNAs (miRNAs) circulantes, pequeños RNAs no codificantes, está abriendo nuevas posibilidades en el campo del diagnostico y de la terapia. Los miRNAs pueden viajar en el interior de pequeñas vesículas extracelulares (sEVs) jugando un papel importante en la comunicación intracelular. Concretamente, el miR-205-5p está involucrado en los procesos de angiogenesis relacionados con el VEGF y además parece regular las vías de señalización asociadas.

Uno de los objetivos de este trabajo es determinar los perfiles de expresión de los miRNAs de las células ARPE-19 y de las sEVs liberadas por las ARPE-19 bajo condiciones oxidantes (H_2O_2). Además, queremos evaluar el papel de los miRNAs identificados y de las sEVs en la progresión de los procesos patológicos relacionados con las alteraciones de la retina.

El perfil de expresión de los miRNAs se llevo a cabo utilizando SeraMir Profiler que incluye 384 miRNAs, cuya expresión se analizó en las células ARPE-19 y en las sEVs liberadas por estas células, tanto en condiciones control como sometidas a 600 μM H_2O_2 durante 24 horas. Por otro lado, el papel de los miRNAs y las sEVs en los procesos angiogenicos se determino mediante el uso de ensayos de matrigel con células HUVEC.

Identificamos un perfil de expresión de miRNAs diferente entre células ARPE-19 sometidas a estrés oxidativo y control (Cell miRNAs) y entre las sEVs liberadas por estas (sEV miRNAs). Como resultado, se detectaron 306 de los 384 Cell miRNAs analizados y 7 de ellos estaban significativamente sobrexpresados en las células tratadas con H_2O_2. Además, se detectaron 218 miRNAs en las sEVs liberadas por células controles y sometidas a H_2O_2 y solamente 2 de ellos estaban significativamente infraexpresados en las sEVs sometidas a H_2O_2. Entre los Cell miRNA desregulados encontramos el miR-205-5p. Nuestros resultados indican que el miR-205-5p está modulado por el OS y regula la angiogenesis mediada por el VEGFA. También determinamos el papel de las sEVs - H_2O_2 en la inducción del OS, el aumento de la muerte celular y la estimulación de la angiogenesis en células ARPE-19 sanas.

Los miRNAs desregulados sugieren su implicación en los desordenes de la retina tras la exposición a OS. Entre los miRNAs desregulados, el miR-205-5p se propone como un candidato contra los procesos proliferativos relacionada con las alteraciones de la retina. Por otra parte, nuestros resultados demuestran la influencia de las sEVs en las células vecinas y la posible utilidad de los sEV miRNAs como biomarcadores.

PALABRAS CLAVE: epitelio pigmentario de la retina; microRNAs; vesículas extracelulares; estrés oxidativo; angiogenesis.

INTRODUCTION

Introduction

1. Ocular anatomy

The vision loss is one of the fears of the population, therefore, sight is one of the most appreciate senses. The eye is the responsible of the visual cycle and is considered as an immune privilege organ. The ocular globe is made up by three layers[1] (Figure 1):

- Outer layer, the sclera, is the fibrous layer which includes the cornea. The sclera comes from the limbus to the optic nerve posteriorly.
- Middle layer, the uvea, is the vascular and nutritive layer formed by the pigmented tissue: iris, choroid and ciliary body. The uvea is between the sclera and the retina.
- Inner layer, the retina, is the sensory and neural part of the eye. The retina is in contact with the vitreous body and the external surface, the choroid.

In addition, the human globe is divided in to three chambers[2] (Figure 1):

- The anterior chamber, located between the posterior part of the cornea and the anterior part of the iris and crystalline lens.
- The posterior chamber is located between the posterior surface of the iris, the anterior surface of the zonular fibers and in the center are the crystalline lens.

- The vitreous chamber is located between the zonular fibers, the ciliary body, the crystalline, the optic nerve and retina.

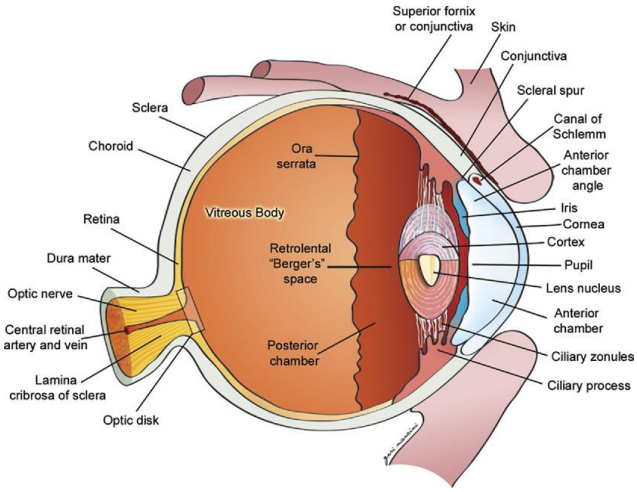

Figure 1. Eye anatomy. Anatomical representation of the human ocular globe. Obtained from Ajay MD, et al. 2011[1].

1.1. The retina

The retina is the sensory inner layer of the globe, a prolongation of the central nervous system and the responsible of encoding visual information. The structure of the retina is conserved across vertebrates[3]. The retina is in contact by the inner part with the vitreous body and with the choroid by the external surface. It is formed by the inner and sensory layer and the outer retinal pigment epithelial (RPE) layer[1].

Different cell types can be found in the retina making up a structure that work in parallel producing a visual output. The photoreceptors are the responsible of coding visual information, transforming the light energy to membrane potential changes. There are two types of photoreceptors: the rods and cones. Cones are the responsible of color

and bright-light vision and rods are in charge of dim-light vision[3]. Furthermore, the bipolar cells of the retina transmit the impulse to retinal ganglion cells which transmit the initial stimuli. The amacrine cells modulate the excitation of ganglion cells, the horizontal cells modulates the communication between bipolar cells and photoreceptors and Müller cells are glial cells responsible of metabolism and homeostasis, being essential for the right functioning of the retina[4].

The retina is formed by 10 layers, from the vitreous to the choroids we can stand out the internal limiting membrane (ILM), nerve fiber layer (NFL), ganglion cell layer (GCL), inner plexiform layer where cone contact with retinal ganglion cells and amacrine cells (IPL), inner nuclear layer formed by bipolar, amacrine and horizontal cells (INL), outer plexiform layer formed by synapses between bipolar cells, photoreceptors and horizontal cells (OPL), outer nuclear layer (ONL), external limiting membrane (ELM), photoreceptors inner segments (IS) and outer segments (POS), and RPE[3,5] (Figure 2).

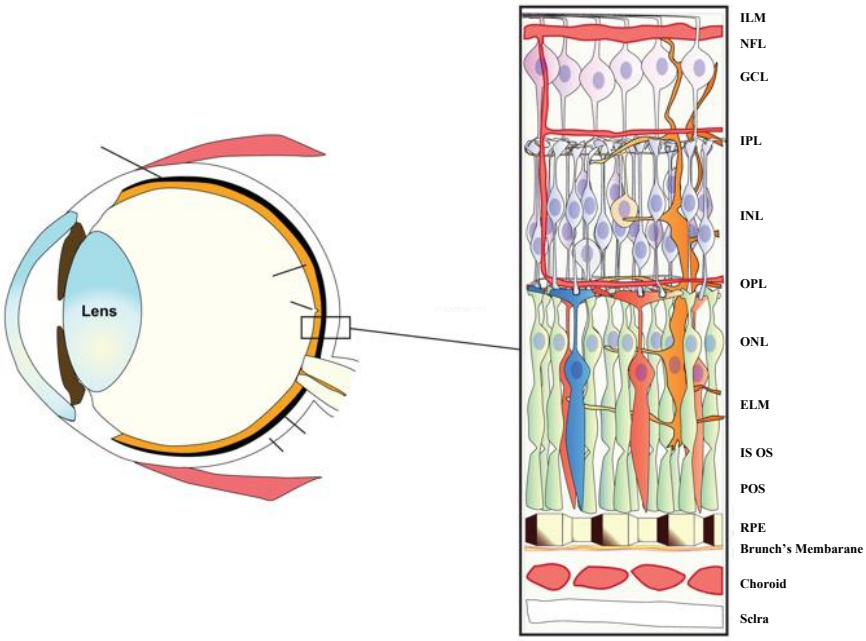

Figure 2. Retinal structure. Cross section of neurons organization of the retina. Obtained and modified from Jarret SG, et al. 2012[6].

1.2. The choroid

The choroid are located between the retina and the sclera attached to the RPE[1,7] formed by melanocytes, fibroblasts, immunocompetent cells, collagenous and connective tissue[8]. It is the vascular layer of the eye providing the metabolic support to the RPE, blood to the optic nerve and absorbing the excess of light[9]. The choriocapillaris, the inner part of the choroids which consist of a network of capillaries associated with the Brunch's membrane, supplies oxygen and nutrients to the RPE and outer retinal layers. The choroidal thickness changes moves the retina allowing the photoreceptors focusing the shot[8]. Therefore, the choroid functions are thermoregulation, adjustment of the position of the retina, secretion of growth factors and absorption of light. The choroids play

an important role in different ocular diseases, such as age-related macular degeneration (AMD) and glaucoma among others[7].

1.3. The retinal pigment epithelium

The RPE is one of the most metabolic active tissue in the human body. It is not involved directly in vision, but their loss leads to photoreceptors and choroid alterations leading to retinal disorders and even loss of vision.

The RPE cell monolayer is formed by pigmented microvilli and is located between the photoreceptor's outer segments and the choroid, essential for vision[10]. The RPE is a quiescent and polarized monolayer able to act different in the apical or basal side, controlling the trafficking of molecules, nutrients, oxygen and waste products[11]. The RPE formed the inner blood retinal barrier and in collaboration with the Brunch Membrane and choriocapillaris constituted the outer blood retinal barrier[12].

The intracellular and extracellular structures such the tight junctions, desmosomes and zonula adherents on RPE, the cytoskeleton and membrane proteins within RPE and the extracellular matrix are essential to maintain the blood retinal barrier (Figure 3)[13].

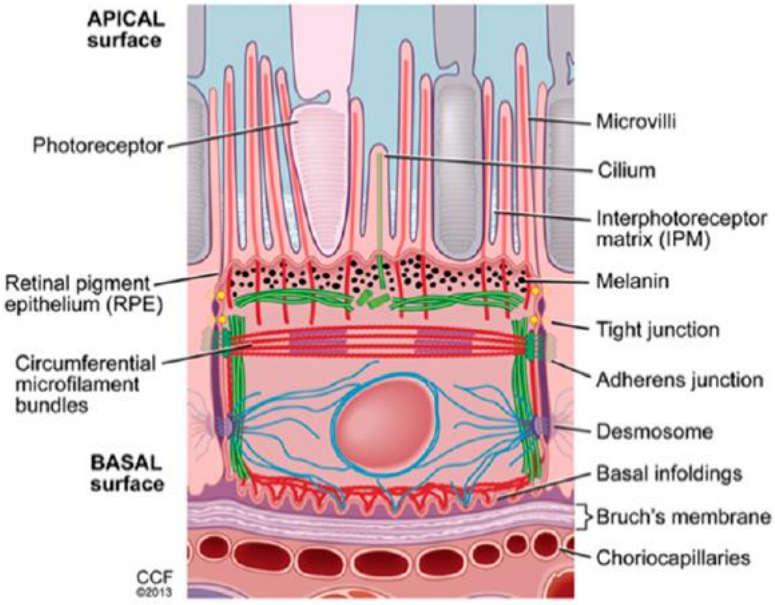

Figure 3. RPE structure. Schematic representation of the RPE structure. Obtained from Tarau I, et al. 2019[13].

The RPE cytoskeleton is formed by actin, microtubules and intermediate filaments. The actin microfilaments support intracellular vesicle trafficking, focal adhesion, cell shape and movement[14]. The microtubules are involved in the phagocytosis of photoreceptors outer segments. At the apical surface there is the microvilli connecting with photoreceptor's outer segments, increasing the surface area. The cytoskeleton of the apical surface is essential for the structure, polarization and orientation of apical process such as phagocytosis and intracellular processing of photoreceptors. Therefore, at the basal surface the actin is joined to zonula adherents and are responsible of cell-shape along with the circumferential microfilament bundles which are contractile. The RPE contact with the extracellular matrix through integrins and cadherins. The extracellular matrix is a dynamic structure

that adapts to the environment being important to cell adhesion and polarity of RPE[13].

1.3.1. Retinal pigment epithelium functions

The RPE has different functions epithelial transport of ions, water and metabolites from the subretinal space to the choroid and from the choroids to the photoreceptors transports fatty acids, retinol and glucose[13], light absorption, glial support, participates in the visual cycle, phagocytosis and secretion of different molecules[15] (Figure 4).

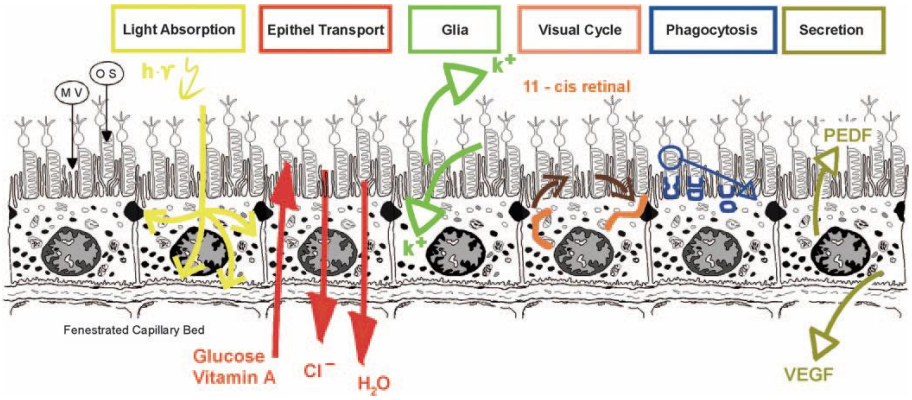

Figure 4. The RPE functions. Summary of the RPE functions: light absorption, Epithelial transport, glial support, visual cycle, phagocytosis and secretion. Obtained from Strauss O. 2005[15].

1.3.1.1. Light absorption and protection

The pigmentation of RPE is essential to increases optical quality and maintenance of visual function. The light when enters the eye is concentrate onto the retina. The retina, due to its anatomical location, is exposed to an oxygen rich environment. The oxygen saturation at the choriocapillaris is higher (90%) than in other retinal blood vessels (45%)[16], inducing the photo-oxidation causing oxidative stress (OS) and in turn increases due to the reactive oxygen species (ROS)

produced by the phagocytosis of photoreceptors outer segments. The absorption and filtering of light is one of the RPE defense mechanism.

For the light absorption the RPE contains different pigments, able to absorb different wavelengths. The melanin, in melanosomes, is the main responsible of light absorption. Therefore, the carotenoids, lutein and zeaxanthin of photoreceptors also participates in the absorption of light[15,17,18]. Furthermore, the RPE is protected from light by enzymatic antioxidants (superoxide dismutase and catalase) and nonenzymatic antioxidants (lutei, zeaxanthin, ascorbate and β-carotene, glutathione and melanin)[19].

1.3.1.2. Epithelial Transport

The RPE transport ions and nutrients from blood to retinal space and to photoreceptors. The RPE transport is bidirectional thanks to the organization of organelles and distribution of membrane proteins, giving rise the polarity. The epithelial transports are essential to the function of the retina, so their imbalance leads to retinal disorders.

Transport from blood to retinal space: The RPE transport ions and water from blood to retina. In the retina, as consequence of the high metabolic rate of photoreceptors, the water is transported by Müller cells, concentrated, constantly renewed and eliminated by RPE. The transepithelial transport of water is facilitated by aquaporin 1. Besides, water is essential to adhesive forces between retina and RPE. Therefore, the RPE is an ion transporting epithelium. The Na^+-K^+-ATPase, located in the apical membrane, establish a Na gradient which facilitates the Cl^-, K^+ and HCO_3^- uptake for pH regulation. The transepithelial transport of ions is linked to pH regulation. By last, the RPE eliminates the

metabolic end products from the photoreceptors such as the lactic acid[15,20].

Transport from blood to the photoreceptors: the RPE transport glucose using the glucose transporters GLUT1 and GLUT3. GLUT3 mediates the basic glucose transport and GLUT1 mediates the inducible glucose transport to metabolic demands. The RPE transport retinol and vitamin A for the retinal supply of photoreceptors and allow the visual cycle. Therefore, the RPE transport from the blood to photoreceptors docosahexaenoic acid (DHA) for the photoreceptor's membrane phospholipids, essential for visual cycle[15] and OS protection[21].

1.3.1.3. Glial

The retinal glial cells protect the retina against infections. There are three types of retinal glial cells: Müller glia, astroglia and microglia.

Müller glia are supporting cells and are essential to structural stabilization. The Müller glia cells are the main retinal glial cells able to move around the whole retina. Their soma is located from the INL to the neuronal cell bodies. Among its functions are the maintenance of blood retinal barrier and ion homeostasis, protection from glutamate excitotoxicity and release of neurotrophic factors to retinal cell maintenance. One of the most important properties of the Müller glia cells are they dedifferentiation to pluripotent stem cells able to replace damaged neurons[22–24].

Astroglia are support cells located in the nerve fiber layer of the retina over the axon of ganglion cells. The astroglia function as part of the blood retinal barrier and axonal sheaths providing energy and

glycogen to the neurons. This cells release different trophic factors and regulate the ionic homeostasis[25,26].

Microglia are macrophage functioning as immune sentinels in the intraocular space. The microglia cells are ramified cells, however when is activated present an oval shape and travel to damage areas and phagocytize pathogens or cells debris. Therefore, the microglia cells act like a phagocytic antigen presenting cells[27,28].

1.3.1.4.Visual cycle

The light is focused onto the retina and is transduced into neural signal in order to produce visual information. This process take place in the outer segments of the photoreceptors, including in the cell membranes and pigment disk membranes of the outer segments[29]. The visual cycle starts with the circulation of all-*trans*-retinal (vitamin A derivate) on the blood stream. The visual chromophore is transferred to rod and cone outer segments where it combines with opsin. Is followed by the absorption of light by rhodopsin and the strike of 11-*cis*-retinal Schiff by the photon to opsin, the all-*trans*-retinal. The conformational changes lead to the activation of the phototransduction cascade and the initiation of the visual response (Figure 5). The 11-*cis*-retinol is regenerated by the isomerization of rhodopsin for the cycle to continue. The isomerase activity take place in the RPE membrane by the RPE65 protein[30].

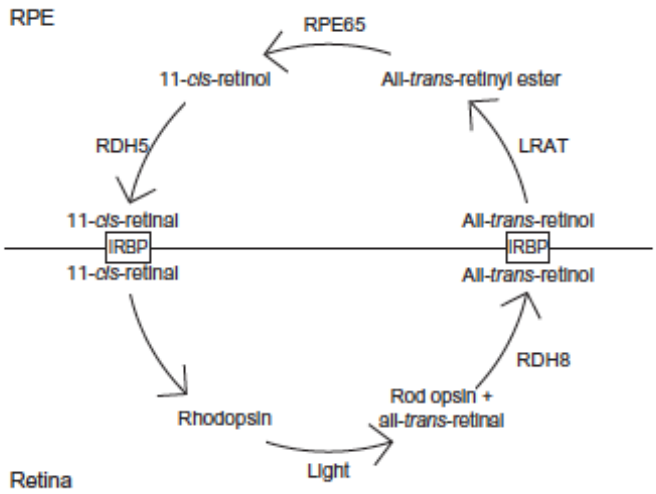

Figure 5. Visual cycle biochemistry. Visual cycle schematic representation. Obtained from Wright C B. et al 2015[31].

1.3.1.5. Phagocytosis

The POS are constantly renew, by RPE phagocytosis, for the proper function of the retina. The POS are phagocyted by the RPE and the retinal or docosahexaenoic acid are digested and delivered to the photoreceptors[32,33]. This POS phagocytosis is a non-inflammatory clearance phagocytosis pathway to remove apoptotic cells and debris. The CD36 and MerTK are the integrin receptors responsible of the POS phagocytosis. The photoreceptors are exposed to intense levels of light leading to the accumulation of photo-damaged proteins and lipids and photo-oxidative radicals[34]. The RPE is exposed to ROS due to the light energy and the high oxygen concentration of the choriocapillaris. Therefore, the inefficient phagocytosis process leads to the debris accumulation and the malfunctioning of photoreceptors.

1.3.1.6. Secretion

The RPE is a polarized pigment layer which regulates light absorption, nutrients and waste transport, phagocytosis of photoreceptors and directional secretion of proteins required in maintaining retinal homeostasis and function, being essential in health and disease. The secretion of growth factors and structural proteins are crucial to photoreceptors survival and maintenance of retinal blood supply[34]. Therefore, the protein secretion is directional, to the apical or basolateral plasma membrane.

Apical secretion

Metalloproteinase

Matrix Metalloproteinase (MMPs) belongs to the zinc-binding calcium-dependent endopeptidases family[35]. The main metalloproteinases release apically by the RPE are MMP-2 and tissue inhibitor of matrix metalloproteinase 1 (TIMP-1). MMPs and TIMPs are usually released apically, however could be present basally on the RPE, in the Bruch's membrane[36,37]. These proteins are the responsible of structural maintenance and turnover of the extracellular matrix (ECM) and could be involved in the POS degradation[38]. It has been suggested that the MMPs/TIMPs balance is essential for the ECM homeostasis and the their disbalance can contribute to age-related changes[35].

Other important MMP is the MMP-9, which together with the MMP-2 play an important role in vasculogenic processes regulating growth factors such as pigment epithelium-derived factor (PEDF)[39] and

degrade basement membrane components, specially type IV collagen[40]. The expression and secretion of MMP are increased by different stimuli; the MMP-1 and MMP-3 are increased by OS[41] and MMP-2 and MMP-9 by angiogenic factors[42].

Hyaluronan

Hyaluronan is a glycosaminoglycan secreted apically by the RPE, is the primary scaffold protein and the major component of the ECM.

αβ crystallin

αβ crystallin is a molecular chaperone that regulates the cytoprotection inhibiting caspase 3, activating the DNA repair and protecting the photoreceptors from OS providing neuroprotection[43].

Pigment epithelium-derived factor

PEDF is an anti-angiogenic factor member of the serine protease inhibitor family. The PEDF is a neurotrophic factor of the retina and ocular tissue. The main functions of PEDF are the neurotrophic support of photoreceptors, the anti-inflammatory properties and the maintenance of a non-angiogenic retinal environment[35,44,45].

Basolateral secretion

Fibroblast growth factor (FGF)

FGF are a survival factor for the RPE and regulates angiogenesis, cell survival and mitogenesis in the retina[45]. The predominant FGF secreted by the RPE are the FGF-1, FGF-2 and FGF-5[35,46].

Endothelin I

Endothelin I is the responsible of the blood flow regulation, inducing vasoconstriction and vasodilatation depending on the receptor they joins[47].

Vascular endothelial growth factor (VEGF)

VEGF is the most important pro-angiogenic growth factor released by the RPE[45]. Therefore, the VEGF acts as a pro-inflammatory molecule. The VEGF is secreted by different cell types in addition to RPE such as Müller cells, endothelial cells, pericytes and ganglion cells (explained in detail in section below).

2. Retinal disorders

Several diseases are related to vision loss such AMD, diabetic retinopathy (DR), glaucoma, retinitis pigmentosa and Stargadt disease.

2.1. Age related macular degeneration

The AMD is the third leading cause of several irreversible vision loss worldwide with a widespread effect on quality of life. AMD is common in persons of 75 years and older. By 2040 the number of people with AMD is expect to be 300 millions being a public health problem with socioeconomic implications[48].

AMD affects the macular region of the retina causing progressive loss of central vision[49]. Traditionally, AMD is classified as early-stage AMD and late-stage. Early stage includes clinical signs such as drusen and abnormalities of RPE, this is often asymptomatic. Late stage AMD can be neovascular (wet or neovascular AMD) and non-neovascular or atrophic (dry AMD)[50]. The neovascular AMD progress rapidly while dry AMD goes slower[51].

The clinical manifestations of neovascular AMD are the presence of fluid or retinal hemorrhage. Therefore, the neovascular AMD is characterized by the choroidal neovascularization and retinal pigment epithelial detachments. The new blood vessels from the choroid breaks the Brunch's membrane by entering the RPE[52]. Angiogenic factors, including VEGF, PEDF and transforming growth factor beta (TGF-β) are related to the progression of neovascular AMD[53].

AMD is a multifactorial disorder and many risk factors have been identified. Its incidence is greater in advanced age groups and in women. There are also genetic factors including rare coding variants in complement factor H, complement factor and TIMP metallopeptidase inhibitor 3 among others. Cardiovascular disease is another risk factor, such as hypertension and hyperlipidemia. Smoking, sunlight exposure, iris color, nutritional factors and alcohol consumption are environmental risk factors for AMD progression[51,52,54].

The most effective treatment so far is based on inhibition of VEGF. The most used drugs are Ranibizumab[55] and Bevacizumab[56], antibodies that binds all VEGFA isoforms, which are supplied as an intravitreal injections. However, these treatments are limited to diminish the evolution of the disease. One of the most challenging issues in

ophthalmic science is to identify early markers for AMD in order to prevent its clinical evolution.

3. Angiogenesis

Angiogenesis is the formation of new blood vessels whereas the vasculogenesis is the process of new blood vessel formation from *de novo*. Both processes are critical during development but uncontrolled growth of blood vessels could take part in numerous disease including ophthalmic diseases. The VEGF is one the most important pro-vasculogenic and pro-angiogenic factors and the responsible of physiological vascular homeostasis in different cells and tissues. Therefore, the VEGF plays an important role in the pathogenesis of tumor growth and in retinopathy associated with blinding diseases such as AMD[57]. As mentioned above, some therapeutic approaches are based in the inhibition of VEGF isoforms, VEGF receptors and associated pathways in order to reduce the pathological neoangiogenesis[58].

3.1. Vascular endothelial growth factor family

The VEGF family includes VEGFA, VEGFB, VEGFC, VEGFD, VEGFE and PIGF (Figure 6). The VEGF members regulates the neoangiogenesis but VEGFC and VEGFD regulates the lymphoangiogenesis. The VEGF expression and driven signaling is regulated, mainly, by hypoxia via hypoxia-inducible factor (HIF) and hypoxia-regulated gens such as epidermal growth factor (EGF) and platelet derived growth factor (PDGF)[59].

VEGFB induce fatty acid uptake by the endothelium and stimulate cardiac endothelial cell promoting revascularization[60]. Phosphatidylinositol-glycan biosynthesis class F (PIGF) promotes inflammation during angiogenic process and stimulates hematopoietic cells proliferation and secretion of proangiogenic growth factors[61].

The VEGFA, the predominant member in the regulation of normal and pathological angiogenesis, is secreted by a wide variety of cells and acts in a paracrine manner. The VEGFA present different isoforms, due to the alternative exon splicing, such as $VEGF_{121}$, $VEGF_{165}$, $VEGF_{189}$, $VEGF_{206}$ and $VEGF_{165}$ the main isoform[62].

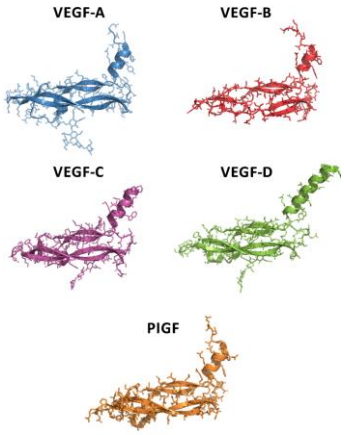

Figure 6. Structure of VEGF isoforms.

3.2. Vascular endothelial growth factor receptors family and signal transduction

There are different VEGF receptors: VEGFR1, VEGFR2 and VEGFR3. The VEGFR are tyrosine kinase membrane-bound proteins with an N-proximal extracellular ligand-binding domain of seven immunoglobulins-like repeats followed by a transmembrane domain, a

juxtamembrane domain, a tyrosine kinase domain and a flexible carboxyl terminus[63].

Each one of the members of the VEGF family has affinity for a specific VEGF receptor. The endothelial cells express predominantly the VEGFR1 and VEGFR2. The main receptor for VEGF is the VEGFR2, its expression is restricted to vascular cells[63], inducing vascular endothelial cell mitogenesis and permeability[57]. To VEGFR1 binds the VEGFB, PIGF and VEGFA. To VEGFR2 binds the VEGFA, VEGFE, VEGFC and VEGFD. Both receptors (VEGFR1 and VEGFR2) activates cell proliferation, migration, survival and vascular permeability. Therefore, VEGFR2 presents two tyrosine residues able to regulate differentially: angiogenesis and vascular permeability[64]. Whereas, VEGFR1 acts as a decoy receptor that binds PIGF to prevent VEGF binding. Although, VEGFA has higher affinity to VEGFR1 than VEGFR2 the complex VEGFR1-VEGFA does not work well in signal transduction[65]. To VEGFR3 binds the VEGFC and VEGFD inducing lymphangiogenesis (Figure 7). Morover, VEGFR3 expression is up regulated in vascular endothelial cells during active angiogenesis[63].

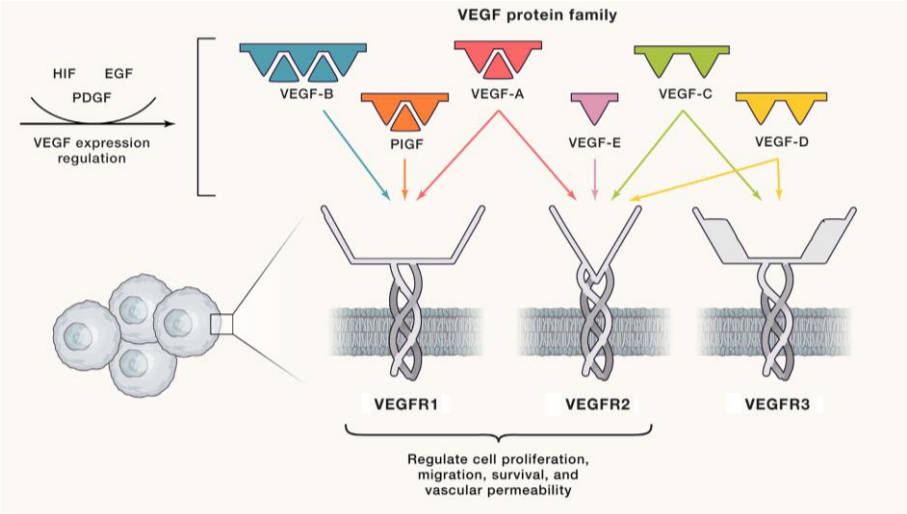

Figure 7. VEGF signaling pathway. Members of the VEGF family including: VEGFB, VEGFA, VEGFC, VEGFD, VEGFE and PIGF. The HIF, EGF and PDGF are genes induced by hypoxia or ischemia able to regulate VEGF. The VEGF receptors areVEGFR1, VEGFR2 and VEGFR3. The VEGFR1 and VEGFR2 induce the VEGF signaling, regulating cell proliferation, migration, survival and vascular permeability. Modified from Apte R S. et al 2019[57].

The VEGFR1/R2 take part in the canonical VEGF signaling inducing cell proliferation, migration, survival and vascular permeability during angiogenesis and vasculogenesis through the activation of kinases[66]. The notch signaling and the expression of notch ligands induce the molecular regulation of the VEGF pathway. But once the VEGF pathway is activated and the notch signaling still increasing a negative feedback loop is induced by notch reducing the VEGFR2 expression in endothelial cells[67]. The canonical signaling is essential to physiological homeostasis but its dysregulation induce pathological angiogenesis.

Concretely, the VEGF binding to VEGFR1 causes the tyrosine phosphorylation and the phosphoinositide-3-kinae (PI3K) and serine/threonine protein kinase Akt inducing endothelial cell proliferation and tubulogenesis[68]. Once activated VEGFR1 the

phospholipase Cγ1 (PLCγ1) is stimulated and cleavage plasma membrane phosphoinositide inducing cytosolic calcium ion flux and altered gene expression[69].

When the VEGFA binds to VEGFR2 a dimerization and trans-autophosphorylation of the cytoplasmic tyrosine residues are induce activating endothelial cell migration and vascular permeability. Therefore, PI3K and Akt are activated increasing the cell survival and nitric oxide production by endothelial nitric oxide synthase (eNOS) promoting vascular permeability[69]. The hyperpermeability in intraocular disorders reflects the formation of aberrant an immature blood vessel with a thin endothelium leading to leakages and bleeding. Additionally, VEGFA stimulates the VEGFR1 and VEGFR2 synthesis through protein kinase C (PKC) activation creating a negative feedback loop[70]. VEGFR2 signaling induces the activation of extracellular signal-regulated kinases 1/2 (ERK1/2) through the RAS-RAF-MAPK signaling pathway, leading to the activating transcription factor 2 (ATF-2) phosphorylation which regulates cell proliferation, migration tubulogenesis and endothelial cell leukocyte adhesion[58,71]. By last, the p38 mitogen-activated protein kinase (MAPK) is activated and promotes actin remodeling, cell migration and a response to stress (Figure 8)[72].

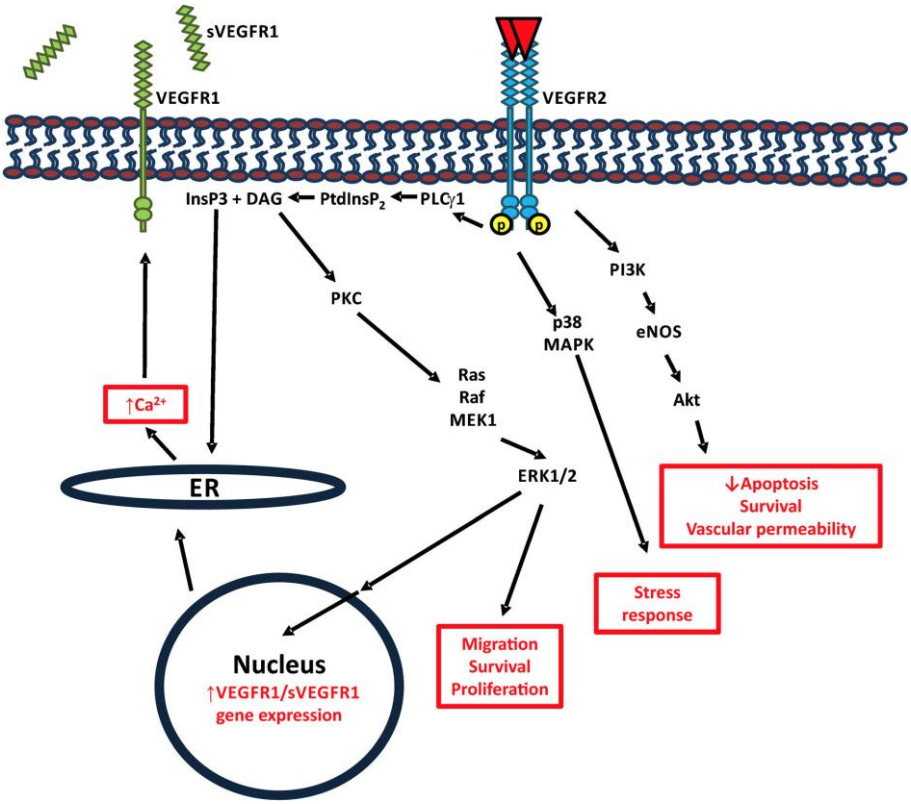

Figure 8. VEGF signaling pathway. Interaction of VEGFA with VEGFR2 inducing tyrosine phosphorylation and ubiquitination. VEGFR2 induce a downstream intracellular signaling events such as p38 MAPK, Akt and ERK1/2 activation promoting cellular response such as: migration, survival, proliferation and vascular permeability inducing a pro-angiogenic response and VEGFR1 expression and plasma membrane translocation. Obtained from Smith G A. et al 2015[63].

3.3. Vasculogenesis and retinal disorders

The retina is a complex neurovascular tissue med up of seven types of neurons, two types of glial cells and a rich network of endothelial cells[73,74]. Retinal ganglion cells in hypoxia conditions release growth factors such as PDGF, which regulates the VEGFA secretion by microglia and Müller cells. As a result, the VEGFA expression is localized in areas of vascular development and in ocular fluids as one

of the main components for the angiogenesis and the regulation of ischemic/hypoxic vasculogenesis induction[75]. Thus, VEGFA plays a critical role in the maintenance of physiologic homeostasis and in retinal vascular disorders[76]. Some treatment strategies are focused on inhibition of angiogenesis by targeting VEGFA such as bevacizumab which is used, not only in retinal disorders but also, in several tumors[63].

In AMD the outer retina and the RPE are affect, the integrity of the Brunch's membrane is compromised, and some vessels sprout from the choriocapillaris into the RPE. Concretely, the VEGFA is the responsible of vascular endothelial cell homeostasis. As said before, RPE in physiological conditions secrets VEGF in a polarized manner. But aging RPE loss their polarity secreting VEGF apically leading to pathological choroidal neovascularization[77]. Hence, the loss of polarity and hypoxia induce VEGFA expression and secretion leading to pathological retinal neovascular processes.

Although the role of VEGFA is well established as one of the main inducers of retinal vasculogenesis processes, it is not the only one. There are other factors that may contribute to these pathological processes that could explain the resistance to treatments based on VEGF blocking[78]. Factors other than VEGFA are PDGF, erythropoietin, stromal-derived factor-1, hyper activation of jack-stat3 and factors associated with abnormal activation of monocyte and glial cells among others[57].

4. Oxidative stress

The eye is susceptible to OS due to their metabolic activity and its susceptibility is related with a great number of retinal pathologies. In

fact, increased OS is one of the underlying factors to pathological retinal vascularization[79]. The OS reflects the imbalance between ROS and the biological ability to detoxify these free radicals to maintain the oxidant homeostasis and guarantee redox signaling[80,81].

4.1. Reactive oxygen species

Living organisms during cellular metabolism produce ROS, mainly in the mitochondrial electron transport chain, the endoplasmic reticulum and peroxisomes[82,83]. ROS can be divided into 2 groups: free radicals and nonradicals. The free radicals are molecules containing one or more unpaired electrons. Nonradicals are formed when two free radicals share the unpaired electrons. The main ROS are: Superoxide anion (O_2^-), Hydrogen peroxide (H_2O_2), Hydroxyl radical ($^{\bullet}OH$), Hypochlorous acid (HOCl), Peroxyl radicals ($ROO^{\bullet}$) and Hydroperoxyl radical ($HOO^{\bullet}$)[84]. All of these ROS can be derived from different intracellular or extracellular sources.

The mitochondria respiratory chain is one of the most important intracellular source of ROS production. Concretely, the complex I and III produce O_2^- and the superoxide dismutase (SOD) produce H_2O_2 from O_2^-. Moreover, the mitochondria produce $^{\bullet}OH$ by Fenton reaction[6,84]. The mitochondrial ROS accumulation induce the mitochondrial DNA (mtDNA) damage associated with progression of retinal disorders among others[85].

Besides, NADPH oxidase is the responsible of the O_2^- production, via the Nox catalytic subunit[86]. Elevated NADPH oxidase shows a strong association with endothelial disfunction and angiogenesis in retina[87]. In fact, NADPH oxidase and mitochondria

take part of a vicious cycle of ROS amplification promoting aging and disease stares.

Moreover, the superfamily of phospholipase A_2, a ubiquitous enzyme involved in cell membrane integrity, are linked to ROS production and lipid peroxidation[6,88]. The enzymes in peroxisomes also take part in ROS production, concretely H_2O_2 and O_2^{-6}.

Therefore, the retina contains chromophores that can be transformed into photosensitizers when excited by a photon inducing a change in electron distribution being excited. In this state interacts with intracellular molecules generating ROS[89].

Apart from this there are exogenous factors that can contribute to ROS generation such as smoking and passive smoking, exercise and alcohol consumption among others[6].

ROS participates in physiological processes when their concentrations are moderate, but when they get out of balance produces adverse modifications of DNA, proteins and lipids inducing disorders and diseases.

Nucleic acids are sensitive to oxidative damage. ROS can lead to DNA modifications in several ways inducing degradation of bases, single- or double-stranded DNA breaks, purine, pyrimidine or sugar-bound modifications, mutations, deletions or translocations and cross-linking with proteins[84]. If oxidative DNA damage is not correctly repaired, it may result in cell death, mutation, replication errors and genomic instability associated with aging and age-related diseases[90].

The lipid peroxidation is another result of oxidative stress, producing a highly reactive electrophilic aldehydes and free radicals disturbing cell function and membrane integrity[91]. Among the most attacked lipids are the polyunsaturated fatty acids (PUFAs) which

generate malondialdehyde and 4-hydroxinonenal (4-HNE) related to pathogenesis of several diseases[92].

Finally, the proteins can be damaged by OS leading to proteins modifications resulting in loss of biological function, cellular and metabolism disorders. Modified proteins tend to degrade quickly by proteases[84].

All of these processes take part in the progression of different disorders including ophthalmic ones.

4.2. Oxidative stress and retinal disorders

The RPE constitutes the blood-retinal barrier playing a pivotal role between blood vessels and photoreceptors. For several reasons such as light, metabolic rate, location, high oxygen tension in the macular area and cellular membrane interactions RPE and retina are continually exposed to OS; a potential risk factor for retinal disorders[6,93,94].

In addition to the OS which the epithelium is subjected regularly external factors such as smoking, sun exposure or bad habits must be added and increases stress levels. On the other hand, over the years the RPE ages with which its sensitivity to stress decreases, unbalancing the balance, promoting retinal disorders[95].

The oxygen levels in the retina regulates the retina vasculature from endothelial cells that forms plexiform layers in the retina[96]. In fact, OS in RPE cells intensifies the production and release of angiogenic factors increasing new blood vessels formation[97–99]. Specifically, OS promotes VEGF production in RPE cells, leading to choroidal neovascularization[100–102].

However, retinal hyperoxia led to blood vessels destruction and hypoxia to new blood vessels formation[103]. In fact, high levels of oxygen led to blood vessels dropout and when the oxygen levels are reset the VEGFA production increase inducing the formation of aberrant blood vessels leading to retinal detachment and blindness[57]. Hypoxia inducible factors 1 and 2 (HIF-1 and HIF-2) plays an important role on angiogenesis. In hypoxic situations HIF-1 and 2 are activated and upregulate the VEGFA expression levels[104]. Besides, ROS production induce growth factor stimulation such as PDGF[83] which can induce retinal disorder.

4.3. Antioxidant defense of retinal pigment epithelium.

The antioxidant defense is made up of enzymes and non-enzymatic molecules. Non-enzymatic antioxidants include vitamins C and E, β-carotene and glutathione. The antioxidant enzymes of RPE are SOD, catalase (CAT) and glutathione peroxidase (GSH-Px)[79,82,84].

Due to the role of OS in the development of retinal diseases, the used of antioxidants has been proposed as a possible treatment such as N-acetylcysteine (NAC) and Diallyl Sulfide (DAS).

NAC is a stable molecule with antioxidant and radical scavenging activity. It is a thiol compound which acts as an antioxidant and disulphide breaking agent. NAC can act as a direct antioxidant agent for some oxidant species or as an indirect antioxidant agent as a GSH precursor and breaking thiolated products, releasing thiols with antioxidant activity[105]. For these reasons, NAC has been proposed for the treatment of diseases in which OS is involved in the onset and progression of it.

Moreover, DAS is a lipophilic thioallyl-ether with antioxidant activity. It acts a selective inhibitor of cytochrome P450 2E1 (CYP2E1), an enzyme involved in xenobiotic metabolism which induces ROS production. CYP2E1 is induced in diabetes-mediated toxicities, after alcohol and drugs consumption and are related to neurological diseases such as Parkinson. Therefore, DAS is able to minimize cellular toxicity induced by ROS inhibiting CYP2E1[106].

Furthermore, the OS is capable of initiate signal transduction cascades which activate different transcriptional factors. Mitogen activated protein kinases (MAPKs), VEGFR and EGFR are OS targets[107]. Among the activated signals are antioxidant pathways such as nuclear factor KB (NFKB) regulating proinflammatory genes[108] and PI3K/Akt which are activated in order to protect the RPE against the OS[109,110]. The apoptosis is an activated mechanism in OS conditions to control the retinal tissue damage. The H_2O_2 exposure activates Bax and p53 leading to cell death by apoptosis[111,112]. Besides, autophagy is activated by OS protecting the RPE cell to OS damage[92,113].

5. microRNA

5.1. microRNAs biogenesis

Nearly the 95% of the genome is noncoding DNA among which are the microRNA (miRNA), small non-coding RNA sequences (21-25 nucleotides), able to regulate the expression of one or more mRNAs[114,115]. miRNAs regulate protein translation by targeting their complementary 3' untranslated regions (UTR) mRNA and by repressing translation or degrading target mRNA. Each miRNA could regulate more than one mRNA involved in different biological

processes including proliferation[116], cell survival[117], inflammation[118], angiogenesis[119], oxidative stress[120] and immune response[121] among others. Some diseases are affected by miRNA dysregulation, a tissue-specific expression profile is needed to decipher the function and mechanism of individual miRNA[122]. MiRNAs could be found intracellularly and extracellularly in different body fluids including plasma, serum, urine, vitreous humor, saliva and in extracellular vesicles (EVs) as circulating miRNAs[123–125]. The circulating miRNAs plays an important role in cell-to-cell communication.

The miRNAs are transcribed by the RNA polymerase II/III as a primary-miRNA(pri-miRNA)[126] generating in the nucleus a RNA transcript with a 5'cap and poliA tail[127]. The pri-miRNA are cleaved by Drosha (an RNA III enzyme) and Di George Syndrome critical region gene 8 (DGCR8) generating the precursor (pre-miRNA) hairpin-shaped with a 5' phosphate group and a 2 nucleotides 3' overhang. However, there are different mechanism of pre-miRNA processing regulation in addition to Drosha. Some transcription factors, hormones, RNA-binding proteins and adenosine deaminases that act on RNA (ADARs) can edit the pri-miRNA[127]. The pre-miRNA is transported by the Ran-GTP dependent Exportin-5 to the cytoplasm[128]. Dicer process the pre-miRNA generating the mature miRNA as RNA duplex of 19-25 nucleotides. The mature miRNA are incorporated into de RNA-induced silencing complex (RISC) assembled by Dicer, transactivation-responsive RNA-binding protein (TRBP) and Argonaute proteins to promote the post-transcriptional regulatory functions[126] mediated by repression, deadenylation and mRNA target degradation[129] (Figure 9).

Different miRNA regulatory mechanisms are propose depending on the complementary degree between miRNA and target. Usually,

when the complementarity is high the mRNA target is degraded while less complementarity leads to translational inhibition[130]. Although, the mRNA 3'UTR is the target region par excellence, the mRNA 5'UTR and coding sequence can also be target sites for miRNA[131].

Approximately 50% of the miRNAs are expressed from non-protein coding transcripts, intergenic miRNAs, and the rest are located in the introns or exons of coding gens, intronic miRNAs[132]. The intragenic miRNAs share the promotor with their encoding gen, are located in the non-protein-coding region of the transcript and are coexpressed with the gen transcripts[122].

The nomenclature of the miRNAs is uniform, are numbered sequentially in the order of discovery as miR and a number. In order to denote the organism 3 letters are added such as hsa form human organism. Identical miRNA sequences from different precursor sequences and genomic locis has a numeric suffix, hsa-miR-XXX-1. When the sequence differs 1 or 2 nucleotides are named with a letter suffix, hsa-miR-XXXa. Therefore, a pre-miRNA can generate more than one mature miRNA after being subjected to different modifications: 5'/3'timming, substitutions, insertions, deletions or additions at 3' end. To difference these miRNAs the suffix 5p and 3p is added. When the miRNAs are closely in the genome they form a cluster[114].

MiRNAs-focused research has grown exponentially due to their potential as biomarkers. The miRNAs are invaluable tools in probing different aspects of a disease such as diagnosis, progression, classification and treatment. In fact, many clinical fields are now focused on the study of miRNA for diagnosis or treatment purpose[123,133].

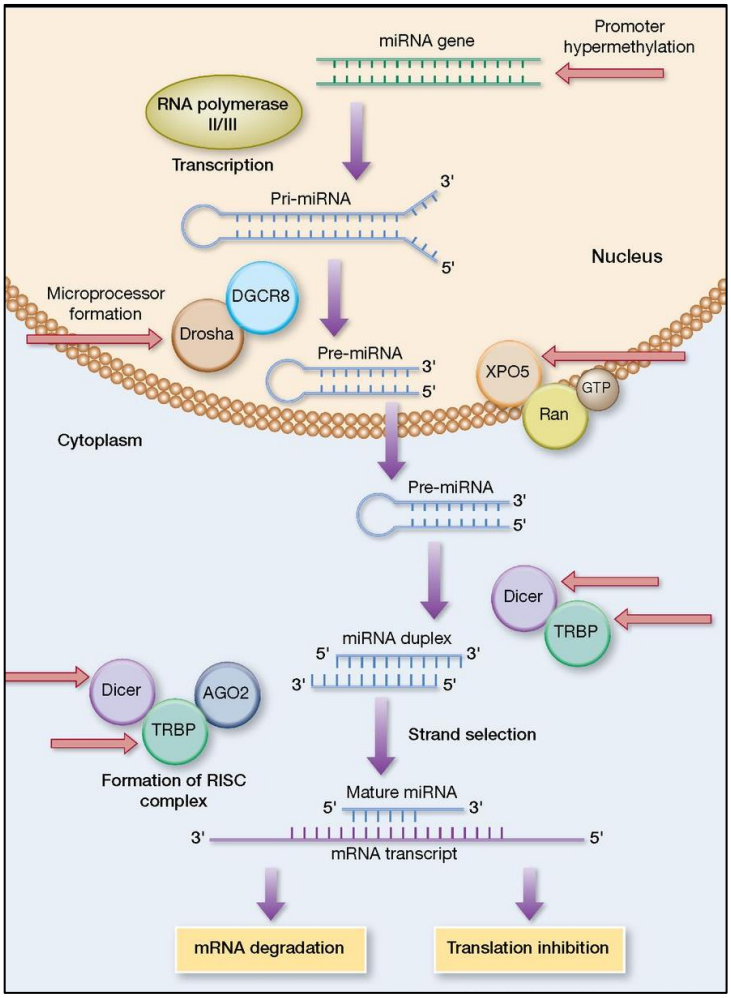

Figure 9. Biogenesis, function and miRNA transport. Figure adapted from Murlane. 2013[134].

5.2. microRNAs and eye disorders

The tissue-specific miRNA expression profile analysis depends on the physiological state of tissue[135]. Recently, the miRNA transcriptome (miRNoma) from human retina are analyze. 480 miRNAs are express

in retina and 416 miRNAs are express in RPE and choroids of which 17% are retina-specific and 29% RPE and choroid-specific[136]. These miRNAs reflect the retina physiology and their expression profile changes on pathological conditions. The abundance of miRNA in retina suggest their implication in visual health maintenance.

The miRNAs play an important role in pathological processes related to eye disorders such as angiogenesis, oxidative stress and immune response. MiRNAs can be easily obtained through different body fluids making them a promising biomarker. The aim of the miRNA profiling is to identify biomarkers and miRNAs related to the pathology progression.

There are different studies that analyze the miRNA expression profile in AMD patients, one of them proposed miR-27a-3p, miR-29b-3p and miR-195-5p as blood biomarkers for AMD, where there are highly express. These miRNAs are involved in cellular process, biological regulation and metabolic process which can be related to AMD pathogenesis[137]. Moreover, the study of miRNA expression profile in serum of AMD patients has demonstrated the presence and usefulness of miR-661 and miR-3121 in wet AMD patients and miR-4258, miR889 and Let-7 in dry AMD as biomarkers[124]. Another body fluid which can be analyzed is the plasma, where the miR-25-3p, miR-410, miR-574-3p and miR-660-5p expression is significantly decreased and miR-139-3p, miR-212-3p, miR-324-3p, miR-324-5p, miR-532-3p, miR-744-5p and Let-7c are highly express in AMD patients[138]. In addition, the miR-146a/miR-106b expression in plasma and vitreous humor has been proposed as a good ratio to discriminate patients with wet AMD[123]. Other miRNAs proposed as potential biomarkers are

miR-9, miR-23a, miR-27a, miR-34a and miR-155 able to regulate pathways linked to neurodegeneration and inflammation[139].

It should be noted, that the analysis of dysregulated miRNA in AMD models provide clues to understand the role of miRNAs in AMD. Different miRNAs were analyzed in RPE model identifying miRNAs related to AMD progression such as miR-92[140], miR-184[141] and miR-155[142] able to regulate angiogenic processes. Another miRNA is miR-34a related to the phagocytosis processes regulation[143].

Other analyzes determine the miRNA expression profile in retinitis pigmentosa noting that miR-96 and miR-183, apoptosis regulators, expressions are increased. However, miR-1 and miR-183, mRNA processing regulators, expressions are decreased in mouse retina[144].

The circulating and retinal miRNA were analyzed in diabetic retinopathy and miR-20a-5p, miR-20a-3p, miR-20b, miR-106a-5p, miR-27a-5p, miR-27b-3p, miR-206-3p and miR-381-3p are dysregulated. These miRNAs regulate VEGF and BDNF expression[139]. However, the closely related miRNAs to diabetic retinopathy are miR-200b, a VEGF regulator, and miR-146a, a modulator of NF-κB inflammatory response[145].

Without a doubt the miRNA expression profile can help to the prevention, diagnosis, monitoring and treatment of the retinal disorder but it would be necessary to improve the miRNA knowledge.

5.2.1. microRNAs and eye oxidative stress

The OS is a factor that can modify the miRNA expression profile in a specific tissue. As already mention the retina is exposed to OS so

the miRNA expression could be modified, and their targets dysregulated promoting OS or protecting cells from them.

Among the dysregulated miRNAs by OS, concretely by H_2O_2 exposure, are miR-30b-5p, miR-192-5p able to regulate cell viability. Although, miR-194-5p, miR-658, miR-382-5p, miR-486-5p, miR-525-5p, miR-518d-3p, miR-29b-1-5p, miR675-5p, miR1238-3p, miR195-3p, miR-1539, miR-490-5p, miR3200-5p, miR-1273d, miR-130a-5p, miR1247-5p, miR-18b-5p, miR-493-3p, miR-27a-5p and miR-1910-5p present an important role in oxidant-antioxidant balance regulation in ARPE-19 cells[146]. In addition to this, the incubation with different compounds such as anti-VEGF drugs[147] and cuurcumin[148] alter the miRNA expression profile in response to OS induce by H_2O_2 exposure.

Some miRNAs have antioxidant enzymes as targets, modulating the antioxidant defense in the tissue. Haque et al demonstrated that ARPE-19 cells exposed to H_2O_2 increase miR-30b levels, which regulates CAT expression, promoting OS reducing the antioxidant mechanism[149]. Another target is the SOD by miR-17-3p aggravating the oxidative damage in RPE cells[150].

Different authors observed the antiapoptotic effect of miR-23a, targeting Fas, in ARPE-19 cells under OS conditions, indicating their pathological effect[120,151]. Moreover, the OS reduce the miR-184 levels which is involved in the photoreceptor's phagocytosis. So miR-184 expression levels are reduced in AMD patients and the phagocytosis processes run-down[152].

Equally other eye pathologies, besides the AMD, has miRNAs dysregulation associated. In a diabetic retinopathy retina, miR-365 expression promotes OS[153]. Additionally, the up-regulation of miR-195 in diabetic retina demonstrate its critical role in OS injury[154]. The

retinitis pigmentosa shows miRNA expression profile dysregulation, concretely of miR-1307, miR-3064, miR-4709, miR-3615 and miR-637 able to target retinitis pigmentosa causative genes[155].

In contrast, not all miRNAs participate in the pathology progression, there are some dysregulate by OS with a protective role including miR-141-3p[156], miR-9[157], miR-187[158], miR-145[159] and miR-29[160] acting as antioxidant miRNAs.

There are different miRNAs like miR-24, miR-21, miR-204, miR-200c and miR-210 relate to OS in different organs and cells, however their role in eye remains to be determined. Therefore, analyzing the role of miRNAs on stressed eye is still a field to explore[161].

5.2.2. microRNAs and eye angiogenesis

The angiogenesis is one of the most important pathological processes related to eye disorders which could be associated with miRNA dysregulation expression profile. Different studies have showed that some miRNAs present proangiogenic roles and other antiangiogenic properties, these miRNAs are considered as angiomiRs. Perturbation of the angiomiRs expression change the gene expression levels rapidly inducing or repressing the angiogenesis process. There are multiple researches focused on determining the relationship of each miRNA with the vascular processes.

One of the most important miRNA targets in angiogenesis processes is VEGF giving to these miRNAs an antiangiogenic role. Although, exist different kind of miRNAs, a group which repress VEGF, antiangiogenic miRNAs, and a group which repress the expression of VEGF inhibitors acting as proangiogenic miRNAs.

Among the miRNAs with VEGF as target are the miR-122 target VEGFC[162], miR-203[163], miR-214[164] and miR-140-5p[165] target VEGFA but some of them have not yet been studied in eye disorder.

Obviously, the expression of these miRNAs should be down-regulated in patients with eye disorders that course with angiogenesis. Other antiangiogenic miRNAs are miR-24[166], miR-21[138], miR-31and miR-184[167] inhibiting neovascularization. Among the multiple functions attributed to miR-146 the angiogenesis modulator capacity is one more, repressing VEGFA in RPE cells acting as antiangiogenic factor[118]. As is mentioned above, the miR-9 present antioxidant properties and it has also been shown that can suppress VEGF expression, adding the antiangiogenic capacity to their protective effect[168].

Therefore, in plasma of AMD patients miR-192-5p and miR-342-3p are downregulated and their target, VEGF, are upregulated inducing pathological angiogenesis and AMD progression[138]. Zhou et al determine that miR-23 and miR-27 have an important role in pathological angiogenesis inducing choroidal neovascularization in AMD[119]. The miR-410 has been identify as angiogenesis modulator in retina thanks to targeting VEGFA[169]. Also, the miR-17 family (miR-17, miR-20a, miR-20b, miR-106a, miR-106b and miR-93) target VEGFA, being important during early angiogenic events in human retina with a downregulated expression[170]. Furthermore, the miR-150[171] and miR-126[172] has been identify as endothelial cell specific inhibitors of pathological angiogenesis.

However, among the proangiogenic miRNAs are the miR-126. This miRNA depending on the context has a anti or proangiogenic effect. One of their targets is the Spread-1 and PI3K regulatory subunit,

VEGFA intracellular inhibitors, promoting the VEGFA expression and blood vessels formation[173]. In addition to this the miR-126 with miR-210 could increase myocardial reperfusion after a heart arrack, thanks to its proangiogenic role[174].

Furthermore, EGF and FGF among others are engaged in angiogenesis regulation. Their expression could be modulated by different miRNAs in the same way as VEGF. The miR-192 targets EGF repressing the new blood vessels formation[175]. miR-101 regulates FGF and promote neovascularization cellular proliferation, survival and migration[176].

The miRNA regulation pathways have been extensively studied in order to provide new knowledge of miRNA regulator mechanisms and treatment strategies. In fact, many clinical fields are now focused on the study of miRNAs for diagnosis or miRNA manipulating for treatment of different pathologies including eye disorders[123,133]. Besides, different researchers are focused on the study of synthetic miRNA administration as a therapeutic drug for different disorders[177].

6. Extracellular vesicles

6.1.Extracellular vesicles and composition

The EVs were discovered three decades ago as a method of intercellular communication[178]. EVs are secreted by multiple cell types and are present in different biological fluids including blood, urine, saliva, breast milk, amniotic fluid among others[179].

The EVs are formed by a lipid bilayer with different size, origin and cargo[180]. The biological cargo includes proteins and genetic material such as mtDNA and small non-coding RNAs among which are

the miRNAs[181,182] (Figure 10). The EVs cargo differs according to the parental cells and their physiological condition[183]. The EVs can transfer their cargo from parental cells to recipient cells, playing an important role on intercellular communication, affecting the recipient cell behavior and the physiological or pathophysiological state of them[184].

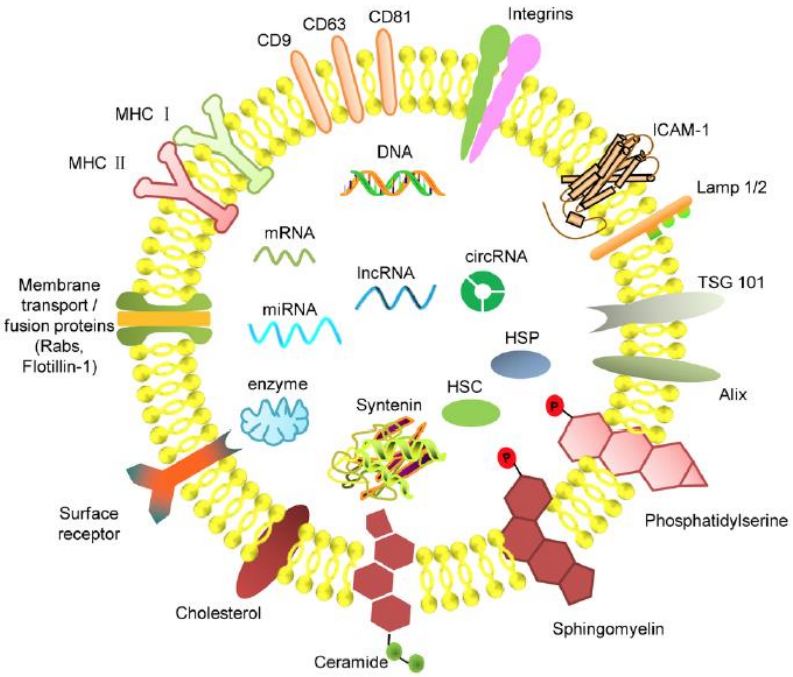

Figure 10. Composition and structure of EVs. Figure adapted from Jiang 2019[183].

Therefore, EVs can be used as a circulating biomarkers for different pathologies because of their presence in biological fluids, their stability and similarity to original cells contents[183]. Recently, EVs are propose as therapeutic targets and as a delivery vehicles of proteins, genetic drugs or chemotherapeutic drugs due to its nature[179,183]. The use of EVs

as therapeutic agents may avoid some important problems of cell therapies such as rejection[184].

The EVs are derived from endocytic compartments, they proceed from early endosomes that mature to late endosomes and multivesicular bodies (MVBs). The endosomal sorting complex required for transports (ESCRT) regulates the formation and the cargo of the late endosome and MVBs[185]. The MVBs membrane germinates producing intraluminal vesicles (ILVs). Rab GTPases 27a and 27b mediates the MVB fusion with cell membrane leading to EVs secretion to the extracellular space[183,186] (Figure 11).

There are different subtypes of EVs according to their size, markers and composition, the most predominant are the small EVs (sEVs), microparticles and ectosomes. The sEVs has a bilipidic layer, diameter of 30-150 nm, 1.09-1.13 g/mL of density and their cell membrane markers are the tetraspanins CD63, CD81 and CD82[187]. Many studies analyze the functional implication of sEVs in different processes like angiogenesis[97,99,188], inflammation[189], cell proliferation[190], migration[191] and invasion[192]. Furthermore, the microparticles and ectosomes are EVs with an heterogeneous size (100– 1500nm), a density of 1.09-1.19 g/mL and are enriched in phosphatidylserine and cholesterol, similar to cell membrane[193]. Finally, the apoptotic bodies are a large particles (0,5- 4 µm) produced by cell death process, when the plasmatic membrane break up leading to small particles enclosing cell content[194].

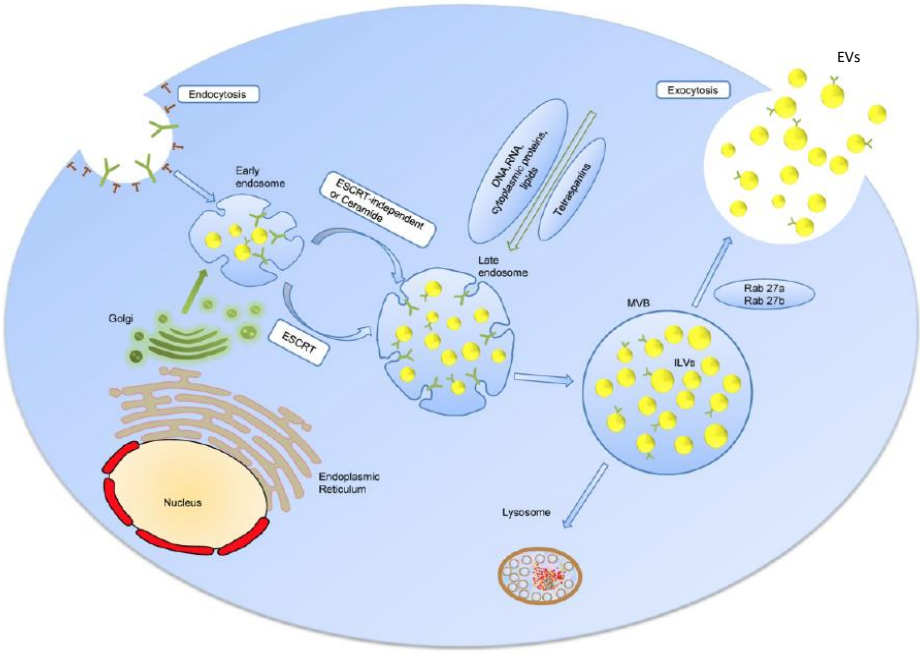

Figure 11. EVs biogenesis process. Figure adapted from Jiang 2019[183].

The nomenclature of the EVs is controversial, according to the minimal information for studies of extracellular vesicles 2018 (MISEV2018)[195] the EVs should be named with operational terms unless the specific markers were detected. However, does not exist a consensus about the markers for the different subtypes of EVs, promoting the use of nomenclature rules of MISEV2018. EVs subtypes will be classified according to their density, biochemical composition, cell origin or size such sEVs with ranges under 100 nm[195], which correspond to the historically called exosomes.

6.2. Functions of extracellular vesicles

EVs are secreted by practically all cell body types and could be found in different biological fluids: blood, urine, saliva, blood and

serum among other[179]. The first function attribute to EVs was the removing of unnecessary molecules[196]. Later, it was observed that EVs are used by all organisms to transport and deliver different substances including signaling molecules and cellular waste[178]. Therefore, EVs could be uses as disease and toxicity biomarkers[197].

Briefly, the most important and studies EVs function is the cell-to-cell communication. EVs can exchange their content (mRNAs, miRNAs and proteins) with their target cells[182,198]. Once in the target cell the EVs are able to modulate different cellular processes including angiogenesis[97,99,199,200], immune response[201] inflammation[202] and act as a protective mechanism[203].

Furthermore, EVs are associated with many common diseases including different types of cancer[204,205], myocardial infraction[206], liver injury[197], neurodegenerative diseases such as Parkinson[207] and retinal disorders[99,208].

EVs can be used as molecular and drugs transporter useful for the treatment of different disorders[178], including eye disorders, thanks to their non-immunogenic nature due to its similar composition to body cells[179]. This field is relatively new, so it needs more research to increase the knowledge about EVs.

6.3. Extracellular vesicles and eye disorders

Due to the EVs functions, they could present an important role in protection and progression of pathological eye disorders. To determine their role is necessary to analyze their cargo and their influence in neighboring cells.

Different studies analyze the proteome profile of EVs released by RPE cells. 72 proteins were found within sEVs released by ARPE-19 cells. However, their cargo depends of the physiological state of cells and are different between stressed and non-stressed cells. Concretely, oxidative stressed-sEVs carry phosphoproteins involved in apoptosis, survival and metabolism pathways[209]. After the study of proteome profile of drusen Wand and collaborators determine its similarity with RPE's EVs composition, suggesting the implication of EVs-proteins released by RPE in drusen formation[210].

Therefore, the EVs effect on neighboring cells depend on their cargo, physiology and environmental conditions. Proof of this is that sEVs from ARPE-19 cells modulate immune response, killing monocytes after cytokine stimulation or downregulating the immune environment in homeostatic conditions[211]. Moreover, the retinal astrocytes sEVs contain antiangiogenic compounds inducing a protective effect[212]. In addition, the intravitreal administration of sEVs from mesenchymal stem cells has a protective effect on retinal ischemia due to the presence of angiogenic growth factors on sEVs[203]. Concluding that the administration of sEVs can be used as treatment for retinal tissues.

Not only the EVs cargo is modified depending on the physiological state of cells but also the amount of EVs that are released. The RPE cells subject to OS release more sEVs than non-stressed cells, and this sEVs promote angiogenesis thanks to the presence of VEGFR1 and VEGFR2 in these stressed-sEVs[97]. In fact, the proangiogenic role of sEVs release by RPE cells has been proved[188].

The EVs could be found in different body fluids including tears[213], blood and aqueous humor. In fact, the aqueous humor from AMD

patients present EVs with a proteome profile different from healthy donors and similar to EVs released by oxidative stressed ARPE-19 cells. Among the EVs-proteins have been founded endosomal proteins, annexins, heat shock proteins, cytoskeleton proteins, adhesion and migrator proteins[214].

Altogether, EVs can be used as biomarkers of disease progression, give information of pathophysiology of the disorder and as therapeutic treatment.

6.4. Extracellular vesicles, miRNAs and eye disorders

Few studies analyze the miRNA expression profile of EVs released by eye tissues and cells. However, different studies analyze EVs-miRNAs able to modulate mechanism related to eye disorders. Angiogenesis is one of the most studied pathological processes related to eye disorders and different angiomiRs travel within EVs including miR-126, miR-214, miR-296, miR-125a, miR-31 and miR-150[215]. Therefore, miR-105 carried in sEVs downregulate ZO-1 enhancing vascular permeability in cancer[216].Nevertheless, these miRNAs have not yet been studied in eye disorders.

Among the few studies focused on eye is found that miR-155, from sEVs released by Burkitt lymphoma cells, induces VEGF expression in RPE cells increasing the new blood vessels formation[217,218]. Moreover, the miR-146a, miR-21 and miR-34 are upregulated in sEVs of vitreous humor from uveal melanoma patients suggesting their utility as diagnostic sEVs-miRNAs[219,220]. The sEVs from blood of AMD patients carry different miRNAs including miR-301-3p, miR-361-5p and miR-

424-5p able to regulate AMD pathological related pathways and this sEVs-miRNAs are proposed as AMD biomarkers[140].

These results suggest the role of sEVs-miRNAs from different body fluids as good biomarkers for different disorders.

HYPOTHESIS AND OBJECTIVES

Hypothesis

The retinal disorders such as RD and AMD are directly linked to neovascular processes and OS[19,94,221–223]. The RPE is continually expose to OS[6,94] intensifying the production of angiogenic factors such as VEGFA, increasing the formation of new blood vessels[101,102,224]. Therefore, sEVs play a crucial role in cellular communication, necessary to the maintenance of visual homeostasis. The OS challenge resulted on significant high sEVs release from RPE. The utility of circulating miRNAs as biomarkers are well known. Unfortunately, there are few studies that analyze the sEVs miRNA expression profile in retinal disorders.

The miRNA expression profile depends on the physiological state of cells and their study allow us to understand the molecular bases of the disease. **Taking together all this information, it is plausible to establish the hypothesis proposed herein that, OS generated by H_2O_2 could be directly involved in the regulation of ARPE-19 cells and sEVs miRNA expression profile.**

Objectives

The aim of the present PhD thesis is to identify the miRNA expression profile of the ARPE-19 cells and the sEVs released under OS conditions in order to identify an early marker for retinal degenerations. To address these issues, we propose the following objectives:

1. **To evaluate the effect of H_2O_2 treatment on ARPE-19 cells in order to determine the oxidative stress production, the cell viability and the release of sEVs.**

2. **To analyze the miRNA expression profile in H_2O_2 stressed ARPE-19 cells and non-stressed ARPE-19 cells and of the sEVs released by cells and to identify the miRNA potential targets and pathways.**

3. **To identify the miR-205-5p targets and pathways regulated by oxidative stress mediated by H_2O_2.**

4. **Determine the effect of H_2O_2 stressed ARPE-19 cells sEVs in oxidative stress production, cell viability on healthy cells and on new blood vessels formation.**

MATERIALS AND METHODS

Materials and Methods

1. Cell Culture and treatment

Arising retinal pigment epithelium (ARPE-19) human cell line was obtained from American Type Culture Collection (ATCC, Barcelona, Spain). ARPE-19 cells were culture in Dublecco's modified Eagle's DMEM/F12 (Gibco, Thermo Fisher, USA) supplemented with HEPES buffer 5mM (Gibco, Thermo Fisher Scientific, USA), 7,5% $NaHCO_3$ (Gibco, Thermo Fisher Scientific, USA), 10% Fetal Bovine Serum (FBS, HyClone, Thermo Fisher Scientific, USA), 1% penicillin/streptomycin (Thermo Fisher Scientific, USA) and 1% amphotericin (Thermo Fisher Scientific, USA). The ARPE-19 cells were maintained at 37ºC and 5% CO_2 and were used from passage 18 to 30.

Mature ARPE-19 cells were seeded in the same conditions as non-mature ARPE-19 cells and maintained 2 months with 1%FBS media.

For cellular passage the media was removed, and cells were rinsed with phosphate-buffered saline (PBS). For cell detachment cells were incubated at 37ºC for 10 min with trypsin-EDTA (HyClone, Thermo Fisher Scientific, USA). Following, cells were collected with completed medium and centrifuged for 5 min at 500 g.

Non-mature and mature ARPE-19 cells were counted after being stained with trypan blue (Thermo Fisher Scientific, USA) using a Neubaure chamber (Thermo Fisher Scientific, USA) [10 µL of cell suspension +10 µL of trypan blue]. The number of cells/mL were calculated using this formula:

Mean of cells x dilution factor x 10.000 = Number of cells/mL

Cells were seeded at a density of 1 x 10^3 cells/cm^2 in conventional flasks. After 2 days the cells reached the 80% of confluence and were ready to treat. For 24 h the cells were treated with H_2O_2 200 µM, 400 µM, 600 µM and 800 µM (Scharlau, Senmenat, Spain) and with 4 mM of N-acetylcysteine (NAC; Sigma Aldrich, Missouri, USA) using media with 1% FBS sEV-free (Gibco, Thermo Fisher Scientific, USA) and filtrated. Cells and supernatant were collected and preserved for further experiments.

ARPE-19 cells were seeded on transwell at a density of 1 x 10^3 cells/cm^2 until reached the confluence, approximately 3-4 weeks. For 24 h the cells were treated with H_2O_2 600 µM (Scharlau, Senmenat, Spain) using media with 1% FBS sEV-free (Gibco, Thermo Fisher Scientific, USA). Cells and supernatant (from up-side and down-side) were collected and preserved for further experiments.

2. Determination of Cell viability

2.1. XTT Assay

Sodium 3'-[1-phenylaminocarbonyl-3,4-tetrazolium-bis(4-methoxy-6-nitro) benzene sulfonic acid hydrate, (XTT, Cell Proliferation Kit II; Roche) was used to determine cell viability as mitochondrial activity. ARPE-19 cells were seeded at 6 x 10^3 cells/well in a 96 well plate for 48 h. ARPE-19 cells were treated with 200 µM, 400 µM, 600 µM and 800 µM H_2O_2 and with 4 mM NAC for 24 h. After two washing with PBS the XTT labeling reagent was mixed with electron coupling reagent, at a final concentration of 0,3 mg/mL to each

well. The solution was incubated for 6 h at 37°C in 5% CO_2. The absorbance was read at 550 nm by microplate reader (Victor, Perkin Elmer). Results were expressed as percentage relative to control group.

2.2. Apoptosis detection

One of the morphological features of apoptosis is the translocation of the membrane phospholipid phosphatidylserine (PS) from the inner to the outer layer of the plasma membrane. Number of dead cells by apoptosis or necrosis was measured by flow cytometry using the FITC Annexin V Apoptosis detection Kit (Immunostep, Salamanca, Spain). The Annexin V, Ca^{2+} dependent phospholipid binding protein, joins to the binding sites of the phospholipids exposed to the extracellular environment. A total of 10.000 cells per condition were analysed using the FACS Verse (Becton Dikinson, New Jersey, USA). Four populations are detected: unmarked Annexin (-)/Propidium Iodide (-) are live cells; double marked Annexin (+)/Propidium Iodide (+) represent apoptotic cells; simple marked Annexin (+)/ Propidium Iodide (-) are early apoptotic cells; and simple marked Annexin (-)/ Propidium Iodade (+) are necrotic cells.

3. Determination of ROS levels

Intracellular ROS levels were measured using dihydroethidium, (DHE; Thermo Fisher Scientific, Waltham, MA, USA) which is a superoxide indicator. This molecule has a blue fluorescence, but, when oxidized to ethidium, it stains DNA in red. ARPE-19 cells were seeded at $6x10^3$ cells/well in a 96 well plate for 48 h. ARPE-19 cells were

treated with 200 µM, 400 µM, 600 µM and 800 µM H_2O_2 and with 4 mM NAC for 24 h. Cells were rinsed with PBS twice and incubated with 5µM of DHE during 30 min at 37°C and 5% CO_2. ROS levels were measured by a fluorescence multiplate reader (Victor X5; Perkin Elmer) excited at 518 nm and read at 605 nm.

4. Transepithelial Resistance Measurement

Transepithelial resistance (TER) was measured by EVOM^2 Epithelial Volhometer (World Precision Instrument, Florida, USA) in ARPE-19 cells seeded in a Corning™ Multiple Well Plate with permeable polyester Membrane inserts (Thermo Fisher Scientific, USA). To calculate the TER a well without cells was used as blank. For 1 well 4 measures were taken, and the average was calculated as:

TER = (TER average – TER blank) x Transwell surface area.

Values were obtained from 3 independent experiments.

5. sEVs isolation

sEVs isolation from media was performed by serial centrifugations with the Optima XPN-100 Ultracentrifuge (Beckman Coulter, USA) using centrifuge tubes polycarbonate (Beckman Coulter, USA). The media from the cell culture was collected and concentrated with Amicon® Ultra-15 Centrifugal Filter Unit (Sigma Aldrich, Missuri, USA). The concentrate was centrifuged at 700 g for 30 min to remove the cellular debris, the supernatant was collected and centrifuged at

14.000 g for 30 min to take out the apoptotic bodies. Then, the supernatant was collected and centrifuged again at 40.000 g for 30 min and at 150.000 g for 90 min. After the last centrifuge the sEVs were at the bottom of the tube, the pellet was washed, resuspended with filtered-PBS and centrifuged at 120.000 g for 60 min, the pellet was collect with filtered-PBS or media and used or stored at -80ºC for further analysis.

From small amounts of medium the sEVs isolation was performed using the Total Exosome Isolation Reagent from cell culture media (Thermo Fisher Scientific, USA). The 2 mL of cell media was centrifuged at 2.000 g for 30 min to remove cells and debris. The supernatant containing the cell-free culture media was mixed with 1 mL of Total Exosome Isolation reagent and incubated overnight at 4 ºC. After incubation, the sample was centrifuged at 10.000 g for 1 h at 4ºC and the pellet was resuspended in cell culture media and stored at -80ºC for further analysis.

6. SEVs Characterization

6.1. Nanoparticle tracking analysis

SEVs identity was confirmed by the nanoparticle tracking system Nanosight NS300 following manufacturer's protocols (Malvern Instruments, Malvern, UK). The Malvern Panalytical Nanosight NS300 uses the technology of Nanoparticle Tracking Analysis. This unique technology utilizes the properties of light scattering and Brownian motion in order to obtain the size distribution and concentration measurement of particles in liquid suspension. A laser beams is passed through the sample chamber, and the particles in suspension in the path

of this beam scatter light in such a manner that can easily be visualized via 20 x magnification microscope onto which is mounted a camera. The camera operates at 30 frames per second, capturing video file of the particle moving under Brownian motion. The software tracks many particles individually and using the Stokes-Einstein equation calculates their hydrodynamic diameters.

SEVs pellet diluted in PBS; a 1/10 dilution went through the capillary of the instrument. The results are express as percentage versus control samples.

6.2. Electron microscopy

SEVs pellets were resuspended in PBS and ultracentrifugated at 120.000 g for 70 min at 4°C. After that, approximately 10 µg of the samples was resuspended in PBS on parafilm. The sample was fixed by depositing a drop of 2% Paraformaldehyde on the parafilm and placing the grid (Mesh with Formvar) on top of the drop. Negative staining was performed with 2% uranyl acetate. Photomicrographs were obtained using the transmission electron microscope FEI Tecnai G2 Spirit (FEI Europe, Eindhoven, Netherlands) using a digital camera Morada (Olympus Soft Image Solutions GmbH, Münster, Germany). sEVs were identified under the microscope solely based on size and morphology.

7. Protein isolation and quantification

7.1. Protein isolation from cells

For protein extraction, cells were tripsinized and centrifuged at 500 g for 5 min. The cells were collected in PBS, centrifuged at 500 g for 5 min and pellets were store at -80ºC until their lysis. Cell pellet was mixed in RIPA lysis buffer (Thermo Fisher Scientific, USA), phosphatase (Thermo Fisher Scientific, USA) and protease (Thermo Fisher, USA) inhibitor cocktail at final concentration of 1:100 and rotated at 4ºC overnight. To complete the lysis the samples were sonicated 3 pulses during 10 s spacing after each pulse samples on ice and centrifuged at 400 g for 20 min at 4 ºC to complete and collect the protein extraction.

7.2. Protein isolation from sEVs

Protein isolation from sEVs was carried out mixing the sEVs pellet with RIPA lysis buffer (Thermo Fisher Scientific, USA), phosphatase (Thermo Fisher Scientific, USA) and protease (Thermo Fisher, USA) inhibitor cocktail at final concentration of 1:100. To complete the lysis the samples were placed in an ultrasonic bath Bandelin Sonorex (Bandelin, Berlin, Germany) 3 pulses of 5 min spacing after each pulse samples on ice and centrifuged at 400 g for 20 min at 4 ºC to complete and collect the protein extraction.

7.3. Protein quantification

The protein concentration of the samples was determined by colorimetric detection based on bicinchoninic acid (BCA) (Thermo Fisher Scientific, USA). This method used the reduction of Cu^{+2} to Cu^{+1} by protein in an alkaline medium with the highly sensitive and selective

colorimetric detection of the Cu^{+1} using the BCA reagent. The purple-colored reaction product of this assay is formed by the chelation of two molecules of BCA with one Cu^{+1}. To determine the protein, amount a standard curve of Bovine Serum Albumin Standard (BSA) of known concentrations, from 2.000 µg/mL to 62,5 µg/mL, was used. The absorbance was read at 562 nm using a multiplate reader (Victor X5; Perkin Elmer).

8. Western Blot Analysis

The western blot is an analytical technique used to separate the denaturalized proteins according to their molecular weight and detect them. Equal amount of protein (30-40 µg) were mixed with sodium dodecyl sulphate (SDS) to denature and charge negatively the proteins, allowing them to migrate and ß-mercaptoethanol to increase the density and give blue colour. Samples were boiled at 95ºC for 10 min to complete the denaturalization. The protein samples were loaded on a 4% stacking - 12% resolving SDS-Polyacrylamide (Thermos Fisher Scientific, USA) electrophoresis gel for 2 h at 120 V.

Then the proteins were electroblotted onto a polyvinylidene difluoride membrane (PVDF; Millipore, MA, USA) by wet transfer for 1 h at 100 V. Membranes were blocked with blocking buffer 3% BSA [Tris-buffered saline with Tween 20 (TTBS); 10mM Tris Base, pH 7,6 NaCl, 0,1% Tween 20 and BSA] for 1 h on a shaking platform. Following, membranes were incubated overnight with the primary antibodies against VEGFA (1:200; Santa Cruz Biotechnology, USA), caspase-3 (1:200; Santa Cruz Biotechnology, USA) and ß-actin (1:1000; Santa Cruz Biotechnology, Texas, USA) as loading control,

diluted in blocking buffer 3% BSA in TTBS. The membranes were washed 3 times with TTBS for 10 min. Finally, membranes were incubated for 2 h at room temperature with a dilution 1:10.000 of anti-mouse and anti-rabbit IgG-HRP antibodies (Santa Cruz Biotechnology, Texas, USA) in TTBS. The membranes were washed 3 times with TTBS for 10 min.

The visualization was done with ECL Western Blotting Detection Reagents (Pierce, Thermo Scientific, Rockford, II, USA) and detected with Image Quant LAS-400 mini (GE Heathcare, Uppsala, Swedem). Protein levels were quantified by densitometry using ImageJ software (NIH, Bethseda, MD, USA). Results were express as percentage respect the control.

9. miRNA expression analysis using microarrays

To the miRNA expression sEV and cell profile, the 384 well SeraMir Profiler (System Biosciences, Palo Alto, CA) were used. For sEV the SBI's ExoQuick Solution (System Biosciences, Palo Alto, CA) was used and RNAs were purified using a phenol-free lysis buffer and rapid spin columns. The SeraMir Kit includes everything needed to accurately and sensitively measure RNAs, the 3' tailing was enabled and simultaneous both 3' and 5' ends were tagged during cDNA synthesis- ready for qPCR. 384 miRNAs were profiled using highly sensitive primers for PCR amplification.

9.1. RNA isolation from cells

ARPE-19 cells were seeded and treated on T_{225} flask, as explained above. The cell pellet was used for RNA purification using the SeraMir RNA Columns (System Biosciences, Palo Alto, CA). 350 µL of Lysis Buffer were added to cell pellet, to break the cells a 15 s vortex were done, and the suspension were placed at room temperature 5 min. In order to determine the efficacy of the RNA purification technique a SeraMir control *RNA spike-in* (System Biosciences, Palo Alto, CA) was added to the solution. To dilute the RNA 100% ethanol was added to the sample and vortexed 10 s. The solution was transferred to the spin column and centrifuged at 13.00 rpm 1 min, the flow-through were discarded and the spin column were placed back into the collection tube. 400 µL of Wash buffer was added, the sample were centrifuged at 13.000 rpm for 1 min (this step was repeated 2 times). To dry the sample, it was centrifuged at 13.000 rpm for 2 min. Following the RNA purification, the RNA elution was performed adding 30 µL of Elution buffer and centrifuged at 2.000 rpm for 2 min. We collect 30 µL of cell-RNA. The quantity and quality (260/280 absorbance ratio) of total RNA were assessed using the NanoDrop 2000 (Thermo Fisher Scientific, USA).

9.2. sEVs isolation and RNA isolation from sEVs

The ARPE-19 media from T_{225} flask were collected and concentrated using Amicon® Utra-15 Centrifugal filters (Cork, Ireland). The collected sample was used to sEVs isolation and lysis. 1 mL of ExoQuick-TC was added to 5 mL of concentrated media and mixed well. The sample was placed at 4ºC overnight, to precipitate the sEVs a 13.000 rpm centrifugation was performed for 2 min. The

supernatant was discarded, and the sEV pellet was used for RNA purification using the SeraMir RNA Columns (System Biosciences, Palo Alto, CA). 350 µL of Lysis Buffer were added to sEV pellet, to break the sEV a 15 s vortex were done, and the suspension were placed at room temperature 5 min. In order to determine the efficacy of the RNA purification technique a SeraMir control *RNA spike-in* (System Biosciences, Palo Alto, CA) was added to the solution. To dilute the RNA 100% ethanol was added to the sample and vortexed 10 s. The solution was transferred to the spin column and centrifuged at 13.00 rpm 1 min, the flow-through were discarded and the spin column were placed back into the collection tube. 400 µL of Wash buffer was added, the sample were centrifuged at 13.000 rpm for 1 min (this step was repeated 2 times). To dry the sample, it was centrifuged at 13.000 rpm for 2 min. Following the RNA purification, the RNA elution was performed adding 30 µL of Elution buffer and centrifuged at 2.000 rpm for 2 min. We collect 30 µL of sEV-RNA. The quantity and quality (260/280 absorbance ratio) of total RNA were assessed using the NanoDrop 2000 (Thermo Fisher Scientific, USA).

9.3. Retro transcription (RT)

Total isolated cell-RNA and sEV-RNA were reversely transcribed (cDNA synthesis) using the SeraMir Kits (System Biosciences, Palo Alto, CA) and PeqSTAR 96 Universal Gradient (peqLAB). The Poly A reaction was performed at 37ºC/ 30 min, following the adaptor anneal reaction at 60ºC/ 5 min and RT/ 2 min. The RT reaction was the last step, 42ºC/ 30 min, 95ºC/ 10 min and held at 15ºC.

9.4. Quantitative Real Time Polimerase Chain Reaction (qRT-PCR)

To test the cDNA a qPCR assay for Spike-in RNA control was performed. Once determined that the RNA is of sufficient quality the 384 well SeraMir Profiler were setup. The appropriate temperature cycles were used: 50ºC/2 min, 95ºC/10 min, 40 cycles; 95ºC/15 s, 6ºC/1 min using RT-PCR QuantStudio™ 3 y 4 system (Thermo Fisher Scientific, USA) from the *Instituto de investigación sanitario* INCLIVA. The miRNA expression values were calculated using the Ct media of 3 endogenous control genes (RNU43, RNU1Q and RNU6) available in the 384 well SeraMir Profiles. The gene expression value was calculated according to the $2^{-\Delta\Delta Ct}$ method, where the ΔΔCt was obtained as following:

$$\Delta Ct = Ct_{(\text{miRNA of interest})} - Ct_{(\text{Ct average of RNU43, RNU1Q and RNU6})}$$

$$\Delta\Delta Ct = \Delta Ct_{(\text{treated sample})} - \Delta Ct_{(\text{mean of control samples})}$$

$$2^{-\Delta\Delta Ct}$$

9.5. Statistical data processing and analysis of miRNA expression

The miRNA expression differences between: ARPE-19 control cells *vs.* ARPE-19 treated with 600µM H_2O_2; sEVs released by ARPE-19 cells treated with 600µM H_2O_2 *vs.* sEVs released by ARPE-19 control cells. Differences were analyzed using t-test study from *genefilter* package from R Bioconductor p_values were adjusted by Benjamini-Hochberg. miRNAs that presented an adjusted p_value< 0,05 were considered statistically significant. Significant miRNAs from

different comparisons were represented in a hierarchical clustering heatmap representation. Heatmaps were performed using *heatmap.3* package from R Bioconductor.

10. RNA isolation and quantification

10.1. RNA isolation from cells

RNA from ARPE-19 cells was isolated using the commercial miRNeasy® Mini Kit (Qiagen, Hilden, Germany). Pellet from 1,5 x 10^6 ARPE-19 cells were resuspended in 700 µL of QIAzol® Lysis Reagent (Qiagen, Hilden, Germany), homogenized with 0,5 x 16 mm syringe and incubated at room temperature. Next, 140 µL of chloroform were added and incubated at room temperature 3 min. The samples were centrifuged at 12.000 g for 15 min at 4ºC to divide the sample in three phases, the upper aqueous phase was transferred, and 100% ethanol was added, mixed and transferred into a RNeasy® Mini column (Qiagen, Hilden, Germany). Next, a wash was carried out with 700 µL of Buffer RWT and two more washes with 500 µL of Buffer RPE, both supplied in the kit. Finally, total RNA was eluted with 30-50 µL of RNase-free water. The isolated RNA was stored at -80ºC for further analysis.

10.2. RNA isolation from sEVs

RNA from sEVs were isolated using the commercial Total sEV RNA and Protein Isolation Kit (Invitrogen, Thermo Fisher Scientific, USA) according to the manufacture instructions. The sEV pellet was resuspended with 200 µL of sEV Resuspension Buffer supplied in the kit, homogenized and incubated at room temperature. Next, 200 µL of

2x Denaturing solution were added and incubated at 4ºC for 5 min. 400 µL of Acid-Phenol: Chloroform were added, vortexed for 60 s and centrifuged at 12.000 g for 5 min at 25ºC to divide the sample in three phases, the upper aqueous phase was transferred. Straightaway, 1.200 µL of 100% ethanol were added to the aqueous phase, mixed and transferred into a Filter Cartridges in a Collection Tube supplied by the kit. Next, a wash was carried out with 700 µL of Wash Solution 1 and two more washes with 500 µL of Wash solution 2/3. Finally, total RNA was eluted with 50 µL of RNase-free water pre-warmed at 95ºC. The isolated RNA was stored at -80ºC for further analysis.

10.3. RNA quantification

The amount of RNA was quantified by UV-Vis spectrophotometers measurements using the NanoDrop 2000 (Thermo Fisher Scientific, USA). The following modification of the Beer-Lambert equation was used for nucleic acid quantification:

$$\mathbf{c = (A^* \varepsilon)/b}$$

c is the nucleic acid concentration in ng/µL

A is the absorbance in AU

ε is the wavelength-dependendt ectinction coefficient in ng-cm/µL

b is the pathlength in cm

The nucleic acid sample concentration was based on the absorbance at 260 nm, the selected analysis constant and a baseline correction. The generally accepted extinction coefficients or constants for RNA were 40 ng-cm/µL. Although purity rations were important indicators of sample quality. A 260/280 ratio of 2.0 was generally accepted as “pure”

for RNA. The 260/280 ratio is dependent on the pH and ionic strength of the buffer used to make the blank measurement and sample measurement. If the ratio was different it indicated the presence of protein, phenol or other contaminants that absorb at 260 nm. A 260/230 ratio of 1,8 – 2,2 were accepted as "pure" nucleic acid. If the ratio was different it indicated the presence of residual phenol, guanidine, magnetic beads, carbohydrates or proteins.

11. qRT-PCR

qRT-PCR was used to analyze the miRNA and mRNA expression profile in an independent sample set.

11.1. qRT-PCR for miRNAs

RT reaction were performed using TaqMan™ MicroRNA Reverse Transcription Kit (Applied Biosystems, CA, USA) and TaqMan® miRNA Assay primers used are in Table 1. The synthesis of cDNA is specific for each mature miRNA. For 20µL of reaction 100-150 ng of total RNA was used with 0,15 µL of 100 mM dNTPs, 1µL MultiScribe™ reverse Transcriptase 50 U/µL, 1,5 µL of 10x Reverse Transcription Buffer, 0,19 µL of RNase Inhibitor 20 U/µL and 3 µL of TaqMan® miRNA Assay primer. The appropriate temperature cycles were used: 16ºC/30 min, 42ºC/30 min, 85ºC/5 min and held at 4ºC using the Mastercycler Nexus Gradient (Eppendorf, Hamburg, Germany).

For qRT-PCR, reactions were performed using TaqMan® Gen expression Master Mix (Applied Biosystems, CA, USA) and TaqMan® miRNA Assay primers (Table 1). For 10 µL of reaction 1,33 µL of RT product, 5 µL of TaqMan® Gene Expression Master Mix 2x, 1 µL

TaqMan® miRNA Assay primer and 2,67 µL of nuclease-free water were used. The amplification conditions were: 50ºC/2 min, 95ºC/10 min and 40-50 cycles of 95ºC/15 s and 60ºC/1 min using Roche 234 LighterCycler 480 (Roche, Basile, Switzerland). For qRT-PCR triplicates was performed for each sample using 96-well plates. Each plate includes the appropriate endogenous control (RNU6B and RNU43), case and control samples to avoid methodological mistakes. The gene expression value was calculated according to the $2^{-\Delta\Delta Ct}$ method, where the ΔΔCt was obtained as following:

$$\Delta Ct = Ct_{(\text{miRNA of interest})} - Ct_{(\text{Ct of RNU43 or RNU6B})}$$

$$\Delta\Delta Ct = \Delta Ct_{(\text{treated sample})} - \Delta Ct_{(\text{control samples})}$$

$$2^{-\Delta\Delta Ct}$$

Table 1. TaqMan® miRNA primer assays

Name	Reference
RNU6B	001093
RNU43	001095
hsa-miR-205-5p	000509
hsa-miR-302c-3p	000533
hsa-miR-521	001122
hsa-miR-130b	000456
hsa-miR-302a-3p	000529
hsa-miR-122	002245

11.2. qRT-PCR for mRNAs

RT reaction were performed with SuperScript III Fisrt-Strand Synthesis System (Thermo Fisher Scientific, USA). For 20 µL of reaction 700 ng of total RNA was used with 1 µL of 10 mM dNTPs and 1µL of Oligo(dT) 20 run at 65ºC/5 min and 4ºC/5 min. To the previous

mix 2 µL of 10x Buffer RT, 2 µL of 50 mM $MgCl_2$, 2 µL of 0,1 M DTT, 1 µL of RNase OUT™ Ribonuclease Inhibitor, 0,25 µL of SuperScript® III RT and 2,75 µL of Nuclease-free water run at 55ºC/50 min and 85ºC/5 min. Finally, 1 µL of RNase H were added to the mix and run at 37ºC/20 min using the Mastercycler Nexus Gradient (Eppendorf, Hamburg, Germany).

For qRT-PCR, reactions were performed using iTaq™ Universal SYBR® Green Supermix (Bio-Rad, CA, USA) and Gene-specific primers used are in Table 2. For 10 µL of reaction 5 ng of cDNA were used with 5 µL of iTaq™ Universal SYBR® Green Supermix and 1,2 µL of forward and reverse 5 µM KiCq Start™ Primers (Sigma-Aldrich, Missouri, USA). The amplification conditions were: 95ºC/5 min and 40-50 cycles of 95ºC/10 s, 60ºC/20 s and 72ºC/30 s and 60ºC/1 min, 97ºC/5 min and 40ºC/30 s using Roche 234 LighterCycler 480 (Roche, Basile, Switzerland). For qRT-PCR triplicates was performed for each sample using 96-well plates. Each plate includes the appropriate endogenous control (GAPDH), case and control samples to avoid methodological mistakes. The gene expression value was calculated according to the $2^{-\Delta\Delta Ct}$ method, where the ΔΔCt was obtained as following:

$$\Delta Ct = Ct_{(mRNA\ of\ interest)} - Ct_{(Ct\ of\ GAPDH)}$$

$$\Delta\Delta Ct = \Delta Ct_{(treated\ sample)} - \Delta Ct_{(control\ samples)}$$

$$2^{-\Delta\Delta Ct}$$

Table 2. Primer sequences

Name	Forward sequence	Reverse sequence
GAPDH	5'-TGAAGGTCGGAGTCAACGGAT- 3'	5'-TTCTCAGCCTTGACGGTGCCA- 3'
VEGFA	5'-GACTTATACCGGGATTTCTTG-3'	5'-AATGTGAATGCAGACCAAAG-3'

12. Analysis of miRNA target genes

In silico analysis of the putative miRNA targets were performed using TargetScanHuman (http://www.targetscan.org/vert_72/) using Tarbase. The pathway analysis in which the detected miRNAs were involved was done using DIANA TOOLS mirPath v.3 algorithm (http://snf-515788.vm.okeanos.grnet.gr/) [225]. Moreover, the analysis of the pathways regulated by the putative targets of the miRNAs was performed with the FUNRICH software using the gen ontology database. With STRING (https://string-db.org/) the networking of the targets was performed.

13. Mimic and siRNA Cell transfection

ARPE-19 cells seeded in a 6 well plate at a 60-80% of confluence were treated with 600 µM H_2O_2 after 24 h were transfected with miR-205-5p mirVana® miRNA mimic (Thermo Fisher Scientific, USA), mirVana™ miRNA mimic negative control (Thermo Fisher Scientific, USA), Silencer® Select Pre-designed siRNA for VEGFA (Thermo Fisher Scientific, USA) and Silencer® negative control #1 siRNA (Thermo Fisher Scientific, USA) at a concentration of 30 pmol using Lipofectamine® RNAiMAX Reagent (Thermo Fisher Scientific, USA) diluted in opti-MEM® Medium (Thermo Fisher Scientific, USA) following the protocol. After 48 h of transfection the cell pellet and the media were collected to further analysis.

14. Human Umbilical Vein Endothelial Cell (HUVEC) isolation and culture

The HUVEC cells were donate by Dr. Carlos Hermenegildo and Dra. Susana Novella from the LinCe laboratory. Isolated from the vein of the umbilical cord of neonates from the Gynecology and Obstetrics services of the Hospital Clínico Universitario Valencia. The study was conducted in accordance with the principles expressed in the Declaration of Helsinki.

The HUVEC cells were isolated on sterile conditions, after the vein cannulation a PBS wash was done followed with a digestion using type II collagenase to detach the HUVEC cells during 15 min at 37°C. the HUVEC cells growth with Endothelial Cell Media (Promo Cell, Heidelberg, Germany) with 20% of FBS inactivated and 1% penicillin/streptomycin and 1% amphotericin. The flask was previously treated with Gelatin from bovine skin Type B (Sigma-Aldrich, Missouri, USA). The cells were growth at 37°C and 5% CO_2 until passage 5.

15. Vasculogenesis Assays

Vasculogenesis was analysed in Matrigel (Becton Dickinson, MA, USA) as previously describe[226]. $8x10^4$ HUVEC cells/well in a 96 well plate were seeded and treated or not with ARPE-19 cells media for 5 h. Matrigel was diluted with DMEM/F12, FBS free and allowed to solidify overnight at 37ºC. Pictures were taken with Olympus CKX41 inverted microscope (Olympus, Tokyo, Japan) and images recorded by

Olympus DP74 digital Camera (Olympus, Tokyo, Japan). The images were analysed with Image J using the Angiogenesis Analyzer.

16. Immunofluorescence

ARPE-19 cells were seeded on glass coverslips after 24 h of treatment were washed with PBS and were fixed by 4% paraformaldehyde (PFA) for 30 min at 4°C. Cells were permeabilized wit 0,01% Triton X-100 (Sigma-Aldrich, Missouri, USA) for 20 min at room temperature. To block nonspecific binding sites 1%BSA-PBS solution was added for 1 h. Primary antibody ZO-1 (Thermo Fisher Scientific, USA) was added at a 1:200 concentration for 1 h at room temperature. After 2 PBS washes the secondary antibody Alexa flour 488 donkey anti-mouse (Invitrogen, Thermo Fisher Scientific, USA) and membrane marker rhodamine phalloidin (Life Technologies, Thermo Fisher Scientific, USA) were added for 1 h at a concentration of 1:200. Finally, the samples were stained with DAPI (Sigma-Aldrich, Missouri, USA) 5 min at a concentration of 1:1000. Cells were mounted in Prolong Gold antifade reagent (Invitrogen, Thermo Fisher Scientific, USA). The images were taken using the confocal microscopy Leica TCS SP2 LSM Zeiss 710 (Wentzler, Germany) with the assistance of Katharina Lueck from the University Collage of London Institute of Ophthalmology.

17. Statistical Analysis

Statistical analysis was performed by using Prism 5.04 software (GraphPad, CA, USA) using 2-way ANOVA and Student's t-test. Statistically significant differences were set at $p < 0.05$.

RESULTS

Results

1. Effect of H_2O_2 in ARPE-19 cells

1.1. H_2O_2-induced oxidative stress in ARPE-19 cells

ARPE-19 cells were exposed for 24 h to different concentrations of H_2O_2 (200 μM, 400 μM, 600 μM and 800 μM) in order to check the proper H_2O_2 concentration on ARPE-19 cells. ARPE-19 cells significantly increased intracellular ROS levels after H_2O_2 exposure: 600 μM H_2O_2 (106 ± 1.69); (p_value < 0.05) and 800 μM H_2O_2 (103.1 ± 0.99); (p_value < 0.05), compare to control group. Nevertheless, 400 μM H_2O_2 (105.0 ± 3.09); (p_value < 0.14), or lower, did not significantly increase ROS levels compared to control (Figure 12).

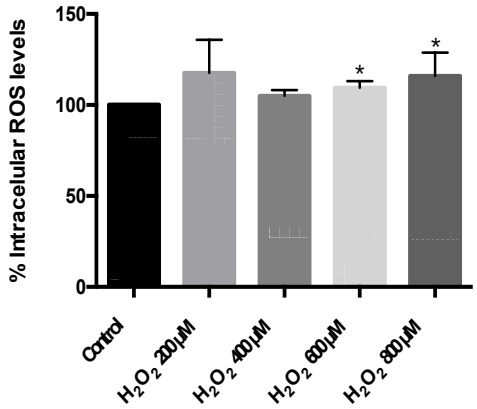

Figure 12. H_2O_2 induces oxidative stress in ARPE-19 cells. Superoxide anions were measured by DHE after 24 h of H_2O_2 treatment. Values are expressed as mean ± SEM (n= 3). The p_value was calculate by T-test and statistically significant differences were set at *p<0.05.

1.2. H_2O_2 reduced ARPE-19 viability

In order to assess whether H_2O_2-induced ROS affected ARPE-19 cells viability, XTT assay was performed. Cell viability was significantly decreased after 800 µM H_2O_2 exposure (95.45 ± 0.99); (p_value < 0.01) in contrast to lower H_2O_2 concentrations (Figure 13 A). Moreover, 800 µM H_2O_2 exposure also increased early apoptosis (3,038 ± 0,17); (p_value < 0.05) compared to control (1.71 ± 0.48) (Figure 13 B and C). Besides, a positive correlation (R^2=0,72) between cell death and ROS production was found (Figure 13 D). Taking in to account the sub-lethal effect of 600 µM H_2O_2 treatment for 24 h, this concentration was used in ARPE-19 cells for the following experiments.

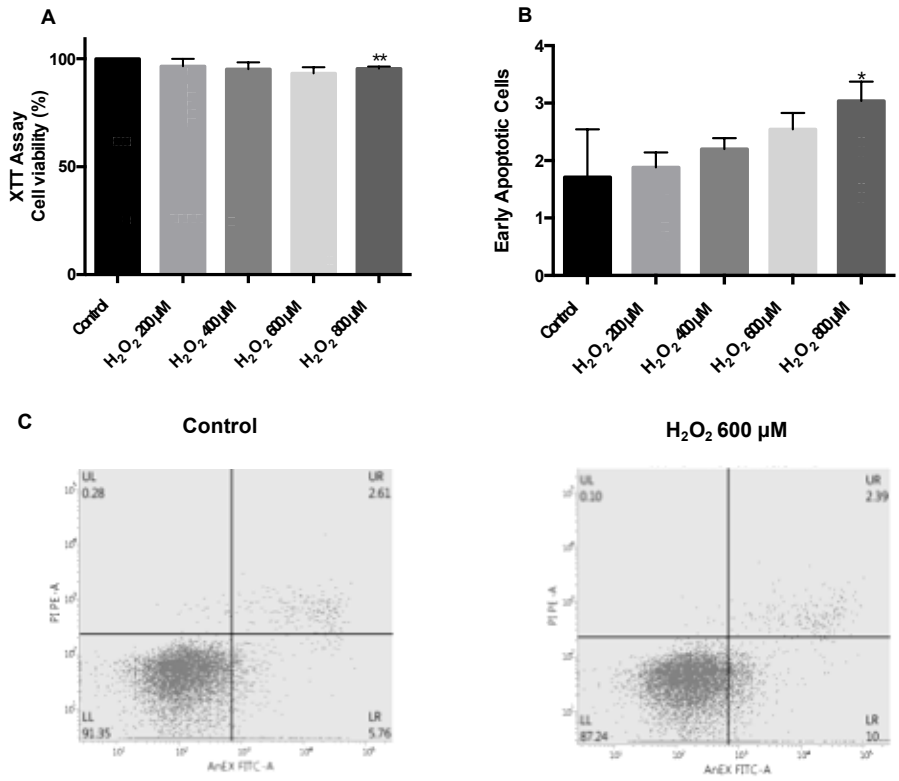

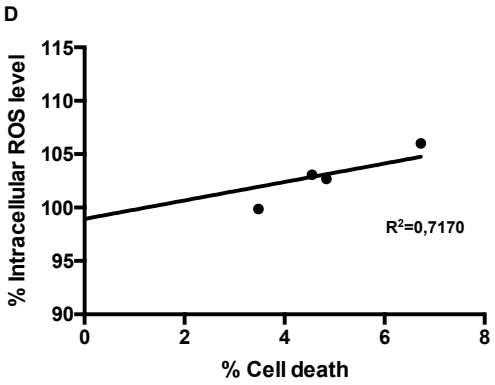

Figure 13.Effect of oxidative stress in ARPE-19 cells. ARPE-19 cell viability after 24 h of H_2O_2 exposure measured by XTT are showed as percentage to control (**A**). Early apoptotic cells measured using Annexin V-IP (**B**). Flow cytometry representative histograms: alive cells (annexin V^-, PI^-), early apoptosis (annexin V^+, PI^-), and necrotic cells (annexin V^*, IP^+) (**C**). Correlation between intracellular ROS production and cell death after 24 h of H_2O_2 exposure (**D**). Values are expressed as mean ± SEM (n= 3). The p_value was calculate by T-test and statistically significant differences were set at *p<0.05 and **p<0.01.

To analyse the effect of 600 µM H_2O_2 exposure, cell morphology was observed. The ARPE-19 cell morphology was not altered after 24 h of 600 µM H_2O_2 treatment (Figure 14 A). On the same way and to check the resistance to H_2O_2 the transepithelial resistance (*Ohm/cm*^{2}) on polarized ARPE-19 cells was measured. After 24 h of 600 µM H_2O_2 treatment, transepithelial resistance was not affected by 600 µM H_2O_2 treatment (Figure 14 B).

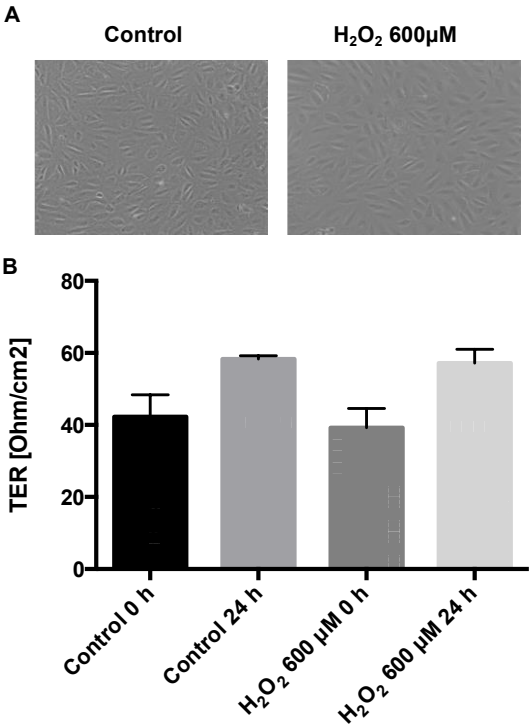

Figure 14. Effect of H_2O_2 600 µM in ARPE-19 cells. Morphology of ARPE-19 cells (**A**). Transepithelial resistance representation [Ohm/cm^2] (**B**). Values are expressed as mean ± SEM (n=3).

1.3. H_2O_2 increased sEVs release in ARPE-19

Matching with previous results on cell viability and ROS production, 600 µM H_2O_2 was used to stress ARPE-19 cells without leading cell death. The number and size of EVs were studied using a nanoparticle tracking system (NanoSight) (Figure 15 A). After 24 h of 600 µM H_2O_2 exposure, ARPE-19 cells increased 40% the number of EVs released to the medium compare to control cells (Figure 15). Besides, EVs were observed under transmission electron microscopy (TEM), which showed that, according to size and morphology, most of

the EVs observed can be classified as small extracellular vesicles (sEVs) (30-150 nm) (Figure 15 B and C).

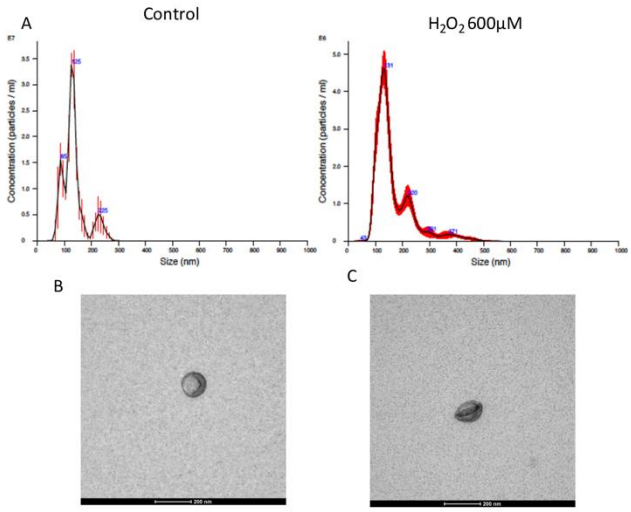

Figure 15. Characterization of sEVs released by ARPE-19 cells. Size-distribution analysis and sEVs number were performed by Nanoparticle Tracking Analysis (**A**). EVs released by ARPE-19 cells control (**B**) and ARPE-19 cells treated by 600 µM H_2O_2 (**C**) were detected by electron microscopy.

2. miRNA expression in ARPE-19 cells and sEVs

The aim of this study was the identification of the miRNA-expression profile after H_2O_2 challenge in ARPE-19 cells. Both, RNA from ARPE-19 cells and their sEVs released to the media, were isolated in order to evaluate the miRNA profile after H_2O_2 exposure. A total number of 384 miRNAs were analysed by the microarray as previously mentioned in material and methods section. The same analysis was performed for ARPE-19 cells and sEVs.

2.1. miRNA expression in ARPE-19 cells (Cell miRNA)

After the microarray analysis and normalization, 306 out of 384 Cell miRNAs were detected by the microarray. After non-supervised hierarchical clustering of expressed miRNAs two different miRNA clusters could be set, related to the physiological state of ARPE-19 cells [Control vs 600 µM H_2O_2 exposure] (Figure 16). As shown in the Heatmap (Figure 16) there was a significant miRNA repression after 600 µM H_2O_2 treatment when compared with control ARPE-19 cells. In addition, the biological replicates correspond to the same cluster and present a similar miRNA expression profile. Not all the detected miRNAs were significantly different expressed. The statistical analysis showed that from the 306 miRNAs detected, 59 were significantly different expressed between control and H_2O_2 treatment (p_value<0.05) (Table 3).

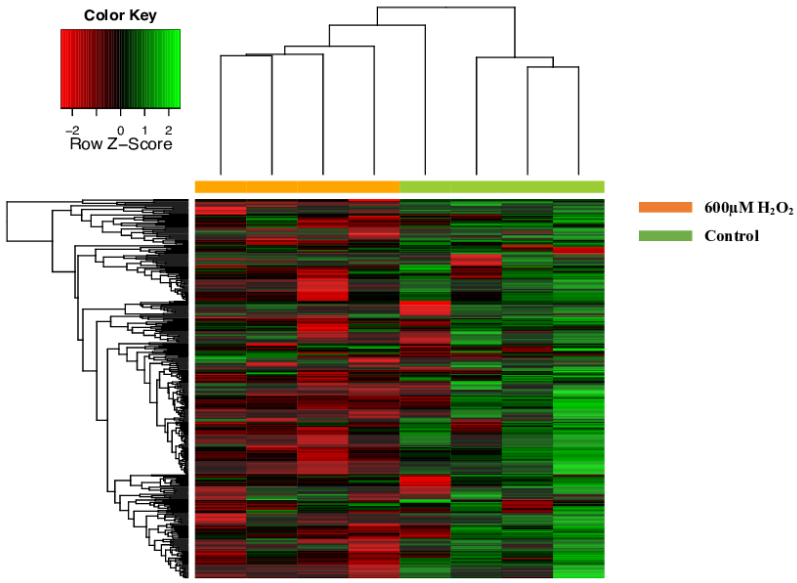

Figure 16. Heatmap of miRNA expression profile from array assay of ARPE-19 cells. After 24 h of 600 µM H_2O_2, the miRNA expression profile was analyzed, using an array for microRNA (System Biosciences, Palo Alto, CA). Hierarchical unsupervised clustering was performed with the expressed miRNAs in ARPE-19 cells. Each column represents an individual cell sample. Orange columns are ARPE-19 cells treat with 600 µM H_2O_2 and green columns ARPE-19 cell controls. Control sample

(n=4) and 600 μM H_2O_2 sample (n=4). The over-expressed miRNAs are shown in green and under-expressed miRNAs in red. Expression values are calculated with respect to the reference genes of the array assay.

Table 3. miRNAs significantly regulated in ARPE-19 cells under oxidative stress. The miRNAs are ranged according to the p_value.

	Statistic	Dm	P_value	Control Mean	Treated mean
miR-139-3p	6,47	0,71	6,49E-04	1,01	0,30
miR-192	5,68	0,74	1,29E-03	1,01	0,27
miR-22	4,09	0,73	6,46E-03	1,04	0,30
miR-15b	4,07	0,73	6,57E-03	1,04	0,31
let-7c	4,06	0,82	6,61E-03	1,06	0,24
let-7b	4,05	0,77	6,70E-03	1,05	0,28
miR-221	3,99	0,66	7,24E-03	1,03	0,37
miR-323-5p	3,60	0,79	1,13E-02	1,05	0,26
miR-15a	3,60	0,67	1,14E-02	1,04	0,37
miR-18b	3,58	0,70	1,16E-02	1,05	0,35
miR-151-3p	3,56	0,78	1,19E-02	1,08	0,30
miR-183	3,54	0,80	1,21E-02	1,08	0,28
miR-518b	3,45	0,76	1,36E-02	1,07	0,31
miR-10a	3,42	0,78	1,41E-02	1,08	0,30
miR-23a	3,40	0,79	1,46E-02	1,08	0,30
miR-151-5p	3,38	0,85	1,49E-02	1,09	0,24
miR-224	3,35	0,78	1,54E-02	1,09	0,30
miR-186	3,34	0,52	1,56E-02	1,03	0,51
let-7f	3,31	0,86	1,62E-02	1,10	0,24
miR-27a	3,25	0,80	1,74E-02	1,09	0,29
miR-148b	3,22	0,66	1,81E-02	1,05	0,39
miR-25	3,16	0,83	1,96E-02	1,11	0,29
miR-98	3,16	1,00	1,97E-02	1,18	0,18
miR-106a	3,14	0,71	2,02E-02	1,06	0,35
let-7a	3,10	1,06	2,10E-02	1,15	0,10
miR-300	3,09	0,89	2,13E-02	1,10	0,21
miR-18a	3,06	0,70	2,21E-02	1,07	0,37
miR-515-3p	3,05	0,89	2,26E-02	1,11	0,22
miR-27b	2,98	0,78	2,45E-02	1,12	0,34
miR-518d-3p	2,96	1,06	2,54E-02	1,20	0,15

	Statistic	Dm	P_value	Control Mean	Treated mean
miR-371-5p	2,92	0,95	2,67E-02	1,18	0,23
miR-92a	2,92	0,70	2,67E-02	1,06	0,37
miR-361-5p	2,92	0,79	2,67E-02	1,10	0,32
miR-521	2,87	1,35	2,85E-02	1,46	0,11
miR-30c	2,85	0,78	2,93E-02	1,10	0,32
miR-335	2,82	0,85	3,05E-02	1,16	0,31
miR-28-5p	2,79	0,94	3,17E-02	1,14	0,21
let-7g	2,78	0,84	3,20E-02	1,09	0,25
miR-29c	2,78	0,82	3,22E-02	1,10	0,28
miR-488	2,76	0,98	3,27E-02	1,16	0,18
miR-532-3p	2,75	0,86	3,32E-02	1,10	0,24
miR-338-5p	2,75	1,11	3,33E-02	1,26	0,15
miR-125a-5p	2,74	0,82	3,35E-02	1,11	0,29
miR-499-3p	2,74	0,72	3,38E-02	1,09	0,37
miR-29a	2,71	0,72	3,51E-02	1,07	0,35
miR-20b	2,70	0,81	3,54E-02	1,10	0,28
miR-148a	2,67	0,90	3,73E-02	1,17	0,27
miR-548b-5p	2,64	1,91	3,85E-02	2,08	0,18
miR-218	2,61	1,00	4,03E-02	1,23	0,23
miR-505	2,60	0,65	4,09E-02	1,10	0,45
miR-205	2,55	2,29	4,35E-02	2,62	0,33
miR-17	2,54	0,78	4,39E-02	1,10	0,32
miR-324-5p	2,53	0,73	4,49E-02	1,15	0,42
miR-320c	2,52	0,82	4,52E-02	1,13	0,31
miR-99a	2,51	0,84	4,59E-02	1,16	0,32
miR-302c	2,51	2,55	4,60E-02	2,70	0,14
miR-30b	2,50	0,85	4,62E-02	1,17	0,32
miR-28-3p	2,49	0,83	4,72E-02	1,13	0,30
miR-99b	2,45	0,77	4,96E-02	1,12	0,35

After the statistical analysis results were selected by focusing on those miRNAs having a fold change (FC) higher or lower than 1 or -1 respectively. Seven out of 59 Cell miRNAs were significantly under-

expressed in H_2O_2-treated cells compared to control conditions. Let-7a (FC= 1,06), miR-518d-3p (FC= 1,06), miR-521 (FC= 1,35), miR-338-5p (FC= 1,11), miR-548b-5p (FC= 1,91), miR-205-5p (FC= 2,29) and miR-302c-3p (FC= 2,55) (Table 4). However, from the analysed miRNAs there were not any miRNA over-expressed in H_2O_2-treated cells. The significant miRNAs are shown in the volcanoplot (Figure 17). It is noteworthy to underline that miR-205-5p and miR-302c-3p presented a dramatic decrease in treated cells when compared to others (FC>2).

Table 4. miRNAs significantly regulated in ARPE-19 cells. Cell miRNAs up-regulated in ARPE-19 cells with FC > 1.

miRNA name	FC	P_value	Control mean	Treated mean
Let-7a	1,06	0,02	1,15	0,10
miR-518d-3p	1,06	0,03	1,20	0,15
miR-521	1,35	0,03	1,46	0,32
miR-338-5p	1,11	0,03	1,26	0,15
miR-548b-5p	1,91	0,04	2,08	0,18
miR-205	2,29	0,04	2,62	0,33
miR-302c	2,55	0,05	2,70	0,15

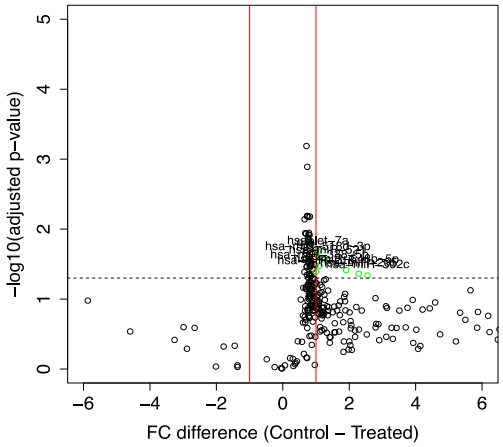

Figure 17. miRNAs significantly regulated in ARPE-19 cells. Volcano plot of Cell miRNA expression profile. The X axis represent the miRNA expression level and the Y axis represents the p_value (T-student Test). The red lines indicate FC ± 1 and p_value < 0.05.

2.2. miRNA expression in ARPE-19 sEVs (SEV miRNA)

The same proceeding was performed for miRNAs on sEVs released to the media. Two clusters were found related to their origin [Control vs 600 µM H_2O_2 treated ARPE-19 cells media] after non-supervised hierarchical clustering of the expressed miRNAs (Figure 18). As above-mentioned, ARPE-19 cells released a significantly higher number of sEVs after 600µM H_2O_2 exposure than control cells. In contrast, these H_2O_2 induced sEVs showed a significant lower miRNA expression compared to control. More concretely, 218 out of 384 sEV miRNAs were detected by the array, 88 less than Cell miRNAs, that its due to its lower cargo/transport capacity. However, only 2 out of 218 sEV miRNAs were significantly lower in sEVs released from treated cells (p<0.05) hsa-miR-302a-3p (FC=1.16) and hsa-miR-122-5p (FC=1.58) than in control sEVs (Table 5 and Figure 19).

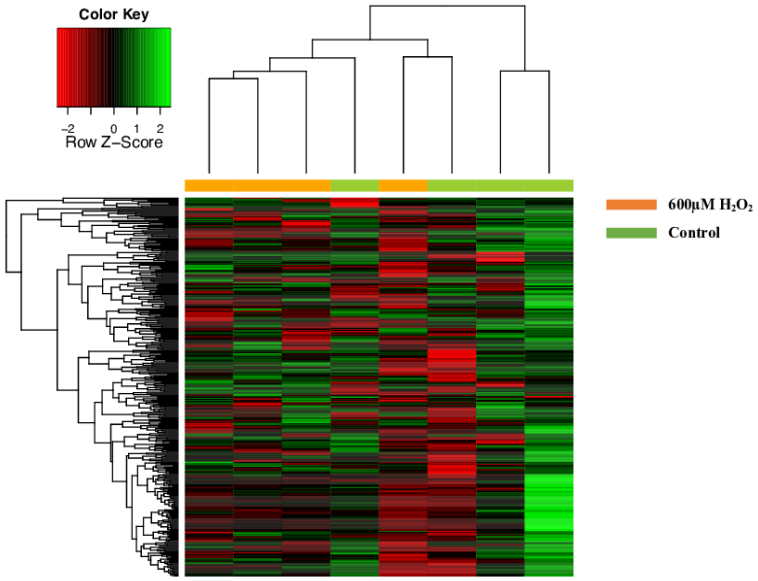

Figure 18. Heatmap of miRNA expression profile from array assay of the sEVs released by ARPE-19 cells. After 24h of 600µM H_2O_2, the miRNA expression profile of sEVs was analyzed, using an array of miRNA. Hierarchical unsupervised clustering was performed with the expressed miRNAs in ARPE-19-released sEVs. Each column represents an individual cell sample. Orange columns are sEVs released by ARPE-19 cells treated with 600µM H_2O_2 and green columns are sEVs released by ARPE-19 control cells. Control samples (n=4) and 600µM H_2O_2 samples (n=4). Over-expressed miRNAS (green) and under-expressed miRNAs (red). The expression values are calculated with respect to the reference genes of the array.

Table 5. miRNAs significantly regulated in sEVs from ARPE-19 cells. sEVs miRNAs up-regulated in ARPE-19 cells with fold change (FC) > 1.

miRNA name	FC	P_value	Control mean	Trate mean
miR-302a-3p	1,16	0,02	1,25	0,09
miR-122-5p	1,58	0,05	1,58	0,01

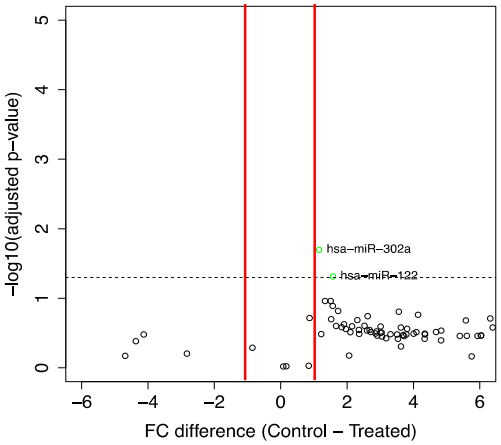

Figure 19. miRNAs significantly regulated in sEVs from ARPE-19 cells. Volcano plot of sEVs miRNA expression profile. The X axis represent the miRNA expression level and the Y axis represents the p_value (T-student Test). The red lines indicate FC ± 1 and p_value < 0.05.

3. Pathway enrichment analysis of miRNA regulated by oxidative stress

Subsequently, the role of the seven under-expressed miRNAs in treated ARPE-19 cells and two under-expressed miRNAs in sEVs from treated cells, were analysed. Two independents ¨*in silico*¨ analysis, one for Cell miRNAs and one for sEVs miRNAs were performed, in order to determine potential biological processes related to OS induction.

The KEGG pathway analysis from the Cell miRNAs identified in the study [Let-7a, miR-518d-3p, miR-521, miR-338-5p, miR-548b-5p, miR-205-5p, and miR-302c-3p] shows 50 deregulated pathways (p_value<0.05). Among the most relevant (p_value<0.001), 5 up to 7 miRNAs are involved in the regulation of cell cycle and adherent junction. 6 up to 7 miRNAS related to both p53 signalling pathway and HIF-1 signalling pathways (Figure 20 and Table 6). Furthermore, it is

remarkable the implication of 7 Cell miRNAs in Thyroid hormone signalling pathway regulation, bladder cancer and cancer related pathways (Figure 20 and Table 6). The full list of deregulated pathways is listed in the Annex I.

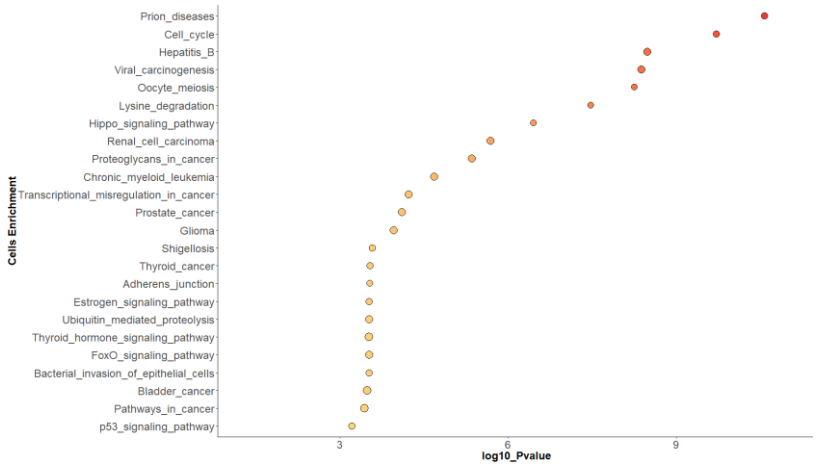

Figure 20. Cell miRNA related pathways after H_2O_2 exposure in ARPE-19 cells. Graphic representation of cellular pathways (Y) and $\log_{10}$ p_value (X), circle size represents the number of involved miRNAs up to 7 deregulated miRNAs.

Table 6. Cell miRNA KEGG pathways deregulated in ARPE-19 cells after H_2O_2 exposure. Enrichment analysis performed by DIANA mirPATH. KEGG pathways with a p_value< 0.001.

KEGG Pathway	FDR	Number of miRNAs	Putative target genes
Prion diseases	$2{,}63x10^{-11}$	5	EGR1 HSPAS FYN PRNP LAMC1 MAP2K1 MAPK1
Cell cycle	$1{,}92x10^{-10}$	5	ESPL1 CCNB2 RBL2 PCNA E2F1 SMC1A YWHAH CCNB1 CDK4 YWHAE CCNA2 ORC2 MCM6 YWHAG CDK2 CCND2 ORC1 DBF4 CDKN1B CUL1 YWHAB WEE1 CDK1 CDK6 MCM7 SKP1 TP53 ATM CCND1 CCNE2 E2F5 SKP2 E2F3 MYC RB1 YWHAZ HDAC2 CDC20 MAD2L1 CDC23 ANAPC5 EP300 CDC27 RBX1 CDKN1A PRKDC E2F4 ANAPC13 CREBBP RAD21 MDM2 ABL1 MCM3 CDC25A
Hepatitis	$3{,}29x10^{-9}$	6	FOS PCNA STAT3 ATP6AP1 E2F1 TGFBR1 NFKB1 CDK4 ATF2 NRAS CCNA2 ATF6B CDK2 CHUK BCL2 CDKN1B YWHAB MAP3K1 TRL4 KRAS CDK6 DDX3X TP53 HSPG2 FADD CREB1 APAF1 MAVS CASP3 CCND1 CCNE2 E2F3 MAPK8 AKT1 MYC IRF3 NFKBIA DDB1 PIK3R1 RB1 YWHAZ TBK1 SRC FAS HRAS EP300 CREB3L2 CREB3L1 CDKN1A MAP2K1 MAP2K4 PTEN NFATC3 MAPK1 CREBBP JAK1 ATK4
Viral carcinogenesis	$4{,}22x10^{-9}$	6	RBL2 STAT3 NFKB1 YWHAH CDK4 ATF2 NRAS IRF9 YWHAE HDAC3 CCNA2 GTF2H1 ATF6B YWHAG CDK2 CCND2 PXN CDKN1B YWHAG CDK2 CCND2 PXN CDKN1B YWHAB CDK1 GTF2B KRAS CDK6

KEGG Pathway	FDR	Number of miRNAs	Putative target genes
			DDX3X TP53 HNRNPK CREB1 GSN PMAIP1 CASP3 CCND1 CCNE2 SKP2 CCR5 IRF3 NFKBIA B_1DDB1 HIST1H2BG PIK3R1 RB1 GTF2A2 YWHAZ HDAC2 KAT2A RAC1 SRC CDC20 RBPJ HIST1H2BL HRAS EP300 CREB3L2 CREB3L1 IL6ST SNW1 CDKN1A MAPK1 SRF CREBBP TBPL1 JAK1 MDM2 ATF4 SCRIB H2BFS HIST1H4D
Oocyte meiosis	$5{,}53x10^{-9}$	4	SLK ESPL1 PPP1CA CAMK2D CCNB2 SMC1A YWHAH CCNB1 YWHAE BTRC CALM3 CALM1 PPP2CA CPEB4 YWHAG CDK2 CUL1 PPP2R5D YWHAB CDK1 IGF1R SKP1 PPP2R5A CCNE2 CPEB2 YWHAZ CDC20 MAD2L1 CDC23 ANAPC5 RPS6KA3 CDC27 RBX1 AURKA SGOL1 MAPK2K1 ANAPC13 ITPR3 MAPK1 ITPR2 FBXW11 ADCY9 PPP1CB RPS6KA2
Lysine degradation	$3{,}32x10^{-8}$	4	WHSC1L1 ALDH7A1 SETD7 SERC1B PLOD2 NSD1 ASH1L KMT2D SUV42OH1 DOT1L SUV420H2 KMT2A ALDH9A1 SUV39H2 KMT2E SETD1A EHMT1 KMT2B
Hippo signaling pathway	$3{,}52x10^{-7}$	4	PPP1CA ACTB FZD5 TGFBR1 YWHAH YAP1 YWHAE BTRC PPP2CA TCF7L2 NF2 YWHAG CCND2 BMP5 ACTG1 GLI2 AREG FZD6 SNAI2 AXIN1 MOB1B YWHAB AMOT BMP6 FZD3 LIMD1 MPP5 DLG4 CCND1 CTNNA1 MYC LLGL1 ID1 FZD2 TEAD1 YWHAZ BMP2 TEAD4 PARD3 SMAD7 MOB1A LATS1 SOX2 LATS2 FBXW11 TGFBR2 WNT9A BMP4 BMPR2 CTGF PPP1CB BIRC2 SCRIB
Renal cell carcinoma	$2{,}09x10^{-6}$	6	BRAF MET SOS2 NRAS CRKL CRK CUL2 PAK2 ARNT KRAS VHL ARNT2 AKT1 PDGFB PIK3R1 RAC1 EGLN2 HRAS EP300 GAB1 RBX1 MAP2K1 SLC2A1 VEGFA MAPK1 CREBBP EGLN1 FLCN
Proteoglycans in cancer	$4{,}50x10^{-6}$	6	ESR1 PPP1CA CAMK2D BRAF ACTB STAT3 FZD5 PDCD4 MET EZR ROCK1 SOS2 CBL NRAS THBS1 CAV1 ARHGEF12 ACTG1 PXN FRS2 FZD6 RDX IGF1R TLR4 ERBB3 KRAS FZD3 MSN RPS6KB2 TP53 HSPG2 CTTN VAV2 PTK2 ITGAV SLC9A1 PPP1R12A DROSHA PLCG1 CASP3 PTPN6 CCND1 AKT1 MYC IGF2 FLNA FZD2 PIK3R1 RAC1 SRC FAS HRAS GAB1 HOXD10 FN1 CDKN1A MAPK2K1 ITPR3 VEGFA FGFR1 MAPK1 ITPR2 MDM2 WNT9A PPP1CB
Chronic myeloid leukemia	$2{,}09x10^{-5}$	6	BRAF E2F1 TGFBR1 NFKB1 SOS2 CDK4 CBL NRAS CRKL CRK RUNX1 CHUK CDKN1B KRAS CDK6 TP53 CCND1 E2F3 AKT1 MYC NFKBIA PIK3R1 RB1 HDAC2 HRAS CDKN1A MAPK2K1 MAPK1 TGFBR2 MDM2 ABL1
Transcriptional misregulation in cancer	$6{,}02x10^{-5}$	6	BMI1 CCNT2 TMPRSS2 MEN1 NFKB1 MET ELK4 RUNX1 HMGA2 AFF1 DUSP6 CCND2 HOXA9 PBX1 LDB1 CDKN1B IGF1R RUNX2 CCR7 TP53 UTY PTK2 ATM RUNX1T1 ARNT2 PBX3 CDK9 MYC KLF3 BMP2K NCOR1 LYL1 JMJD1C HDAC2 H3F3A KDM6A SP1 MAX DOT1L H3F3B SPINT1 KMT2A MYCN CDKN1A BIRC3 EWSR1 FOXO1 JUP TGFBR2 MDM2 SIN3A PAX3
Prostate cancer	$7{,}86x10^{-5}$	6	BRAF E2F1 NFKB1 SOS2 NRAS TCF7L2 CDK2 CHUK BCL2 CDKN1B IGF1R KRAS TP53 CREB1 CCND1 CCNE2 E2F3 AKT1 PDGFB NFKBIA PIK3R1 RB1 HSP90B1 HRAS EP300 NKX3-1 CREB3L2 CREB3L1 CDKN1A MAP2K1 PTEN FGFR1 FOCO1 MAPK1 CREBBP MDM2 ATF4
Glioma	$1x10^{-4}$	6	CAMK2D BRAF E2F1 SOS2 CDK4 NRAS CALM3 CALM1 IGF1R KRAS CDK6 TP53 PLCG1 CCND1 E2F3 AKT1 PDGFB PIK3R1 RB1 HRAS CDKN1A MAP2K1 PTEN MAPK1 MDM2
Shigellosis	$3x10^{-4}$	5	PFN1 ACTB ARPC5L NFKB1 ROCK1 WASL RIPK2 CRKL BTRC CRK ACTG1 CHUK ELMO2 NOD1 VCL CTTN PFN2 MAPK8 DIAPH1 ARPC2 WASF2 NFKBIA RAC1 SRC MAPK1 FBXW11 ABL1 RHOG
Adherent junction	$3x10^{-4}$	4	ACTB CSNK2A2 TGFBR1 MET WASL TCF7L2 ACTG1 SNAI2 PTPN1 IGF1R VCL TJP1 FYN NLK PTPN6 CTNNA1 WASF2 CSNK2A1 FARP2 RAC1 INSR SRC SSX2IP EP300 PARD3 YES1 PTPRB FGFR1 MAPK1 MAP3K7 CREBBP TGFBR2
Thyroid cancer	$3x10^{-4}$	5	BRAF NRAS TPR TCF7L2 KRAS TP53 CCND1 MYC HRAS MAP2K1 MAPK1 TFG NCOA4
Estrogen signaling pathway	$3x10^{-4}$	5	ESR1 HSPA2 FOS SOS2 ATF2 NRAS CALM3 CALM1 ATF6B KRAS PLCB3 CREB1 AKT1 PIK3R1 HSP90B1 SRC HSPA8 SP1 HRAS GNAQ CREB3L2 CREB3L1 MAP2K1 ITPR3 MAPK1 ITPR2 ADCY9 PLCB4 ATF4

KEGG Pathway	FDR	Number of miRNAs	Putative target genes
Bacterial invasion of epithelial cells	$3x10^{-4}$	5	ACTB ARPC5L MET WASL CBL CRKL SEPT8 CRK CAV1 SEPT11 ACTG1 PXN ELMO2 CLTC VCL CTTN PTK2 CTNNA1 ARPC2 WASF2 PIK3R1 RAC1 SRC GAB1 FN1 SEPT2 SEPT9 RHOG
FoxO signaling pathway	$3x10^{-4}$	6	IRS2 BRAF CCNB2 RBL2 STAT3 TGFBR1 CCNB1 SOS2 NRAS STK4 SETD7 KLF2 CDK2 CCND2 CHUK CDKN1B IGF1R TNFSF10 KRAS HOMER2 ATM NLK CCD1 S1PR1 SKP2 MAPK8 AKT1 PRKAG1 PLK2 GABARAPL1 PIK3R1 INSR PRKAA1 PRMT1 HRAS PRKAB2 EP300 SOD2 CDKN1A MAP2K1 ATG12 PTEN SGK3 FOXO1 MAPK1 CREBBP CCNG2 TGFBR2 MDM2 BCL2L11
Ubiquitin mediated proteolysis	$3x10^{-4}$	6	UBE2Q2 UBE3B CBL BTRC TRIM37 CUL2 NEDD4L HUWE1 CUL1 UBE4A MAP3K1 UBE2J1 UBE2I HERC1 MID1 VHL SKP1 CDC34 TRIP12 SOCS3 SKP2 SOCS1 DDB1 UBE2K CDC20 CDC23 ANAPC5 PIAS4 UBE2D3 UBE2G2 CDC27 RBX1 UBE2G1 BIRC3 CUL3 UBE2W ANAPC13 FBXW11 RHOBTB2 UBE4B TRIM32 PIAS1 MDM2 UBE2J2 BURC2 UBOX5
Thyroid hormone signaling pathway	$3x10^{-4}$	7	ESR1 ACTB MED13L NRAS HDAC3 MED14 MED12 ACTG1 MED13 SLC16A10 THRA KRAS NOTCH4 NCOA3 TP53 PLCB3 ITGAV SLC9A1 PLCG1 CCND1 AKT1 MYC NCOR1 NCOA2 PIK3R1 HDAC2 KAT2A SRC HRAS EP300 MAP2K1 SLC2A1 PFKFB2 ATP2A2 ATP1A1 FOXO1 MAPK1 CREBBP MDM2 PLCB4 BMP4 SIN3A
Bladder cancer	$3x10^{-4}$	7	BRAF E2F1 CDK4 NRAS RPS6KA5 TP53 CCND1 E2F3 MYC DAPK1 RB1 HRAS CDKN1A MAP2K1 MDM2
Pathways in cancer	$4x10^{-4}$	7	BRAF FOS STAT3 FZD5 E2F1 TGFBR1 NFKB1 MET ROCK1 SOS2 CDK4 CBL NRAS CRKL STK4 BID CRK RUNX1 RAD51 CUL2 TPR TCF7L2 ARHGEF12 CDK2 GLI2 BDKRB2 ARNT FZD6 CHUK BCL2 CDKN1B AXIN1 IGF1R GNB1 KRAS CDK6 FZD3 VHL MLH1 TP53 FADD PLCB3 PTK2 LAMC3 ITGAV RUNC1T1 ARNT2 PLCG1 CASP3 CCND1 LPAR1 MSH6 CTNNA1 CCNE2 SKP2 COL4A2 E2F3 MAPK8 AKT1 F2R MYC DAPK1 PDGFB NFKBIA KIT PTGS2 FZD2 PIK3R1 RB1 HSP90B1 HDAC2 RAC1 BMP2 EGLN2 MAX FAS HRAS LAMC1 EP300 GNAQ NKX3-1 RBX1 FN1 CDKN1A MAP2K1 BIRC3 SLC2A1 VEGFA PTEN FGFR1 FOXO1 MAPK1 CREBBP GNG5 ADCY9 JUP TGFBR2 TFG JAK1 MDM2 WNT9A ABL1 PLCB4 BMP4 EGLN1 COL4A1 BIRC2 NCOA4
p53 signaling pathway	$6x10^{-4}$	5	CCNG1 ZMAT3 CCNB2 CCNB2 CDK4 BID THBS1 CDK2 CCND2 CDK1 CDK6 TP53 APAF1 ATM PMAIP1 CASP3 CCND1 CCNE2 SHISA5 SESN1 SESN2 TNFRSF10B MDM4 FAS CDKN1A RRM2 PTEN CCNG2 MDM2

When performed the *"in silico"* analysis on sEVs miRNAs [miR-302a-3p and miR-122-5p] 25 KEGG pathways regulated by these miRNAs were showed ($p_value<0.05$). Among them, Proteoglycans in cancer, Chronic myeloid leukaemia, TGF-beta signalling pathway and Transcriptional misregulation in cancer were regulated by the 2 sEVs miRNAs (Figure 21 and Table 7). The complete list of deregulated pathways by these miRNAs is listed in the Annex II.

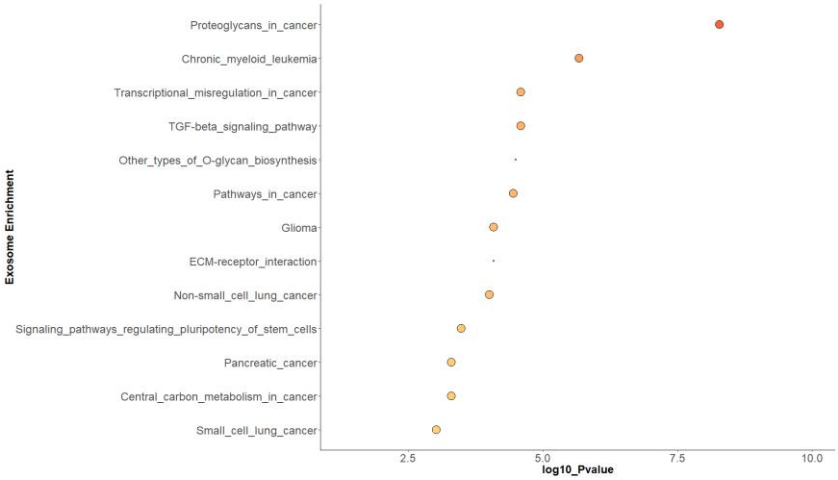

Figure 21. sEV miRNA related pathways after H_2O_2 exposure in ARPE-19 cells. Graphic representation of cellular pathways (Y) and $\log_{10}$ p_value (X), circle size represents the number of involved miRNAs up to 2 deregulated miRNAs.

Table 7. sEVs miRNA KEGG pathways deregulated in ARPE-19 cells after H_2O_2 exposure. Enrichment analysis performed by DIANA mirPATH. KEGG pathways with a p_value < 0.001.

KEGG pathway	FDR	Number of miRNAs	Putative target genes
Proteoglycans in cancer	$5{,}23 \times 10^{-9}$	2	ACTB FZD5 ITGB1 EZR SOS2 SMAD2 CBL ARHGEF12 ROCK2 FZD6 IQGAP1 RAF1 IGF1R EGFR FZD3 PAK1 TP53 CTTN SLC9A1 DCN PLCG1 PIK3CD CCND1 AKT1 MYC FLNB PIK3CG PTPN11 RAC1 FZD1 ANK1 PDPK1 VMP1 MTOR FGFR1 MAPK1 MDM2 RPS6KB1 CD44 PRKACB PPP1CB
Chronic myeloid leukemia	$2{,}14 \times 10^{-6}$	2	E2F1 TGFBR1 SOS2 CDK4 CBL E2F2 RUNX1 CTBP1 RAF1 CDKN1B TP53 PIK3CD CCND1 SMAD4 E2F3 AKT1 MYC NFKBIA PIK3CG PTPN11 MEDOM MAPK1 TGFBR2 MDM2
TGF-beta signaling pathway	$2{,}58 \times 10^{-5}$	2	TGFBR1 ID2 SMAD2 NODAL SMURF2 BMPR1B LEFTY1 ID4 ACVR2B ZFYVE16 DCN SMAD4 MYC RBL1 LTBP1 E2F4 MAPK1 SMAD1 TGFBR2 RPS6KB1
Transcriptional misregulation in cancer	$2{,}58 \times 10^{-5}$	2	CCNT2 NFKBIZ ID2 FUS ETV6 ELK4 RUNX1 AFF1 CCND2 CDKN1B MLLT3 IGF1R RUNX2 TP53 ATM MYC KLF3 PLAT FLT1 JMJD1C ETV1 BCL6 DOT1L PPARG KMT2A BCL2A1 EWSR1 SMAD1 TGFBR2 MDM2 TAF15
Other types of O-glycan biosynthesis	$3{,}19 \times 10^{-5}$	1	ST3GAL3 OGT POMT2 MFNG GXYLT1 B3GAT2 B4GALT1 POFUT1
Pathways in cancer	$3{,}55 \times 10^{-5}$	2	FZD5 E2F1 TGFBR1 ITGB1 SOS2 CDK4 LAMB1 SMAD2 CBL E2F2 CXCR4 STK4 GNAS LAMA5 RUNX1 TPR CTBP1 ARHGEF12 BAX ROCK2 FZD6 RAF1 CDKN1B TRAF4 PLD1 LPAR2 BRCA2 IGF1R EGFR APPL1 FZD3 VHL TP53 LAMC3 PLCG1 PIK3CD CCND1 SMAD4 MSH6 COL4A2 E2F3 AKT1 PGF F2R MYC NFKBIA KIT COL4A3 PIK3CG HSP90B1 RAC1 FGF18 FZD1 PPARG GNAQ PIAS2 CCNE1 MECOM CYCS MTOR FGFR1 MAPK1 TGFBR2 MDM2 PLCB4 PRKACB

KEGG pathway	FDR	Number of miRNAs	Putative target genes
ECM-receptor interaction	$8{,}31x10^{-5}$	1	ITGB1 ITGB8 LAMB1 PAMA5 COL27A1 AGRN LAMC3 COL4A2 COL5A3 CD44
Glioma	$8{,}31x10^{-5}$	2	E2F1 SOS2 CDK4 E2F2 RAF1 IGF1R EGFR TP53 PLCG1 PIK3CD CCND1 E2F3 AKT1 PIK3CG MTOR MAK1 MDM2
Non-small cell lung cancer	$9{,}84x10^{-5}$	2	E2F1 SOS2 CDK4 E2F2 STK4 RAF1 EGFR TP53 PLCG1 PIK3CD CCND1 E2F3 AKT1 PIK3CG PDPK1 MAPK1
Signaling pathways regulating pluripotency of stem cells	$3x10^{-4}$	2	JARID2 FZD5 ID2 SMAD2 NODAL REST BMPR1B TBX3 FZD6 RAF1 IGF1R ZFHX3 ID4 FZD3 ACVR2B RIF1 PIK3CD JAK2 SMAD4 AKT1 MYC SKIL PIK3CG FZD1 ISL1 FGFR1 SOX2 MAPK1 SMAD1
Pancreatic cancer	$5x10^{-4}$	2	E2F1 TGFBR1 CDK4 SMAD2 E2F2 RAF1 PLD1 BRCA2 EGFR TP53 PIK3CD CCND1 SMAD4 E2F3 AKT1 PIK3CG RAC1 MAPK1 TGFBR2
Central carbon metabolism in cancer	$5x10^{-4}$	2	PKM RAF1 EGFR SLC7A5 SLC16A3 G6PD TP53 PIK3CD AKT1 MYC KIT PIK3CG IDH1 MTOR FGFR1 MAPK1 SLC1A5
Small cell lung cancer	$1x10^{-3}$	2	E2F1 ITGB1 CDK4 LAMB1 E2F2 LAMA5 CDKN1B TRAF4 TP53 LAMC3 PIK3CD CCND1 COL4A2 E2F3 AKT1 MYC NFKBIA COL4A3 PIK3CG PIAS2 CCNE1 CYCS

4. Microarray validation of miRNA expression in ARPE-19 cells.

Because of the nature of the data and the methods used, false positive can be obtained due to the technique used or to the stochastic processes. Therefore, it is mandatory to evaluate the robustness of the data and to confirm that the miRNAs are deregulated by H_2O_2. For this aim, a study of miRNA expression was carried out by using a different technique, the qRT-PCR with independent RNA samples.

Among the miRNAs differentially expressed in ARPE-19 cells, seven out of 59 presented a significant fold-change. We selected three out of seven significant miRNAs (those with the highest differences observed): miR-205-5p, miR-521, and miR-302c-3p. The miR-130b was used as control. After miRNA amplification by qRT-PCR, we analysed the mean Ct for replicates, the standard deviation and calculated the $\Delta\Delta$Ct, as previously described in material and methods

section. The outcome confirmed the results obtained, miR-205-5p (p_value=$5.69x10^{-5}$), miR-521 (p_value=$1.07x10^{-3}$) and miR302c-3p (p_value=$2.28x10^{-5}$) were down-regulated by 600µM H_2O_2 compared to control (Figure 22).

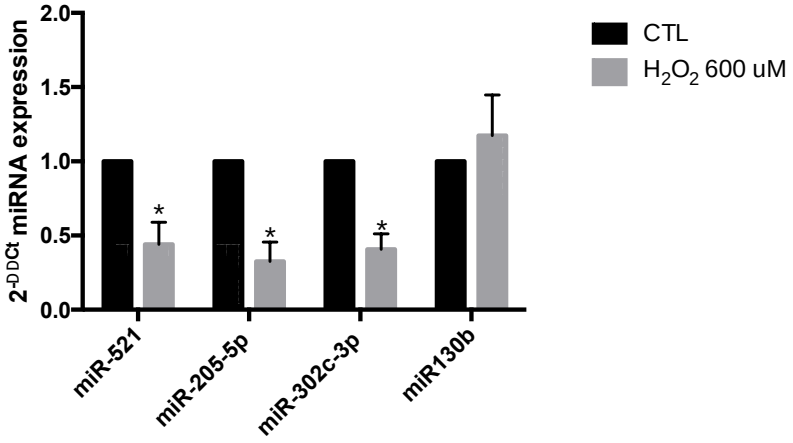

Figure 22. Cell miRNAs validation in ARPE-19 cells. Relative expression of selected Cell miRNAs with FC>1 (control vs 600 µM H_2O_2). miRNA expression was quantified by qRT-PCR and calculate using $2^{-\Delta\Delta Ct}$. Results are expressed as mean ± SEM of n=3-4. The p_value was calculated by T-test and statistically significant differences were set at *p_value<0.05 vs Control.

To assess the Cell miRNA profile reproducibility, the miRNA expression in mature ARPE-19 cells was analysed. The miRNA expression profile in mature ARPE-19 cells replicated the results obtained from non-mature ARPE-19 cells showed above, the miR-205-5p (p_value=0.05), miR-521 (p_value=$4x10^{-4}$) and miR-302c-3p (p_value=0.04) were down-regulated by 600µM H_2O_2 compared to control (Figure 23). These results indicate that non-mature ARPE-19 cells are a suitable model for the miRNA study.

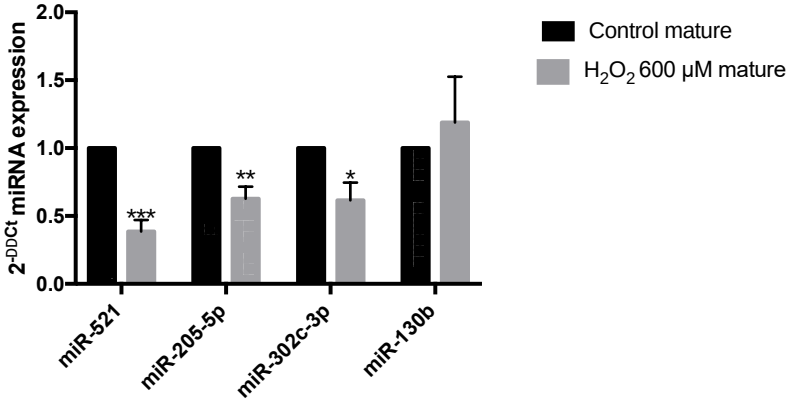

Figure 23. Cell miRNAs in mature ARPE-19 cells. Relative expression of selected Cell miRNAs with FC>1 (control vs 600 µM H_2O_2). miRNA expression was quantified by qRT-PCR and calculate using $2^{-\Delta\Delta Ct}$.. Results are expressed as mean ± SEM of n=3-4. The p_value was calculated by T-test and statistically significant differences were set at *p_value<0.05, **p_value<0.01 and ***p_value<0.001vs Control.

The same qRT-PCR procedure was performed by using the two sEV miRNAs differently expressed: hsa-miR-302a-3p and hsa-miR-122-5p. As expected, miRNAs were under-expressed in sEVs released from H_2O_2-treated ARPE-19 cells compared to sEVs released from control ARPE-19 cells (p_value<$1x10^{-3}$) (Figure 24).

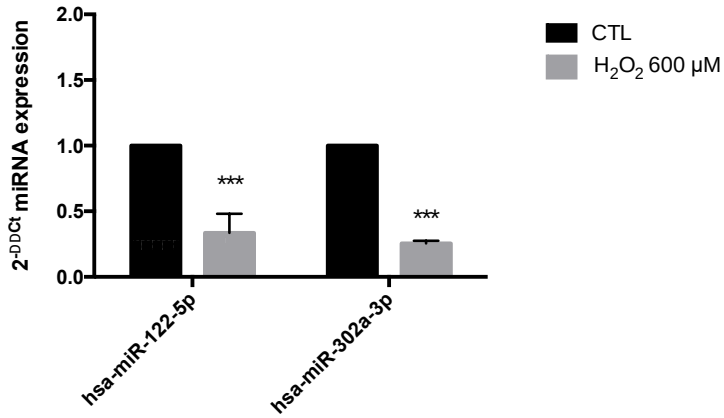

Figure 24. sEVs miRNAs validation in ARPE-19 cells. Relative expression of selected sEVs miRNAs with FC>1 (control vs 600 µM H_2O_2). miRNA expression was

quantified by qRT-PCR and calculate using $2^{-\Delta\Delta Ct}$. Results are expressed as mean ± SEM of n=3-4. The p_value was calculated by Two-way ANOVA and statistically significant differences were set at ***p_value<0.001 vs Control.

5. Potential Targets of miRNAs

In order to identify biological functions of the validated miRNAs and to select their putative targets, TargetScan Human (http://www.targetscan.org/vert_72/) were handled. The outcome on validated Cell miRNAs are listed in Annex III, IV and V and those on sEVs miRNA in Annex VI and VII.

5.1. Potential Target of Cell miRNA

To analyse the biological pathways and networks regulated by the predicted targets of each miRNA were entered into the FUNRICH software (version 3.1.3). The functional enrichment analysis of miR-205-5p showed more than 2,800 biological processes regulated by at least one of the 593 mRNA target of miR-205-5p. The top 20 biological processes regulated by miR-205-5p are shown in Figure 25. The enrichment pathway analysis showed interesting pathways deregulated, 1.3% of genes are involved in positive regulation of endothelial cell migration, 3.5% in angiogenesis and 1.9% in negative regulation of angiogenesis. Moreover, the functional enrichment analysis of miR-521 showed 2,453 biological processes regulated by at least one of the 631 mRNA target of miR-521 (Figure 26). Among the top biological processes were iris morphogenesis regulated by 0.6% of genes, regulation of feeding behaviour by 0.6% and positive regulation of dendritic spine morphogenesis by 0.7% of genes. Besides, the analysis

of miR-302c-3p showed more than 3,020 biological processes regulated by at least one of the 703 mRNA target (Figure 27). The Wnt receptor signalling pathway, calcium modulation pathway was regulated by 1.1.% of genes, 0.5% of genes regulate positively the mesenchymal stem cell differentiation and the 0.8% the cartilage development.

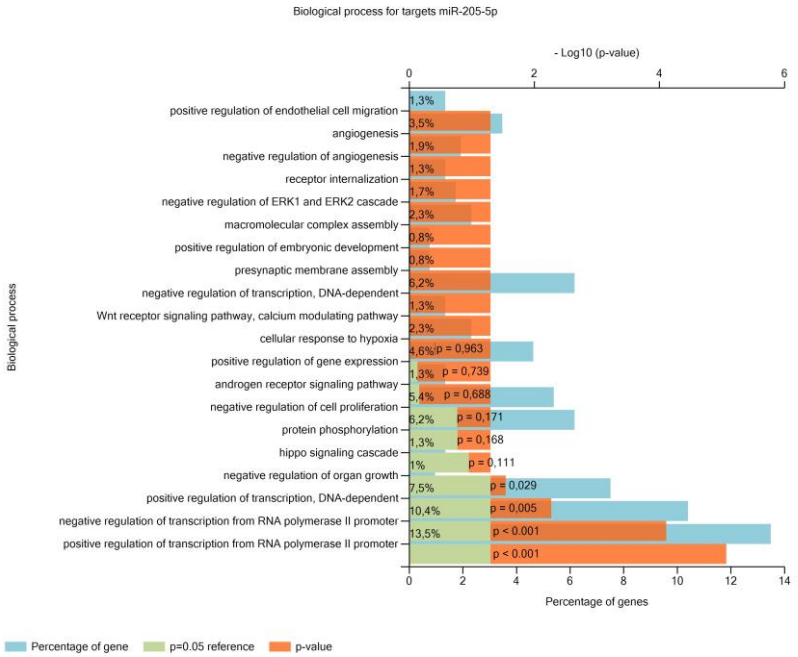

Figure 25. miR-205-5p protein target related pathways. Top 20 biological processes regulated by miR-205-5p predicted targets, using FUNRICH and the gen ontology database.

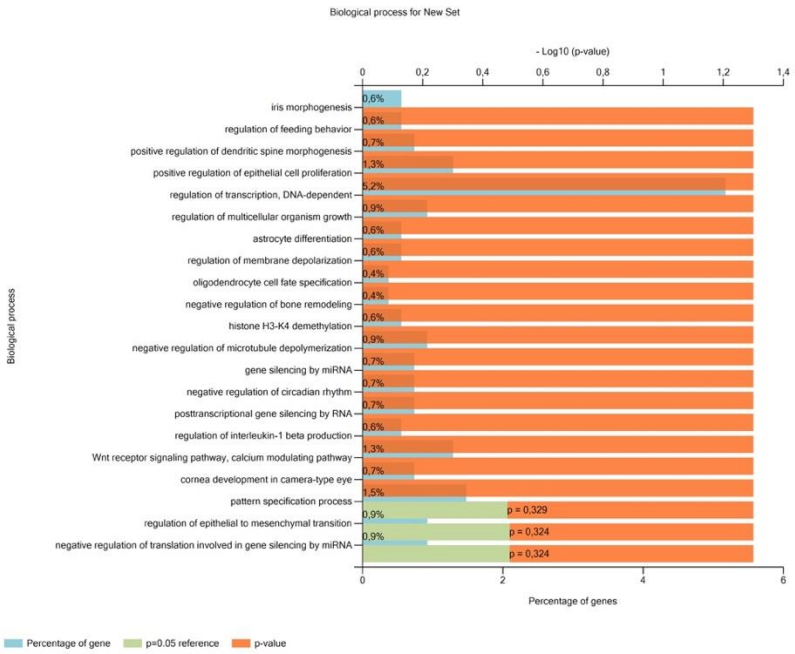

Figure 26. miR-521 protein target related pathways. Top 20 biological processes regulated by miR-521 predicted targets, using FUNRICH and the gen ontology database.

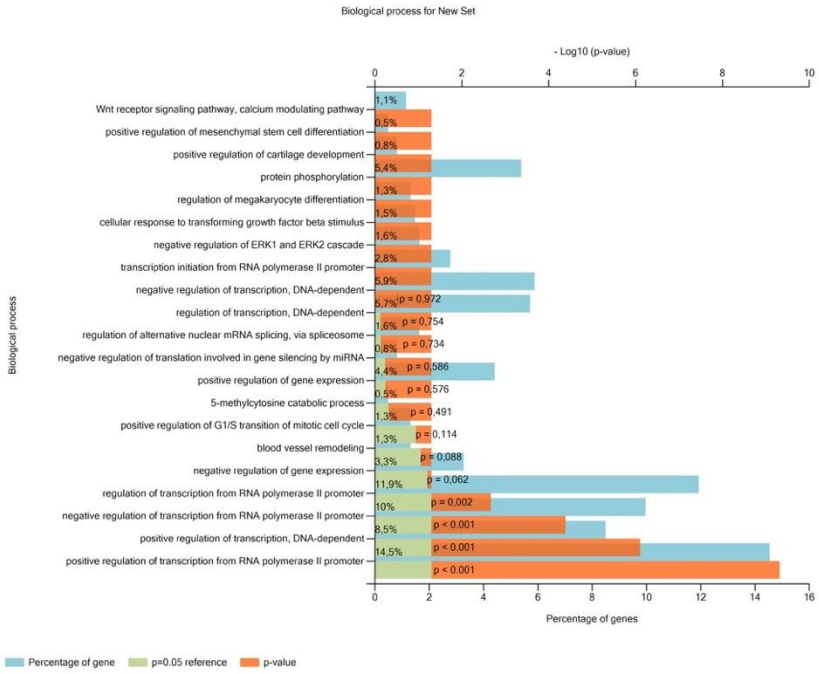

Figure 27. miR-302c-3p protein target related pathways. Top 20 biological processes regulated by miR-302c-3p predicted targets, using FUNRICH and the gen ontology database.

5.2. Potential Target of SEV miRNA

Similarly, to the Cell miRNAs, the biological pathways and networks regulated by the predicted targets were entered into the FUNRICH software (version 3.1.3) to perform the functional analysis. The functional enrichment analysis of miR-302a-3p showed 607 biological processes regulated by at least one of the 1,019 mRNA target of miR-302a-3p. Among the top pathways, the GTPase activity was regulated by 1.3% of genes, dentate gyrus development by 0.7% of genes and the response to DNA damage by 3% of genes. Finally, the analysis of miR-122-5p targets showed 266 biological processes

regulate by at least one of the 226 mRNA targets. 1% of genes were involved in the regulation of o-linked glycosylation via threonine, monocyte activation and endochondral bone growth. The top 20 biological processes regulated by miR-302a-3p and miR-122-5p are shown in Figure 28 and Figure 29 respectively.

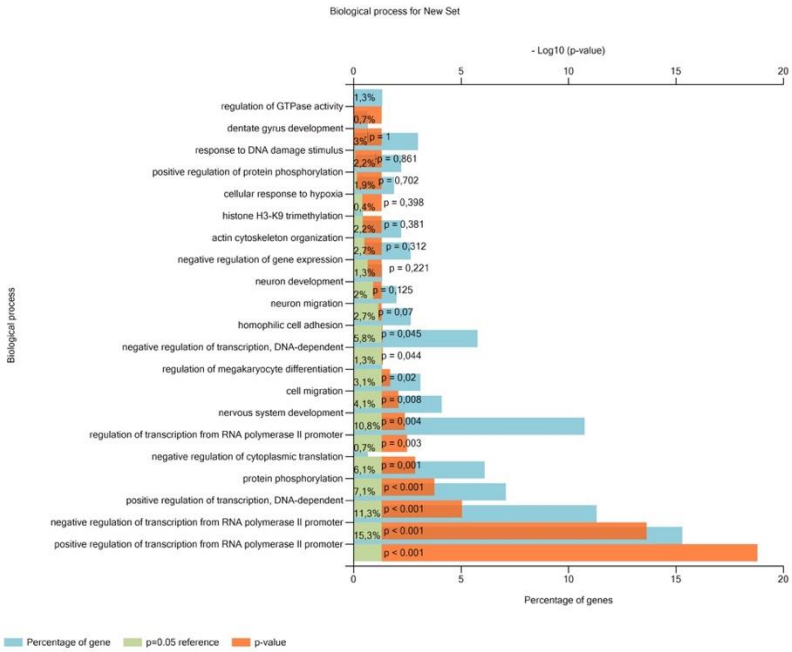

Figure 28. miR-302a-3p protein target related pathways. Top 20 biological processes regulated by miR-302a-3p predicted targets, using FUNRICH and the gen ontology database.

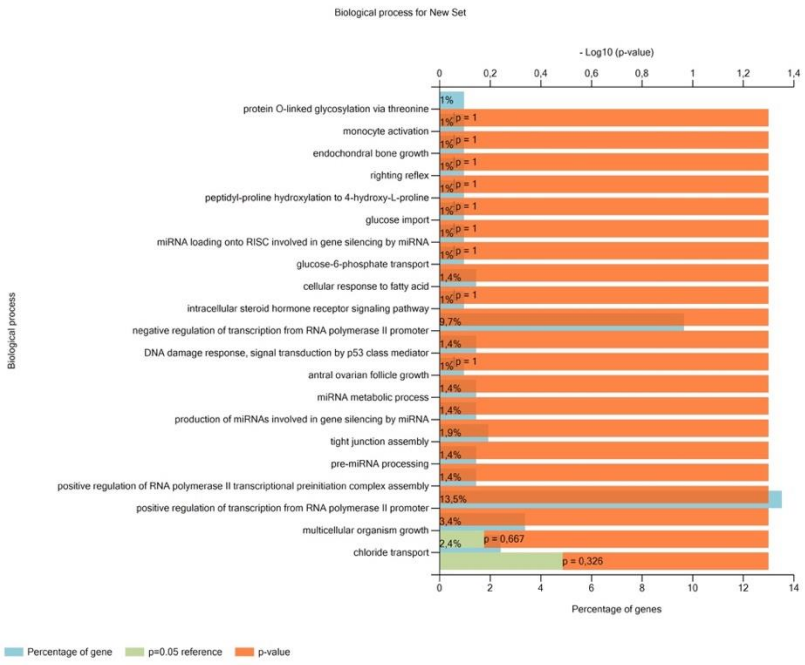

Figure 29. miR-122-5p protein target related pathways. Top 20 biological processes regulated by miR-122-5p predicted targets, using FUNRICH and the gen ontology database.

6. Oxidative stress down-regulates miR-205-5p

As previously observed, ARPE-19 cells resulted in a significant ROS production after H_2O_2 exposure, concretely at 600 µM and 800 µM of H_2O_2. 600 µM H_2O_2 was used to stress ARPE-19 cells without killing them. However, this phenomenon was normalized by the antioxidant N-acetylcysteine 4 mM (NAC) (p_value=0.04) (Figure 30 A). A significant reduction of miR-205-5p levels were observed in ARPE-19 cells after H_2O_2 exposure compared to control cells (p_value=0.03) (Figure 30 B). In order to assess whether this increase is oxidative stress-dependent, the antioxidant NAC (4 mM) was added.

NAC normalized the miR-205-5p levels reduced by H_2O_2 (p_value=0.01). However, no significant changes in miR-205-5p expression levels were found in control ARPE-19 cells after NAC exposure (p_value=0.37) (Figure 30 B).

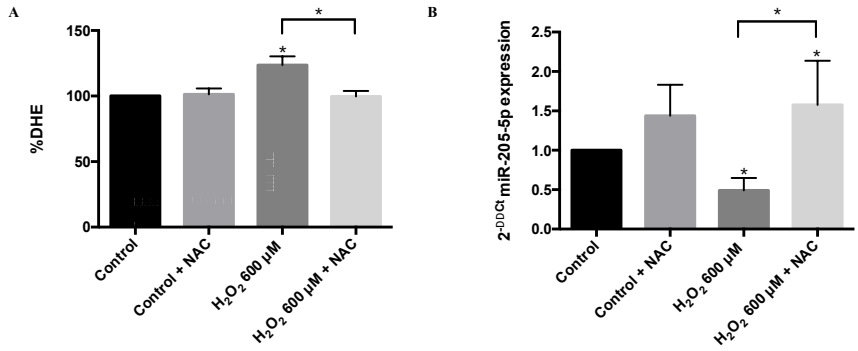

Figure 30. Oxidative stress regulates miR-205-5p expression. Superoxide anions were measured by DHE after H_2O_2 and NAC exposure (**A**). APRE-19 miR-205-5p expression was analyzed by qRT-PCR (**B**). Values are expressed as mean ± SEM (n=3). The p_value was calculated by T-test and statistically significant differences were set at *p<0.05.

Mature H_2O_2 treated ARPE-19 cells also resulted on the same response after NAC treatment, miR-205-5p expression was normalized by NAC administration (Figure 31). This suggest a potential REDOX sole of the miR-205-5p. In the same way, as occurring with non-mature ARPE-19 cells, NAC normalized the miR-205-5p expression levels (p_value=0.04).

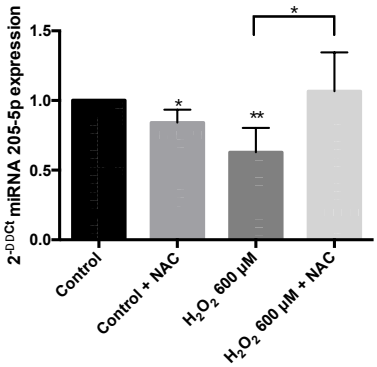

Figure 31. Oxidative stress regulates miR-205-5p expression in mature ARPE-19 cells. Mature APRE-19 miR-205-5p expression was analyzed by qRT-PCR. Values are expressed as mean ± SEM (n=3). The p_value was calculated by T-test and statistically significant differences were set at *p<0.05 and **p<0.01.

7. miR-205-5p targets are related to vascular processes

Potential biological processes regulated by miR-205-5p were assessed using *in silico* analysis with TargetScan Human 7.2. (http://www.targetscan.org/vert_72/). As explain in the section above, 592 putative mRNA targets were able to regulate more than 2,800 biological processes. The 592 mRNAs were entered into FUNRICH software (version 3.1.3) and the mRNAs related to angiogenic and vasculogenic processes were selected. Finally, 32 mRNA predicted targets were found (Table 8). Using STRING (https://string-db.org/) the functional network of the mRNA targets related to vasculogenic processes were represented (Figure 33).

Table 8. mRNA targets of miR-205-5p related to vascular processes.

Abbreviation	Name	Function
RORA	RAR Related Orphan Receptor A	pro-angiogenic[227]

Abbreviation	Name	Function
MED1	Mediator of RNA polymerase II transcription subunit 1	not founded
QKI	Protein quaking	pro-angiogenic[228]
GATA3	Trans-ating T-cell-specific transcription factor GATA-3	anti-angiogenic[229]
AGO1	Protein argonaute-1	pro-angiogenic[230]
INSR	Insulin receptor	pro-angiogenic[231]
PLET1	Placenta-expressed transcript 1 protein	not founded
ROCK2	Rho-associated protein kinase 2	pro-angiogenic[232]
HMGB1	High mobility group protein B1	pro-angiogenic[233]
ARID1A	AT-rich interactive domain-containing protein 1A	anti-angiogenesis[234]
RUNX1	Runt-related transcription factor 1	pro-angiogenic[235]
PTEN	Phosphatidylinositol 3,4,5-trisphosphate 3-phosphatase and dual-specificity protein phosphatase	pro-angiogenic[236]
ANGPT2	Angioprotein-2	pro-angiogenic[237]
ERBB4	Receptor tyrosine-protein kinase erbB-4	pro-angiogenic[238]
MAPK3	Mitogen-activated protein kinase 3	pro-angiogenic[239]
PRKCE	Protein kinase C epsilon type	anti-angiogenic[240]
PRKCA	Protein kinase C alpha type	anti-angiogenic[241]

Abbreviation	Name	Function
S1PR1	Sphingosine 1-phosphate receptor 1	pro-angiogenic[242]
LYN	Tyrosine-protein kinase Lyn	pro-angiogenic[243]
CSF1	Macrophage colony-stimulating factor 1 receptor	pro-angiogenic[244]
LPAR1	Lysophosphatidic acid receptor 1	pro-angiogenic[245]
SMAD1	Mothers against decapentaplegic homolog 1	pro-angiogenic[246]
YAP1	Transcriptional coactivator YAP1	pro-angiogenic[247]
AMOT	Angiomotin	anti-angiogenic[248]
THBS1	Thrombospondin-1	anti-angiogenic[249]
EREG	Proepiregulin	pro-angiogenic[250]
VEGFA	Vascular endothelial growth factor-A	pro-angiogenic[251]
NRCAM	Neuronal cell adhesion molecule	pro-angiogenic[252]
PTPRJ	Receptor-type tyrosine-protein phosphatase eta	pro-angiogenic[253]
CALCRL	Calcitonin gene-related peptide type 1 receptor	pro-angiogenic[254]
RNF213	E3 ubiquitin-protein ligase RNF213	anti-angiogenic[255]
CTH	Cystathionine gamma-lyase	pro-angiogenic[256]

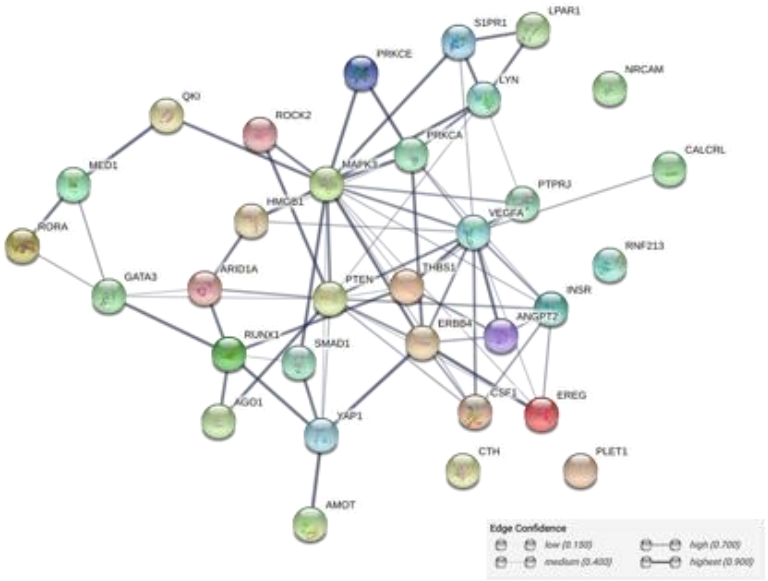

Figure 32. miR-205-5p protein target related angiogenic pathways. Interactional Network of miR-205-5p angiogenic related targets.

8. VEGFA mRNA is a direct target of miR-205-5p

Consistently with previous results, *in silico* analysis showed that VEGFA mRNA is a predicted target of miR-205-5p (Table 8 and Figure 32). TargetScan predicted a 3'-UTR binding site for VEGFA mRNA and miR-205-5p (Figure 33). In order to confirm the relation between VEGFA mRNA and miR-205-5p, VEGFA mRNA expression was analysed after H_2O_2 treatment. We observed that VEGFA mRNA levels were up-regulated after H_2O_2 exposure (p_value=0.0230) (Figure 34 B), indicating a negative correlation with miR-205-5p levels (Figure 34 A and C). Matching with the aforementioned results on miR-205-5p levels, VEGFA mRNA levels were also normalized by NAC exposure

(p_value=0.0197; H_2O_2 600 µM vs H_2O_2 600 µM + NAC) (Figure 34 D).

	Predicted consequential pairing of target region (top) and miRNA (bottom)
Position 166-173 of VEGFA 3' UTR	5' ...AUCCAGAAACCUGAAAUGAAGGA...
hsa-miR-205-5p	3' GUCUGAGGCCACCUUACUUCCU

Figure 33. VEGFA and miR-205-5p. The predicted biding site of miR-205-5p with the 3'UTR mRNA VEGFA.

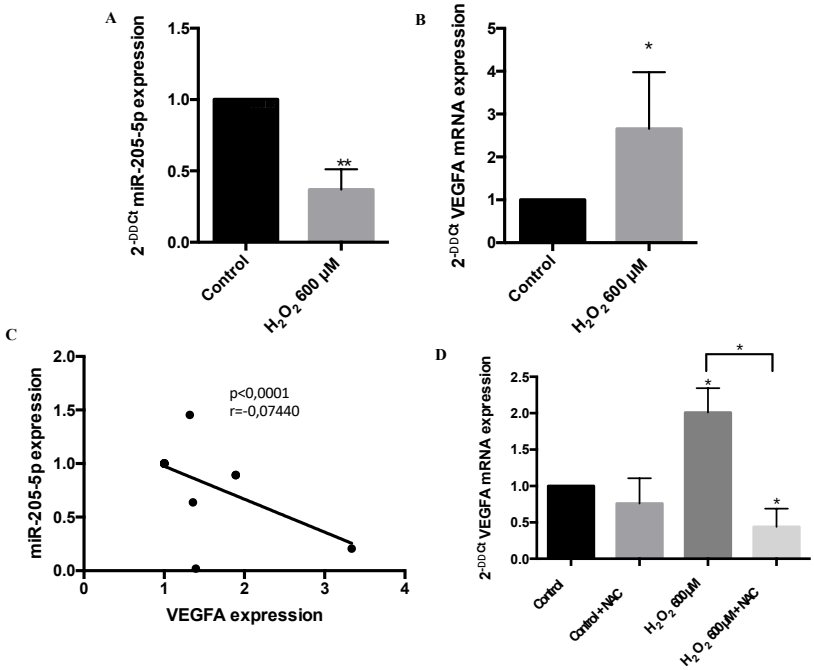

Figure 34. VEGFA is predicted as a direct target of miR-205-5p. After 24h of H_2O_2 600 µM exposure the miR-205-5p expression (**A**) and the mRNA VEGFA expression (**B**) was analysed by qRT-PCR. The expression correlation between miR-205-5p and VEGFA was analysed using a Spearman correlation (**C**). After the co-treatment with N-acetylcysteine, VEGFA expression was analysed in ARPE-19 cells by qRT-PCR (**D**). Values are expressed as mean ± SEM (n=3). The p_value was calculated by T-test and statistically significant differences were set at *p<0,05 and **p<0,01.

9. VEGFA expression is regulated by miR-205-5p

In order to test the role of miR-205-5p on VEGFA mRNA expression, ARPE-19 cells were transfected with miR-205-5p mimic. It is worth to mention that the transfection process did not affect the ARPE-19 cell viability (Figure 35) and thus can be considered as a suitable method.

The transfection with a negative control did not affect the miR-205-5p expression. As expected, mimic transfected ARPE-19 cells with the mimic increased miR-205-5p levels as we expected (Control vs Control + mimic miR-205-5p; p_value<0.0001 and H_2O_2 600 µM vs H_2O_2 600 µM + mimic miR-205-5p; p_value=0.01) (Figure 36 A). In contrast, decreased VEGFA mRNA levels (Control vs Control + mimic miR-205-5p; p_value<0.0002 and H_2O_2 600 µM vs H_2O_2 600 µM + mimic miR-205-5p; p_value=0.0468) (Figure 36 B). Similarly, transfected ARPE-19 cells also decreased VEGFA mRNA levels after H_2O_2 exposure (Control vs H_2O_2 600 µM; p_value=0.0079) (Figure 36 B). These results were confirmed by blotting analysis, showing a significant decrease of VEGFA protein expression after miR-205-5p mimic transfection in H_2O_2 treated cells (Control vs Control + mimic miR-205-5p; p_value<0.03 and H_2O_2 600 µM vs H_2O_2 600 µM + mimic miR-205-5p; p_value=0.0025, Control vs H_2O_2 600 µM; p_value=0.0024) (Figure 36 C).

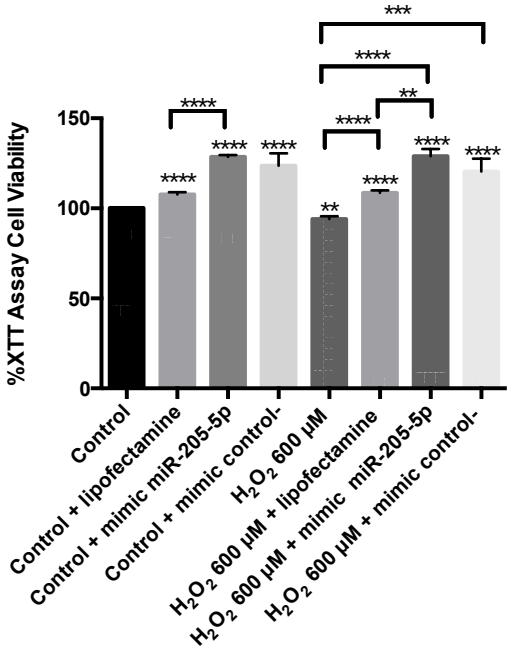

Figure 35. ARPE-19 cell viability after mimic miR-205-5p transfection. XTT assay was performed to analyzed cell viability, values are express as percentage to control ± SEM (n=3-4). The p_value was calculated by T-test and statistically significant differences were set at ** p_value < 0.01, ***p_value < 0.0001 and ****p_value < 0.00001.

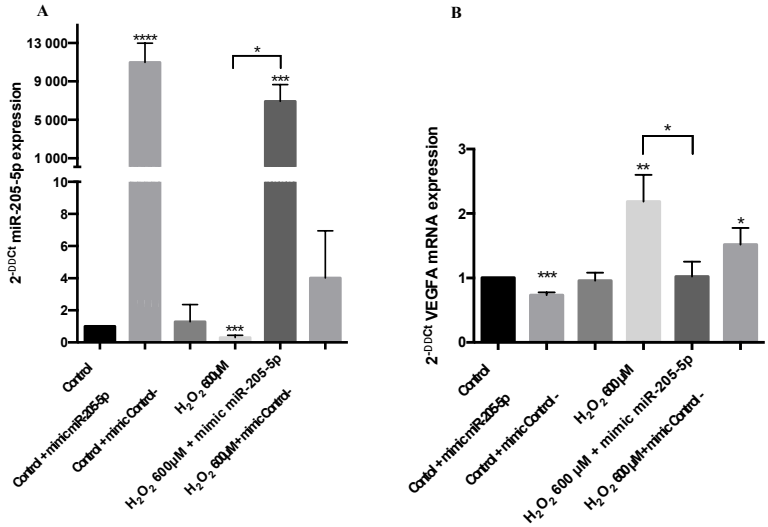

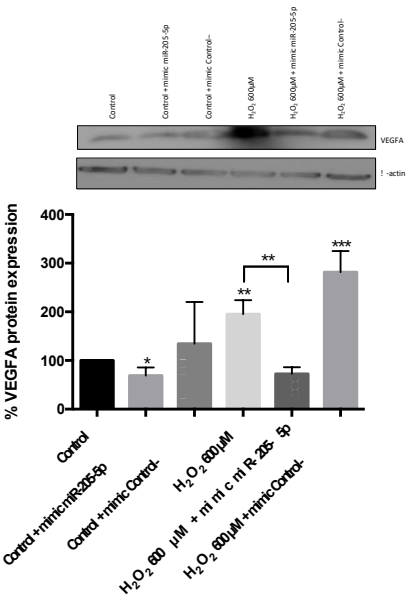

Figure 36. VEGFA expression is regulated by miR-205-5p. MiR-205-5p expression levels after 48 h of miR-205-5p mimic transfection and mimic negative control (**A**). VEGFA mRNA expression levels after 48 h of transfection with miR-205-5p mimic and mimic negative control were measured by qRT-PCR (**B**). Western blot analysis for VEGFA protein after miR-205-5p mimic and mimic negative control transfection (**C**). Values are expressed as mean ± SEM (n=3). The p_value was calculated by T-test and statistically significant differences were set at *p<0.05, **p<0.01, ***p<0.001 and ****p<0.0001.

10. Vasculogenesis is affected by miR-205-5p deregulation via VEGFA

HUVEC cells spontaneously produce tube formation, where cells are divided and arranged as a capillary network without external stimulus. The tub formation could be accelerated or inhibited by factors found in the cell culture media.

Functional vasculogenesis assay was performed to confirm the inhibitory effect of miR-205-5p on VEGFA. HUVEC cells, grown with cell culture media obtained from control ARPE-19 cells, produced few

vascular processes (Figure 37 A and I). However, culture media obtained from 600 µM H_2O_2 treated ARPE-19 cells significantly promoted angiogenic changes in HUVEC cells compared to control (131.7 ± 4.39) (p_value<0.0001; Control vs H_2O_2 600 µM) (Figure 37 E and I). Interestingly, HUVEC cells cultured on miR-205-5p-mimic-transfected ARPE-19 cell culture media significantly abolished these angiogenic changes (90.52 ± 7.46) (p_value=0.01; H_2O_2 600 µM + mimic(miR-205-5p) vs H_2O_2 600 µM) (Figure 37 F and I). Cell culture media from mimic-transfected control ARPE-19 cells also reduced angiogenesis in HUVEC cells (82.74 ± 5.04) (p_value=0.0004; Control + mimic(miR-205-5p) vs Control) (Figure 37 B and I). Otherwise, in order to confirm the implication of miR-205-5p-VEGFA regulation in the vasculogenic process, ARPE-19 cells were transfected with siVEGFA and co-transfected with mimic(miR-205-5p)-siVEGFA. As expected, HUVEC cells grown with siVEGFA transfected 600 µM H_2O_2 treated ARPE-19 cell culture media, prevented the angiogenic process (103.9 ± 6.97) (p_value=0.0062; H_2O_2 600 µM + siVEGFA vs H_2O_2 600 µM) (Figure 37 G and I). In the same way, the culture media obtainedfrom co-transfected ARPE-19 cells in 600 µM H_2O_2 conditions the angiogenesis processes was reduced (100.1 ± 6.84) (p_value=0.0028; H_2O_2 600 µM + siVEGFA + mimic(miR-205-5p) vs H_2O_2 600 µM) (Figure 37 D, H and I).

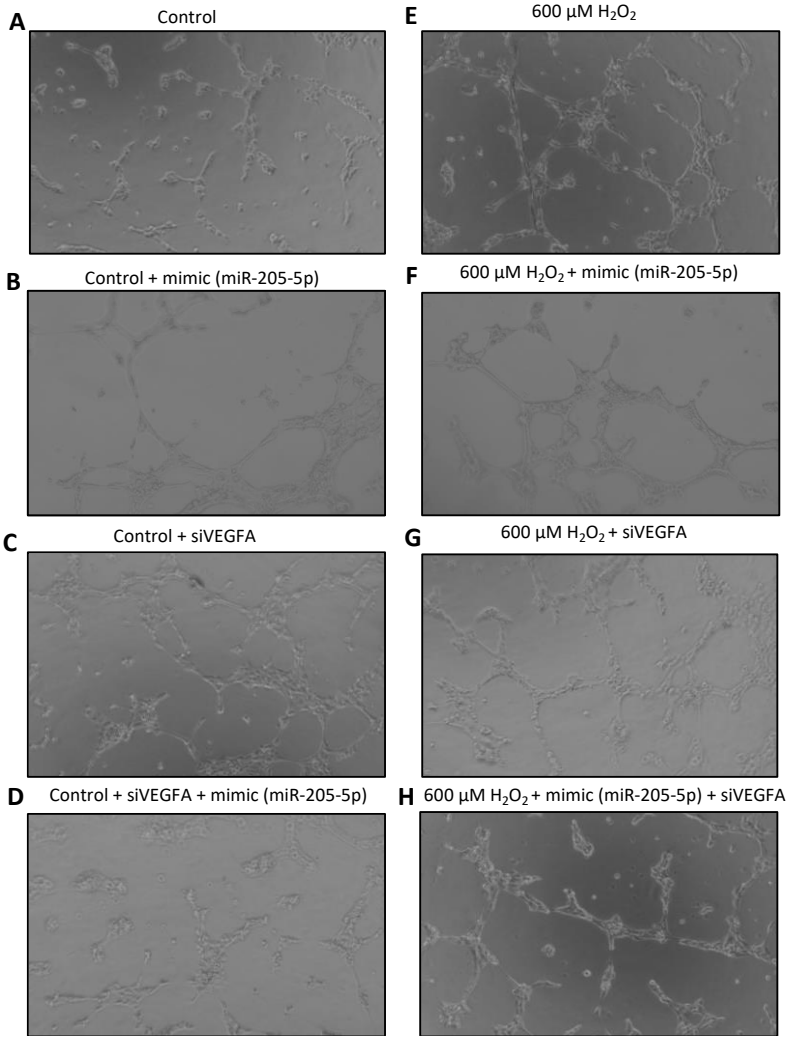
A
Control
E
600 µM H_2O_2
B
Control + mimic (miR-205-5p)
F
600 µM H_2O_2 + mimic (miR-205-5p)
C
Control + siVEGFA
G
600 µM H_2O_2 + siVEGFA
D
Control + siVEGFA + mimic (miR-205-5p)
H
600 µM H_2O_2 + mimic (miR-205-5p) + siVEGFA

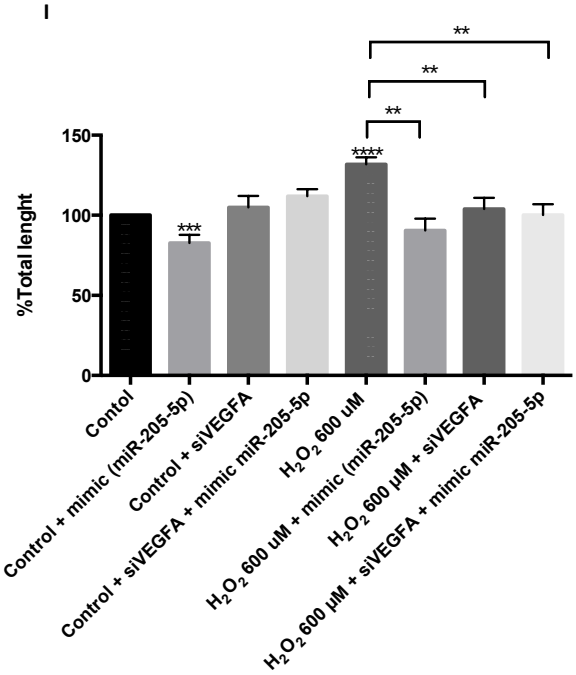

Figure 37.VEGFA-mediated Vasculogenesis is regulated by miR-205-5p. HUVEC cell tube formation under different ARPE-19 cell culture media conditions. ARPE-19 control medium (**A**), mimic(miR-205-5p)-treated ARPE-19 control (**B**), siVEGFA-treated ARPE-19 control (**C**), mimic(miR-205-5p)+siVEGFA-treated ARPE-19 control (**D**), H_2O_2 600 µM treated ARPE-19 (**E**), mimic(miR-205-5p)-treated ARPE-19 + H_2O_2 600 µM medium (**F**), siVEGFA-treated ARPE-19 + H_2O_2 600 µM medium (**G**) and mimic(miR-205-5p)+siVEGFA-treated ARPE-19 + H_2O_2 600 µM medium (**H**). Scale bar 100µM. Total length (**I**) were calculated. Values are expressed as mean ± SEM (n=3). The p_value was calculated by T-test and statistically significant differences were set at *p<0.05, **p<0.01, ***p<0.001 and ****p<0.0001.

11. H_2O_2- sEVs and their influence in neighboring cells

To analyze the influence of the H_2O_2-stressed sEVs in the neighboring cells (ARPE-19), sEVs released from control and 600 µM H_2O_2 treated ARPE-19 cells were isolated and exposed to naïve ARPE-19 cells. sEVs released from control treated ARPE-19 cells did not produce oxidatice-induced response. However, sEVs obtained from

600 µM H_2O_2 treated ARPE-19 cells induced OS responses in ARPE-19 cells (113.5 ± 3.32) (p_value=0.0152) at the same level as the treatment with 600 µM H_2O_2 treatment (111.7 ± 3.22) (p_value=0.0222) (Figure 38).

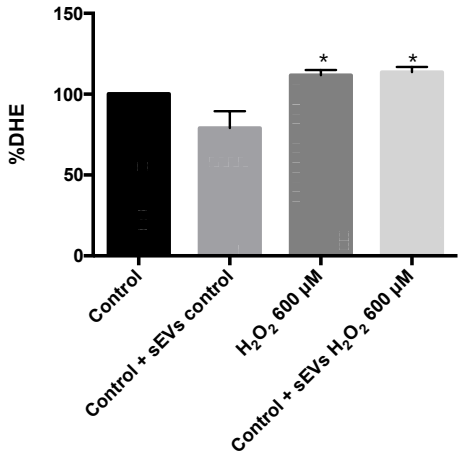

Figure 38. sEVs induce oxidative stress. Superoxide anions were measured by DHE after H_2O_2 600µM exposure. Values are expressed as mean ± SEM (n=3). The p_value was calculated by T-test and statistically significant differences were set at *p<0.05.

In the same way, we analyzed the effect of the H_2O_2-induced sEVs on ARPE-19 cell viability, as previously detailed sEVs from control and 600 µM H_2O_2 treated ARPE-19 cells were isolated and administrated to treated ARPE-19 cell culture. Fitting with the previous results on oxidative stress-induced response, control-sEVs did not affect the ARPE-19 cells viability (96.13 ± 3.344). However and as expected, the H_2O_2-sEVs significantly decreased ARPE-19 cell viability (90.28 ± 3.056) (p_value=0.0335) (Figure 39).

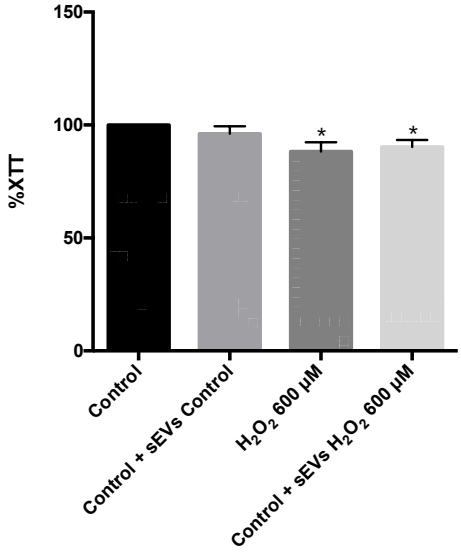

Figure 39. sEVs affect cell viability. XTT assay was performed to analyzed cell viability, values are express as percentage to control ± SEM (n=3). The p_value was calculated by T-test and statistically significant differences were set at * p_value < 0.05.

The polarized nature of the RPE is essential for the health of the eye, not only regarding nutrient and waste transport, but also in the synthesis and directional secretion of proteins and sEVs. Polarized ARPE-19 cells release sEVs to the apical and basal side. After the polarization of ARPE-19 cells the sEVs from the apical and basal media were isolated separately in order to assess their influence in non-stressed ARPE-19 cells. Zona occludens protein 1 (ZO-1) is one of the most important proteins in the tight junctions presents in RPE tissue. The immunofluorescence against ZO-1 showed a cualitative decrease of ZO-1 expression when cells were treated with sEVs from 600 µM H_2O_2 stressed ARPE-19 cells (Figure 40).

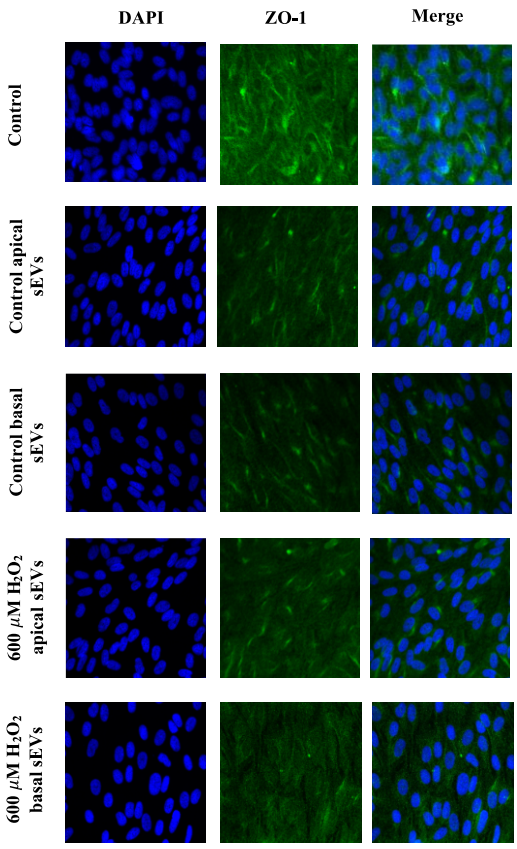

Figure 40. sEVs from H_2O_2 stressed ARPE-19 cells decrease barrier function. The immunofluorescence of ZO-1 was done in order to analyze the influence of sEVs from H_2O_2 stressed ARPE-19 cells on ARPE-19 cells during 24 h.

12. H_2O_2- sEVs increase angiogenesis

Additionally, we performed a functional angiogenic assay to elucidate the effect of induced VEGFA expression by sEVs. As we see before, HUVEC cells grown with cell culture media obtained from control ARPE-19 cells, produced few vascular processes (Figure 40 A and E) and culture media obtained from H_2O_2 treated ARPE-19 cells

significantly induced angiogenic changes in HUVEC cells (121.4 ± 3.49) (p_value=0.0036; Control vs H_2O_2 600 µM) (Figure 40 C and E). Interestingly, HUVEC cells grown with sEVs from H_2O_2 treated ARPE-19 cells significantly induced angiogenic changes in HUVEC cells (128,7 ± 9.52) (p_value=0.0393; H_2O_2 600 µM sEVs vs Control) (Figure 40 D and E). However, sEVs from control ARPE-19 cells did not induced angiogenesis in HUVEC cells (97.9 ± 1.79) (Figure 40 B and D).

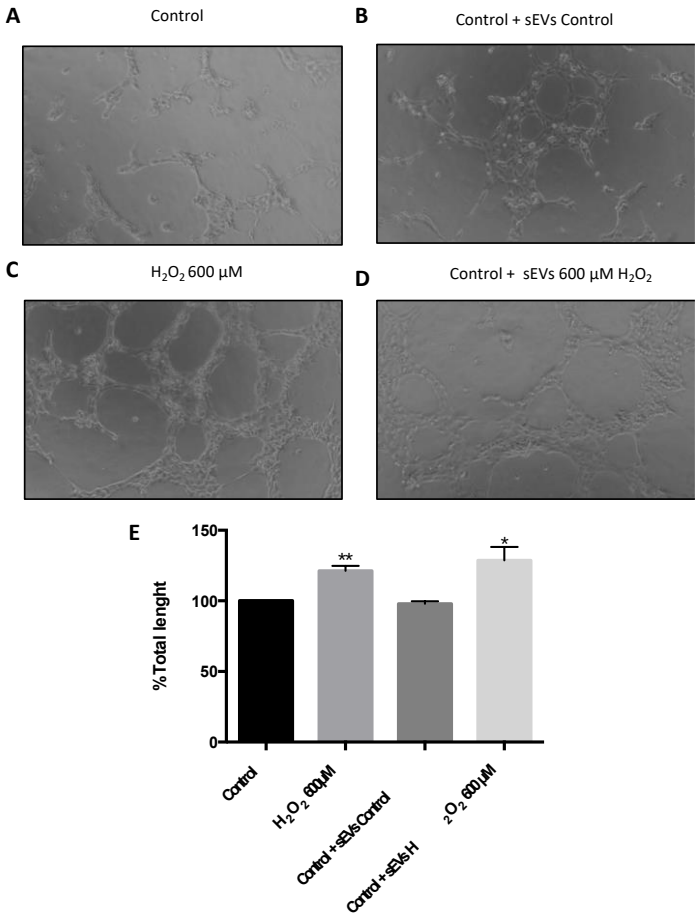

Figure 40. sEVs-mediated Vasculogenesis. HUVEC cell tube formation under different ARPE-19 cell culture media conditions. ARPE-19 control medium (**A**),

control sEVs (**B**), H_2O_2 600 µM ARPE-19 media (**C**) and sEVs H_2O_2 600 µM (**D**). Scale bar 100µM. Total length (**E**) were calculated. Values are expressed as mean ± SEM (n=3). The p_value was calculated by T-test and statistically significant differences were set at *p<0.05 and **p<0.01.

13. H_2O_2- sEVs increase VEGFA production

As previously observed, EVs modify affect neighboring cells. To assess the effect of EVs in the VEGFA expression, both sEVs obtained from control and 600 µM H_2O_2 treated ARPE-19 cells were isolated and used on naïve ARPE-19 cells. Cells treated with control-sEVs did not induced VEGFA response (0.87 ± 0.23). However, the treatment with 600 µM H_2O_2-sEVs increase VEGFA expression (2.19 ± 0.55) at the same level as the treatment with 600 µM H_2O_2 (1.83 ± 0.41) (Figure 41).

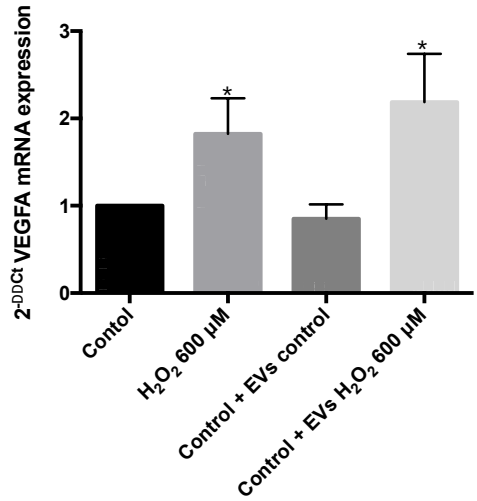

Figure 41. VEGFA expression induced by sEVs. After 24h of H_2O_2 600 µM, EVs control and EVs H_2O_2 600 µM exposure the mRNA VEGFA expression was analysed by qRT-PCR. Values are expressed as mean ± SEM (n=6). The p_value was calculated by T-test and statistically significant differences were set at *p<0,05.

DISSCUSION

Discussion

1. Effect of H_2O_2 in ARPE-19 cells

According to its anatomical location and function, RPE is continuously exposed to OS. OS can result from excessive light and metabolic activity finally affecting the normal eye function. ARPE-19 cells are useful for *in vitro* studies thanks to their structural and functional characteristics[257]. On this line, the use of ARPE-19 cell under oxidative challenges results useful to study the RPE response to oxidative stimuli. Different oxidizing agents have been used including EtOH[97,258], glucose[188] and H_2O_2[146,259] as herein. Non-mature ARPE-19 cells have been widely used as RPE cellular models in ophthalmology and cellular biology in recent years[97,99,146,188,209].

One preliminary aspect is that referred to the H_2O_2 concentration selected for the study. A dose-response study was performed to find the sublethal H_2O_2 concentration in order to study the cellular response. 600 μM H_2O_2 for 24 h was the highest concentration increasing ROS levels without showing early apoptotic signs. In fact, the cellular morphology of these cells was unchanged respect to the control cells. Higher H_2O_2 concentrations (> 800 μM H_2O_2) significantly increased early apoptosis on ARPE-19 cells. ROS overproduction activates cellular self-defense mechanisms, but when the production is excessive, cell death occurs. However, other authors have used different H_2O_2 ranges (200-600 μM) and some differences can be found in terms of cell viability (XTT or MTT), apoptosis and ROS production[120,147,148]. Plausibly, the difference on time exposure (12-24 h) or cell confluence level could explain these discrepancies. In fact, polarized ARPE-19 cells are more resistant to OS than non-polarized ARPE-19 cells[260].

Fitting with the lack of apoptotic signs, a significant positive correlation between cell viability and ROS production was also observed in ARPE-19 cells. Taking into account the sub-lethal effect of 24 h of 600 μM H_2O_2 treatment, this concentration was used to stimulate the pathophysiology in ARPE-19 cells for the following experiments.

The finding that polarized ARPE-19 cells are more resistant to OS than non-polarized ARPE-19 cells[260] could explain the lack of change in the transepithelial resistance after 24 h of 600 μM H_2O_2 treatment.

It is well documented that different oxidizing agents such as EtOH[97], high glucose[188], photo-oxidative blue-light[261] and rotenone[262] promote sEVs release from ARPE-19 cells. Fitting with this, H_2O_2 pro-oxidant challenge significantly increased EVs release from ARPE-19 cells. These EVs ranged from 30 to 150 nm diameter, as observed by NanoSight and TEM, being classified as sEVs.

2. miRNA expression profile in ARPE-19 cells and sEVs

Because of their critical role in various biological processes such as OS and angiogenesis[138,149] related to retinal pathology, miRNAs, a novel class of non-coding RNAs, have been proposed by numerous studies as promising and therapeutic tools for retinal disorders[123,133].

2.1.miRNA expression profile in ARPE-19 cells

The miRNA expression profile showed two different clusters according to the ARPE-19 cells treatment. Specifically, we identify 59 miRNAs significantly expressed in ARPE-19 cells, but only 7 miRNAs were significantly under-expressed in 600 μM H_2O_2 treated ARPE-19 cells regarding to control conditions.

Several works focused on retinal disorders, have reported significant changes on miRNAs (Table 9). Among them, let-7a[138,263], miR-518d-3p[147], miR-205[123] and miR-302c are present[148]. However, the miR-521 and miR-548b-5p had not been related to retinal disorders so far.

Table 9. Relevant miRNAs identified on eye-related disorders.

miRNA	Reference
miR-139-3p	Szemraj et al 2015 and Ertekin et al 2014[124,138]
miR-192	Grassmann et al 2014 and Ertekin et al 2014 and [140,138,264]
let-7c	Ren et al 2017 and Szemraj et al 2015[124,137]
miR-18b	Ren et al 2017 and Wang et al 2014[137,265]
miR-183	Karali et al 2016, Loscher et al 2007 and

	Xiang et al 2017[136,144,266]
miR-23a	Li et al 2016, Lin et al 2011, Romano et al 2017, Szemraj et al 2015 and Zhou et al 2011[119,120,124,139,151]
miR-27a	Ren et al 2017; Romano et al 2017; Szemraj et al 2015[124,137,139]
miR-25	Ren et al 2017 and Zhang et al 2017[137,267]
miR-106a	Ertekin et al 2014[138]
let-7a	Ertekin et al 2014 and SanGiovanni et al 2017[138,263]
miR-27b	Ertekin et al 2014 and Howell et al 2013[138,148]
miR-518d-3p	Dinç et al 2018[147]
miR-92a	Dinç et al 2018, Howell et al 2013, Desjarlais et al 2019 and Walz et al 2019[147,148,268,269]
miR-361-5p	Grassmann et al 2014 and Szemraj et al 2015[124,140]
miR-335	Ertekin et al 2014 and Grassmann et al 2014[138,140]
miR-30c	Ren et al 2017[137]
miR-28-5p	Ren et al 2017[137]
miR-29a	Ertekin et al 2014, Howell et al 2013, Walz et al 2019, Zhang et al 2017 and Zhang et al 2017 (2)[138,148,269–271]
miR-205	Ménard et al 2016 and Blasiak et al[123,272]
miR-17	Ertekin et al 2014, Barber et al 2017 and Tian et al 2016[138,150,273]
miR-324-5p	Ertekin et al 2014[138]
miR-302c	Howell et al 2013[148]
miR-30b	Dinç et al 2018, Romano et al 2017, Mazzeo et al 2019 and Haque et al 2012[139,147,149,274]
miR-28-3p	Howell et al 2013[148]
miR-338-5p	Zhou et al 2019[275]

The enrichment analysis of the 7 miRNAs under-expressed show different pathways related to retinal disorders including cell cycle, adherent junctions, p53 signaling pathway and HIF-1 signaling pathway. In addition, the mRNA targets regulated by miR-205, whose expression was validated, are capable of regulating endothelial cell

migration and angiogenesis as shown in some articles[276–278]. Besides, the mRNA targets regulated by the other validated Cell miRNAs regulated iris morphogenesis (miR-521 mRNA targets) and Wnt receptor signaling pathway (miR-302c-3p mRNA targets), also related to eye disorders[279]

2.2.miRNA expression profile in sEVs from ARPE-19 cells

Extracellular or circulating miRNAs can be included on sEVs, associated to lipoproteins or proteins[280]. Although 600 μM H_2O_2 treated ARPE-19 cells released more sEVs, the miRNAs content was lower. Two different clusters of miRNA expression obtained from sEVs could be identified according to control or 600 μM H_2O_2 treated ARPE-19 cells.

In spite of the fact that in sEVs only 218 out of 384 sEVs miRNAs were detected by the array, 88 less than in Cell miRNAs, probably due to its lowe cargo capacity. Only two sEVs miRNAs were significantly highly expressed in control released sEVs than in sEVs from treated cells. The miR-302a and miR-122 have already been seen in sEVs confirming our results[281–285].

Multiple pathways obtained in the enrichment analysis were observed. Most of them were related with signaling pathways important in cancer. Additionally, we identify the mRNA targets of validated miRNAs involved in processes related to retinal disorders[286,287]. Specifically, miR-122 mRNA targets could regulate the miRNA loading into RISC complex and the thigh junction assembling. On the other hand, the miR-302a mRNA targets are related to DNA damage stimulus response, cellular response to hypoxia and cell migration.

When comparing the two sEVs miRNAs, miR-302a and miR-122, to those miRNAs on ARPE-19 cells, no matches could be found. Surprisingly, the sEV miR-302a and the Cell miR-302c belong to the miR 302/367 *La-related protein 7 (LARP7)* intragenic cluster. This includes miR-367, miR-302d, miR-302a, miR-302c and miR-302b. This cluster is involved in several processes coordinating proliferation, differentiation, pluripotency maintenance and cell reprograming[288]. Moreover, the cluster, regulates TFG pathway, PI3K-AKT and BMP cell signaling[289–291]. Additionally, miR-302a acts as a tumor suppressor[292] and repressor of cell division, more concretely, VEGFA is one of the direct targets for this miRNA[293]. In addition, miR-122 has been related to VEGFC[294]. Interestingly, low miR-302a/miR-122 expression levels are inversely related to VEGF levels in hepatocellular carcinoma, promoting vascular changes[162,293]. On this line, miR-122 seems to have a role against OS, since the use of pre-miR-122 protects from H_2O_2 induced OS[295], targeting the mitochondrial ribosomal protein S11[296].

Recent data form other groups indicate how diverse oxidative insults as EtOH or high glucose, and now H_2O_2 lead to increase sEVs release from ARPE-19 cells[97,188]. Furthermore, those oxidative-induced sEVs were capable of promoting neovascular processes in endothelial cell cultures, whereas control-released sEVs inhibited this phenomenon[97,188]. In view of these findings, we hypothesize that sEVs miR-122 and miR-302 decreased levels could play a role on angiogenesis involving OS related pathways.

Different reports locate the sEVs-miRNAs in eye tissue. MiR-302 expression was observed already in RPE cells by Li and collaborators, playing an important role in the RPE differentiation[297]. Other authors

observed a miR-122 differentially expression on canine retina[298], in aqueous humor[299] and are related in fact to DR[300].

In agreement with others, up/down regulated miRNAs are related to several and different signaling pathways. After seeing the results in both sEV miRNA and Cell miRNAs related pathways, cancer related pathways are commonly involved in many of the deregulated miRNAs. Circulating miRNAs can be easily obtain through a blood draw, turning them into promising targets to investigate as potential liquid biopsy markers.

3. miR-205-5p, oxidative stress, vasculogenesis

The miR-205-5p was mapped in the mammalian eye, it was found in the epidermis and the anterior segmental epithelia but was not found in RPE[301]. Other studies have found that miR-125b[302] and miR-23a[151] are over expressed in oxidative stress-induced RPE cells[146]. However, is the first time that the presence of miR-205-5p has been demonstrated in ARPE-19 cells as an RPE cell model. In contrast to the relevance of this miRNA on glioblastoma[278] or hepatocellular carcinoma[303], little information is available about the presence of miR-205-5p in the eye.

Our results show that, 600 μM H_2O_2 exposure resulted in a significant decrease in miR-205-5p levels in ARPE-19 cells. It has been suggested that miR-205-5p positively regulates the peroxiredoxin 2 (PRDX2) pathway[304]. PRDX2 reduces ROS derived from H_2O_2 transformation. In addition, miR-205-5p was identified as protective against OS via EGLN2 suppression[305]. Once considering this, reducing miR-205-5p levels after oxidative challenge is opposed to this proposed antioxidant mechanism. Perhaps excessive OS challenge leads to a different scenario, far from the physiological conditions that occur in

wet AMD or cancer. Future research must address the antioxidant role of miR-205-5p. Another relevant finding is that NAC normalized those decreased miR-205-5p levels, indicating that miR-205-5p is sensitive to ROS, both in mature and non-mature ARPE-19 cells.

According to Yue et al., VEGFA 3'UTR-mRNA is one of the putative targets of miR-205-5p[251]. In addition, we have identified some potential targets of miR-205-5p and their biological processes. Among the potential mRNA regulated by miR-205-5p, 3.5% are angiogenic and 1.3% are related to endothelial cell migration. In fact, it is well documented that miR-205-5p acts as a tumor suppressor by regulating cell migration and proliferation[251,277,278,306,307]. Moreover, it has been suggest that miR-205-5p could interact indirectly via PI3K/AKT also involved in angiogenesis[278]. We have observed that VEGFA and miR-205-5p are inversely expressed, inducing angiogenesis.

Additionally, we confirm the fact that OS increases VEGFA expression levels[97,308,309]. On the one hand, H_2O_2 induction significantly increased both VEGFA mRNA and protein expression in ARPE-19 cells. On the other hand, the addition of NAC normalized H_2O_2-induced ROS and VEGFA levels. This double result matches with the normalized miR-205-5p levels found after NAC exposure. NAC is a precursor of L-cysteine with scavenging properties and antioxidant effects, interacting with the antioxidant glutathione system[310,311]. In addition to direct VEGFA regulation, miR-205-5p also indirectly regulates ERK1/2 and PI3K/AKT pathways[278,312,313]. The PI3K/AKT signaling pathway induces the Nrf2/ARE antioxidant pathway[314], and miR-205-5p could be involved in this route. Future research should be focused on the antioxidant machinery regulated by miR-205-5p.

VEGFA mRNA expression levels negatively correlated with miR-205-5p expression, highlighting the transcriptional regulation of VEGFA mRNA by this miRNA. Previous studies have already identified the regulation of VEGFA by miR-205-5p[277,278,306,313]. Additionally, the results reported here indicate that the VEGFA/miR-205-5p correlation might be regulated by OS in ARPE-19 cells.

As already mentioned above, different oxidative stimuli, including EtOH[97] an high glucose[188], promoted angiogenesis in ARPE-19 cells. More concretely, OS increased EVs released from ARPE-19 cells, promoting these vascular changes[97,99]. Moreover, we demonstrated the effect of miR-205-5p/VEGFA regulation on vasculogenic processes induced by oxidative stimuli. OS is a common factor on retinal disorders such as DR and AMD, supporting the possibility that oxidative challenges on RPE lead to proliferative vascular responses found in AMD and DR.

Anti-VEGF administration is currently used to control neovascular processes in both wet AMD and DR[315]. Similarly, anti-VEGF therapies are also helpful against different forms of cancer, such as glioblastoma and colorectal cancer[316]. In agreement with this, miR-205-5p suppresses VEGFA expression in glioblastoma[251] and also inhibits the PI3K/AKT pathway[278]. In accordance with this, reducing VEGF-angiogenesis and PI3K/AKT could decrease tumor cell viability and proliferation. Thus, miR-205-5p could be considered as a plausible target against local vascular proliferative retinal processes. Moreover, increasing miR-205-5p levels could be beneficial for these ocular proliferative disorders not only by the direct anti-VEGFA blockade but also by the PI3K/AKT pathway interaction.

4. H_2O_2-sEVs influence

EVs are secreted by multiple cell types including RPE[97,261,262,317,318]. As mentioned before, different oxidative stimuli induce greater release of sEVs by ARPE-19 cells[97,188,261,262] confirming our results.

The sEVs have an important role on intercellular communication when transferring their cargo to the neighboring cells[319]. Among their cargo the sEVs carry miRNAs, as shown herein. The RPE sEVs are able to induce new blood vessels[97,99,188], communicate stress messages[320], modulate immune response[211] and inflammation[262]. After exposure of healthy ARPE-19 cells to sEVs released by ARPE-19 subject to OS, $H_2O_2$600 μM, it is observed that their cell viability is reduced to levels similar to those seen when directly treated with 600 μM H_2O_2. Besides, our results show that 600 μM H_2O_2 sEVs induces OS in healthy ARPE-19 cells in the same way as 600 μM H_2O_2 treatment levels. Therefore, sEVs released by stressed cells contribute to RPE dysfunction, matching with previous reports[320].

Angiogenic capacity is among the functions attributed to sEVs[188], partly thanks to the presence of VEGFR1 and VEGFR2 in stressed-sEVs[97]. Our results follow the same direction, noting that 600 μM H_2O_2 sEVs induce blood vessels formation, reaching similar levels as with direct exposure to 600 μM H_2O_2. Further, our results suggest that after 600 μM H_2O_2-sEVs exposure the VEGFA expression levels increase in recipient ARPE-19 cells. The sEVs cargo, including the sEVs-miRNAs observed in our study, could be involved in the regulation of VEGFA expression in the recipient cell inducing the angiogenic processes and therefore influencing the pathological state of the RPE. More research must be performed on sEVs-miRNAs to determine the concrete role of

these complex in the angiogenic processes and pathology of RPE and retinal disorders.

CONCLUSIONS

Conclusions

1. H_2O_2 exposure induces oxidative stress in ARPE-19 cells at concentrations above 600 μM. These cells are resistant to H_2O_2-induced-oxidative stress at 800 μM. Polarized ARPE-19 cells are more resistant to H_2O_2 exposure than non-polarized cells. 24 hours of 600 μM H_2O_2 exposure increases sEVs release on ARPE-19 cells.

2. ARPE-19 miRNA expression profilie shows a significant repression after H_2O_2 600 μM treatment: let-7a, miR-518d-3p, miR-521, miR-338-5p, miR-548b-5p, miR-205-5p and miR-302c-3p are under expressed in ARPE-19 cells exposed to H_2O_2 compared to control ARPE-19 cells.

3. There is a different miRNA expression profile on sEVs released by control ARPE-19 cells versus H_2O_2 treated ones: miR-302a-3p and miR-122-5p are under expressed in sEVs released by H_2O_2 treated ARPE-19 cells compared to sEVs released by control cells.

4. Pathway enrichment analysis points up that Cell miRNAs significantly underrepresented regulates genes involved in cell cycle, adherent junction, p53 signaling pathway, HIF-1 signaling pathway and cancer related pathways. Otherwise, sEVs miRNAs modulate characteristic pathways including TGF-beta signaling pathway, FoxO signaling pathway and cell cycle.

5. The functional enrichment analysis of the validated ARPE-19 miRNAs show interesting pathways dysregulated after H_2O_2 exposure. Specifically, the miR-205-5p includes positive regulation of endothelial cell migration and angiogenesis.

6. H_2O_2 induced oxidative stress decreases miR-205-5p expression in non-mature and mature ARPE-19 cells. The antioxidant N-Acetylcysteine normalize those decreased miR-205-5p levels, indicating that miR-205-5p is sensitive to oxidative stress.

7. Different targets related to vasculogenic processes are regulated by miR-205-5p. Among them the VEGFA, whose expression is regulated by miR-205-5p and oxidative stress. miR-205-5p overexpression decreases HUVEC tube formation by inhibiting VEGFA expression.

8. The sEVs released by H_2O_2-treated ARPE-19 cells promote changes in neighboring cells. ARPE-19 cells exposed to sEVs released by H_2O_2-treated ARPE-19 cells increased oxidative stress and reduce cell viability. These sEVs also induces HUVEC cell tube formation.

REFERENCES

References

1. Malhotra, A., Minja, F. J., Crum, A. & Burrowes, D. Ocular anatomy and cross-sectional imaging of the eye. *Semin. Ultrasound. CT. MR* **32**, 2–13 (2011).
2. Kels, B. D., Grzybowski, A. & Grant-Kels, J. M. Human ocular anatomy. *Clin. Dermatol.* **33**, 140–6
3. Hoon, M., Okawa, H., Della Santina, L. & Wong, R. O. Functional Architecture of the Retina: Development and Disease. (2014). doi:10.1016/j.preteyeres.2014.06.003
4. Joyce, C., Le, P. H. & Sadiq, N. M. *Histology, Retina. StatPearls* (2019).
5. Normal Retinal Anatomy - The Retina Reference. Available at: http://www.retinareference.com/anatomy/. (Accessed: 12th November 2019)
6. Jarrett, S. G. & Boulton, M. E. Consequences of oxidative stress in age-related macular degeneration. *Mol. Aspects Med.* **33**, 399–417 (2012).
7. Chen, Q., Niu, S., Yuan, S., Fan, W. & Liu, Q. Choroidal vasculature characteristics based choroid segmentation for enhanced depth imaging optical coherence tomography images. *Med. Phys.* **43**, 1649–1661 (2016).
8. Nickla, D. L. & Wallman, J. The multifunctional choroid. *Progress in Retinal and Eye Research* **29**, 144–168 (2010).
9. Tian, J., Marziliano, P., Baskaran, M., Tun, T. A. & Aung, T. Automatic segmentation of the choroid in enhanced depth imaging optical coherence tomography images. *Biomed. Opt. Express* **4**, 397–411 (2013).
10. Chiba, C. The retinal pigment epithelium: An important player of retinal disorders and regeneration. *Exp. Eye Res.* **123**, 107–114 (2014).
11. Marmorstein, A. D. The polarity of the retinal pigment epithelium. *Traffic* **2**, 867–872 (2001).
12. Rizzolo, L. J. Barrier properties of cultured retinal pigment epithelium. *Experimental Eye Research* **126**, 16–26 (2014).
13. Tarau, I.-S., Berlin, A., Curcio, C. A. & Ach, T. The Cytoskeleton of the Retinal Pigment Epithelium: from Normal Aging to Age-Related Macular Degeneration. *Int. J. Mol. Sci.* **20**, 3578 (2019).
14. Rotty, J. D. & Bear, J. E. Competition and collaboration between different actin assembly pathways allows for homeostatic control of the actin cytoskeleton. *Bioarchitecture*

5, 27–34 (2014).
15. Strauss, O., Introduction, I. & Strauss, O. The Retinal Pigment Epithelium in Visual Function. *Physiol. Rev.* **85**, 845–881 (2005).
16. Alm, A. & Bill, A. The Oxygen Supply to the Retina, I. Effects of Changes in Intraocular and Arterial Blood Pressures, and in Arterial PO2 and Pco2 on the Oxygen Tension in the Vitreous Body of the Cat. *Acta Physiol. Scand.* **84**, 261–274 (1972).
17. Bone, R. A. *et al.* Distribution of lutein and zeaxanthin stereoisomers in the human retina. *Exp. Eye Res.* **64**, 211–218 (1997).
18. Handelman, G. J., Dratz, E. A., Reay, C. C. & Van Kuijk, F. J. G. M. Carotenoids in the human macula and whole retina. *Investig. Ophthalmol. Vis. Sci.* **29**, 850–855 (1988).
19. Beatty, S., Koh, H., Phil, M., Henson, D. & Boulton, M. The role of oxidative stress in the pathogenesis of age-related macular degeneration. *Surv. Ophthalmol.* **45**, 115–34 (2000).
20. Caceres, P. S. & Rodriguez-Boulan, E. Retinal pigment epithelium polarity in health and blinding diseases. *Curr. Opin. Cell Biol.* **62**, 37–45 (2020).
21. Liu, Y., Zhang, D., Wu, Y. & Ji, B. Docosahexaenoic acid aggravates photooxidative damage in retinal pigment epithelial cells via lipid peroxidation. *J. Photochem. Photobiol. B Biol.* **140**, 85–93 (2014).
22. Kumar, A., Pandey, R. K., Miller, L. J., Singh, P. K. & Kanwar, M. Müller glia in retinal innate immunity: A perspective on their roles in endophthalmitis. *Crit. Rev. Immunol.* **33**, 119–135 (2013).
23. Bringmann, A. *et al.* Müller cells in the healthy and diseased retina. *Progress in Retinal and Eye Research* **25**, 397–424 (2006).
24. Bringmann, A. *et al.* Cellular signaling and factors involved in Müller cell gliosis: Neuroprotective and detrimental effects. *Progress in Retinal and Eye Research* **28**, 423–451 (2009).
25. Coorey, N. J., Shen, W., Chung, S. H., Zhu, L. & Gillies, M. C. The role of glia in retinal vascular disease. *Clinical and Experimental Optometry* **95**, 266–281 (2012).
26. Abbott, N. J., Rönnbäck, L. & Hansson, E. Astrocyte-endothelial interactions at the blood-brain barrier. *Nature Reviews Neuroscience* **7**, 41–53 (2006).
27. Li, L., Eter, N. & Heiduschka, P. The microglia in healthy and diseased retina. *Experimental Eye Research* **136**, 116–130

(2015).
28. Langmann, T. Microglia activation in retinal degeneration. *J. Leukoc. Biol.* **81**, 1345–1351 (2007).
29. Grossniklaus, H. E., Geisert, E. E. & Nickerson, J. M. Introduction to the Retina. in *Progress in Molecular Biology and Translational Science* **134**, 383–396 (Elsevier B.V., 2015).
30. Rando, R. R. The biochemistry of the visual cycle. *Chemical Reviews* **101**, 1881–1896 (2001).
31. Wright, C. B., Redmond, T. M. & Nickerson, J. M. A History of the Classical Visual Cycle. in *Progress in Molecular Biology and Translational Science* **134**, 433–448 (Elsevier B.V., 2015).
32. Gordon, W. C., Rodriguez de Turco, E. B. & Bazan, N. G. Retinal pigment epithelial cells play a central role in the conservation of docosahexaenoic acid by photoreceptor cells after shedding and phagocytosis. *Curr. Eye Res.* **11**, 73–83 (1992).
33. Nguyen-Legros, J. & Hicks, D. Renewal of photoreceptor outer segments and their phagocytosis by the retinal pigment epithelium. *International Review of Cytology* **196**, 245–313 (2000).
34. Strauss, O. The retinal pigment epithelium in visual function. *Physiological Reviews* **85**, 845–881 (2005).
35. Ponnalagu, M., Subramani, M., Jayadev, C., Shetty, R. & Das, D. Retinal pigment epithelium-secretome: A diabetic retinopathy perspective. *Cytokine* **95**, 126–135 (2017).
36. Vranka, J. A. *et al.* Discrete expression and distribution pattern of TIMP-3 in the human retina and choroid. *Curr. Eye Res.* **16**, 102–110 (1997).
37. Guo, L., Hussain, A. A., Limb, G. A. & Marshall, J. Age-dependent variation in metalloproteinase activity of isolated human Bruch's membrane and choroid. *Invest. Ophthalmol. Vis. Sci.* **40**, 2676–82 (1999).
38. Padgett, L. C., Lui, G. M., Werb, Z. & Lavail, M. M. Matrix metalloproteinase-2 and tissue inhibitor of metalloproteinase-1 in the retinal pigment epithelium and interphotoreceptor matrix: Vectorial secretion and regulation. *Exp. Eye Res.* **64**, 927–938 (1997).
39. Chung, C. *et al.* Ethanol Exposure Depletes Hepatic Pigment Epithelium-Derived Factor, a Novel Lipid Regulator. *Gastroenterology* **136**, (2009).
40. Bandyopadhyay, M. & Rohrer, B. Matrix metalloproteinase activity creates pro-angiogenic environment in primary human

retinal pigment epithelial cells exposed to complement. *Invest. Ophthalmol. Vis. Sci.* **53**, 1953–1961 (2012).
41. Kernt, M. *et al.* Indocyanine green increases light-induced oxidative stress, senescence, and matrix metalloproteinases 1 and 3 in human RPE cells. *Acta Ophthalmol.* **90**, 571–579 (2012).
42. Hoffmann, S. *et al.* MMP-2 and MMP-9 Ssecretion by RPE is stimulated by angiogenic molecules found in choroidal neovascular membranes. *Retina* **26**, 454–461 (2006).
43. Sreekumar, P. G. *et al.* αB crystallin is apically secreted within exosomes by polarized human retinal pigment epithelium and provides neuroprotection to adjacent cells. *PLoS One* **5**, (2010).
44. Cayouette, M., Smith, S. B., Becerra, S. P. & Gravel, C. Pigment epithelium-derived factor delays the death of photoreceptors in mouse models of inherited retinal degenerations. *Neurobiol. Dis.* **6**, 523–532 (1999).
45. Kay, P., Yang, Y. C. & Paraoan, L. Directional protein secretion by the retinal pigment epithelium: Roles in retinal health and the development of age-related macular degeneration. *J. Cell. Mol. Med.* **17**, 833–843 (2013).
46. Dunn, K. C. *et al.* Use of the ARPE-19 cell line as a model of RPE polarity: Basolateral secretion of FGF5. *Investig. Ophthalmol. Vis. Sci.* **39**, 2744–2749 (1998).
47. Narayan, S., Brun, A. M. & Yorio, T. Endothelin-1 distribution and basolateral secretion in the retinal pigment epithelium. *Exp. Eye Res.* **79**, 11–19 (2004).
48. Wong, W. L. *et al.* Global prevalence of age-related macular degeneration and disease burden projection for 2020 and 2040: A systematic review and meta-analysis. *Lancet Glob. Heal.* **2**, (2014).
49. Lim, L. S., Mitchell, P., Seddon, J. M., Holz, F. G. & Wong, T. Y. Age-related macular degeneration. *Lancet* **379**, 1728–1738 (2012).
50. Ferris, F. L. *et al.* Clinical classification of age-related macular degeneration. *Ophthalmology* **120**, 844–851 (2013).
51. Mitchell, P., Liew, G., Gopinath, B. & Wong, T. Y. Age-related macular degeneration. *The Lancet* **392**, 1147–1159 (2018).
52. A, G., L, M. & O, M. AGE-RELATED MACULAR DEGENERATION. *Rom. J. Ophthalmol.* **59**, (2015).
53. Kersten, E. *et al.* Systemic and ocular fluid compounds as potential biomarkers in age-related macular degeneration. *Survey of Ophthalmology* **63**, 9–39 (2018).

54. Lambert, N. G. *et al.* Risk factors and biomarkers of age-related macular degeneration. *Progress in Retinal and Eye Research* **54**, 64–102 (2016).
55. Rosenfeld, P. J. *et al.* Ranibizumab for neovascular age-related macular degeneration. *N. Engl. J. Med.* **355**, 1419–1431 (2006).
56. Michels, S., Rosenfeld, P. J., Puliafito, C. A., Marcus, E. N. & Venkatraman, A. S. Systemic bevacizumab (Avastin) therapy for neovascular age-related macular degeneration: Twelve-week results of an uncontrolled open-label clinical study. *Ophthalmology* **112**, 1035-1047.e9 (2005).
57. Apte, R. S., Chen, D. S. & Ferrara, N. VEGF in Signaling and Disease: Beyond Discovery and Development. *Cell* **176**, 1248–1264 (2019).
58. Ferrara, N. & Adamis, A. P. Ten years of anti-vascular endothelial growth factor therapy. *Nature Reviews Drug Discovery* **15**, 385–403 (2016).
59. Semenza, G. L. HIF-1: Mediator of physiological and pathophysiological responses to hypoxia. *Journal of Applied Physiology* **88**, 1474–1480 (2000).
60. Li, X. *et al.* Reevaluation of the role of VEGF-B suggests a restricted role in the revascularization of the ischemic myocardium. *Arterioscler. Thromb. Vasc. Biol.* **28**, 1614–1620 (2008).
61. Carmeliet, P. *et al.* Synergism between vascular endothelial growth factor and placental growth factor contributes to angiogenesis and plasma extravasation in pathological conditions. *Nat. Med.* **7**, 575–583 (2001).
62. Ferrara, N. Binding to the extracellular matrix and proteolytic processing: Two key mechanisms regulating vascular endothelial growth factor action. *Mol. Biol. Cell* **21**, 687–690 (2010).
63. Smith, G. A. *et al.* Vascular endothelial growth factors: multitasking functionality in metabolism, health and disease. *Journal of Inherited Metabolic Disease* **38**, 753–763 (2015).
64. Sakurai, Y., Ohgimoto, K., Kataoka, Y., Yoshida, N. & Shibuya, M. Essential role of Flk-1 (VEGF receptor 2) tyrosine residue 1173 in vasculogenesis in mice. *Proc. Natl. Acad. Sci. U. S. A.* **102**, 1076–1081 (2005).
65. De Vries, C. *et al.* The fms-like tyrosine kinase, a receptor for vascular endothelial growth factor. *Science (80-.).* **255**, 989–991 (1992).
66. Robinson, C. J. & Stringer, S. E. The splice variants of vascular

endothelial growth factor (VEGF) and their receptors. *J. Cell Sci.* **114**, 853–865 (2001).
67. Okabe, K. *et al.* Neurons limit angiogenesis by titrating VEGF in retina. *Cell* **159**, 584–596 (2014).
68. Cai, J. *et al.* Activation of Vascular Endothelial Growth Factor Receptor-1 Sustains Angiogenesis and Bcl-2 Expression Via the Phosphatidylinositol 3-Kinase Pathway in Endothelial Cells. *Diabetes* **52**, 2959–2968 (2003).
69. Roskoski, R. Vascular endothelial growth factor (VEGF) signaling in tumor progression. *Critical Reviews in Oncology/Hematology* **62**, 179–213 (2007).
70. Raikwar, N. S., Liu, K. Z. & Thomas, C. P. Protein kinase C regulates FLT1 abundance and stimulates its cleavage in vascular endothelial cells with the release of a soluble PlGF/VEGF antagonist. *Exp. Cell Res.* **319**, 2578–2587 (2013).
71. Fearnley, G. W. *et al.* VEGF-A isoforms differentially regulate ATF-2-dependent VCAM-1 gene expression and endothelial-leukocyte interactions. *Mol. Biol. Cell* **25**, 2509–2521 (2014).
72. Lamalice, L., Houle, F. & Huot, J. Phosphorylation of Tyr 1214 within VEGFR-2 triggers the recruitment of Nck and activation of Fyn leading to SAPK2/p38 activation and endothelial cell migration in response to VEGF. *J. Biol. Chem.* **281**, 34009–34020 (2006).
73. Macosko, E. Z. *et al.* Highly parallel genome-wide expression profiling of individual cells using nanoliter droplets. *Cell* **161**, 1202–1214 (2015).
74. Wechsler-Reya, R. J. & Barres, B. A. Retinal development: Communication helps you see the light. *Curr. Biol.* **7**, R433–R436 (1997).
75. Olsson, A. K., Dimberg, A., Kreuger, J. & Claesson-Welsh, L. VEGF receptor signalling - In control of vascular function. *Nature Reviews Molecular Cell Biology* **7**, 359–371 (2006).
76. Jager, R. D., Mieler, W. F. & Miller, J. W. Age-related macular degeneration. *New England Journal of Medicine* **358**, 2606 (2008).
77. Miller, J. W., Le Couter, J., Strauss, E. C. & Ferrara, N. Vascular endothelial growth factor a in intraocular vascular disease. *Ophthalmology* **120**, 106–114 (2013).
78. Sene, A., Chin-Yee, D. & Apte, R. S. Seeing through VEGF: Innate and adaptive immunity in pathological angiogenesis in the eye. *Trends in Molecular Medicine* **21**, 43–51 (2015).
79. Heesterbeek, T. J., Lorés-Motta, L., Hoyng, C. B., Lechanteur,

Y. T. E. & den Hollander, A. I. Risk factors for progression of age-related macular degeneration. *Ophthalmic Physiol. Opt.* (2020). doi:10.1111/opo.12675

80. Cai, J., Nelson, K. C., Wu, M., Sternberg, P. & Jones, D. P. Oxidative damage and protection of the RPE. *Progress in Retinal and Eye Research* **19**, 205–221 (2000).
81. Bellezza, I., Giambanco, I., Minelli, A. & Donato, R. Nrf2-Keap1 signaling in oxidative and reductive stress. *Biochimica et Biophysica Acta - Molecular Cell Research* **1865**, 721–733 (2018).
82. Bellezza, I. Oxidative Stress in Age-Related Macular Degeneration: Nrf2 as Therapeutic Target. *Front. Pharmacol.* **9**, 1280 (2018).
83. Holmström, K. M. & Finkel, T. Cellular mechanisms and physiological consequences of redox-dependent signalling. *Nature Reviews Molecular Cell Biology* **15**, 411–421 (2014).
84. Birben, E., Sahiner, U. M., Sackesen, C., Erzurum, S. & Kalayci, O. Oxidative stress and antioxidant defense. *World Allergy Organization Journal* **5**, 9–19 (2012).
85. Lin, H. *et al.* Mitochondrial DNA damage and repair in rpe associated with aging and age-related macular degeneration. *Investig. Ophthalmol. Vis. Sci.* **52**, 3521–3529 (2011).
86. Desouki, M. M., Kulawiec, M., Bansal, S., Das, G. & Singh, K. K. Cross talk between mitochondria and superoxide generating NADPH oxidase in breast and ovarian tumors. *Cancer Biol. Ther.* **4**, 1367–1373 (2005).
87. Elizabeth Hartnett, M. The effects of oxygen stresses on the development of features of severe retinopathy of prematurity: Knowledge from the 50/10 OIR model. *Documenta Ophthalmologica* **120**, 25–39 (2010).
88. Braca, A. *et al.* Triterpene Derivatives as Inhibitors of Protein Involved in the Inflammatory Process: Molecules Interfering with Phospholipase A2, Cycloxygenase, and Lipoxygenase. *Curr. Drug Targets* **12**, 302–321 (2012).
89. Kruft I, B. & Greer, A. Photosensitization Reactions In Vitro and In Vivo. *Bone* **23**, 1–7 (2008).
90. Wadhwa, R., Gupta, R. & Maurya, P. K. Oxidative Stress and Accelerated Aging in Neurodegenerative and Neuropsychiatric Disorder. *Curr. Pharm. Des.* **24**, 4711–4725 (2019).
91. A, A., MF, M. & S, A. Lipid Peroxidation: Production, Metabolism, and Signaling Mechanisms of Malondialdehyde and 4-hydroxy-2-nonenal. *Oxid. Med. Cell. Longev.* **2014**,

(2014).
92. Flores-Bellver, M. *et al.* Autophagy and mitochondrial alterations in human retinal pigment epithelial cells induced by ethanol: Implications of 4-hydroxy-nonenal. *Cell Death Dis.* **5**, e1328-13 (2014).
93. Beatty, S., Koh, H.-H., Phil, M., Henson, D. & Boulton, M. The Role of Oxidative Stress in the Pathogenesis of Age-Related Macular Degeneration. *Surv. Ophthalmol.* **45**, 115–134 (2000).
94. Tangvarasittichai, O. & Tangvarasittichai, S. Oxidative Stress, Ocular Disease and Diabetes Retinopathy. *Curr. Pharm. Des.* **24**, 4726–4741 (2019).
95. Datta, S., Cano, M., Ebrahimi, K., Wang, L. & Handa, J. T. The impact of oxidative stress and inflammation on RPE degeneration in non-neovascular AMD. *Progress in Retinal and Eye Research* **60**, 201–218 (2017).
96. Ashton, N. Oxygen and the growth and development of retinal vessels. In vivo and in vitro studies The XX Francis I. Proctor Lecture. *Am. J. Ophthalmol.* **62**, 412–435 (1966).
97. Atienzar-Aroca, S. *et al.* Oxidative stress in retinal pigment epithelium cells increases exosome secretion and promotes angiogenesis in endothelial cells. *J. Cell. Mol. Med.* **20**, 1457–1466 (2016).
98. Simão, S., Santos, D. F. & Silva, G. A. Aliskiren decreases oxidative stress and angiogenic markers in retinal pigment epithelium cells. *Angiogenesis* **20**, 175–181 (2017).
99. Atienzar-Aroca, S. *et al.* Role of retinal pigment epithelium-derived exosomes and autophagy in new blood vessel formation. *J. Cell. Mol. Med.* **22**, 5244–5256 (2018).
100. Marneros, A. G. Increased VEGF-A promotes multiple distinct aging diseases of the eye through shared pathomechanisms. *EMBO Mol. Med.* **8**, 208–231 (2016).
101. Marazita, M. C., Dugour, A., Marquioni-Ramella, M. D., Figueroa, J. M. & Suburo, A. M. Oxidative stress-induced premature senescence dysregulates VEGF and CFH expression in retinal pigment epithelial cells: Implications for Age-related Macular Degeneration. *Redox Biol.* **7**, 78–87 (2016).
102. Dong, A. *et al.* Oxidative stress promotes ocular neovascularization. *J. Cell. Physiol.* **219**, 544–552 (2009).
103. Smith, L. E. H. Pathogenesis of retinopathy of prematurity. *Seminars in Neonatology* **8**, 469–473 (2003).
104. Maher, E. R., Neumann, H. P. H. & Richard, S. Von Hippel-Lindau disease: A clinical and scientific review. *European*

Journal of Human Genetics **19**, 617–623 (2011).
105. Aldini, G. *et al.* N-Acetylcysteine as an antioxidant and disulphide breaking agent: the reasons why. *Free Radical Research* **52**, 751–762 (2018).
106. Suman, S. & Shukla, Y. Diallyl sulfide and its role in chronic diseases prevention. in *Advances in Experimental Medicine and Biology* **929**, 127–144 (Springer New York LLC, 2016).
107. Mateos, M. V, Tenconi, P. E., Giusto, N. M. & Salvador, G. A. *Inflammation and Oxidative Stress in Retinal Diseases: The Role of Intracellular Signaling in the Retinal Pigment Epithelium*. *Int J Ophthalmol Clin Res* **2**, (2015).
108. Qiu, Y. *et al.* Downregulating p22phox ameliorates inflammatory response in Angiotensin II-induced oxidative stress by regulating MAPK and NF- B pathways in ARPE-19 cells. *Sci. Rep.* **5**, (2015).
109. Faghiri, Z. & Bazan, N. G. PI3K/Akt and mTOR/p70S6K pathways mediate neuroprotectin D1-induced retinal pigment epithelial cell survival during oxidative stress-induced apoptosis. *Exp. Eye Res.* **90**, 718–725 (2010).
110. Song, C. *et al.* Oxidative stress-mediated NFeκB phosphorylation upregulates p62/SQSTM1 and promotes retinal pigmented epithelial cell survival through increased autophagy. *PLoS One* **12**, 1–26 (2017).
111. Ho, T. C. *et al.* Activation of mitogen-activated protein kinases is essential for hydrogen peroxide -induced apoptosis in retinal pigment epithelial cells. *Apoptosis* **11**, 1899–1908 (2006).
112. Sharma, A. *et al.* 4-Hydroxynonenal induces p53-mediated apoptosis in retinal pigment epithelial cells. *Arch. Biochem. Biophys.* **480**, 85–94 (2008).
113. Bonet-Ponce, L. *et al.* On the mechanism underlying ethanol-induced mitochondrial dynamic disruption and autophagy response. *Biochim. Biophys. Acta* **1852**, 1400–9 (2015).
114. Bhaskaran, M. & Mohan, M. MicroRNAs: history, biogenesis, and their evolving role in animal development and disease. *Vet. Pathol.* **51**, 759–74 (2014).
115. Kumar, S., Vijayan, M., Bhatti, J. S. & Reddy, P. H. MicroRNAs as Peripheral Biomarkers in Aging and Age-Related Diseases. in *Progress in molecular biology and translational science* **146**, 47–94 (2017).
116. Wang, L. *et al.* MicroRNA-182 Suppresses HGF/SF-Induced Increases in Retinal Pigment Epithelial Cell Proliferation and Migration through Targeting c-Met. *PLoS One* **11**, e0167684

(2016).
117. Tasharrofi, N. *et al.* Survival Improvement in Human Retinal Pigment Epithelial Cells via Fas Receptor Targeting by miR-374a. *J. Cell. Biochem.* **118**, 4854–4861 (2017).
118. Hao, Y., Zhou, Q., Ma, J., Zhao, Y. & Wang, S. miR-146a is Upregulated During Retinal Pigment Epithelium (RPE)/Choroid Aging in Mice and Represses IL-6 and VEGF-A Expression in RPE Cells. *J. Clin. Exp. Ophthalmol.* **7**, (2016).
119. Zhou, Q. *et al.* Regulation of angiogenesis and choroidal neovascularization by members of microRNA-23~27~24 clusters. *Proc. Natl. Acad. Sci. U. S. A.* **108**, 8287–92 (2011).
120. Lin, H. *et al.* Effect of miR-23 on Oxidant-Induced Injury in Human Retinal Pigment Epithelial Cells. *Investig. Opthalmology Vis. Sci.* **52**, 6308 (2011).
121. He, J.-F., Du, Y., Jiang, B.-L. & He, J.-F. Increased microRNA-155 and decreased microRNA-146a may promote ocular inflammation and proliferation in Graves' ophthalmopathy. *Med. Sci. Monit.* **20**, 639–643 (2014).
122. Ying, S.-Y., Chang, D. C. & Lin, S.-L. The MicroRNA. in 1–25 (2018). doi:10.1007/978-1-4939-7601-0_1
123. Ménard, C. *et al.* MicroRNA signatures in vitreous humour and plasma of patients with exudative AMD. *Oncotarget* **7**, 19171–19184 (2016).
124. Szemraj, M. *et al.* Serum MicroRNAs as Potential Biomarkers of AMD. *Med. Sci. Monit.* **21**, 2734–2742 (2015).
125. Elshelmani, H. & Rani, S. Exosomal microRNA discovery in age-related macular degeneration. in *Methods in Molecular Biology* **1509**, 93–113 (Humana Press Inc., 2017).
126. Bartel, D. P. MicroRNAs: genomics, biogenesis, mechanism, and function. *Cell* **116**, 281–97 (2004).
127. Tran, N. & Hutvagner, G. Biogenesis and the regulation of the maturation of miRNAs. *Essays Biochem.* **54**, 17–28 (2013).
128. Yi, R., Qin, Y., Macara, I. G. & Cullen, B. R. Exportin-5 mediates the nuclear export of pre-microRNAs and short hairpin RNAs. *Genes Dev.* **17**, 3011–6 (2003).
129. Djuranovic, S., Nahvi, A. & Green, R. miRNA-Mediated Gene Silencing by Translational Repression Followed by mRNA Deadenylation and Decay. *Science (80-.).* **336**, 237–240 (2012).
130. Hutvágner, G. & Zamore, P. D. A microRNA in a multiple-turnover RNAi enzyme complex. *Science (80-.).* **297**, 2056–2060 (2002).
131. Lytle, J. R., Yario, T. A. & Steitz, J. A. Target mRNAs are

repressed as efficiently by microRNA-binding sites in the 5′ UTR as in the 3′ UTR. *Proc. Natl. Acad. Sci. U. S. A.* **104**, 9667–9672 (2007).
132. Saini, H. K., Griffiths-Jones, S. & Enright, A. J. Genomic analysis of human microRNA transcripts. *Proc. Natl. Acad. Sci.* **104**, 17719–17724 (2007).
133. Elbay, A., Ercan, Ç., Akbaş, F., Bulut, H. & Ozdemir, H. Three new circulating microRNAs may be associated with wet age-related macular degeneration. *Scand. J. Clin. Lab. Invest.* 1–7 (2019). doi:10.1080/00365513.2019.1637931
134. Mulrane, L., Mcgee, S. F., Gallagher, W. M. & O'connor, D. P. miRNA Dysregulation in Breast Cancer. (2013). doi:10.1158/0008-5472.CAN-13-1841
135. Londin, E. *et al.* Analysis of 13 cell types reveals evidence for the expression of numerous novel primate- and tissue-specific microRNAs. (2015). doi:10.1073/pnas.1420955112
136. Karali, M. *et al.* High-resolution analysis of the human retina miRNome reveals isomiR variations and novel microRNAs. *Nucleic Acids Res.* **44**, 1525–1540 (2016).
137. Ren, C. *et al.* Circulating miRNAs as potential biomarkers of age-related macular degeneration. *Cell. Physiol. Biochem.* **41**, 1413–1423 (2017).
138. Ertekin, S. *et al.* Evaluation of circulating miRNAs in wet age-related macular degeneration. *Mol. Vis.* **20**, 1057–1066 (2014).
139. Romano, G. L. *et al.* Retinal and Circulating miRNAs in Age-Related Macular Degeneration: An In vivo Animal and Human Study. *Front. Pharmacol.* **8**, 168 (2017).
140. Grassmann, F. *et al.* A circulating MicroRNA profile is associated with late- stage neovascular age-related macular degeneration. *PLoS One* **9**, 1–8 (2014).
141. Lambert, V. *et al.* Laser-induced choroidal neovascularization model to study age-related macular degeneration in mice. *Nat. Protoc.* **8**, 2197–2211 (2013).
142. Yan, L. *et al.* Single and compound knock-outs of microRNA (miRNA)-155 and its angiogenic gene target CCN7 in mice alter vascular and neovascular growth in the retina via resident microglia. *J. Biol. Chem.* **290**, 23264–23281 (2015).
143. Bhattacharjee, S., Zhao, Y., Dua, P., Rogaev, E. I. & Lukiw, W. J. microRNA-34a-Mediated Down-Regulation of the Microglial-Enriched Triggering Receptor and Phagocytosis-Sensor TREM2 in Age-Related Macular Degeneration. *PLoS One* **11**, e0150211 (2016).

144. Loscher, C. J. *et al.* Altered retinal microRNA expression profile in a mouse model of retinitis pigmentosa. *Genome Biol.* **8**, R248 (2007).
145. Gong, Q. & Su, G. Roles of miRNAs and long noncoding RNAs in the progression of diabetic retinopathy. *Bioscience Reports* **37**, (2017).
146. Ayaz, L. & Dinç, E. Evaluation of microRNA responses in ARPE-19 cells against the oxidative stress. *Cutan. Ocul. Toxicol.* **37**, 121–126 (2018).
147. Dinç, E., Ayaz, L. & Kurt, A. H. Effects of Bevacizumab, Ranibizumab, and Aflibercept on MicroRNA Expression in a Retinal Pigment Epithelium Cell Culture Model of Oxidative Stress. *J. Ocul. Pharmacol. Ther.* **34**, 1–8 (2018).
148. Howell, J. C. *et al.* Global microRNA expression profiling: curcumin (diferuloylmethane) alters oxidative stress-responsive microRNAs in human ARPE-19 cells. *Mol. Vis.* **19**, 544–60 (2013).
149. Haque, R. *et al.* MicroRNA-30b-Mediated Regulation of Catalase Expression in Human ARPE-19 Cells. *PLoS One* **7**, e42542 (2012).
150. Tian, B. *et al.* miR-17-3p Exacerbates Oxidative Damage in human Retinal Pigment Epithelial Cells. **11**, e0160887 (2016).
151. Li, D. dan *et al.* Inhibition of the oxidative stress-induced miR-23a protects the human retinal pigment epithelium (RPE) cells from apoptosis through the upregulation of glutaminase and glutamine uptake. *Mol. Biol. Rep.* **43**, 1079–1087 (2016).
152. Murad, N. *et al.* MiR-184 regulates ezrin, LAMP-1 expression, affects phagocytosis in human retinal pigment epithelium and is downregulated in age-related macular degeneration. *FEBS J.* **281**, 5251–5264 (2014).
153. Wang, J. *et al.* miR-365 promotes diabetic retinopathy through inhibiting Timp3 and increasing oxidative stress. *Exp. Eye Res.* **168**, 89–99 (2018).
154. Zhang, R. *et al.* Upregulation of miR-195 accelerates oxidative stress-induced retinal endothelial cell injury by targeting mitofusin 2 in diabetic rats. *Mol. Cell. Endocrinol.* **452**, 33–43 (2017).
155. Donato, L. *et al.* miRNAexpression profile of retinal pigment epithelial cells under oxidative stress conditions. *FEBS Open Bio* **8**, 219–233 (2018).
156. Cheng, L. B. *et al.* miRNA-141 attenuates UV-induced oxidative stress via activating Keap1-Nrf2 signaling in human

retinal pigment epithelium cells and retinal ganglion cells. *Oncotarget* **8**, 13186–13194 (2017).
157. Kutty, R. K. *et al.* MicroRNA expression in human retinal pigment epithelial (ARPE-19) cells: increased expression of microRNA-9 by N-(4-hydroxyphenyl)retinamide. *Mol. Vis.* **16**, 1475–86 (2010).
158. Zhang, Q. L. *et al.* Down-regulated miR-187 promotes oxidative stress-induced retinal cell apoptosis through P2X7 receptor. *Int. J. Biol. Macromol.* **120**, 801–810 (2018).
159. Hui, Y. & Yin, Y. MicroRNA-145 attenuates high glucose-induced oxidative stress and inflammation in retinal endothelial cells through regulating TLR4/NF-κB signaling. *Life Sci.* **207**, 212–218 (2018).
160. Cai, J., Zhang, H., Zhang, Y. feng, Zhou, Z. & Wu, S. MicroRNA-29 enhances autophagy and cleanses exogenous mutant αB-crystallin in retinal pigment epithelial cells. *Exp. Cell Res.* **374**, 231–248 (2019).
161. Wang, S., Koster, K. M., He, Y. & Zhou, Q. miRNAs as potential therapeutic targets for age-related macular degeneration. *Future Med. Chem.* **4**, 277–287 (2012).
162. Wang, Y. *et al.* MiR-122 targets VEGFC in bladder cancer to inhibit tumor growth and angiogenesis. *Am. J. Transl. Res.* **8**, 3056–3066 (2016).
163. Liu, F. *et al.* MiR-203 contributes to pre-eclampsia via inhibition of VEGFA expression. *Mol. Med. Rep.* **17**, 5627–5634 (2018).
164. Li, Y., Zhao, L., Qi, Y. & Yang, X. MicroRNA-214 upregulates HIF-1α and VEGF by targeting ING4 in lung cancer cells. *Mol. Med. Rep.* **19**, 4935–4945 (2019).
165. Lu, Y. *et al.* MicroRNA-140-5p inhibits invasion and angiogenesis through targeting VEGF-A in breast cancer. *Cancer Gene Ther.* **24**, 386–392 (2017).
166. Zhou, Q. *et al.* Repression of choroidal neovascularization through actin cytoskeleton pathways by MicroRNA-24. *Mol. Ther.* **22**, 378–389 (2014).
167. Shen, J. *et al.* MicroRNAs Regulate Ocular Neovascularization. *Mol. Ther.* **16**, 1208–1216 (2008).
168. Yoon, C. *et al.* MiR-9 regulates the post-transcriptional level of VEGF165a by targeting SRPK-1 in ARPE-19 cells. *Graefe's Arch. Clin. Exp. Ophthalmol.* **252**, 1369–1376 (2014).
169. Chen, N. *et al.* MicroRNA-410 reduces the expression of vascular endothelial growth factor and inhibits oxygen-induced

retinal neovascularization. *PLoS One* **9**, (2014).
170. Nunes, D. N. *et al.* Synchronous down-modulation of miR-17 family members is an early causative event in the retinal angiogenic switch. *Proc. Natl. Acad. Sci. U. S. A.* **112**, 3770–3775 (2015).
171. Liu, C.-H. *et al.* Endothelial microRNA-150 is an intrinsic suppressor of pathologic ocular neovascularization. doi:10.1073/pnas.1508426112
172. Wang, S. *et al.* The Endothelial-Specific MicroRNA miR-126 Governs Vascular Integrity and Angiogenesis. *Dev. Cell* **15**, 261–271 (2008).
173. Hunter, M. P. *et al.* Detection of microRNA Expression in Human Peripheral Blood Microvesicles. *PLoS One* **3**, e3694 (2008).
174. Zhu, H. & Fan, G. C. Role of microRNAs in the reperfused myocardium towards post-infarct remodelling. *Cardiovasc. Res.* **94**, 284–292 (2012).
175. Wu, S. Y. *et al.* A miR-192-EGR1-HOXB9 regulatory network controls the angiogenic switch in cancer. *Nat. Commun.* **7**, (2016).
176. Kottakis, F. *et al.* FGF-2 Regulates Cell Proliferation, Migration, and Angiogenesis through an NDY1/KDM2B-miR-101-EZH2 Pathway. *Mol. Cell* **43**, 285–298 (2011).
177. Tiwari, A., Mukherjee, B. & Dixit, M. MicroRNA Key to Angiogenesis Regulation: MiRNA Biology and Therapy. *Curr. Cancer Drug Targets* **18**, 266–277 (2017).
178. Raposo, G. & Stoorvogel, W. Extracellular vesicles: Exosomes, microvesicles, and friends. *J. Cell Biol.* **200**, 373–383 (2013).
179. Ha, D., Yang, N. & Nadithe, V. Exosomes as therapeutic drug carriers and delivery vehicles across biological membranes: current perspectives and future challenges. *Acta Pharm. Sin. B* **6**, 287–296 (2016).
180. You, Y. & Ikezu, T. Emerging roles of extracellular vesicles in neurodegenerative disorders. *Neurobiol. Dis.* 104512 (2019). doi:10.1016/j.nbd.2019.104512
181. Thompson, A. G. *et al.* Extracellular vesicles in neurodegenerative disease — pathogenesis to biomarkers. *Nat. Rev. Neurol.* **12**, 346–357 (2016).
182. Valadi, H. *et al.* Exosome-mediated transfer of mRNAs and microRNAs is a novel mechanism of genetic exchange between cells. *Nat. Cell Biol.* **9**, 654–9 (2007).
183. Jiang, L., Gu, Y., Du, Y. & Liu, J. Exosomes: diagnostic

biomarkers and therapeutic delivery vehicles for cancer. *Mol. Pharm.* acs.molpharmaceut.9b00409 (2019). doi:10.1021/acs.molpharmaceut.9b00409

184. Mol, E. A., Goumans, M.-J., Doevendans, P. A., Sluijter, J. P. G. & Vader, P. Higher functionality of extracellular vesicles isolated using size-exclusion chromatography compared to ultracentrifugation. *Nanomedicine* **13**, 2061–2065 (2017).
185. Henne, W. M., Buchkovich, N. J. & Emr, S. D. The ESCRT Pathway. *Dev. Cell* **21**, 77–91 (2011).
186. Stenmark, H. Rab GTPases as coordinators of vesicle traffic. *Nat. Rev. Mol. Cell Biol.* **10**, 513–25 (2009).
187. Greening, D. W. & Simpson, R. J. Understanding extracellular vesicle diversity – current status. *Expert Rev. Proteomics* **15**, 887–910 (2018).
188. Maisto, R. *et al.* ARPE-19-derived VEGF-containing exosomes promote neovascularization in HUVEC: the role of the melanocortin receptor 5 has been built and requires approval. *Cell Cycle* (2019).
189. Xu, H., Jia, S. & Xu, H. Therapeutic potential of exosomes in autoimmune diseases. *Clin. Immunol.* (2019). doi:10.1016/j.clim.2019.06.006
190. Zhang, S. *et al.* MSC exosomes mediate cartilage repair by enhancing proliferation, attenuating apoptosis and modulating immune reactivity. *Biomaterials* **156**, 16–27 (2018).
191. Harada, T. *et al.* Wnt5b-associated exosomes promote cancer cell migration and proliferation. *Cancer Sci.* **108**, 42–52 (2017).
192. Hou, J., Wang, F., Liu, X., Song, M. & Yin, X. Tumor-derived exosomes enhance invasion and metastasis of salivary adenoid cystic carcinoma cells. *J. Oral Pathol. Med.* **47**, 144–151 (2018).
193. van Niel, G., D'Angelo, G. & Raposo, G. Shedding light on the cell biology of extracellular vesicles. *Nat. Rev. Mol. Cell Biol.* **19**, 213–228 (2018).
194. Atkin-Smith, G. K. *et al.* A novel mechanism of generating extracellular vesicles during apoptosis via a beads-on-a-string membrane structure. *Nat. Commun.* **6**, 7439 (2015).
195. Théry, C. *et al.* Minimal information for studies of extracellular vesicles 2018 (MISEV2018): a position statement of the International Society for Extracellular Vesicles and update of the MISEV2014 guidelines. *J. Extracell. vesicles* **7**, 1535750 (2018).
196. Johnstone, R. M., Mathew, A., Mason, A. B. & Teng, K.

Exosome formation during maturation of mammalian and avian reticulocytes: Evidence that exosome release is a major route for externalization of obsolete membrane proteins. *J. Cell. Physiol.* **147**, 27–36 (1991).
197. Yang, X., Weng, Z., Mendrick, D. L. & Shi, Q. Circulating extracellular vesicles as a potential source of new biomarkers of drug-induced liver injury. *Toxicol. Lett.* **225**, 401–406 (2014).
198. Turturici, G., Tinnirello, R., Sconzo, G. & Geraci, F. Extracellular membrane vesicles as a mechanism of cell-to-cell communication: advantages and disadvantages. *AJP Cell Physiol.* **306**, C621–C633 (2014).
199. Salomon, C. *et al.* Exosomal Signaling during Hypoxia Mediates Microvascular Endothelial Cell Migration and Vasculogenesis. *PLoS One* **8**, 1–24 (2013).
200. Cantaluppi, V. *et al.* Microvesicles Derived from Endothelial Progenitor Cells Enhance Neoangiogenesis of Human Pancreatic Islets. *Cell Transplant.* **21**, 1305–1320 (2012).
201. Aharon, A. & Brenner, B. Microparticles, thrombosis and cancer. *Best Practice and Research: Clinical Haematology* **22**, 61–69 (2009).
202. Lanyu, Z. & Feilong, H. Emerging role of extracellular vesicles in lung injury and inflammation. *Biomedicine and Pharmacotherapy* **113**, (2019).
203. Moisseiev, E. *et al.* Protective Effect of Intravitreal Administration of Exosomes Derived from Mesenchymal Stem Cells on Retinal Ischemia. *Curr. Eye Res.* **42**, 1358–1367 (2017).
204. Crow, J. *et al.* Exosomes as mediators of platinum resistance in ovarian cancer. *Oncotarget* **8**, 11917–11936 (2017).
205. Bebelman, M. P., Smit, M. J., Pegtel, D. M. & Baglio, S. R. Biogenesis and function of extracellular vesicles in cancer. *Pharmacology and Therapeutics* **188**, 1–11 (2018).
206. Wang, N. *et al.* Mesenchymal stem cells-derived extracellular vesicles, via miR-210, improve infarcted cardiac function by promotion of angiogenesis. *Biochim. Biophys. Acta - Mol. Basis Dis.* **1863**, 2085–2092 (2017).
207. Vella, L. J., Hill, A. F. & Cheng, L. Focus on extracellular vesicles: Exosomes and their role in protein trafficking and biomarker potential in Alzheimer's and Parkinson's disease. *International Journal of Molecular Sciences* **17**, (2016).
208. Sahaboglu, A., Vidal-Gil, L. & Sancho-Pelluz, J. Release of Retinal Extracellular Vesicles in a Model of Retinitis

Pigmentosa. in *Advances in Experimental Medicine and Biology* **1185**, 431–436 (Springer, 2019).
209. Biasutto, L., Chiechi, A., Couch, R., Liotta, L. A. & Espina, V. Retinal pigment epithelium (RPE) exosomes contain signaling phosphoproteins affected by oxidative stress. *Exp. Cell Res.* **319**, 2113–2123 (2013).
210. Wang, A. L. *et al.* Autophagy and Exosomes in the Aged Retinal Pigment Epithelium: Possible Relevance to Drusen Formation and Age-Related Macular Degeneration. *PLoS One* **4**, e4160 (2009).
211. Knickelbein, J. E. *et al.* Modulation of immune responses by extracellular vesicles from retinal pigment epithelium. *Investig. Ophthalmol. Vis. Sci.* **57**, 4101–4107 (2016).
212. Hajrasouliha, A. R. *et al.* Exosomes from retinal astrocytes contain antiangiogenic components that inhibit laser-induced choroidal neovascularization. *J. Biol. Chem.* **288**, 28058–28067 (2013).
213. Grigor'eva, A. E. *et al.* Characteristics of exosomes andmicroparticles discovered in human tears. *Biomeditsinskaya Khimiya* **62**, 99–106 (2016).
214. Kang, G. Y. *et al.* Exosomal proteins in the aqueous humor as novel biomarkers in patients with neovascular age-related macular degeneration. *J. Proteome Res.* **13**, 581–595 (2014).
215. Todorova, D., Simoncini, S., Lacroix, R., Sabatier, F. & Dignat-George, F. Extracellular vesicles in angiogenesis. *Circ. Res.* **120**, 1658–1673 (2017).
216. Zhou, W. *et al.* Cancer-Secreted miR-105 destroys vascular endothelial barriers to promote metastasis. *Cancer Cell* **25**, 501–515 (2014).
217. Yoon, C. *et al.* Delivery of miR-155 to retinal pigment epithelial cells mediated by Burkitt's lymphoma exosomes. *Tumor Biol.* **37**, 313–321 (2016).
218. Kong, W. *et al.* Upregulation of miRNA-155 promotes tumour angiogenesis by targeting VHL and is associated with poor prognosis and triple-negative breast cancer. *Oncogene* **33**, 679–89 (2014).
219. Eldh, M. *et al.* MicroRNA in exosomes isolated directly from the liver circulation in patients with metastatic uveal melanoma. *BMC Cancer* **14**, (2014).
220. Ragusa, M. *et al.* miRNA profiling in vitreous humor, vitreal exosomes and serum from uveal melanoma patients: Pathological and diagnostic implications. *Cancer Biol. Ther.* **16**,

1387–1396 (2015).
221. Li, C. *et al.* Oxidative Stress-Related Mechanisms and Antioxidant Therapy in Diabetic Retinopathy. *Oxidative Medicine and Cellular Longevity* **2017**, (2017).
222. Shaw, P. X. *et al.* Oxidative stress, innate immunity, and age-related macular degeneration. *AIMS Mol. Sci.* **3**, 196–221 (2016).
223. Kim, J. M. *et al.* Responses of Types 1 and 2 Neovascularization in Age-Related Macular Degeneration to Anti-Vascular Endothelial Growth Factor Treatment: Optical Coherence Tomography Angiography Analysis. *Semin. Ophthalmol.* **34**, 168–176 (2019).
224. Marneros, A. G. VEGF-A and the NLRP3 Inflammasome in Age-Related Macular Degeneration. in 79–85 (2016). doi:10.1007/978-3-319-17121-0_12
225. Vlachos, I. S. *et al.* DIANA-miRPath v3.0: deciphering microRNA function with experimental support. *Nucleic Acids Res.* **43**, W460-6 (2015).
226. Bueno-Betí, C. *et al.* An affordable method to obtain cultured endothelial cells from peripheral blood. *J. Cell. Mol. Med.* **17**, 1475–1483 (2013).
227. Sun, Y. *et al.* RORα modulates semaphorin 3E transcription and neurovascular interaction in pathological retinal angiogenesis. *FASEB J.* **31**, 4492–4502 (2017).
228. Cochrane, A. *et al.* Quaking Is a Key Regulator of Endothelial Cell Differentiation, Neovascularization, and Angiogenesis. *Stem Cells* **35**, 952–966 (2017).
229. Asselin-Labat, M.-L. *et al.* Gata-3 Negatively Regulates the Tumor-Initiating Capacity of Mammary Luminal Progenitor Cells and Targets the Putative Tumor Suppressor Caspase-14. *Mol. Cell. Biol.* **31**, 4609–4622 (2011).
230. Zhao, C. & Popel, A. S. Computational Model of MicroRNA Control of HIF-VEGF Pathway: Insights into the Pathophysiology of Ischemic Vascular Disease and Cancer. *PLOS Comput. Biol.* **11**, e1004612 (2015).
231. Heidegger, I., Kern, J., Ofer, P., Klocker, H. & Massoner, P. Oncogenic functions of IGF1R and INSR in prostate cancer include enhanced tumor growth, cell migration and angiogenesis. *Oncotarget* **5**, 2723–35 (2014).
232. Tagashira, T. *et al.* Afadin Facilitates Vascular Endothelial Growth Factor–Induced Network Formation and Migration of Vascular Endothelial Cells by Inactivating Rho-Associated

Kinase Through ArhGAP29. *Arterioscler. Thromb. Vasc. Biol.* **38**, 1159–1169 (2018).
233. Nishihiro, S. *et al.* High-Mobility Group Box-1-Induced Angiogenesis After Indirect Bypass Surgery in a Chronic Cerebral Hypoperfusion Model. *NeuroMolecular Med.* (2019). doi:10.1007/s12017-019-08541-x
234. Hu, C. *et al.* Arid1a regulates response to anti-angiogenic therapy in advanced hepatocellular carcinoma. *J. Hepatol.* **68**, 465–475 (2018).
235. Lam, J. D. *et al.* Identification of RUNX1 as a Mediator of Aberrant Retinal Angiogenesis. *Diabetes* **66**, 1950–1956 (2017).
236. Zhang, Y. *et al.* Ionizing Radiation-inducible microRNA-21 Induces Angiogenesis by Directly Targeting PTEN. *Asian Pacific J. Cancer Prev.* **20**, 1587–1593 (2019).
237. Ren, L., Wei, C., Li, K. & Lu, Z. LncRNA MALAT1 up-regulates VEGF-A and ANGPT2 to promote angiogenesis in brain microvascular endothelial cells against oxygen–glucose deprivation via targetting *miR-145*. *Biosci. Rep.* **39**, BSR20180226 (2019).
238. Russell, K. S., Stern, D. F., Polverini, P. J. & Bender, J. R. Neuregulin activation of ErbB receptors in vascular endothelium leads to angiogenesis. *Am. J. Physiol. Circ. Physiol.* **277**, H2205–H2211 (1999).
239. Chen, D.-B., Feng, L., Hodges, J. K., Lechuga, T. J. & Zhang, H. Human trophoblast-derived hydrogen sulfide stimulates placental artery endothelial cell angiogenesis†. *Biol. Reprod.* **97**, 478–489 (2017).
240. Hafeez, B. B. *et al.* Genetic Ablation of PKC Epsilon Inhibits Prostate Cancer Development and Metastasis in Transgenic Mouse Model of Prostate Adenocarcinoma. *Cancer Res.* **71**, 2318–2327 (2011).
241. Mountain, D. J. H., Singh, M. & Singh, K. Downregulation of VEGF-D expression by interleukin-1β in cardiac microvascular endothelial cells is mediated by MAPKs and PKCα/β1. *J. Cell. Physiol.* **215**, 337–343 (2008).
242. Liu, S. *et al.* S1PR1 regulates the switch of two angiogenic modes by VE-cadherin phosphorylation in breast cancer. *Cell Death Dis.* **10**, 200 (2019).
243. Hang, T.-C. *et al.* Vascular Endothelial Growth Factor (VEGF) and Platelet (PF-4) Factor 4 Inputs Modulate Human Microvascular Endothelial Signaling in a Three-Dimensional

Matrix Migration Context* □ S. (2013). doi:10.1074/mcp.M113.030528
244. Zheng, Q. *et al.* Granulocyte-macrophage colony-stimulating factor increases tumor growth and angiogenesis directly by promoting endothelial cell function and indirectly by enhancing the mobilization and recruitment of proangiogenic granulocytes. *Tumor Biol.* **39**, 101042831769223 (2017).
245. Kanehira, M. *et al.* A Lysophosphatidic Acid Receptors 1 and 3 Axis Governs Cellular Senescence of Mesenchymal Stromal Cells and Promotes Growth and Vascularization of Multiple Myeloma. *Stem Cells* **35**, 739–753 (2017).
246. Oh, M.-K. & Kim, I.-S. Involvement of placental growth factor upregulated via TGF-β1-ALK1-Smad1/5 signaling in prohaptoglobin-induced angiogenesis. *PLoS One* **14**, e0216289 (2019).
247. Han, N., Tian, W., Yu, N. & Yu, L. YAP1 is required for the angiogenesis in retinal microvascular endothelial cells via the inhibition of MALAT1-mediated miR-200b-3p in high glucose-induced diabetic retinopathy. *J. Cell. Physiol.* jcp.29047 (2019). doi:10.1002/jcp.29047
248. Dai, X. *et al.* Phosphorylation of angiomotin by Lats1/2 kinases inhibits F-actin binding, cell migration, and angiogenesis. *J. Biol. Chem.* **288**, 34041–51 (2013).
249. Foulsham, W. *et al.* Thrombospondin-1 in ocular surface health and disease. *Ocul. Surf.* **17**, 374–383 (2019).
250. Cai, Y., Xie, K., Wu, H. & Wu, K. Functional suppression of Epiregulin impairs angiogenesis and aggravates left ventricular remodeling by disrupting the extracellular-signal-regulated kinase1/2 signaling pathway in rats after acute myocardial infarction. *J. Cell. Physiol.* **234**, jcp.28503 (2019).
251. Yue, X. *et al.* MicroRNA-205 functions as a tumor suppressor in human glioblastoma cells by targeting VEGF-A. *Oncol. Rep.* **27**, 1200–6 (2012).
252. Slevin, M. *et al.* Identification of pro-angiogenic markers in blood vessels from stroked-affected brain tissue using laser-capture microdissection. *BMC Genomics* **10**, 113 (2009).
253. Fournier, P., Dussault, S., Fusco, A., Rivard, A. & Royal, I. Tyrosine Phosphatase PTPRJ/DEP-1 Is an Essential Promoter of Vascular Permeability, Angiogenesis, and Tumor Progression. *Cancer Res.* **76**, 5080–5091 (2016).
254. Dong, Y.-L. *et al.* Calcitonin Gene-Related Peptide (CALCA) Is a Proangiogenic Growth Factor in the Human Placental

Development1. *Biol. Reprod.* **76**, 892–899 (2007).
255. Ito, A. *et al.* Enhanced post-ischemic angiogenesis in mice lacking RNF213; a susceptibility gene for moyamoya disease. *Brain Res.* **1594**, 310–320 (2015).
256. van den Born, J. C. *et al.* Cystathionine γ-lyase is expressed in human atherosclerotic plaque microvessels and is involved in micro-angiogenesis. *Sci. Rep.* **6**, 34608 (2016).
257. Dunn, K. C., Aotaki-Keen, A. E., Putkey, F. R. & Hjelmeland, L. M. ARPE-19 , A Human Retinal Pigment Epithelial Cell Line with. *Exp Eye Res* **62**, 155–169 (1996).
258. Martinez-Gil, N. *et al.* CYP2E1 in the human retinal pigment epithelium: Expression, activity, and induction by ethanol. *Investig. Ophthalmol. Vis. Sci.* **56**, 6855–6863 (2015).
259. Dinc, E., Ayaz, L. & Kurt, A. H. Protective Effect of Combined Caffeic Acid Phenethyl Ester and Bevacizumab Against Hydrogen Peroxide-Induced Oxidative Stress in Human RPE Cells. *Curr. Eye Res.* **42**, 1659–1666 (2017).
260. Hsiung, J., Zhu, D. & Hinton, D. R. Polarized human embryonic stem cell-derived retinal pigment epithelial cell monolayers have higher resistance to oxidative stress-induced cell death than nonpolarized cultures. *Stem Cells Transl. Med.* **4**, 10–20 (2015).
261. Zhang, W. *et al.* Photo-Oxidative Blue-Light Stimulation in Retinal Pigment Epithelium Cells Promotes Exosome Secretion and Increases the Activity of the NLRP3 Inflammasome. *Curr. Eye Res.* **44**, 67–75 (2019).
262. Ke, Y. *et al.* Exosomes derived from RPE cells under oxidative stress mediate inflammation and apoptosis of normal RPE cells through Apaf1/caspase-9 axis. *J. Cell. Biochem.* (2020). doi:10.1002/jcb.29713
263. SanGiovanni, J. P., SanGiovanni, P. M., Sapieha, P. & De Guire, V. miRNAs, single nucleotide polymorphisms (SNPs) and age-related macular degeneration (AMD). *Clin. Chem. Lab. Med.* **55**, 763–775 (2017).
264. Wu, J. *et al.* Protective effects of methane-rich saline on diabetic retinopathy via anti-inflammation in a streptozotocin-induced diabetic rat model. *Biochem. Biophys. Res. Commun.* **466**, 155–161 (2015).
265. Wang, H.-C. *et al.* Profiling the microRNA Expression in Human iPS and iPS-derived Retinal Pigment Epithelium. *Cancer Inform.* **13**, 25–35 (2014).
266. Xiang, L. *et al.* miR-183/96 plays a pivotal regulatory role in

mouse photoreceptor maturation and maintenance. *Proc. Natl. Acad. Sci.* **114**, 6376–6381 (2017).
267. Zhang, J. *et al.* miR-25 Mediates Retinal Degeneration Via Inhibiting ITGAV and PEDF in Rat. *Curr. Mol. Med.* **17**, 359–374 (2017).
268. Desjarlais, M. *et al.* MicroRNA expression profile in retina and choroid in oxygen-induced retinopathy model. *PLoS One* **14**, e0218282 (2019).
269. Walz, J. M. *et al.* Impact of angiogenic activation and inhibition on miRNA profiles of human retinal endothelial cells. *Exp. Eye Res.* **181**, 98–104 (2019).
270. Zhang, Y. *et al.* Regulation of Matrix Metalloproteinase-2 Secretion from Scleral Fibroblasts and Retinal Pigment Epithelial Cells by miR-29a. *Biomed Res. Int.* **2017**, 1–7 (2017).
271. Zhang, Y. *et al.* miR-29a regulates the proliferation and differentiation of retinal progenitors by targeting Rbm8a. *Oncotarget* **8**, 31993–32008 (2017).
272. Blasiak, J. *et al.* Expression of VEGFA-regulating miRNAs and mortality in wet AMD. *J. Cell. Mol. Med.* **23**, 8464–8471 (2019).
273. Berber, P., Grassmann, F., Kiel, C. & Weber, B. H. F. F. An Eye on Age-Related Macular Degeneration: The Role of MicroRNAs in Disease Pathology. *Mol. Diagnosis Ther.* **21**, 31–43 (2017).
274. Mazzeo, A. *et al.* Functional analysis of miR-21-3p, miR-30b-5p and miR-150-5p shuttled by extracellular vesicles from diabetic subjects reveals their association with diabetic retinopathy. *Exp. Eye Res.* **184**, 56–63 (2019).
275. Zhou, P. & Li, X. Serum miR-338-5p has potential for use as a tumor marker for retinoblastoma. *Oncol. Lett.* **18**, 307–313 (2019).
276. Gao, C., Zhang, C. C., Yang, H. X. & Hao, Y. N. MALAT1 Protected the Angiogenesis Function of Human Brain Microvascular Endothelial Cells (HBMECs) Under Oxygen Glucose Deprivation/re-oxygenation (OGD/R) Challenge by Interacting with miR-205-5p/VEGFA Pathway. *Neuroscience* **435**, 135–145 (2020).
277. Cao, W., Zhao, Y., Wang, L. & Huang, X. Circ0001429 regulates progression of bladder cancer through binding miR-205-5p and promoting VEGFA expression. *Cancer Biomarkers* 1–13 (2019). doi:10.3233/CBM-182380
278. An, G., Liang, S., Sheng, C., Liu, Y. & Yao, W. Upregulation

of microRNA-205 suppresses vascular endothelial growth factor expression-mediated PI3K/Akt signaling transduction in human keloid fibroblasts. *Exp. Biol. Med.* **242**, 275–285 (2017).
279. Wang, Z., Liu, C. H., Huang, S. & Chen, J. Wnt Signaling in vascular eye diseases. *Progress in Retinal and Eye Research* **70**, 110–133 (2019).
280. Creemers, E. E., Tijsen, A. J. & Pinto, Y. M. Circulating MicroRNAs. *Circ. Res.* **110**, 483–495 (2012).
281. Bukong, T. N., Momen-Heravi, F., Kodys, K., Bala, S. & Szabo, G. Exosomes from hepatitis C infected patients transmit HCV infection and contain replication competent viral RNA in complex with Ago2-miR122-HSP90. *PLoS Pathog.* **10**, e1004424 (2014).
282. Mittelbrunn, M. *et al.* Unidirectional transfer of microRNA-loaded exosomes from T cells to antigen-presenting cells. *Nat. Commun.* **2**, 282 (2011).
283. van Balkom, B. W. M., Eisele, A. S., Pegtel, D. M., Bervoets, S. & Verhaar, M. C. Quantitative and qualitative analysis of small RNAs in human endothelial cells and exosomes provides insights into localized RNA processing, degradation and sorting. *J. Extracell. vesicles* **4**, 26760 (2015).
284. Jiao, X. *et al.* Serum and exosomal miR-122 and miR-199a as a biomarker to predict therapeutic efficacy of hepatitis C patients. *J. Med. Virol.* **89**, 1597–1605 (2017).
285. Lou, G. *et al.* Exosomes derived from MIR-122-modified adipose tissue-derived MSCs increase chemosensitivity of hepatocellular carcinoma. *J. Hematol. Oncol.* **8**, (2015).
286. Kong, Y., Naggert, J. K. & Nishina, P. M. The impact of adherens and tight junctions on physiological function and pathological changes in the retina. in *Advances in Experimental Medicine and Biology* **1074**, 545–551 (Springer New York LLC, 2018).
287. Lin, Y. *et al.* SIRT1 deletion impairs retinal endothelial cell migration through downregulation of VEGF-A/VEGFR-2 and MMP14. *Investig. Ophthalmol. Vis. Sci.* **59**, 5431–5440 (2018).
288. Gao, Z., Zhu, X. & Dou, Y. The miR-302/367 cluster: a comprehensive update on its evolution and functions. *Open Biol.* **5**, 150138 (2015).
289. Kuo, C.-H., Deng, J. H., Deng, Q. & Ying, S.-Y. A novel role of miR-302/367 in reprogramming. *Biochem. Biophys. Res. Commun.* **417**, 11–16 (2012).
290. Barroso-del Jesus, A., Lucena-Aguilar, G. & Menendez, P. The

miR-302-367 cluster as a potential stemness regulator in ESCs. *Cell Cycle* **8**, 394–8 (2009).
291. Lipchina, I., Studer, L. & Betel, D. The expanding role of miR-302–367 in pluripotency and reprogramming. *Cell Cycle* **11**, 1517–1523 (2012).
292. Chen, W., Zhuang, X., Qi, R. & Qiao, T. MiR-302a-5p suppresses cell proliferation and invasion in non-small cell lung carcinoma by targeting ITGA6. *Am. J. Transl. Res.* **11**, 4348–4357 (2019).
293. Qin, C. *et al.* MicroRNA-302a inhibits cell proliferation and invasion, and induces cell apoptosis in hepatocellular carcinoma by directly targeting VEGFA. **16**, 6360–6367 (2017).
294. Li, C. *et al.* Chronic inflammation contributes to the development of hepatocellular carcinoma by decreasing miR-122 levels. *Oncotarget* **7**, 17021–34 (2016).
295. Bai, J. *et al.* DNA Methylation of miR-122 Aggravates Oxidative Stress in Colitis Targeting SELENBP1 Partially by p65NF- κ B Signaling. *Oxid. Med. Cell. Longev.* **2019**, 1–14 (2019).
296. Song, L. *et al.* MicroRNA-122 is involved in oxidative stress in isoniazid-induced liver injury in mice. *Genet. Mol. Res.* **14**, 13258–65 (2015).
297. Li, W.-B. *et al.* Development of Retinal Pigment Epithelium from Human Parthenogenetic Embryonic Stem Cells and MicroRNA Signature. *Investig. Opthalmology Vis. Sci.* **53**, 5334 (2012).
298. Genini, S., Guziewicz, K. E., Beltran, W. A. & Aguirre, G. D. Altered miRNA expression in canine retinas during normal development and in models of retinal degeneration. *BMC Genomics* **15**, 172 (2014).
299. Drewry, M. D. *et al.* Differentially expressed microRNAs in the aqueous humor of patients with exfoliation glaucoma or primary open-angle glaucoma. *Hum. Mol. Genet.* **27**, 1263–1275 (2018).
300. Pastukh, N., Meerson, A., Kalish, D., Jabaly, H. & Blum, A. Serum miR-122 levels correlate with diabetic retinopathy. *Clin. Exp. Med.* **19**, 255–260 (2019).
301. Ryan, D. G., Oliveira-Fernandes, M. & Lavker, R. M. MicroRNAs of the mammalian eye display distinct and overlapping tissue specificity. *Mol. Vis.* **12**, 1175–84 (2006).
302. Liu, G., Zhang, C.-D., Wang, J. & Jia, W.-C. Inhibition of the oxidative stress-induced miR-125b protects glucose metabolic disorders of human retinal pigment epithelium (RPE) cells. *Cell.*

Mol. Biol. (Noisy-le-grand). **64**, 1–5 (2018).
303. Shao, P. *et al.* MicroRNA-205-5p regulates the chemotherapeutic resistance of hepatocellular carcinoma cells by targeting PTEN/JNK/ANXA3 pathway. *Am. J. Transl. Res.* **9**, 4300–4307 (2017).
304. Patil, K. S. *et al.* A Proteomics Approach to Investigate miR-153-3p and miR-205-5p Targets in Neuroblastoma Cells. *PLoS One* **10**, e0143969 (2015).
305. Muratsu-Ikeda, S. *et al.* Downregulation of miR-205 modulates cell susceptibility to oxidative and endoplasmic reticulum stresses in renal tubular cells. *PLoS One* **7**, e41462 (2012).
306. Zhao, X. *et al.* MicroRNA-205 is downregulated in hepatocellular carcinoma and inhibits cell growth and metastasis via directly targeting vascular endothelial growth factor A. *Oncol. Lett.* **16**, 2207–2214 (2018).
307. Li, L. & Li, S. miR-205-5p inhibits cell migration and invasion in prostatic carcinoma by targeting ZEB1. *Oncol. Lett.* **16**, 1715–1721 (2018).
308. Kim, Y.-W. & Byzova, T. V. Oxidative stress in angiogenesis and vascular disease. *Blood* **123**, 625–631 (2014).
309. R., K. *et al.* Stimulation of apical and basolateral vascular endothelial growth factor-A and vascular endothelial growth factor-C secretion by oxidative stress in polarized retinal pigment epithelial cells. *Mol. Vis.* **12**, 1649–1659 (2006).
310. Samuni, Y., Goldstein, S., Dean, O. M. & Berk, M. The chemistry and biological activities of N-acetylcysteine. *Biochim. Biophys. Acta - Gen. Subj.* **1830**, 4117–4129 (2013).
311. Tardiolo, G., Bramanti, P. & Mazzon, E. Overview on the effects of N-acetylcysteine in neurodegenerative diseases. *Molecules* **23**, 3305 (2018).
312. Tao, W., Sun, W., Zhu, H. & Zhang, J. miR-205-5p suppresses pulmonary vascular smooth muscle cell proliferation by targeting MICAL2-mediated Erk1/2 signaling. *Microvasc. Res.* **124**, 43–50 (2019).
313. Huang, J., Wang, X., Wen, G. & Ren, Y. MiRNA-205-5p functions as a tumor suppressor by negatively regulating VEGFA and PI3K/Akt/mTOR signaling in renal carcinoma cells. *Oncol. Rep.* **42**, 1677–1688 (2019).
314. Thangapandiyan, S. & Miltonprabu, S. Epigallocatechin gallate supplementation protects against renal injury induced by fluoride intoxication in rats: Role of Nrf2/HO-1 signaling. *Toxicol. reports* **1**, 12–30 (2014).

315. Salcedo-Villanueva, G. *et al.* Anti-VEGF treatment switch in neovascular age-related macular degeneration: a comparison of aflibercept versus ranibizumab after a single-dose switch. *Int. Ophthalmol.* (2018). doi:10.1007/s10792-018-1038-4
316. Brandes, A. A. *et al.* A Randomized Phase II Trial (TAMIGA) Evaluating the Efficacy and Safety of Continuous Bevacizumab Through Multiple Lines of Treatment for Recurrent Glioblastoma. *Oncologist* **24**, 521–528 (2019).
317. Tong, Y., Zhou, Y. L., Wang, Y. X., Zhao, P. Q. & Wang, Z. Y. Retinal pigment epithelium cell-derived exosomes: Possible relevance to CNV in wet-age related macular degeneration. *Med. Hypotheses* **97**, 98–101 (2016).
318. Klingeborn, M., Stamer, W. D. & Bowes Rickman, C. Polarized exosome release from the retinal pigmented epithelium. in *Advances in Experimental Medicine and Biology* **1074**, 539–544 (Springer New York LLC, 2018).
319. Morris, D. R. *et al.* Exosomal MiRNA transfer between retinal microglia and RPE. *Int. J. Mol. Sci.* **21**, (2020).
320. Shah, N. *et al.* Extracellular vesicle-mediated long-range communication in stressed retinal pigment epithelial cell monolayers. *Biochim. Biophys. Acta - Mol. Basis Dis.* **1864**, 2610–2622 (2018).

ANNEXES

Annexes

Annex I. Cell miRNAs pathway enrichment analysis after H_2O_2 exposure in ARPE-19 cells. Enrichment analysis performed by DIANA mirPATH. KEGG pathways with a p_value < 0.05.

KEGG Pathway	FDR	Number of miRNAs	Putative target genes
Prion diseases	$2{,}63\times10^{-11}$	5	EGR1 HSPAS FYN PRNP LAMC1 MAP2K1 MAPK1
Cell cycle	$1{,}92\times10^{-10}$	5	ESPL1 CCNB2 RBL2 PCNA E2F1 SMC1A YWHAH CCNB1 CDK4 YWHAE CCNA2 ORC2 MCM6 YWHAG CDK2 CCND2 ORC1 DBF4 CDKN1B CUL1 YWHAB WEE1 CDK1 CDK6 MCM7 SKP1 TP53 ATM CCND1 CCNE2 E2F5 SKP2 E2F3 MYC RB1 YWHAZ HDAC2 CDC20 MAD2L1 CDC23 ANAPC5 EP300 CDC27 RBX1 CDKN1A PRKDC E2F4 ANAPC13 CREBBP RAD21 MDM2 ABL1 MCM3 CDC25A
Hepatitis	$3{,}29\times10^{-9}$	6	FOS PCNA STAT3 ATP6AP1 E2F1 TGFBR1 NFKB1 CDK4 ATF2 NRAS CCNA2 ATF6B CDK2 CHUK BCL2 CDKN1B YWHAB MAP3K1 TRL4 KRAS CDK6 DDX3X TP53 HSPG2 FADD CREB1 APAF1 MAVS CASP3 CCND1 CCNE2 E2F3 MAPK8 AKT1 MYC IRF3 NFKBIA DDB1 PIK3R1 RB1 YWHAZ TBK1 SRC FAS HRAS EP300 CREB3L2 CREB3L1 CDKN1A MAP2K1 MAP2K4 PTEN NFATC3 MAPK1 CREBBP JAK1 ATK4
Viral carcinogenesis	$4{,}22\times10^{-9}$	6	RBL2 STAT3 NFKB1 YWHAH CDK4 ATF2 NRAS IRF9 YWHAE HDAC3 CCNA2 GTF2H1 ATF6B YWHAG CDK2 CCND2 PXN CDKN1B YWHAG CDK2 CCND2 PXN CDKN1B YWHAB CDK1 GTF2B KRAS CDK6 DDX3X TP53 HNRNPK CREB1 GSN PMAIP1 CASP3 CCND1 CCNE2 SKP2 CCR5 IRF3 NFKBIA B¡DDB1 HIST1H2BG PIK3R1 RB1 GTF2A2 YWHAZ HDAC2 KAT2A RAC1 SRC CDC20 RBPJ HIST1H2BL HRAS EP300 CREB3L2 CREB3L1 IL6ST SNW1 CDKN1A MAPK1 SRF CREBBP TBPL1 JAK1 MDM2 ATF4 SCRIB H2BFS HIST1H4D
Oocyte meiosis	$5{,}53\times10^{-9}$	4	SLK ESPL1 PPP1CA CAMK2D CCNB2 SMC1A YWHAH CCNB1 YWHAE BTRC CALM3 CALM1 PPP2CA CPEB4 YWHAG CDK2 CUL1 PPP2R5D YWHAB CDK1 IGF1R SKP1 PPP2R5A CCNE2 CPEB2 YWHAZ CDC20 MAD2L1 CDC23 ANAPC5 RPS6KA3 CDC27 RBX1 AURKA SGOL1 MAPK2K1 ANAPC13

KEGG Pathway	FDR	Number of miRNAs	Putative target genes
			ITPR3 MAPK1 ITPR2 FBXW11 ADCY9 PPP1CB RPS6KA2
Lysine degradation	$3{,}32 \times 10^{-8}$	4	WHSC1L1 ALDH7A1 SETD7 SERC1B PLOD2 NSD1 ASH1L KMT2D SUV42OH1 DOT1L SUV420H2 KMT2A ALDH9A1 SUV39H2 KMT2E SETD1A EHMT1 KMT2B
Hippo signaling pathway	$3{,}52 \times 10^{-7}$	4	PPP1CA ACTB FZD5 TGFBR1 YWHAH YAP1 YWHAE BTRC PPP2CA TCF7L2 NF2 YWHAG CCND2 BMP5 ACTG1 GLI2 AREG FZD6 SNAI2 AXIN1 MOB1B YWHAB AMOT BMP6 FZD3 LIMD1 MPP5 DLG4 CCND1 CTNNA1 MYC LLGL1 ID1 FZD2 TEAD1 YWHAZ BMP2 TEAD4 PARD3 SMAD7 MOB1A LATS1 SOX2 LATS2 FBXW11 TGFBR2 WNT9A BMP4 BMPR2 CTGF PPP1CB BIRC2 SCRIB
Renal cell carcinoma	$2{,}09 \times 10^{-6}$	6	BRAF MET SOS2 NRAS CRKL CRK CUL2 PAK2 ARNT KRAS VHL ARNT2 AKT1 PDGFB PIK3R1 RAC1 EGLN2 HRAS EP300 GAB1 RBX1 MAP2K1 SLC2A1 VEGFA MAPK1 CREBBP EGLN1 FLCN
Proteoglycans in cancer	$4{,}50 \times 10^{-6}$	6	ESR1 PPP1CA CAMK2D BRAF ACTB STAT3 FZD5 PDCD4 MET EZR ROCK1 SOS2 CBL NRAS THBS1 CAV1 ARHGEF12 ACTG1 PXN FRS2 FZD6 RDX IGF1R TLR4 ERBB3 KRAS FZD3 MSN RPS6KB2 TP53 HSPG2 CTTN VAV2 PTK2 ITGAV SLC9A1 PPP1R12A DROSHA PLCG1 CASP3 PTPN6 CCND1 AKT1 MYC IGF2 FLNA FZD2 PIK3R1 RAC1 SRC FAS HRAS GAB1 HOXD10 FN1 CDKN1A MAPK2K1 ITPR3 VEGFA FGFR1 MAPK1 ITPR2 MDM2 WNT9A PPP1CB
Chronic myeloid leukemia	$2{,}09 \times 10^{-5}$	6	BRAF E2F1 TGFBR1 NFKB1 SOS2 CDK4 CBL NRAS CRKL CRK RUNX1 CHUK CDKN1B KRAS CDK6 TP53 CCND1 E2F3 AKT1 MYC NFKBIA PIK3R1 RB1 HDAC2 HRAS CDKN1A MAPK2K1 MAPK1 TGFBR2 MDM2 ABL1
Transcriptional misregulation in cancer	$6{,}02 \times 10^{-5}$	6	BMI1 CCNT2 TMPRSS2 MEN1 NFKB1 MET ELK4 RUNX1 HMGA2 AFF1 DUSP6 CCND2 HOXA9 PBX1 LDB1 CDKN1B IGF1R RUNX2 CCR7 TP53 UTY PTK2 ATM RUNX1T1 ARNT2 PBX3 CDK9 MYC KLF3 BMP2K NCOR1 LYL1 JMJD1C HDAC2 H3F3A KDM6A SP1 MAX DOT1L H3F3B SPINT1 KMT2A MYCN CDKN1A BIRC3 EWSR1 FOXO1 JUP TGFBR2 MDM2 SIN3A PAX3

KEGG Pathway	FDR	Number of miRNAs	Putative target genes
Prostate cancer	$7{,}86 \times 10^{-5}$	6	BRAF E2F1 NFKB1 SOS2 NRAS TCF7L2 CDK2 CHUK BCL2 CDKN1B IGF1R KRAS TP53 CREB1 CCND1 CCNE2 E2F3 AKT1 PDGFB NFKBIA PIK3R1 RB1 HSP90B1 HRAS EP300 NKX3-1 CREB3L2 CREB3L1 CDKN1A MAP2K1 PTEN FGFR1 FOCO1 MAPK1 CREBBP MDM2 ATF4
Glioma	0,0001	6	CAMK2D BRAF E2F1 SOS2 CDK4 NRAS CALM3 CALM1 IGF1R KRAS CDK6 TP53 PLCG1 CCND1 E2F3 AKT1 PDGFB PIK3R1 RB1 HRAS CDKN1A MAP2K1 PTEN MAPK1 MDM2
Shigellosis	0,0003	5	PFN1 ACTB ARPC5L NFKB1 ROCK1 WASL RIPK2 CRKL BTRC CRK ACTG1 CHUK ELMO2 NOD1 VCL CTTN PFN2 MAPK8 DIAPH1 ARPC2 WASF2 NFKBIA RAC1 SRC MAPK1 FBXW11 ABL1 RHOG
Adherent junction	0,0003	4	ACTB CSNK2A2 TGFBR1 MET WASL TCF7L2 ACTG1 SNAI2 PTPN1 IGF1R VCL TJP1 FYN NLK PTPN6 CTNNA1 WASF2 CSNK2A1 FARP2 RAC1 INSR SRC SSX2IP EP300 PARD3 YES1 PTPRB FGFR1 MAPK1 MAP3K7 CREBBP TGFBR2
Thyroid cancer	0,0003	5	BRAF NRAS TPR TCF7L2 KRAS TP53 CCND1 MYC HRAS MAP2K1 MAPK1 TFG NCOA4
Estrogen signaling pathway	0,0003	5	ESR1 HSPA2 FOS SOS2 ATF2 NRAS CALM3 CALM1 ATF6B KRAS PLCB3 CREB1 AKT1 PIK3R1 HSP90B1 SRC HSPA8 SP1 HRAS GNAQ CREB3L2 CREB3L1 MAP2K1 ITPR3 MAPK1 ITPR2 ADCY9 PLCB4 ATF4
Bacterial invasion of epithelial cells	0,0003	5	ACTB ARPC5L MET WASL CBL CRKL SEPT8 CRK CAV1 SEPT11 ACTG1 PXN ELMO2 CLTC VCL CTTN PTK2 CTNNA1 ARPC2 WASF2 PIK3R1 RAC1 SRC GAB1 FN1 SEPT2 SEPT9 RHOG
FoxO signaling pathway	0,0003	6	IRS2 BRAF CCNB2 RBL2 STAT3 TGFBR1 CCNB1 SOS2 NRAS STK4 SETD7 KLF2 CDK2 CCND2 CHUK CDKN1B IGF1R TNFSF10 KRAS HOMER2 ATM NLK CCD1 S1PR1 SKP2 MAPK8 AKT1 PRKAG1 PLK2 GABARAPL1 PIK3R1 INSR PRKAA1 PRMT1 HRAS PRKAB2 EP300 SOD2 CDKN1A MAP2K1 ATG12 PTEN SGK3 FOXO1 MAPK1 CREBBP CCNG2 TGFBR2 MDM2 BCL2L11
Ubiquitin mediated proteolysis	0,0003	6	UBE2Q2 UBE3B CBL BTRC TRIM37 CUL2 NEDD4L HUWE1 CUL1 UBE4A MAP3K1 UBE2J1 UBE2I HERC1 MID1

KEGG Pathway	FDR	Number of miRNAs	Putative target genes
			VHL SKP1 CDC34 TRIP12 SOCS3 SKP2 SOCS1 DDB1 UBE2K CDC20 CDC23 ANAPC5 PIAS4 UBE2D3 UBE2G2 CDC27 RBX1 UBE2G1 BIRC3 CUL3 UBE2W ANAPC13 FBXW11 RHOBTB2 UBE4B TRIM32 PIAS1 MDM2 UBE2J2 BURC2 UBOX5
Thyroid hormone signaling pathway	0,0003	7	ESR1 ACTB MED13L NRAS HDAC3 MED14 MED12 ACTG1 MED13 SLC16A10 THRA KRAS NOTCH4 NCOA3 TP53 PLCB3 ITGAV SLC9A1 PLCG1 CCND1 AKT1 MYC NCOR1 NCOA2 PIK3R1 HDAC2 KAT2A SRC HRAS EP300 MAP2K1 SLC2A1 PFKFB2 ATP2A2 ATP1A1 FOXO1 MAPK1 CREBBP MDM2 PLCB4 BMP4 SIN3A
Bladder cancer	0,0003	7	BRAF E2F1 CDK4 NRAS RPS6KA5 TP53 CCND1 E2F3 MYC DAPK1 RB1 HRAS CDKN1A MAP2K1 MDM2
Pathways in cancer	0,0004	7	BRAF FOS STAT3 FZD5 E2F1 TGFBR1 NFKB1 MET ROCK1 SOS2 CDK4 CBL NRAS CRKL STK4 BID CRK RUNX1 RAD51 CUL2 TPR TCF7L2 ARHGEF12 CDK2 GLI2 BDKRB2 ARNT FZD6 CHUK BCL2 CDKN1B AXIN1 IGF1R GNB1 KRAS CDK6 FZD3 VHL MLH1 TP53 FADD PLCB3 PTK2 LAMC3 ITGAV RUNC1T1 ARNT2 PLCG1 CASP3 CCND1 LPAR1 MSH6 CTNNA1 CCNE2 SKP2 COL4A2 E2F3 MAPK8 AKT1 F2R MYC DAPK1 PDGFB NFKBIA KIT PTGS2 FZD2 PIK3R1 RB1 HSP90B1 HDAC2 RAC1 BMP2 EGLN2 MAX FAS HRAS LAMC1 EP300 GNAQ NKX3-1 RBX1 FN1 CDKN1A MAP2K1 BIRC3 SLC2A1 VEGFA PTEN FGFR1 FOXO1 MAPK1 CREBBP GNG5 ADCY9 JUP TGFBR2 TFG JAK1 MDM2 WNT9A ABL1 PLCB4 BMP4 EGLN1 COL4A1 BIRC2 NCOA4
p53 signaling pathway	0,0006	5	CCNG1 ZMAT3 CCNB2 CCNB2 CDK4 BID THBS1 CDK2 CCND2 CDK1 CDK6 TP53 APAF1 ATM PMAIP1 CASP3 CCND1 CCNE2 SHISA5 SESN1 SESN2 TNFRSF10B MDM4 FAS CDKN1A RRM2 PTEN CCNG2 MDM2
Huntington's disease	0,001	5	POLR2B NDUFS2 COX8A SDHB HIP1 CYC1 REST AP2B1 HTT NDUFA5 RCOR1 IFT57 CLTC VDAC2 ATP5B TP53 DNAH1 PLCB3 CREB1 APAF1 POLR2D ATP5G3 DLG4 POLR2A CASP3 UQCR1O NDUFA3 NDUFV3 UQCRH NDUFA4 HDAC2 AP2A1 NDUFA10 SP1 EP300 SLC25A4 GNAQ TGM2 CREB3L2 SOD2 CREB3L1 PPIF AP2S1 CREBBP

KEGG Pathway	FDR	Number of miRNAs	Putative target genes
			TBPL1 PLCB4 SIN3A ATP5C1 ATP50 MT-CO1 MT-ATP8
Endocytosis	0,002	5	RNF41 VPS4A HSPA2 RAB4A ARFGEF1 TGFBR1 MET ADRBK1 DNAJC6 CBL AGAP3 CAV1 AP2B1 CHMP1B NEDD4L EEA1 EHD4 VPS36 AGAP1 ADRB2 IGF1R CLTC CHMP2A ERBB3 RAB31 VPS37B GBF1 RABEP1 ASAP1 RAB11FIP2 ARFGAP2 GIT2 CCR5 F2R SMAP1 TFRC CHMP5 RAB11A KIT SRC AP2A1 HSPA8 HRAS GRK6 ZFYVE20 STAMBP CYTH1 VPS37C RAB22A ARF6 PARD3 SMAD7 VPS25 RAB5C EHD1 AP2S1 TGFBR2 MDM2 ARRB1 ASAP2
Epstein-Barr virus infection	0,002	5	POLR2B HSPA2 POLR3D STAT3 CSNK2A2 NFKB1 YWHAH EIF2AK1 ATF2 YWHAE CCNA2 YWHAG CDK2 PSMD2 TYK2 EIF2AK4 CHUK BCL2 CDKN1B YWHAB CDK1 GTF2B TAB2 PSMD14 TP53 POLR2D NUP214 POLR3A PLCG1 POLR2A NCOR2 SKP2 MAPK8 AKT1 MYC HLA-DPA1 PSMD11 VIM IRF3 PSMD14 NFKBIA PSMC4 PIK3R1 RB1 CSNK2A1 TWHAZ HDAC2 TNK1 PSMD1 HSPA8 RBPJ EP300 PSMD7 SNW1 CDKN1A POLR3B RAN MAP2K4 XPO1 MAP3K7 CREBBP TBPL1 PSMC6 JAK1 MDM2
Small cell lung cancer	0,003	5	E2F1 NFKB1 CDK4 CDK2 BCL2 CDKN1B CDK6 TP53 APAF1 PTK2 LAMC3 ITGAV CCND1 CCNE2 SKP2 COL4A2 E2F3 AKT1 MYC NFKBIA PTGS2 PIK3R1 RB1 MAX LAMC1 FN1 BIRC3 PTEN COL4A1 BIRC2
Protein processing in endoplasmic reticulum	0,003	7	HSPA2 RPN1 EIF2AK1 SSR1 UGGT1 MBTPS1 ERO1L YOD1 ATF6B NPLOC4 EDEM2 SEL1L UBQLN1 SEC23A DNAJB11 EIF2AK4 HSPA5 BCL2 CUL1 FBXO6 MBTPS2 UBE2J1 STT3B HSPH1 CANX SKP1 PREB SEC63 EDEM3 SEC24C MAPK8 PRKCSH VCP SEC24A HSP90B1 SEC31A DDOST HSPA8 UBE2D3 CKAP4 UBE2G2 SEC24B RBX1 UBE2G1 RPN2 CALR DNAJA2 UBE4B OS9 ERO1LB UBE2J2 ATF4
HIF-1 signaling pathway	0,004	4	CAMK2D STAT3 NFKB1 CUL2 ARNT BCL2 CDKN1B EIF4EBP1 IGF1R TLR4 VHL RPS6KB2 PLCG1 ENO1 AKT1 TFRC PIK3R1 INSR EGLN2 EP300 EIF4E2 RBX1 CDKN1A MAP2K1 SLC2A1 PFKFB2 EDN1 MKNK2 ALDOA PFKL VEGFA MAPK1 CREBBP TEK EGLN1 PFKFB3 IL6R

KEGG Pathway	FDR	Number of miRNAs	Putative target genes
Glycosaminoglycan biosynthesis-keratan sulfate	0,005	3	B4GALT1 B3GNT1 B4GALT3 B3BNT2
Proteasome	0,007	5	PSMB8 PSMD2 PSMB7 PSME4 PSME2 PSMD13 PSMA2 PSMD11 PSMD14 PSMC4 PSMB2 PSMD1 PSMD7 POMP PSMA4 PSMC6 PSMB5 PSMB3
Acute myeloid leukemia	0,007	5	BRAF STAT3 NFKB1 SOS2 NRAS RUNX1 TCF7L2 CHUK EIF4EBP1 KRAS RPS6KB2 RUNX1T1 CCND1 AKT1 MYC KIT PIK3R1 HRAS MAP2K1 MAPK1 JUP
HTLV-I infection	0,011	7	EGR1 FOS CCNB2 PCNA FZD5 E2F1 TGFBR1 NFKB1 IL1R1 CDK4 ATF2 NRAS ELK4 MAP3K3 CCND2 ETS2 FZD6 ZFP36 CHUK VCAM1 MAP3K1 KRAS VDAC2 FZD3 CANX TP53 CREB1 ATM CCND1 E2F3 MAPK8 AKT1 POLD3 MYC HLA-DPA1 TP53INP1 PDGFB NFKBIA FZD2 PIK3R1 RB1 NRP1 KAT2A POLE4 CDC20 MAD2L1 CDC23 ANAPC5 HRAS EP300 SLC25A4 CDC27 KAT5 ATF3 CALR CDKN1A SLC2A1 RAN TRRAP FOSL1 MAP2K4 XPO1 NFATC3 TLN1 SRF CREBBP TBPL1 ADCY9 MYBL2 TGFBR2 JAK1 WNT9A ATF4
ECM-receptor interaction	0,011	4	GP5 THBS1 THBS2 COL27A1 COL3A1 HSPG2 LAMC3 ITGAV COL4A2 RELN COL5A1 COL1A1 DAG1 COL1A2 LAMC1 FN1 CD47 COL4A1
TGF-beta signaling pathway	0,013	4	TGFBR1 ROCK1 INHBC THBS1 PPP2CA ACVR1B BMP5 CUL1 INHBA LEFTY1 BMP6 SKP1 RPS6KB2 ACVR2B E2F5 MYC SMAD5 ID1 BMP2 SP1 ACVR1C EP300 RBX1 SMAD7 E2F4 MAPK1 CREBBP LEFTY2 TGFBR2 BMP4 BMPR2
Melanoma	0,013	6	BRAF E2F1 MET CDK4 NRAS IGF1R KRAS CDK6 TP53 CCND1 E2F3 AKT1 PDGFB PIK3R1 RB1 HRAS CDKN1A MAP2K1 PTEN FGFR1 MAPK1 MDM2
RNA degradation	0,015	5	DCP1A CNOT6 TOB2 CNOT4 SKIV2L2 LSM8 DDX6 PABPC4 LSM6 BTG2 ENO1 DCP2 CNOT7 MPHOSPH6 RQCD1 XRN1 HSPA9 DCPS CNOT10 BTG3 CNOT10 BTG3 CNOT1 PFKM PAN3 NUDT16 XRN2 PFKL BTG1 PATL1
Neurotrophin signaling pathway	0,016	6	CAMK2D BRAF NFKB1 SOS2 RIPK2 NRAS CRKL YWHAE CALM3 CALM1 MAP3K1 KRAS RPS6KA5 TP53 PLCG1 MAPK8 AKT1 NFKBIA ARHGDIA PIK3R1 RAC1 HRAS RPS6KA3 GAB1 MAP2K1 IRAK2 SH2B1 PRDM4 MAPK1 ABL1 ATF4 RPS6KA2

KEGG Pathway	FDR	Number of miRNAs	Putative target genes
Regulation of actin cytoskeleton	0,020	6	PPP1CA PFN1 BRAF ACTB ARPC5L SSH2 EZR ROCK1 WASL SOS2 NRAS CRKL CRK PAK2 ARHGEF12 ACTG1 PXN BDKRB2 RDX MYH9 VCL KRAS MSN PIP4K2A VAV2 PTK2 ITGAV GSN SLC9A1 PIKFYVE PPP1R12A PFN2 F2R DIAPH1 ARPC2 MYL9 PDGFB WASF2 CFL2 PIK3R1 RAC1 SRC HRAS MYLK3 FN1 MAP2K1 ARHGEF7 NCKAP1 VAV3 FGFR1 MAPK1 PIP4K2C PPP1CB PIP4K2B
Colorectal cancer	0,025	4	BRAF FOS TGFBR1 TCF7L2 BCL2 AXIN1 KRAS MLH1 TP53 CASP3 CCND1 MSH6 MAPK8 AKT1 MYC PIK3R1 RAC1 MAP2K1 MAPK1 TGFBR2
Signaling pathways regulating pluripotency of stem cells	0,031	5	BMI1 STAT3 FZD5 KAT6A INHBC NRAS REST ACVR1B HAND1 FZD6 SMARCAD1 INHBA AXIN1 IGF1R ZFHX3 KRAS FZD3 ACVR2B AKT1 MYC LIFR SKIL SMAD5 ID1 FZD2 PIK3R1 BMP2 ACVR1C HRAS IL6ST MAO2K1 FGFR1 SOX2 MAPK1 PCGF3 LEFTY2 JAK1 WNT9A BMP4 BMPR2
PI3K-Akt signaling pathway	0,033	6	PRLR RBL2 TSC1 NFKB1 MET YWHAH SOS2 PKN4 CDK4 ATF2 NRAS YWHAE THBS1 ATF6B THBS2 PPP2CA YWHAG MCL1 CDK2 CCND2 COL27A1 CHUK BCL2 CDKN1B PPP2R5D YWHAB EIF4EBP1 IGF1R GNB1 TLR4 KRAS CDK6 COL3A1 IFNAR2 RPS6KB2 PPP2R5A TP53 CREB1 PTK2 LAMC3 ITGAV DDIT4 CCND1 LPAR1 CCNE2 COL4A2 AKT1 F2R MYC RELN COL5A1 PDGFB COL1A1 KIT PIK3R1 HSP90B1 YWHAZ PHLPP1 PPP2R3C EPHA2 RAC1 INSR PRKAA1 COL1A2 HRAS LAMC1 EIF4E2 CREB3L2 CREB3L1 FN1 PKN2 CDKN1A MAP2K1 VEGFA PTEN FGFR1 SGK3 MAPK1 GNG5 TEK JAK1 MDM2 ATF4 BCL2L11 COL4A1 IL6R EFNA1 NR4A1
TNF signaling pathway	0,033	5	MAGI2 FOS NFKB1 ATF2 BCL3 ATF6B CHUK VCAM1 TAB2 TAB3 RPS6KA5 FADD SOCS3 CREB1 CASP3 JUNB MAPK8 AKT1 NFKBIA PTGS2 PIK3R1 DNM1L JAG1 FAS CREB3L2 CREB3L1 MAP2K1 BIRC3 EDN1 MAP2K4 MAPK1 MAP3K7 MMP14 ATF4 BIRC2
Other types of O-glycan biosynthesis	0,036	2	OGT POMT2 GXYLT1 LFNG B4GALT1 EOGT B4GALT3
Pancreatic cancer	0,036	5	BRAF STAT3 E2F1 TGFBR1 NFKB1 CDK4 RAD51 CHUK KRAS CDK6 TP53 CCND1 E2F3 MAPK8 AKT1 PIK3R1 RB1 RAC1 MAP2K1 VEGFAA MAPK1 TGFBR2 JAK1

KEGG Pathway	FDR	Number of miRNAs	Putative target genes
MAPK signaling pathway	0,040	6	BRAF DUSP4 HSPA2 FOS ECSIT TGFBR1 NFKB1 IL1R1 SOS2 ATF2 NRAS DUSP2 CRKL STK4 ELK4 MAP3K3 CRK PAK2 DUSP6 CHUK MAP4K3 MAP3K1 TAB2 KRAS TAOK1 RPS6KA5 TP53 NLK DUSP10 CASP3 MAPKPK5 RAPGEF2 MAPK8 AKT1 MYC PPM1A PDGFB FLNA RAC1 HSPA8 DUSP7 DUSP3 MAX FAS HRAS RPS6KA3 MAP2K1 MAP3K2 DUSP5 MAP2K4 NFATC3 FGFR1 MAPK1 MAP3K7 SRF DUSP1 TGFBR2 ATF4 DAXX ARRB1 NR4A1 RPS6KA2
Salmonella infection	0,041	4	PFN1 ACTB FOS ARPC5L NFKB1 ROCK1 WASL PKN3 PLEKHM2 IL18 ACTG1 DYNC1H1 MYH9 TLR4 TJP1 PFN2 DYNC1LI2 MAPK8 ARPC2 WASF2 FLNA RAC1 KLC1 PKN2 MAPK1 RHOG
Prolactin signaling pathway	0,047	5	ESR1 PRLR FOS STAT3 NFKB1 SOS2 NRAS CCND2 TNFRSF11A KRAS SOCS3 CCND1 SOCS1 MAPK8 AKT1 SOCS5 PIK3R1 SRC HRAS MAP2K1 MAPK1 IRF1 SOCS7
ErbB signaling pathway	0,047	6	CAMK2D BRAF SOS2 CBL NRAS CRKL CRK PAK2 AREG CDKN1B EIF4EBP1 ERBB3 KRAS RPS6KB2 PTK2 PLCG1 MAPK8 AKT1 MYC PIK3R1 SRC HRAS GAB1 CDKN1A MAP2K1 MAPK1 ABL2 ABL1

Annex II. sEV miRNAs pathway enrichment analysis after H_2O_2 exposure in ARPE-19 cells. Enrichment analysis performed by DIANA mirPATH. KEGG pathways with a p_value < 0.05.

KEGG pathway	FDR	Number of miRNAs	Putative target genes
Proteoglycans in cancer	$5{,}23 \times 10^{-9}$	2	ACTB FZD5 ITGB1 EZR SOS2 SMAD2 CBL ARHGEF12 ROCK2 FZD6 IQGAP1 RAF1 IGF1R EGFR FZD3 PAK1 TP53 CTTN SLC9A1 DCN PLCG1 PIK3CD CCND1 AKT1 MYC FLNB PIK3CG PTPN11 RAC1 FZD1 ANK1 PDPK1 VMP1 MTOR FGFR1 MAPK1 MDM2 RPS6KB1 CD44 PRKACB PPP1CB
Chronic myeloid leukemia	$2{,}14 \times 10^{-6}$	2	E2F1 TGFBR1 SOS2 CDK4 CBL E2F2 RUNX1 CTBP1 RAF1 CDKN1B TP53 PIK3CD CCND1 SMAD4 E2F3 AKT1 MYC NFKBIA PIK3CG PTPN11 MEDOM MAPK1 TGFBR2 MDM2
TGF-beta signaling pathway	$2{,}58 \times 10^{-5}$	2	TGFBR1 ID2 SMAD2 NODAL SMURF2 BMPR1B LEFTY1 ID4 ACVR2B ZFYVE16 DCN SMAD4 MYC RBL1

KEGG pathway	FDR	Number of miRNAs	Putative target genes
			LTBP1 E2F4 MAPK1 SMAD1 TGFBR2 RPS6KB1
Transcriptional misregulation in cancer	$2{,}58x10^{-5}$	2	CCNT2 NFKBIZ ID2 FUS ETV6 ELK4 RUNX1 AFF1 CCND2 CDKN1B MLLT3 IGF1R RUNX2 TP53 ATM MYC KLF3 PLAT FLT1 JMJD1C ETV1 BCL6 DOT1L PPARG KMT2A BCL2A1 EWSR1 SMAD1 TGFBR2 MDM2 TAF15
Other types of O-glycan biosynthesis	$3{,}19x10^{-5}$	1	ST3GAL3 OGT POMT2 MFNG GXYLT1 B3GAT2 B4GALT1 POFUT1
Pathways in cancer	$3{,}55x10^{-5}$	2	FZD5 E2F1 TGFBR1 ITGB1 SOS2 CDK4 LAMB1 SMAD2 CBL E2F2 CXCR4 STK4 GNAS LAMA5 RUNX1 TPR CTBP1 ARHGEF12 BAX ROCK2 FZD6 RAF1 CDKN1B TRAF4 PLD1 LPAR2 BRCA2 IGF1R EGFR APPL1 FZD3 VHL TP53 LAMC3 PLCG1 PIK3CD CCND1 SMAD4 MSH6 COL4A2 E2F3 AKT1 PGF F2R MYC NFKBIA KIT COL4A3 PIK3CG HSP90B1 RAC1 FGF18 FZD1 PPARG GNAQ PIAS2 CCNE1 MECOM CYCS MTOR FGFR1 MAPK1 TGFBR2 MDM2 PLCB4 PRKACB
ECM-receptor interaction	$8{,}31x10^{-5}$	1	ITGB1 ITGB8 LAMB1 PAMA5 COL27A1 AGRN LAMC3 COL4A2 COL5A3 CD44
Glioma	$8{,}31x10^{-5}$	2	E2F1 SOS2 CDK4 E2F2 RAF1 IGF1R EGFR TP53 PLCG1 PIK3CD CCND1 E2F3 AKT1 PIK3CG MTOR MAK1 MDM2
Non-small cell lung cancer	$9{,}84x10^{-5}$	2	E2F1 SOS2 CDK4 E2F2 STK4 RAF1 EGFR TP53 PLCG1 PIK3CD CCND1 E2F3 AKT1 PIK3CG PDPK1 MAPK1
Signaling pathways regulating pluripotency of stem cells	0,0003	2	JARID2 FZD5 ID2 SMAD2 NODAL REST BMPR1B TBX3 FZD6 RAF1 IGF1R ZFHX3 ID4 FZD3 ACVR2B RIF1 PIK3CD JAK2 SMAD4 AKT1 MYC SKIL PIK3CG FZD1 ISL1 FGFR1 SOX2 MAPK1 SMAD1
Pancreatic cancer	0,0005	2	E2F1 TGFBR1 CDK4 SMAD2 E2F2 RAF1 PLD1 BRCA2 EGFR TP53 PIK3CD CCND1 SMAD4 E2F3 AKT1 PIK3CG RAC1 MAPK1 TGFBR2
Central carbon metabolism in cancer	0,0005	2	PKM RAF1 EGFR SLC7A5 SLC16A3 G6PD TP53 PIK3CD AKT1 MYC KIT PIK3CG IDH1 MTOR FGFR1 MAPK1 SLC1A5
Small cell lung cancer	0,0010	2	E2F1 ITGB1 CDK4 LAMB1 E2F2 LAMA5 CDKN1B TRAF4 TP53 LAMC3 PIK3CD CCND1 COL4A2 E2F3 AKT1 MYC NFKBIA COL4A3 PIK3CG PIAS2 CCNE1 CYCS
FoxO signaling pathway	0,0012	2	TGFBR1 CCNB1 SOS2 SMAD2 STK4 CCND2 RAF1 CDKN1B IGF1R EGFR

KEGG pathway	FDR	Number of miRNAs	Putative target genes
			GADD45A IL7R G6PC3 ATM PIK3CD CCND1 SMAD4 AKT1 PIK3CG INSR PRKAA1 BCL6 PRKAB2 PRKAG2 PDPK1 MAPK1 TGFBR2 MDM2 BCL2L11
Thyroid hormone signaling pathway	0,0013	2	ACTB MED13L RAF1 MED13 ATP1B1 THRA MED17 NCOA3 TP53 SLC9A1 NOTCH1 PLCG1 PIK3CD CCND1 AKT1 MYC PIK3CG PDPK1 PFKFB2 MTOR MAPK1 MDM2 PLCB4 NCOA1 PRKACB
Colorectal cancer	0,0014	2	TGFBR1 SMAD2 BAX RAF1 APPL1 TP53 PIK3CD CCND1 SMAD4 MSH6 AKT1 MYC PIK3CG RAC1 CYCS MAPK1 TGFBR2
Insulin signaling pathway	0,0018	2	PHKA2 TSC1 SOS2 CBL RAF1 PTPRF G6PC3 PPP1R3A PIK3CD AKT1 PIK3CG PRKAR2A INSR PRKAA1 PHKA1 PRKAB2 PRKAR1A ACACB PRKAG2 MKNK1 PDPK1 MKNK2 MTOR GYS1 EXOC7 MAPK1 PPP1R3E RPS6KB1 PRKACB PPP1CB ACACA
Prostate cancer	0,0018	2	E2F1 SOS2 E2F2 RAF1 CDKN1B IGF1R EGFR TP53 CREB1 PIK3CD CCND1 E2F3 AKT1 NFKBIA PIK3CG HSP90B1 CCNE1 PDPK1 MTOR FGFR1 MAPK1 MDM2
Lysine degradation	0,0028	2	WHSC1L1 NSD1 ASH1L PHTKPL DOT1L SUV420H2 KMT2A KMT2E KMT2C
Cell cycle	0,0069	2	E2F1 CCNB1 CDK4 SMAD2 E2F2 ORC2 CCND2 SMC3 CDKN1B WEE1 GADD45A TP53 ATM TFDP2 CCND1 SMAD4 E2F3 MYC RBL1 ANAPC5 CCNE1 ORD6 E2F4 RAD21 MDM2 CDC25A
Melanoma	0,0069	2	E2F1 CDK4 E2F2 RAF1 IGF1R EGFR TP53 PIK3CD CCND1 E2F3 AKT1 PIK3CG FDF18 FGFR1 MAPK1 MDM2
Adherent junction	0,0077	2	ACTB CSNK2A2 TGFBR1 WASF1 SMAD2 LMO7 IQGAP1 IGF1R EGFR PTPRF SMAD4 PTPRJ RAC1 INSR SSX2IP FGFR1 MAPK1 TGFBR2
P53 signaling pathway	0,0103	2	CCNG1 CCNB1 CDK4 CCND2 BAX GADD45A TP53 ATM CCND1 TP73 SESN2 MDM4 CCNE1 CYCS GTSE1 MDM2
AMPK signaling pathway	0,0259	2	TSC1 SCD5 IGF1R CAMKK2 G6PC3 CREB1 PIK3CD CCND1 AKT1 PPP2R2A PIK3CG INSR PRKAA1 PRKAB2 PPARG ACACB PRKAG2 PDPK1 PFKFB2 MTOR GYS1 RPS6KB1 ACACA

KEGG pathway	FDR	Number of miRNAs	Putative target genes
Bladder cancer	0,0329	2	E2F1 CDK4 E2F2 RAF1 EGFR TP53 CCND1 E2F3 MYC MAPK1 MDM2

Annex III. miR-205-5p predicted mRNA targets. Top 100 predicted mRNA targets by TargetScan Human 7.2.

Target gene	Gene name
BICC1	bicaudal C homolog 1 (Drosophila)
TNFAIP8	tumor necrosis factor, alpha-induced protein 8
CHN1	chimerin 1
NEU1	sialidase 1 (lysosomal sialidase)
C11orf86	chromosome 11 open reading frame 86
HSD17B11	hydroxysteroid (17-beta) dehydrogenase 11
C10orf131	chromosome 10 open reading frame 131
TIMM17A	translocase of inner mitochondrial membrane 17 homolog A (yeast)
HS3ST1	heparan sulfate (glucosamine) 3-O-sulfotransferase 1
TMEM144	transmembrane protein 144
SLC35B3	solute carrier family 35 (adenosine 3'-phospho 5'-phosphosulfate transporter), member B3
ABI2	abl-interactor 2
FAM136A	family with sequence similarity 136, member A
LRP1	low density lipoprotein receptor-related protein 1
RNF146	ring finger protein 146
ACSL1	acyl-CoA synthetase long-chain family member 1
CALCRL	calcitonin receptor-like
SLC35A1	solute carrier family 35 (CMP-sialic acid transporter), member A1
CFL2	cofilin 2 (muscle)
CXorf21	chromosome X open reading frame 21
CCNJ	cyclin J
CLTC	clathrin, heavy chain (Hc)
EVA1C	eva-1 homolog C (C. elegans)
TGFA	transforming growth factor, alpha
YES1	v-yes-1 Yamaguchi sarcoma viral oncogene homolog 1
CLDN11	claudin 11
SEPT4	septin 4
GXYLT1	glucoside xylosyltransferase 1
ARHGAP17	Rho GTPase activating protein 17
BTBD3	BTB (POZ) domain containing 3

Target gene	Gene name
BMPER	BMP binding endothelial regulator
NACC2	NACC family member 2, BEN and BTB (POZ) domain containing
CTPS2	CTP synthase 2
SORBS1	sorbin and SH3 domain containing 1
PET117	PET117 homolog (S. cerevisiae)
TP53BP2	tumor protein p53 binding protein, 2
CDH11	cadherin 11, type 2, OB-cadherin (osteoblast)
LRRK2	leucine-rich repeat kinase 2
DSC2	desmocollin 2
NDUFA4	NADH dehydrogenase (ubiquinone) 1 alpha subcomplex, 4, 9kDa
GEMIN6	gem (nuclear organelle) associated protein 6
ADAMTS9	ADAM metallopeptidase with thrombospondin type 1 motif, 9
DLG2	discs, large homolog 2 (Drosophila)
AAK1	AP2 associated kinase 1
SGMS1	sphingomyelin synthase 1
CDK14	cyclin-dependent kinase 14
C3orf80	chromosome 3 open reading frame 80
PTP4A1	protein tyrosine phosphatase type IVA, member 1
ENC1	ectodermal-neural cortex 1 (with BTB domain)
CREBRF	CREB3 regulatory factor
PCNX	pecanex homolog (Drosophila)
RAP2B	RAP2B, member of RAS oncogene family
SRSF10	serine/arginine-rich splicing factor 10
CDK19	cyclin-dependent kinase 19
FOXF1	forkhead box F1
AL626787.1	
PICALM	phosphatidylinositol binding clathrin assembly protein
FRK	fyn-related kinase
PTPRM	protein tyrosine phosphatase, receptor type, M
ONECUT1	one cut homeobox 1
SH3GL3	SH3-domain GRB2-like 3
MARCKS	myristoylated alanine-rich protein kinase C substrate

Target gene	Gene name
SH3BGRL3	SH3 domain binding glutamic acid-rich protein like 3
CMTM4	CKLF-like MARVEL transmembrane domain containing 4
CBX1	chromobox homolog 1
GLRB	glycine receptor, beta
CASC4	cancer susceptibility candidate 4
SATB2	SATB homeobox 2
DDX5	DEAD (Asp-Glu-Ala-Asp) box helicase 5
VEGFA	vascular endothelial growth factor A
LYN	v-yes-1 Yamaguchi sarcoma viral related oncogene homolog
B4GALT6	UDP-Gal:betaGlcNAc beta 1,4- galactosyltransferase, polypeptide 6
ZFYVE16	zinc finger, FYVE domain containing 16
ARRB2	arrestin, beta 2
EPB41L4B	erythrocyte membrane protein band 4.1 like 4B
LPCAT1	lysophosphatidylcholine acyltransferase 1
ZNF536	zinc finger protein 536
ESRRG	estrogen-related receptor gamma
FGF14	fibroblast growth factor 14
USP13	ubiquitin specific peptidase 13 (isopeptidase T-3)
PHYHIPL	phytanoyl-CoA 2-hydroxylase interacting protein-like
MICU3	mitochondrial calcium uptake family, member 3
NAA11	N(alpha)-acetyltransferase 11, NatA catalytic subunit
NECAP1	NECAP endocytosis associated 1
NSF	N-ethylmaleimide-sensitive factor
PSMA4	proteasome (prosome, macropain) subunit, alpha type, 4
SIAH1	siah E3 ubiquitin protein ligase 1
ZEB1	zinc finger E-box binding homeobox 1
TSHZ3	teashirt zinc finger homeobox 3
EFCAB4A	EF-hand calcium binding domain 4A
PGAP3	post-GPI attachment to proteins 3
TTC19	tetratricopeptide repeat domain 19
TM9SF2	transmembrane 9 superfamily member 2
RP11-17M16.1	Homo sapiens FLJ44313 protein (FLJ44313), mRNA.

Target gene	Gene name
ABCD2	ATP-binding cassette, sub-family D (ALD), member 2
PSTK	phosphoseryl-tRNA kinase
CREB1	cAMP responsive element binding protein 1
ZEB2	zinc finger E-box binding homeobox 2
TAOK1	TAO kinase 1

Annex IV. miR-521 predicted mRNA targets. Top 100 predicted mRNA targets by TargetScan Human 7.2.

Target gene	Gene name
WDYHV1	WDYHV motif containing 1
GABPB1	GA binding protein transcription factor, beta subunit 1
PLEKHA1	pleckstrin homology domain containing, family A (phosphoinositide binding specific) member 1
RPS6KB2	ribosomal protein S6 kinase, 70kDa, polypeptide 2
LTB	lymphotoxin beta (TNF superfamily, member 3)
MC2R	melanocortin 2 receptor (adrenocorticotropic hormone)
GGACT	gamma-glutamylamine cyclotransferase
RNF144B	ring finger protein 144B
AP4S1	adaptor-related protein complex 4, sigma 1 subunit
NAIP	NLR family, apoptosis inhibitory protein
RNF152	ring finger protein 152
NEU3	sialidase 3 (membrane sialidase)
TBX5	T-box 5
RNF121	ring finger protein 121
DNAJC5	DnaJ (Hsp40) homolog, subfamily C, member 5
DECR2	2,4-dienoyl CoA reductase 2, peroxisomal
KDM5D	lysine (K)-specific demethylase 5D
RASSF1	Ras association (RalGDS/AF-6) domain family member 1
MTDH	metadherin
PSTPIP1	proline-serine-threonine phosphatase interacting protein 1
FAM215A	family with sequence similarity 215, member A (non-protein coding)
KIAA0947	KIAA0947
WIPI2	WD repeat domain, phosphoinositide interacting 2

Target gene	Gene name
RNGTT	RNA guanylyltransferase and 5'-phosphatase
HAND2	heart and neural crest derivatives expressed 2
UBE2E1	ubiquitin-conjugating enzyme E2E 1
FAM167A	family with sequence similarity 167, member A
RPA1	replication protein A1, 70kDa
EBF1	early B-cell factor 1
SKAP2	src kinase associated phosphoprotein 2
TRIB2	tribbles pseudokinase 2
SERINC2	serine incorporator 2
PPP2R3B	protein phosphatase 2, regulatory subunit B", beta
SNX13	sorting nexin 13
PTCH2	patched 2
RSPO1	R-spondin 1
ART4	ADP-ribosyltransferase 4
GPX8	glutathione peroxidase 8 (putative)
TCF7L2	transcription factor 7-like 2 (T-cell specific, HMG-box)
C20orf144	chromosome 20 open reading frame 144
TNRC6C	trinucleotide repeat containing 6C
HNRNPA2B1	heterogeneous nuclear ribonucleoprotein A2/B1
NKX2-5	NK2 homeobox 5
STX1B	syntaxin 1B
EFNB2	ephrin-B2
COL24A1	collagen, type XXIV, alpha 1
PROS1	protein S (alpha)
CD99L2	CD99 molecule-like 2
PHF17	PHD finger protein 17
CYB5D1	cytochrome b5 domain containing 1
SLCO4C1	solute carrier organic anion transporter family, member 4C1
FAM19A1	family with sequence similarity 19 (chemokine (C-C motif)-like), member A1
HIF1AN	hypoxia inducible factor 1, alpha subunit inhibitor
HOXC13	homeobox C13
BTNL9	butyrophilin-like 9

Target gene	Gene name
KDSR	3-ketodihydrosphingosine reductase
IKBKG	inhibitor of kappa light polypeptide gene enhancer in B-cells, kinase gamma
IDH2	isocitrate dehydrogenase 2 (NADP+), mitochondrial
ARMCX1	armadillo repeat containing, X-linked 1
GALNT2	UDP-N-acetyl-alpha-D-galactosamine:polypeptide N-acetylgalactosaminyltransferase 2 (GalNAc-T2)
UBN2	ubinuclein 2
BCL2L14	BCL2-like 14 (apoptosis facilitator)
TFAP2C	transcription factor AP-2 gamma (activating enhancer binding protein 2 gamma)
WDR1	WD repeat domain 1
ARHGAP17	Rho GTPase activating protein 17
AXIN2	axin 2
COL23A1	collagen, type XXIII, alpha 1
NETO1	neuropilin (NRP) and tolloid (TLL)-like 1
GULP1	GULP, engulfment adaptor PTB domain containing 1
ZNF791	zinc finger protein 791
PI4K2A	Phosphatidylinositol 4-kinase type 2-alpha; Uncharacterized protein
OSBPL3	oxysterol binding protein-like 3
AKIRIN1	akirin 1
RANGRF	RAN guanine nucleotide release factor
CLASP1	cytoplasmic linker associated protein 1
HEBP2	heme binding protein 2
CCNE1	cyclin E1
ASB6	ankyrin repeat and SOCS box containing 6
PPAPDC3	phosphatidic acid phosphatase type 2 domain containing 3
CRY1	cryptochrome 1 (photolyase-like)
TMEM201	transmembrane protein 201
PLD6	phospholipase D family, member 6
ADRM1	adhesion regulating molecule 1
LAGE3	L antigen family, member 3
PIH1D3	PIH1 domain containing 3
C7orf72	chromosome 7 open reading frame 72
PHB2	prohibitin 2

Target gene	Gene name
COIL	coilin
DAZAP1	DAZ associated protein 1
MYT1	myelin transcription factor 1
CASP9	caspase 9, apoptosis-related cysteine peptidase
ELOVL2	ELOVL fatty acid elongase 2
FAM49B	family with sequence similarity 49, member B
WNT9A	wingless-type MMTV integration site family, member 9A
SLC1A7	solute carrier family 1 (glutamate transporter), member 7
KIAA0753	KIAA0753
ZNF83	zinc finger protein 83
MID1	midline 1 (Opitz/BBB syndrome)
MAFB	v-maf avian musculoaponeurotic fibrosarcoma oncogene homolog B

Annex V. miR-302c-3p predicted mRNA targets. Top 100 predicted mRNA targets by TargetScan Human 7.2.

Target gene	Gene name
C2orf69	chromosome 2 open reading frame 69
CROT	carnitine O-octanoyltransferase
FGF16	fibroblast growth factor 16
LMO3	LIM domain only 3 (rhombotin-like 2)
LCOR	ligand dependent nuclear receptor corepressor
CFL2	cofilin 2 (muscle)
OLFM3	olfactomedin 3
AEBP2	AE binding protein 2
KCNJ6	potassium inwardly-rectifying channel, subfamily J, member 6
STX11	syntaxin 11
UBL3	ubiquitin-like 3
MAP3K2	mitogen-activated protein kinase kinase kinase 2
LDOC1	leucine zipper, down-regulated in cancer 1
KCNJ2	potassium inwardly-rectifying channel, subfamily J, member 2
NFYA	nuclear transcription factor Y, alpha
ARID4B	AT rich interactive domain 4B (RBP1-like)
NOVA1	neuro-oncological ventral antigen 1
KDM1B	lysine (K)-specific demethylase 1B
TNFAIP1	tumor necrosis factor, alpha-induced protein 1 (endothelial)
GALNT3	UDP-N-acetyl-alpha-D-galactosamine:polypeptide N-acetylgalactosaminyltransferase 3 (GalNAc-T3)
CD83	CD83 molecule
RARB	retinoic acid receptor, beta
RALGPS2	Ral GEF with PH domain and SH3 binding motif 2
KCNK10	potassium channel, subfamily K, member 10
PICALM	phosphatidylinositol binding clathrin assembly protein
TRERF1	transcriptional regulating factor 1
CXXC5	CXXC finger protein 5
GAS2	growth arrest-specific 2
TMPRSS11F	transmembrane protease, serine 11F
MTF1	metal-regulatory transcription factor 1

Target gene	Gene name
RAP1A	RAP1A, member of RAS oncogene family
C10orf11	chromosome 10 open reading frame 11
EFEMP1	EGF containing fibulin-like extracellular matrix protein 1
ZKSCAN1	zinc finger with KRAB and SCAN domains 1
KCNB1	potassium voltage-gated channel, Shab-related subfamily, member 1
MUC7	mucin 7, secreted
RAB22A	RAB22A, member RAS oncogene family
TMEM74	transmembrane protein 74
IL6ST	interleukin 6 signal transducer (gp130, oncostatin M receptor)
PKN2	protein kinase N2
KIF23	kinesin family member 23
PDIK1L	PDLIM1 interacting kinase 1 like
ONECUT1	one cut homeobox 1
RASSF2	Ras association (RalGDS/AF-6) domain family member 2
ZNF367	zinc finger protein 367
C8orf46	chromosome 8 open reading frame 46
ZNF654	zinc finger protein 654
DDHD1	DDHD domain containing 1
PRC1	protein regulator of cytokinesis 1
ZNF2	zinc finger protein 2
CHMP4C	charged multivesicular body protein 4C
CAMK2N1	calcium/calmodulin-dependent protein kinase II inhibitor 1
ZBTB47	zinc finger and BTB domain containing 47
ARHGEF3	Rho guanine nucleotide exchange factor (GEF) 3
PAK7	p21 protein (Cdc42/Rac)-activated kinase 7
SYT14	synaptotagmin XIV
INSIG2	insulin induced gene 2
LGI1	leucine-rich, glioma inactivated 1
SSX2IP	synovial sarcoma, X breakpoint 2 interacting protein
TMEM154	transmembrane protein 154
HN1	hematological and neurological expressed 1
ESR1	estrogen receptor 1

Target gene	Gene name
C20orf62	chromosome 20 open reading frame 62
SPRED1	sprouty-related, EVH1 domain containing 1
LIF	leukemia inhibitory factor
JAK1	Janus kinase 1
DAPP1	dual adaptor of phosphotyrosine and 3-phosphoinositides
ASCC1	activating signal cointegrator 1 complex subunit 1
NAPEPLD	N-acyl phosphatidylethanolamine phospholipase D
NHLRC2	NHL repeat containing 2
NXT2	nuclear transport factor 2-like export factor 2
SAMD12	sterile alpha motif domain containing 12
IGDCC3	immunoglobulin superfamily, DCC subclass, member 3
UBE2E2	ubiquitin-conjugating enzyme E2E 2
PPAP2B	phosphatidic acid phosphatase type 2B
TUBG1	tubulin, gamma 1
IRF9	interferon regulatory factor 9
PDCD1LG2	programmed cell death 1 ligand 2
MARCH5	membrane-associated ring finger (C3HC4) 5
WDR26	WD repeat domain 26
VAMP3	vesicle-associated membrane protein 3
IKZF2	IKAROS family zinc finger 2 (Helios)
LARP1B	La ribonucleoprotein domain family, member 1B
LAMA3	laminin, alpha 3
MEF2C	myocyte enhancer factor 2C
IRF2	interferon regulatory factor 2
PBX3	pre-B-cell leukemia homeobox 3
LEFTY1	left-right determination factor 1
ADAMTSL3	ADAMTS-like 3
CDCA7	cell division cycle associated 7
CYP26B1	cytochrome P450, family 26, subfamily B, polypeptide 1
MCL1	myeloid cell leukemia sequence 1 (BCL2-related)
WNT5A	wingless-type MMTV integration site family, member 5A
LAMP5	lysosomal-associated membrane protein family, member 5
DERL2	derlin 2

Target gene	Gene name
AKT3	v-akt murine thymoma viral oncogene homolog 3
MYCBP	MYC binding protein
SOCS3	suppressor of cytokine signaling 3
TSEN34	TSEN34 tRNA splicing endonuclease subunit

Annex VI. miR-122-5p predicted mRNA targets. Top 100 predicted mRNA targets by TargetScan Human 7.2.

Target gene	Gene name
CTDNEP1	CTD nuclear envelope phosphatase 1
ALDOA	aldolase A, fructose-bisphosphate
RFXAP	regulatory factor X-associated protein
PLEKHB2	pleckstrin homology domain containing, family B (evectins) member 2
MASP1	mannan-binding lectin serine peptidase 1 (C4/C2 activating component of Ra-reactive factor)
CLIC4	chloride intracellular channel 4
SLC52A2	solute carrier family 52 (riboflavin transporter), member 2
PRKRA	protein kinase, interferon-inducible double stranded RNA dependent activator
NICN1	nicolin 1
AC002451.1	Protein LOC100996577
ST6GALNAC4	ST6 (alpha-N-acetyl-neuraminyl-2,3-beta-galactosyl-1,3)-N-acetylgalactosaminide alpha-2,6-sialyltransferase 4
P4HA1	prolyl 4-hydroxylase, alpha polypeptide I
FUNDC2	FUN14 domain containing 2
CLIC1	chloride intracellular channel 1
RBP5	retinol binding protein 5, cellular
CCNG1	cyclin G1
EPO	erythropoietin
BAI2	brain-specific angiogenesis inhibitor 2
TBR1	T-box, brain, 1
PIGS	phosphatidylinositol glycan anchor biosynthesis, class S
G6PC3	glucose 6 phosphatase, catalytic, 3
ZNF827	zinc finger protein 827
DUSP4	dual specificity phosphatase 4
CD320	CD320 molecule
SLC25A34	solute carrier family 25, member 34
FOXK2	forkhead box K2
SLC1A5	solute carrier family 1 (neutral amino acid transporter), member 5
RIMS1	regulating synaptic membrane exocytosis 1
SLC7A1	solute carrier family 7 (cationic amino acid transporter, y+ system), member 1

Target gene	Gene name
PDK4	pyruvate dehydrogenase kinase, isozyme 4
NPEPPS	aminopeptidase puromycin sensitive
MICU3	mitochondrial calcium uptake family, member 3
CCAR1	cell division cycle and apoptosis regulator 1
IGSF5	immunoglobulin superfamily, member 5
TBC1D10B	TBC1 domain family, member 10B
PIP4K2A	phosphatidylinositol-5-phosphate 4-kinase, type II, alpha
GRHL2	grainyhead-like 2 (Drosophila)
GALNTL6	UDP-N-acetyl-alpha-D-galactosamine:polypeptide N-acetylgalactosaminyltransferase-like 6
SLC41A1	solute carrier family 41 (magnesium transporter), member 1
CLIC5	chloride intracellular channel 5
SSR2	signal sequence receptor, beta (translocon-associated protein beta)
PEG10	paternally expressed 10
KDELC2	KDEL (Lys-Asp-Glu-Leu) containing 2
ADSS	adenylosuccinate synthase
MIPOL1	mirror-image polydactyly 1
C20orf112	chromosome 20 open reading frame 112
GRAMD3	GRAM domain containing 3
DUSP2	dual specificity phosphatase 2
FKBP5	FK506 binding protein 5
MAF1	MAF1 homolog (S. cerevisiae)
ANKRD13C	ankyrin repeat domain 13C
NT5C3A	5'-nucleotidase, cytosolic IIIA
CCNYL1	cyclin Y-like 1
CANX	calnexin
MMGT1	membrane magnesium transporter 1
SUCLA2	succinate-CoA ligase, ADP-forming, beta subunit
BRPF1	bromodomain and PHD finger containing, 1
ARL2	ADP-ribosylation factor-like 2
NOD2	nucleotide-binding oligomerization domain containing 2
CHMP3	charged multivesicular body protein 3
RNF103-CHMP3	RNF103-CHMP3 readthrough

Target gene	Gene name
CALM3	calmodulin 3 (phosphorylase kinase, delta)
SPRY2	sprouty homolog 2 (Drosophila)
FOXP2	forkhead box P2
CPEB1	cytoplasmic polyadenylation element binding protein 1
OCLN	occludin
RP11-181C3.1	Uncharacterized protein
SLC25A51	solute carrier family 25, member 51
HNRNPU	heterogeneous nuclear ribonucleoprotein U (scaffold attachment factor A)
CTNND2	catenin (cadherin-associated protein), delta 2
TBC1D22B	TBC1 domain family, member 22B
CS	citrate synthase
KIF5B	kinesin family member 5B
AC137932.1	
ARFGEF1	ADP-ribosylation factor guanine nucleotide-exchange factor 1 (brefeldin A-inhibited)
HECTD3	HECT domain containing E3 ubiquitin protein ligase 3
DENND2C	DENN/MADD domain containing 2C
KLHL18	kelch-like family member 18
SMARCD1	SWI/SNF related, matrix associated, actin dependent regulator of chromatin, subfamily d, member 1
PLAG1	pleiomorphic adenoma gene 1
ZNF668	zinc finger protein 668
KCNJ13	potassium inwardly-rectifying channel, subfamily J, member 13
PLXNA2	plexin A2
MEIS2	Meis homeobox 2
GCNT4	glucosaminyl (N-acetyl) transferase 4, core 2
BCAT2	branched chain amino-acid transaminase 2, mitochondrial
NPAS3	neuronal PAS domain protein 3
SLC13A5	solute carrier family 13 (sodium-dependent citrate transporter), member 5
SLC39A8	solute carrier family 39 (zinc transporter), member 8
KAT2A	K(lysine) acetyltransferase 2A
SORT1	sortilin 1
SLC25A29	solute carrier family 25 (mitochondrial carnitine/acylcarnitine carrier), member 29

Target gene	Gene name
STX16	syntaxin 16
UBE2G1	ubiquitin-conjugating enzyme E2G 1
CCDC97	coiled-coil domain containing 97
TEAD3	TEA domain family member 3
C17orf105	chromosome 17 open reading frame 105
GNPDA1	glucosamine-6-phosphate deaminase 1
STK24	serine/threonine kinase 24

Annex VII. miR-302a predicted mRNA targets. Top 100 predicted mRNA targets by TargetScan Human 7.2.

Target gene	Gene name
FMR1	fragile X mental retardation 1
CROT	carnitine O-octanoyltransferase
FAM169A	family with sequence similarity 169, member A
GRIK1-AS2	GRIK1 antisense RNA 2
RAB22A	RAB22A, member RAS oncogene family
DYRK4	dual-specificity tyrosine-(Y)-phosphorylation regulated kinase 4
TGFBR2	transforming growth factor, beta receptor II (70/80kDa)
TNRC6A	trinucleotide repeat containing 6A
LATS2	large tumor suppressor kinase 2
ZNF367	zinc finger protein 367
MCCD1	mitochondrial coiled-coil domain 1
ARID4B	AT rich interactive domain 4B (RBP1-like)
MARCH5	membrane-associated ring finger (C3HC4) 5
FGF16	fibroblast growth factor 16
TSEN34	TSEN34 tRNA splicing endonuclease subunit
GUCY1A3	guanylate cyclase 1, soluble, alpha 3
BTG1	B-cell translocation gene 1, anti-proliferative
LEFTY1	left-right determination factor 1
UBE2B	ubiquitin-conjugating enzyme E2B
LCOR	ligand dependent nuclear receptor corepressor

Target gene	Gene name
GALNT3	UDP-N-acetyl-alpha-D-galactosamine:polypeptide N-acetylgalactosaminyltransferase 3 (GalNAc-T3)
ZKSCAN1	zinc finger with KRAB and SCAN domains 1
MBD2	methyl-CpG binding domain protein 2
NFIB	nuclear factor I/B
CLOCK	clock circadian regulator
EDNRB	endothelin receptor type B
ZNF77	zinc finger protein 77
CAMK2N1	calcium/calmodulin-dependent protein kinase II inhibitor 1
DCAF6	DDB1 and CUL4 associated factor 6
KREMEN1	kringle containing transmembrane protein 1
LIN52	lin-52 homolog (C. elegans)
CFL2	cofilin 2 (muscle)
C2orf88	chromosome 2 open reading frame 88
DAZAP2	DAZ associated protein 2
APOC2	apolipoprotein C-II
MAP3K2	mitogen-activated protein kinase kinase kinase 2
UBE2W	ubiquitin-conjugating enzyme E2W (putative)
ZNF2	zinc finger protein 2
YOD1	YOD1 deubiquitinase
RELA	v-rel avian reticuloendotheliosis viral oncogene homolog A
YIPF7	Yip1 domain family, member 7
HN1	hematological and neurological expressed 1
FGD4	FYVE, RhoGEF and PH domain containing 4
IKZF2	IKAROS family zinc finger 2 (Helios)
PRDM4	PR domain containing 4
PRDM8	PR domain containing 8
IRF2	interferon regulatory factor 2
LYRM2	LYR motif containing 2
SLAIN1	SLAIN motif family, member 1
OXR1	oxidation resistance 1
IRF9	interferon regulatory factor 9
SUV39H1	suppressor of variegation 3-9 homolog 1 (Drosophila)
TMEM100	transmembrane protein 100

Target gene	Gene name
MSL1	male-specific lethal 1 homolog (Drosophila)
MSANTD4	Myb/SANT-like DNA-binding domain containing 4 with coiled-coils
ZNF800	zinc finger protein 800
LEFTY2	left-right determination factor 2
ATAD2	ATPase family, AAA domain containing 2
REEP3	receptor accessory protein 3
TIMM17A	translocase of inner mitochondrial membrane 17 homolog A (yeast)
LHX6	LIM homeobox 6
GLIS3	GLIS family zinc finger 3
PFN2	profilin 2
RPS6KA3	ribosomal protein S6 kinase, 90kDa, polypeptide 3
DDHD1	DDHD domain containing 1
E2F7	E2F transcription factor 7
PBX3	pre-B-cell leukemia homeobox 3
NR4A2	nuclear receptor subfamily 4, group A, member 2
HAUS8	HAUS augmin-like complex, subunit 8
PLAG1	pleiomorphic adenoma gene 1
ELAVL2	ELAV like neuron-specific RNA binding protein 2
PRRG4	proline rich Gla (G-carboxyglutamic acid) 4 (transmembrane)
SAR1B	SAR1 homolog B (S. cerevisiae)
DYRK2	dual-specificity tyrosine-(Y)-phosphorylation regulated kinase 2
PDCD1LG2	programmed cell death 1 ligand 2
POLK	polymerase (DNA directed) kappa
MYT1L	myelin transcription factor 1-like
SNTB2	syntrophin, beta 2 (dystrophin-associated protein A1, 59kDa, basic component 2)
CXorf67	chromosome X open reading frame 67
ST8SIA2	ST8 alpha-N-acetyl-neuraminide alpha-2,8-sialyltransferase 2
GPM6A	glycoprotein M6A
TFAP4	transcription factor AP-4 (activating enhancer binding protein 4)
MIXL1	Mix paired-like homeobox
RTN1	reticulon 1

Target gene	Gene name
KDM1B	lysine (K)-specific demethylase 1B
GDF11	growth differentiation factor 11
LAMP5	lysosomal-associated membrane protein family, member 5
ZBTB7A	zinc finger and BTB domain containing 7A
AMER2	APC membrane recruitment protein 2
DUSP2	dual specificity phosphatase 2
DERL2	derlin 2
GPR6	G protein-coupled receptor 6
PPP6C	protein phosphatase 6, catalytic subunit
ATF6B	activating transcription factor 6 beta
ANKRD50	ankyrin repeat domain 50
NR2C2	nuclear receptor subfamily 2, group C, member 2
C10orf11	chromosome 10 open reading frame 11
SAMD12	sterile alpha motif domain containing 12
KCNJ8	potassium inwardly-rectifying channel, subfamily J, member 8

Annex VIII. Related publications

1. **Maria Oltra**, Lorena Vidal-Gil, Rosa Maisto, Javier Sancho-Pelluz, and Jorge M. Barcia. Oxidative stress-induced angiogenesis is mediated by miR-205-5p (Journal of Celular and Molecular Medicine, January 2020). DOI: 10.1111/jcmm.14822.
2. **Maria Oltra**, Lorena Vidal-Gil, Rosa Maisto, Sara S. Oltra, Francisco Javier Romero, Javier Sancho-Pelluz, and Jorge M. Barcia. miR302a and 122 are deregulated in small extracellular vesicles from ARPE-19 cells cultured with H_2O_2 (Scientific Reports, November 2019). DOI: 10.1038/s41598-019-54373-x.

Received: 28 May 2019 | Revised: 17 October 2019 | Accepted: 4 November 2019

DOI: 10.1111/jcmm.14822

ORIGINAL ARTICLE

WILEY

Oxidative stress-induced angiogenesis is mediated by miR-205-5p

Maria Oltra[1,2,3] | Lorena Vidal-Gil[1,2,3] | Rosa Maisto[4] | Javier Sancho-Pelluz[2,3] | Jorge M. Barcia[2,3]

[1]Escuela de Doctorado, Universidad Católica de Valencia San Vicente Mártir, Valencia, Spain

[2]Neurobiología y Neurofisiología, Facultad de Medicina y Ciencias de la Salud, Universidad Católica de Valencia San Vicente Mártir, Valencia, Spain

[3]Centro de Investigación Traslacional San Alberto Magno, Universidad Católica de Valencia San Vicente Mártir, Valencia, Spain

[4]Department of Experimental Medicine, Università degli studi della Campania Luigi Vanvitelli, Napoli, Italy

Correspondence
Javier Sancho-Pelluz, Neurobiología y Neurofisiología, Centro de Investigación Traslacional San Alberto Magno, Universidad Católica de Valencia San Vicente Mártir, Valencia, Spain.
Email: fj.sancho@ucv.es

Funding information
Universidad Católica de Valencia San Vicente Mártir research Fund and Centro de Investigación Traslacional San Alberto Magno, Universidad Católica de Valencia San Vicente Mártir, Grant/Award Number: 2018-128-001, 2019-128-001; Escuela de Doctorado Universidad Católica de Valencia San Vicente Mártir, Grant/Award Number: EDUCV-PRE-2015-006 and EDUCV-PRE-2016-005

Abstract

miR-205-5p is known to be involved in VEGF-related angiogenesis and seems to regulate associated cell signalling pathways, such as cell migration, proliferation and apoptosis. Therefore, several studies have focused on the potential role of miR-205-5p as an anti-angiogenic factor. Vascular proliferation is observed in diabetic retinopathy and the 'wet' form of age-related macular degeneration. Today, the most common treatments against these eye-related diseases are anti-VEGF therapies. In addition, both AMD and DR are typically associated with oxidative stress; hence, the use of antioxidant agents is accepted as a co-adjuvant therapy for these patients. According to previous data, ARPE-19 cells release pro-angiogenic factors when exposed to oxidative insult, leading to angiogenesis. Matching these data, results reported here, indicate that miR-205-5p is modulated by oxidative stress and regulates VEGFA-angiogenesis. Hence, miR-205-5p is proposed as a candidate against eye-related proliferative diseases.

KEYWORDS

angiogenesis, microRNAs, retinal pigment epithelial cells

1 | INTRODUCTION

MicroRNAs (miRNAs) are non-coding RNAs [1,2] able to repress or degrade complementary mRNA of target genes involved in different biological processes including cell proliferation,[3] cell survival,[4] inflammation [5] and angiogenesis.[6] Vascular endothelial growth factor A (VEGFA) is one of the most important angiogenic factors involved in different types of cancer.[7] In fact, anti-VEGF therapies are widely used against cancer.[8-10] Actually, several reports indicate a direct role of miR-205-5p on VEGFA expression.[7,11-13] It has been observed that miR-205-5p directly suppresses expression of VEGFA and reduces cell proliferation-migration in human glioblastoma cells.[7] Moreover, An et al. showed that miR-205-5p inhibited the VEGF-PI3K/AKT pathway.[13] Other studies confirmed that miR-205-5p

This is an open access article under the terms of the Creative Commons Attribution License, which permits use, distribution and reproduction in any medium, provided the original work is properly cited.
© 2019 The Authors. *Journal of Cellular and Molecular Medicine* published by John Wiley & Sons Ltd and Foundation for Cellular and Molecular Medicine.

could inhibit the progression of tumour cells, targeting FOXO1[14] and CBX1,[15] among others, and promotes LRRK2-mediated apoptosis.[16]

Enhancement of VEGFA and neovascular overgrowth are behind two associated proliferative retinal disorders: diabetic retinopathy (DR)[17] and the neovascular—aka 'wet' —age-related macular degeneration (AMD).[18,19] Even though the significant release of VEGF has been reported several times,[20–22] little is known about the role of miR-205-5p in these diseases. VEGFA is released by retinal cells, including the retinal pigment epithelium (RPE).[23,24] This layer constitutes the blood-retinal barrier, playing a pivotal role between the bloodstream and photoreceptors.[25] For several reasons (light, metabolic rate, cellular membrane interactions, etc), RPE is continually exposed to oxidative stress (OS) [26–28]; hence, OS is considered a relevant risk factor for AMD.[27–29] Recent reports point out that OS in RPE cells intensifies the production and release of angiogenic factors, thus increasing the formation of new blood vessels.[20,30,31] Specifically, OS promotes VEGF production in RPE cells, leading to choroidal neovascularization.[18,32,33] In agreement with this, miR-205-5p overexpression also reduced reactive oxygen species (ROS) by increasing peroxiredoxin 2 levels,[34] suggesting that miR-205-5p could be sensitive to oxidative stimuli. Besides, OS is involved in eye diseases, such as AMD, and VEGFA-mediated angiogenesis plays a crucial role in the evolution of these diseases.[27,29,35,36] Indeed, VEGF inhibitors are widely used in both cancer and wet AMD, with beneficial results.[37,38]

The present work focuses on the response of miR-205-5p-VEGFA in ARPE-19 cells to oxidative challenge as an approach to the potential therapeutic target of eye-related proliferative disorders.

2 | MATERIALS AND METHODS

2.1 | Cell culture

The ARPE-19 human cell line was obtained from American Type Culture Collection (ATCC). Cells were cultured in Dulbecco's modified Eagle's medium DMEM/F12 (Invitrogen), as previously described.[20] Cells from passage numbers 11-30 were used and cultured to 80%–90% confluence at a starting density of 1×10^6 cells/cm^2 on different plates depending on the technique. After 2 days, the cells were treated for 24 hours with 600 μmol/L H_2O_2 (Scharlau) and 4 mM N-acetylcysteine (NAC) (Sigma-Aldrich) using media with 1% of fetal bovine serum (FBS). Cells and supernatant were collected and preserved for further experiments.

Human umbilical vein endothelial cells (HUVEC) were isolated from umbilical veins as previously described.[39] HUVEC were grown in Endothelial Cell Media supplemented with 20% FBS, penicillin/streptomycin and amphotericin at 37°C and 5% CO_2.

2.2 | Determination of intracellular ROS

Intracellular ROS levels were measured using dihydroethidium (DHE; Thermo Fisher Scientific), which is a superoxide indicator. This molecule has a blue fluorescence but, when oxidized to ethidium, it stains DNA red. ARPE-19 cells were seeded at 6×10^3 cells/well in a 96 well plate. Cells were rinsed with PBS (phosphate-buffered saline) twice and incubated with 5 μmol/L DHE for 30 min at 37°C and 5% CO_2. ROS levels were measured by a fluorescence multiplate reader (Victor X5; Perkin Elmer) excited at 518 nm and read at 605 nm.

2.3 | Mimic and inhibitor transfection

ARPE-19 cells seeded in a 6 well plate at 60%–80% confluence were transfected with miR-205-5p mirVana® miRNA mimic (Thermo Fisher Scientific) miR-205-5p mirVana® miRNA inhibitor and mirVana™ miRNA mimic negative control #1 (Thermo Fisher Scientific), as a negative control of transfection process, at a concentration of 30 pmol (10 μM), using Lipofectamine® RNAiMAX Reagent (Thermo Fisher Scientific) diluted in opti-MEM® Medium (Thermo Fisher Scientific). After 48 hours of transfection, the cell pellet and the media were collected for further analysis.

The groups were classified as: Control (physiological condition without transfection), Control + mimic miR-205-5p (physiological condition and transfection), Control + mimic Control- (physiological condition and transfection control), H_2O_2 600 μmol/L (oxidative stress condition), H_2O_2 600 μmol/L + mimic miR-205-5p (oxidative stress condition and transfection) and H_2O_2 600 μmol/L + mimic Control- (oxidative stress condition and transfection control).

2.4 | RNA isolation and miRNA expression analysis

The RNA was isolated from ARPE-19 cells using the miRNeasy Mini Kit (Qiagen) according to the manufacturer's instructions. Total RNA quantity and quality (260/280 absorbance ratio) were assessed using NanoDrop 2000 (Thermo Fisher Scientific). Quantitative real-time PCR (qRT-PCR) was used to analyse the miRNA expression profile of the selected miRNAs. For miRNA expression analysis, 100-300 ng of RNA were retrotranscribed using TaqMan MicroRNA Reverse Transcription Kit (Applied Biosystems) using specific TaqMan RT primers and the thermocycler PeqSTAR 96 Universal Gradient (PeqLAB), with cycles of 16°C/30 min, 42°C/30 min, 85°C/5 min and 4°C/infinity. qRT-PCR was performed using TaqMan™ microRNA Assays (Thermo Fisher Scientific) with TaqMan Gene Expression Master Mix (Applied Biosystems) and RT-PCR Roche 234 LighterCycler 480 with the appropriate temperature cycles. Normalization was done with RNU6B snoRNA. Relative expression was calculated as $2^{-\Delta\Delta Ct}$. For mRNA expression analysis, 1,000 ng of RNA were retrotranscribed with SuperScript III First-Strand Synthesis System (Life Technologies, Thermo Fisher Scientific) and the thermocycler PeqSTAR 96 Universal Gradient (PeqLAB), with cycles of 65°C/5 min, 4°C/5 min, 55°C/50 min, 85°C/5 min 37°C/20 min and 4°C/infinity. Quantitative real-time PCR was performed using Sybr Green Supermix (BioRad) and RT-PCR Roche 234 LighterCycler 480

with the appropriate temperature cycles. Normalization was done with GAPDH. Relative expression was calculated as $2^{-\Delta\Delta Ct}$.

2.5 | Analysis of miRNA target genes

In silico analysis of the putative targets of miR-205-5p was performed using Target Scan Human (http://www.targetscan.org/vert_72/). We analysed the pathways regulated by the putative targets of miR-205-5p with FUNRICH using the gene ontology database. With STRING (https://string-db.org/) we performed the networking of the targets related to angiogenic pathways.

2.6 | Western blotting

ARPE-19 cells, treated or control, were collected in RIPA Buffer (Thermo Fisher Scientific) and a protease/phosphatase inhibitor cocktail (Sigma-Aldrich). Equal amounts of protein (30 µg) were loaded and measured by SDS-PAGE on 4%-12% SDS-Polyacrylamide gel electrophoresis and electro-blotted onto a polyvinylidene difluoride membrane (PVDF; Millipore) by wet transfer. Membranes were incubated overnight with antibodies against VEGFA (1:200; Santa Cruz Biotechnology) and ß-actin (1:1,000; Santa Cruz Biotechnology) as loading control. Finally, the membranes were incubated for 2 hours at room temperature with anti-mouse and anti-rabbit IgG-HRP antibodies (Santa Cruz Biotechnology). The visualization was performed with ECL (Pierce, Thermo Fisher Scientific) and detected with Image Quant LAS-100 mini (GE Healthcare). Protein levels were quantified by densitometry using ImageJ software (NIH).

2.7 | Vasculogenesis assay

Vasculogenesis was analysed in normal Matrigel (Becton Dickinson) as previously described.[39] Briefly, 8 × 10^4 HUVEC cells/well in a 96 well plate were seeded and treated or not with ARPE-19 cells media for 5 hours. The different conditions were determined by the media used; control media, 600 µmol/L H_2O_2 media, miR-205-5p mimic-transfected control media and miR-205-5p mimic-transfected-600 µmol/L H_2O_2 media from ARPE-19 cells. Matrigel was diluted with DMEM/F12, FBS-free and allowed to solidify overnight at 37°C. Pictures were taken with a CKX41 inverted microscope (Olympus) and images recorded by an DP74 digital camera (Olympus). The images were analysed with Image J using the Angiogenesis Analyzer.

2.8 | Statistical analysis

Results of each experiment are presented as mean ± SEM. Statistical significance was set at 0.05 by using *t* test and 2-way–ANOVA.

3 | RESULTS

3.1 | Oxidative stress down-regulates miR-205-5p expression

As previously observed, ARPE-19 cells resulted in a significant ROS production after 600 µM H_2O_2 exposure.[40,41] This phenomenon was normalized by N-acetylcysteine (NAC) (Figure 1A). Significantly reduced miR-205-5p levels were observed in ARPE-19 cells after H_2O_2 exposure compared with control cells (Figure 1B). In order to assess whether this increase is oxidative stress-dependent, the antioxidant NAC (4 mmol/L) was added. NAC normalized the miR-205-5p levels reduced by H_2O_2. No significant changes in miR-205-5p expression levels were found in control ARPE-19 cells after NAC exposure (Figure 1B).

3.2 | miR-205-5p targets are related to vascular processes

Potential biological processes regulated by miR-205-5p were assessed using in silico analysis with TargetScan (http://www.targe

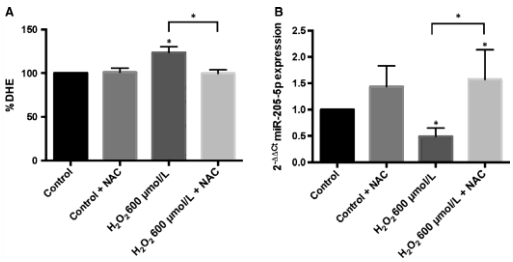

FIGURE 1 Oxidative stress regulates miR-205-5p expression. Superoxide anions were measured by DHE after H_2O_2 and NAC exposure (A). ARPE-19 miR-205-5p expression was analysed by qRT-PCR (B). Values are expressed as mean ± SEM (n = 3). Statistically significant differences were set at $^*P < .05$

tscan.org/vert_72/). Actually, 592 putative mRNA targets were found. To analyse the biological pathways and networks regulated by the predicted targets of miR-205-5p, these 592 mRNAs were entered into FUNRICH software (version 3.1.3). Functional enrichment analysis showed more than 2800 biological processes regulated by at least one mRNA target of miR-205-5p. The top 20 biological

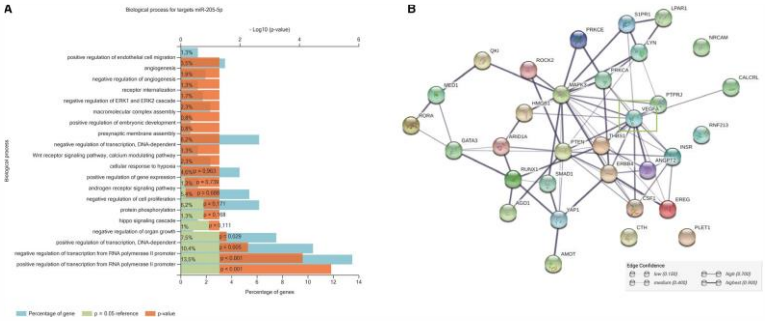

FIGURE 2 miR-205-5p protein target-related pathways. Top 20 biological processes regulated by miR-205-5p predicted targets, using FUNRICH and the gene ontology database (A). Interactional Network of miR-205-5p angiogenic related targets (B)

FIGURE 3 VEGFA is predicted as direct target of miR-205-5p. Predicted binding site of miR-205-5p with the 3'UTR mRNA VEGFA (A). qRT-PCR H_2O_2 exposure of miR-205-5p expression (B) and VEGFA mRNA expression (C). Spearman's correlation between miR-205-5p and VEGFA mRNA (D). qRT-PCR VEGFA mRNA expression after NAC exposure (E). Values are expressed as mean ± SEM (n = 3). Statistically significant differences were set at $^*P < .05$ and $^{**}P < .01$

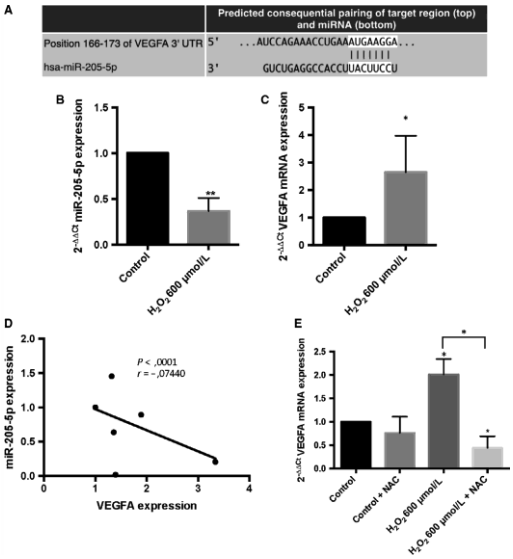

processes regulated by miR-205-5p are shown in Figure 2A. After selecting angiogenic and vasculogenic related processes, 32 mRNA predicted targets were found according to their functional protein association network, using STRING (https://string-db.org/) (Figure 2B and File S1).

3.3 | VEGFA mRNA is a direct target of miR-205-5p

Consistently with previous results, in silico analysis showed that VEGFA mRNA is a predicted target for miR-205-5p (Figure 2B). Target Scan predicted a 3'-UTR binding site for VEGFA mRNA and miR-205-5p (Figure 3A). In order to confirm the relation between VEGFA mRNA and miR-205-5p, VEGFA mRNA expression was analysed after H_2O_2 treatment. We observed that VEGFA mRNA levels were up-regulated after H_2O_2 exposure (Figure 3C), indicating a negative correlation with miR-205-5p levels (Figure 3B and 3D). Matching with the aforementioned results on miR-205-5p levels, VEGFA mRNA levels were also normalized by NAC exposure (Figure 3E).

3.4 | VEGFA expression is regulated by miR-205-5p

In order to test the role of miR-205-5p on VEGFA mRNA expression, ARPE-19 cells were transfected with a miR-205-5p mimic. The transfection process did not affect the ARPE-19 cells viability (File S2). The transfection with a negative control did not affect miR-205-5p expression. Transfected ARPE-19 cells with the mimic, increased miR-205-5p levels (Figure 4A), decreasing VEGFA mRNA levels (Figure 4B). Similarly, transfected ARPE-19 cells also decreased VEGFA mRNA levels after H_2O_2 exposure (Figure 4B). These results were confirmed by Western blotting analysis, showing a significant decrease of VEGFA protein expression after miR-205-5p mimic transfection in H_2O_2 treated cells (Figure 4C). MiR-205-5p was inhibited in untreated ARPE-19 cells and expression of mRNA VEGFA studied. No significant changes were found (File S3).

3.5 | Vasculogenesis is affected by miR-205-5p deregulation via VEGFA

A functional vasculogenesis assay was performed to confirm the inhibiting effect of miR-205-5p on VEGFA. HUVEC cells, grown with cell culture media obtained from control ARPE-19 cells, produced few vascular processes (Figure 5A, 5E and 5F). However, culture media obtained from H_2O_2 treated ARPE-19 cells significantly induced angiogenic changes in HUVEC cells (Figure 5C, 5E and 5F). Interestingly, HUVEC cells grown with mimic-transfected ARPE-19 cell culture media significantly abolished these angiogenic changes (Figure 5D, 5E and 5F). Cell culture media from mimic-transfected ARPE-19 cells also reduced angiogenesis in control HUVEC cells (Figure 5B, 5E and 5F).

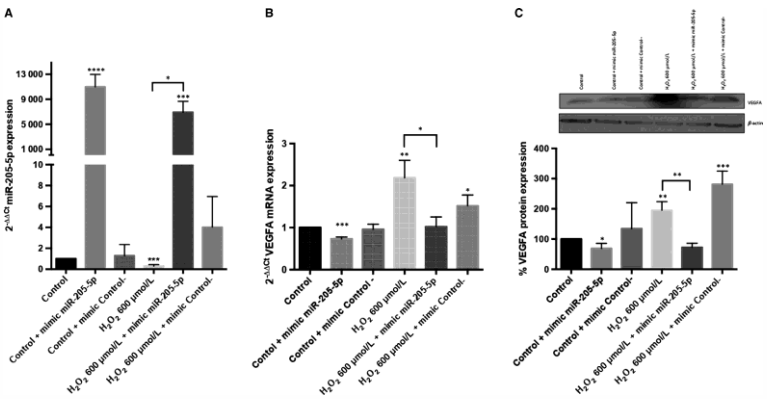

FIGURE 4 VEGFA expression is regulated by miR-205-5p. MiR-205-5p expression levels after 48 h of miR-205-5p mimic transfection and mimic negative control (A). VEGFA mRNA expression levels after 48 h of transfection with miR-205-5p mimic and mimic negative control were measured by qRT-PCR (B). Western blot analysis for VEGFA protein after miR-205-5p mimic and mimic negative control transfection (C). Values are expressed as mean ± SEM (n = 3). Statistically significant differences were set at *$P < .05$, **$P < .01$, ***$P < .001$ and ****$P < .0001$

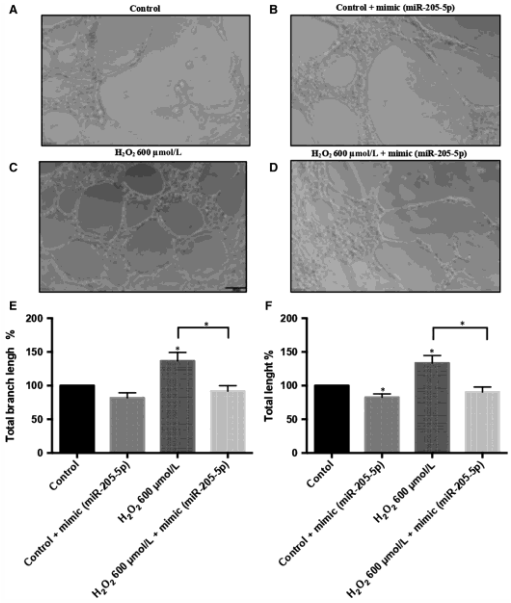

FIGURE 5 VEGFA-mediated Vasculogenesis is regulated by miR-205-5p. HUVEC cell tube formation under different ARPE-19 cell culture media conditions. ARPE-19 control medium (A), mimic(miR-205-5p)-treated ARPE-19 control (B), H_2O_2 600 µmol/L treated ARPE-19 (C) and mimic-treated ARPE-19 + H_2O_2 600 µmol/L medium (D). Scale bar 100 µmol/L. Total branch length (E) and total length (F) were calculated. Values are expressed as mean ± SEM (n = 3). Statistically significant differences were set at $^*P < .05$

4 | DISCUSSION

In a previous report, in which miR-205-5p was mapped in the mammalian eye, it was found in the epidermis and the anterior segmental epithelia and was not found in RPE.[42] Other studies have found that miR-125b[43] and miR-23a[44] are overexpressed in oxidative stress-induced RPE cells.[41] This current report is the first one indicating the presence of miR-205-5p in ARPE-19 cells as an RPE cell type. In contrast to the relevance of this miRNA on glioblastoma[13] or hepatocellular carcinoma,[45] little information is available about the presence of miR-205-5p in the eye.

4.1 | Oxidative stress down-regulates miR-205-5p expression

As mentioned above, H_2O_2 exposure resulted in a significant decrease in miR-205-5p levels in ARPE-19 cells. It has been suggested that miR-205-5p positively regulates the peroxiredoxin 2 (PRDX2) pathway.[34] PRDX2 reduces ROS derived from H_2O_2 transformation. In addition, miR-205-5p was identified as protective against OS via EGLN2 suppression.[46] Once considering this, reducing miR-205-5p levels after oxidative challenge is opposed to this proposed antioxidant mechanism. Perhaps excessive OS challenge (24 hours H_2O_2 600 µmol/L) leads to a different scenario, far from the physiological conditions that occur in wet AMD or cancer. Future research must address the antioxidant role of miR-205-5p. Another relevant finding is that NAC normalized those decreased miR-205-5p levels, indicating that miR-205-5p is sensitive to ROS.

4.2 | VEGFA mRNA as a miR-205-5p target

According to Yue et al., VEGFA 3'UTR-mRNA is one of the putative targets of miR-205-5p.[7] In addition, we have identified some potential targets of miR-205-5p and their biological processes. Among the potential mRNAs regulated by miR-205-5p, 3.5% are angiogenic and 1.3% are related to endothelial cell migration (Figure 2). In fact, it

is well documented that miR-205-5p acts as a tumour suppressor by regulating cell migration and proliferation.[7,11-13,47] Moreover, it has been suggested that miR-205-5p could interact indirectly via PI3K/AKT also involved in angiogenesis.[13] In the present report, we have observed that VEGFA and miR-205-5p are inversely expressed (Figure 3), inducing angiogenesis.

The results shown here confirm the fact that OS increases VEGFA expression levels.[20,48,49] On the one hand, H_2O_2 induction significantly increased both VEGFA mRNA and protein expression in ARPE-19. On the other hand, the addition of NAC normalized H_2O_2-induced ROS and VEGFA levels. This double result matches with the normalized miR-205-5p levels found after NAC exposure. NAC is a precursor of L-cysteine with scavenging properties and antioxidant effects, interacting with the antioxidant glutathione system.[50,51] In addition to direct VEGFA regulation, miR-205-5p also indirectly regulates ERK1/2 and PI3K/AKT pathways.[13,52] The PI3K/AKT signalling pathway induces the Nrf2/ARE antioxidant pathway,[53] and miR-205-5p could be involved in this route. Future research should be focused on the antioxidant machinery regulated by miR-205-5p.

VEGFA mRNA expression levels negatively correlated with miR-205-5p expression, highlighting the transcriptional regulation of VEGFA mRNA by this miRNA. Previous studies have already identified the regulation of VEGFA by miR-205-5p.[11-13] Additionally, the results reported here indicate that the VEGFA/miR-205-5p correlation might be regulated by OS in ARPE-19 cells.

Previous data have shown how different oxidative stimuli (ethanol [20] and high glucose[54]) promoted angiogenesis in ARPE-19 cells. More concretely, OS increased extracellular vesicles released from ARPE-19 cells, promoting these vascular changes.[20,31] Moreover, in this report, we demonstrated the effect of miR-205-5p/VEGFA regulation on vasculogenic processes induced by oxidative stimuli. OS is a common factor on DR and AMD, supporting the possibility that oxidative challenges on RPE lead to proliferative vascular responses found in AMD and DR.

Anti-VEGF administration is currently used to control neovascular processes in both DR and wet AMD.[37] Similarly, anti-VEGF therapies are also helpful against different forms of cancer, such as glioblastoma and colorectal cancer.[55] In agreement with this, miR-205-5p suppresses VEGFA expression in glioblastoma [7] and also inhibits the PI3K/AKT pathway.[13] In accordance with this, reducing VEGF-angiogenesis and PI3K/AKT could decrease tumour cell viability and proliferation. Thus, miR-205-5p could be considered as a plausible target against local vascular proliferative retinal processes. Moreover, increasing miR205-5p levels could be beneficial for these ocular proliferative disorders not only by the direct anti-VEGFA blockade but also by the PI3K/AKT pathway interaction.

ACKNOWLEDGEMENTS

The present work was funded by internal funds from Universidad Católica de Valencia San Vicente Mártir (2018-128-001) and the Centro de Investigación Traslacional San Alberto Magno, Universidad Católica de Valencia San Vicente Mártir (2019-128-001). Maria Oltra's salary came from a scholarship offered by Escuela de Doctorado Universidad Católica de Valencia San Vicente Mártir (EDUCV-PRE-2016-005). Lorena Vidal-Gil's salary came from a scholarship offered by Escuela de Doctorado Universidad Católica de Valencia San Vicente Mártir (EDUCV-PRE-2015-006).

CONFLICT OF INTEREST

The authors have no conflicts of interest to declare.

AUTHOR CONTRIBUTIONS

JSP and JMB designed the research programme. MO, LVG and RM performed the research. MO analysed the data. MO, JSP and JMB wrote the paper.

ORCID

Maria Oltra https://orcid.org/0000-0001-6397-2702
Rosa Maisto https://orcid.org/0000-0003-2952-8493
Javier Sancho-Pelluz https://orcid.org/0000-0001-5409-5760
Jorge M. Barcia https://orcid.org/0000-0002-3660-7977

DATA AVAILABILITY STATEMENT

The data that support the findings of this study are available from the corresponding author upon reasonable request.

REFERENCES

1. Ren C, Liu Q, Wei Q, et al. Circulating miRNAs as potential biomarkers of age-related macular degeneration. *Cell Physiol Biochem*. 2017;41:1413-1423.
2. Bhaskaran M, Mohan M. MicroRNAs: history, biogenesis, and their evolving role in animal development and disease. *Vet Pathol*. 2014;51:759-774.
3. Wang L, Dong F, Reinach PS, et al. MicroRNA-182 Suppresses HGF/SF-Induced Increases in retinal pigment epithelial cell proliferation and migration through targeting c-met. *PLoS ONE*. 2016;11:e0167684.
4. Tasharrofi N, Kouhkan F, Soleimani M, et al. Survival improvement in human retinal pigment epithelial cells via Fas receptor targeting by miR-374a. *J Cell Biochem*. 2017;118:4854-4861.
5. Hao Y, Zhou Q, Ma J, Zhao Y, Wang S. miR-146a is upregulated during retinal pigment epithelium (RPE)/choroid aging in mice and represses IL-6 and VEGF-A expression in RPE cells. *J Clin Exp Ophthalmol*. 2016;7(3):562.
6. Zhou Q, Gallagher R, Ufret-Vincenty R, Li X, Olson EN, Wang S. Regulation of angiogenesis and choroidal neovascularization by members of microRNA-23–27–24 clusters. *Proc Natl Acad Sci U S A*. 2011;108:8287-8292.
7. Yue X, Wang P, Xu J, et al. MicroRNA-205 functions as a tumor suppressor in human glioblastoma cells by targeting VEGF-A. *Oncol Rep*. 2012;27:1200-1206.
8. Dinç E, Ayaz L, Kurt AH. Effects of bevacizumab, ranibizumab, and aflibercept on MicroRNA expression in a retinal pigment epithelium cell culture model of oxidative stress. *J Ocul Pharmacol Ther*. 2018;34:1-8.
9. CATT Research Group, Martin DF, Maguire MG, et al. Ranibizumab and bevacizumab for neovascular age-related macular degeneration. *N Engl J Med*. 2011;364:1897-1908.
10. Frezzetti D, Gallo M, Maiello MR, et al. VEGF as a potential target in lung cancer. *Expert Opin Ther Targets*. 2017;21:959-966.

11. Zhao X, Zhou S, Wang D, He W, Li J, Zhang S. MicroRNA-205 is downregulated in hepatocellular carcinoma and inhibits cell growth and metastasis via directly targeting vascular endothelial growth factor A. *Oncol Lett*. 2018;16:2207-2214.
12. Cao W, Zhao Y, Wang L, Huang X. Circ0001429 regulates progression of bladder cancer through binding miR-205-5p and promoting VEGFA expression. *Cancer Biomark*. 2019;25(1):101-113.
13. An G, Liang S, Sheng C, Liu Y, Yao W. Upregulation of microRNA-205 suppresses vascular endothelial growth factor expression-mediated PI3K/Akt signaling transduction in human keloid fibroblasts. *Exp Biol Med*. 2017;242:275-285.
14. Lu Z, Xu Y, Yao Y, Jiang S. miR-205-5p contributes to paclitaxel resistance and progression of endometrial cancer by downregulating FOXO1. *Oncol Res*. 2019. https://doi.org/10.3727/096504018X15452187888839. [Epub ahead of print]
15. Hu A, Zhang Y, Zhao X, Li J, Ying Y. CBX1 is a direct target of miR-205-5p and contributes to the progression of pituitary tumor. *Pharmazie*. 2019;74:154-156.
16. Chen Q, Huang X, Li R. lncRNA MALAT1/miR-205-5p axis regulates MPP+-induced cell apoptosis in MN9D cells by directly targeting LRRK2. *Am J Transl Res*. 2018;10:563-572.
17. Li E-H, Huang Q-Z, Li G-C, Xiang Z-Y, Zhang X. Effects of miRNA-200b on the development of diabetic retinopathy by targeting *VEGFA* gene. *Biosci Rep*. 2017;37(2):BSR20160572.
18. Marneros AGVEGF-A. and the NLRP3 Inflammasome in Age-Related Macular. *Degeneration*. 2016;79-85. https://doi.org/10.1007/978-3-319-17121-0_12.
19. Penn JS, Madan A, Caldwell RB, Bartoli M, Caldwell RW, Hartnett ME. Vascular endothelial growth factor in eye disease. *Prog Retin Eye Res*. 2008;27:331-371.
20. Atienzar-Aroca S, Flores-Bellver M, Serrano-Heras G, et al. Oxidative stress in retinal pigment epithelium cells increases exosome secretion and promotes angiogenesis in endothelial cells. *J Cell Mol Med*. 2016;20:1457-1466.
21. Witmer A, Vrensen GFJ, Van Noorden CJ, Schlingemann R. Vascular endothelial growth factors and angiogenesis in eye disease. *Prog Retin Eye Res*. 2003;22:1-29.
22. Rubio RG, Adamis AP. Ocular angiogenesis: vascular endothelial growth factor and other factors. *Dev Ophthalmol*. 2016;55:28-37.
23. Miller JW. Age-related macular degeneration revisited–piecing the puzzle: the LXIX Edward Jackson memorial lecture. *Am J Ophthalmol*. 2013;155(1–35):e13.
24. Bellezza I. Oxidative stress in age-related macular degeneration: Nrf2 as therapeutic target. *Front Pharmacol*. 2018;9:1280.
25. Cunha-Vaz J, Bernardes R, Lobo C. Blood-retinal barrier. *Eur J Ophthalmol*. 2011;21:3-9.
26. Jarrett SG, Boulton ME. Consequences of oxidative stress in age-related macular degeneration. *Mol Aspects Med*. 2012;33:399-417.
27. Beatty S, Koh H, Phil M, Henson D, Boulton M. The role of oxidative stress in the pathogenesis of age-related macular degeneration. *Surv Ophthalmol*. 2000;45:115-134.
28. Tangvarasittichai O, Tangvarasittichai S. Oxidative stress, ocular disease and diabetes retinopathy. *Curr Pharm Des*. 2019;24:4726-4741.
29. Shaw PX, Stiles T, Douglas C, et al. Oxidative stress, innate immunity, and age-related macular degeneration. *AIMS Mol Sci*. 2016;3:196-221.
30. Simão S, Santos DF, Silva GA. Aliskiren decreases oxidative stress and angiogenic markers in retinal pigment epithelium cells. *Angiogenesis*. 2017;20:175-181.
31. Atienzar-Aroca S, Serrano-Heras G, Freire Valls A, et al. Role of retinal pigment epithelium-derived exosomes and autophagy in new blood vessel formation. *J Cell Mol Med*. 2018;22:5244-5256.
32. Marazita MC, Dugour A, Marquioni-Ramella MD, Figueroa JM, Suburo AM. Oxidative stress-induced premature senescence dysregulates VEGF and CFH expression in retinal pigment epithelial cells: Implications for Age-related Macular Degeneration. *Redox Biol*. 2016;7:78-87.
33. Dong A, Xie B, Shen J, et al. Oxidative stress promotes ocular neovascularization. *J Cell Physiol*. 2009;219:544-552.
34. Patil KS, Basak I, Pal R, et al. A Proteomics approach to investigate miR-153-3p and miR-205-5p targets in neuroblastoma cells. *PLoS ONE*. 2015;10(12):e0143969.
35. Reuter S, Gupta SC, Chaturvedi MM, Aggarwal BB. Oxidative stress, inflammation, and cancer: how are they linked? *Free Radic Biol Med*. 2010;49:1603-1616.
36. Lugrin J, Rosenblatt-Velin N, Parapanov R, Liaudet L. The role of oxidative stress during inflammatory processes. *Biol Chem*. 2014;395:203-230.
37. Salcedo-Villanueva G, Feria-Anzaldo E, Romo-Aguas JC, et al. Anti-VEGF treatment switch in neovascular age-related macular degeneration: a comparison of aflibercept versus ranibizumab after a single-dose switch. *Int Ophthalmol*. 2019;39(9):2023-2031.
38. Loizzi V, Del Vecchio V, Gargano G, et al. Biological pathways involved in tumor angiogenesis and bevacizumab based anti-angiogenic therapy with special references to ovarian cancer. *Int J Mol Sci*. 2017;18:1967.
39. Bueno-Betí C, Novella S, Lázaro-Franco M, et al. An affordable method to obtain cultured endothelial cells from peripheral blood. *J Cell Mol Med*. 2013;17:1475-1483.
40. Dinc E, Ayaz L, Kurt AH. Protective effect of combined caffeic acid phenethyl ester and bevacizumab against hydrogen peroxide-induced oxidative stress in human RPE cells. *Curr Eye Res*. 2017;42:1659-1666.
41. Ayaz L, Dinç E. Evaluation of microRNA responses in ARPE-19 cells against the oxidative stress. *Cutan Ocul Toxicol*. 2018;37:121-126.
42. Ryan DG, Oliveira-Fernandes M, Lavker RM. MicroRNAs of the mammalian eye display distinct and overlapping tissue specificity. *Mol Vis*. 2006;12:1175-1184.
43. Liu G, Zhang C-D, Wang J, Jia W-C. Inhibition of the oxidative stress-induced miR-125b protects glucose metabolic disorders of human retinal pigment epithelium (RPE) cells. *Cell Mol Biol (Noisy-Le-Grand)*. 2018;64:1-5.
44. Li D-D, Zhong B-W, Zhang H-X, et al. Inhibition of the oxidative stress-induced miR-23a protects the human retinal pigment epithelium (RPE) cells from apoptosis through the upregulation of glutaminase and glutamine uptake. *Mol Biol Rep*. 2016;43:1079-1087.
45. Shao P, Qu W-K, Wang C-Y, et al. MicroRNA-205-5p regulates the chemotherapeutic resistance of hepatocellular carcinoma cells by targeting PTEN/JNK/ANXA3 pathway. *Am J Transl Res*. 2017;9:4300-4307.
46. Muratsu-Ikeda S, Nangaku M, Ikeda Y, Tanaka T, Wada T, Inagi R. Downregulation of miR-205 modulates cell susceptibility to oxidative and endoplasmic reticulum stresses in renal tubular cells. *PLoS ONE*. 2012;7:e41462.
47. Li L, Li S. miR-205-5p inhibits cell migration and invasion in prostatic carcinoma by targeting ZEB1. *Oncol Lett*. 2018;16:1715-1721.
48. Kim Y-W, Byzova TV. Oxidative stress in angiogenesis and vascular disease. *Blood*. 2014;123:625-631.
49. Kannan R, Zhang N, Sreekumar PG, et al. Stimulation of apical and basolateral vascular endothelial growth factor-A and vascular endothelial growth factor-C secretion by oxidative stress in polarized retinal pigment epithelial cells. *Mol Vis*. 2006;12:1649-1659.
50. Samuni Y, Goldstein S, Dean OM, Berk M. The chemistry and biological activities of N-acetylcysteine. *Biochim Biophys Acta - Gen Subj*. 2013;1830:4117-4129.
51. Tardiolo G, Bramanti P, Mazzon E. Overview on the effects of N-acetylcysteine in neurodegenerative diseases. *Molecules*. 2018;23:3305.
52. Tao W, Sun W, Zhu H, Zhang J. miR-205-5p suppresses pulmonary vascular smooth muscle cell proliferation by targeting MICAL2-mediated Erk1/2 signaling. *Microvasc Res*. 2019;124:43-50.

53. Thangapandiyan S, Miltonprabu S. Epigallocatechin gallate supplementation protects against renal injury induced by fluoride intoxication in rats: Role of Nrf2/HO-1 signaling. *Toxicol Rep*. 2014;1:12-30.
54. Maisto R, Oltra M, Vidal Gil L, et al. ARPE-19-derived VEGF-containing exosomes promote neovascularization in HUVEC: the role of the melanocortin receptor 5 has been built and requires approval. *Cell Cycle*. 2019;18:413-424.
55. Brandes AA, Gil-Gil M, Saran F, et al. A randomized phase II Trial (TAMIGA) evaluating the efficacy and safety of continuous bevacizumab through multiple lines of treatment for recurrent glioblastoma. *Oncologist*. 2019;24:521-528.

SUPPORTING INFORMATION

Additional supporting information may be found online in the Supporting Information section.

How to cite this article: Oltra M, Vidal-Gil L, Maisto R, Sancho-Pelluz J, Barcia JM. Oxidative stress-induced angiogenesis is mediated by miR-205-5p. *J Cell Mol Med*. 2019;00:1–9. https://doi.org/10.1111/jcmm.14822

SCIENTIFIC REPORTS
nature research

OPEN

miR302a and 122 are deregulated in small extracellular vesicles from ARPE-19 cells cultured with H_2O_2

Maria Oltra[1,2,3], Lorena Vidal-Gil[1,2,3], Rosa Maisto[4], Sara S. Oltra[5], Francisco Javier Romero[6], Javier Sancho-Pelluz[2,3]* & Jorge Miguel Barcia[2,3]

Age related macular degeneration (AMD) is a common retina-related disease leading to blindness. Little is known on the origin of the disease, but it is well documented that oxidative stress generated in the retinal pigment epithelium and choroid neovascularization are closely involved. The study of circulating miRNAs is opening new possibilities in terms of diagnosis and therapeutics. miRNAs can travel associated to lipoproteins or inside small Extracellular Vesicles (sEVs). A number of reports indicate a significant deregulation of circulating miRNAs in AMD and experimental approaches, but it is unclear whether sEVs present a significant miRNA cargo. The present work studies miRNA expression changes in sEVs released from ARPE-19 cells under oxidative conditions (i.e. hydrogen peroxide, H_2O_2). H_2O_2 increased sEVs release from ARPE-19 cells. Moreover, 218 miRNAs could be detected in control and H_2O_2 induced-sEVs. Interestingly, only two of them (hsa-miR-302a and hsa-miR-122) were significantly under-expressed in H_2O_2-induced sEVs. Results herein suggest that the down regulation of miRNAs 302a and 122 might be related with previous studies showing sEVs-induced neovascularization after oxidative challenge in ARPE-19 cells.

microRNA (miRNA) are small non-coding RNA sequences (21-25 nucleotides) able to regulate the expression of one or more mRNAs[1,2]. miRNAs regulate protein translation by targeting their complementary mRNAs and by repressing translation or degrading a target mRNA. Nowadays, miRNA research has been rocketed from 214 publications in 2014 to 11,610 in 2018 (source: Pubmed). Many clinical fields are now focused on the study of miRNA for diagnosis or treatment purposes[3,4]. Moreover, miRNAs play an important role in different cellular processes such as angiogenesis[5,6], oxidative stress[7], and immune responses[8].

Most of the cells can release extracellular vesicles (EVs), which may interact with both neighbouring or distant target cells[9,10]. EVs typically include genetic material and proteins, making these vesicles key in cell to cell communication[11]. Among these EVs, are the small EVs (sEVs; <100 nm diameter)[12], which were observed to carry miRNAs[13]. Cargo of sEVs depends on the cellular origin and the homeostatic state[14].

Recent studies analysed miRNA expression in biological samples from patients with age related macular degeneration (AMD), in order to identify those miRNAs related to the pathophysiology and progression of the disease. Among these, miR-9, miR-23a, miR-27a, miR-34a, miR-146a, miR-155 have been proposed as potential candidates[15–19]. The "wet" form of AMD is characterized by neovascularization[20]. The retinal pigment epithelium (RPE) plays a pivotal role between the photoreceptor cell layer and the choroid, the vascular network surrounding the eye. This interaction is critical for retinal homeostasis[21]. Ren and collaborators analysed circulating miRNAs from AMD patients and proposed miR-27a-3p, miR-29b-3p, and miR-195-5p as candidate biomarkers for AMD diagnosis[19].

One of the most challenging issues in ophthalmological sciences is to identify early markers for AMD in order to prevent its clinical evolution. To date AMD treatments are limited to diminish the evolution of the disease as anti-VEGF drugs (eg. Bevacizumab)[22]. The present work studies the oxidative-induced response in RPE cells, in order to find potential miRNAs related to neovascularization within sEVs.

[1]Escuela de Doctorado Universidad Católica de Valencia San Vicente Mártir, Valencia, Spain. [2]Neurobiología y Neurofisiología, Facultad de Medicina y Ciencias de la Salud, Universidad Católica de Valencia San Vicente Mártir, Valencia, Spain. [3]Centro de Investigación Traslacional San Alberto Magno, Universidad Católica de Valencia San Vicente Mártir, Valencia, Spain. [4]Università degli studi della Campania Luigi Vanvitelli, Naples, Italy. [5]INCLIVA Biomedical Research Institute, Hospital Clínico Universitario Valencia, University of Valencia, Valencia, Spain. [6]Hospital General de Requena, Valencia, Spain. *email: fj.sancho@ucv.es

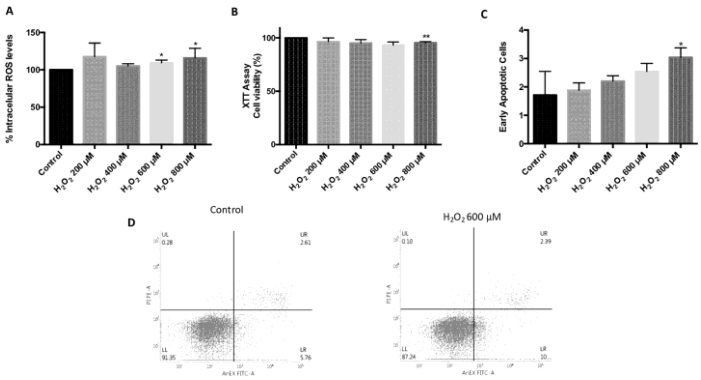

Figure 1. Effect of oxidative stress in ARPE-19 cells. Superoxide anions were measured by DHE after 24 h of H_2O_2 treatment. (**A**) XTT cell viability as percentage to control. (**B**) Early apoptotic cells measured using AnnexinV-IP. (**C**) Flow cytometry histograms: alive cells (annexin V^-, PI^-), early apoptosis (annexin V^+, PI^-) and necrotic cells (annexin V^+, IP^+). (**D**) Values are expressed as mean ± SEM (n = 3). Statistically significant differences were set at $^*p < 0.05$ and $^{**}p < 0.01$.

Results

H_2O_2-induced oxidative stress in ARPE-19 cells. ARPE-19 cells exposed for 24 h to H_2O_2 significantly increased intracellular reactive oxygen species (ROS) levels when using a concentration of 600 µM (106 ± 1.69) and 800 µM (103.1 ± 0.9892), compared to control (100 ± 0). Nevertheless, 400 µM H_2O_2, or lower, did not increase ROS levels compared to control (Fig. 1A). In order to assess whether H_2O_2-induced ROS affected ARPE-19 cell viability, a XTT assay was performed. Cell viability was significantly decreased when using 800 µM H_2O_2 (95.45 ± 0.9999) but not with lower concentrations (Fig. 1B). Moreover, 800 µM H_2O_2 concentration also increased early apoptosis (3.038 ± 0.1689) with respect to control (1.713 ± 0.4796) (Fig. 1C,D).

H_2O_2 increased sEVs release in ARPE-19. Matching previous results on cell viability (see Fig. 1), 600 µM H_2O_2 was used to stress ARPE-19 cells without killing them (sub-lethal concentration). After 24 h of 600 µM H_2O_2 exposure, ARPE-19 cells significantly increased the number of EVs released to the medium (Fig. 2). More precisely, a 40% increase in the release of EVs was observed after 600 µM H_2O_2 exposure, compared to controls. Number and size of EVs were studied using a nanoparticle tracking system (NanoSight) (Fig. 2A). Besides, EVs were observed using transmission electron microscopy (TEM), which showed that, according to size and morphology, most of the EVs observed can be classified as sEVs (Fig. 2B,C).

miRNA Expression in ARPE-19 cells and sEVs. In the present study, 384 miRNAs were analysed, and two different miRNA clusters could be set after hierarchical clustering (Fig. 3). The same proceeding was performed with the extracellular medium to collect sEVs and miRNAs providing also two clusters (Fig. 4).

miRNA Expression in ARPE-19 cells (Cell miRNA). As shown in Fig. 3, there is a significant miRNA repression after H_2O_2 treatment when compared with control ARPE-19 cells. As a result, 306 out of 384 Cell miRNAs were detected by the array. From those, 59 Cell miRNAs were significantly expressed in ARPE-19 cells ($p < 0.05$) (Table 1). Moreover, seven out of 59 Cell miRNAs were significantly under-expressed in H_2O_2-treated cells (fold change, FC > 1) than in control conditions. Different detected miRNAs are shown in Fig. 5A,C. It is noteworthy to underline that hsa-miR-205 and hsa-miR-302c presented a dramatic decrease in treated cells when compared to others (FC > 2).

miRNA Expression in ARPE-19 sEVs (sEV miRNA). As above-mentioned, ARPE-19 cells released a significantly higher number of sEVs after 600 µM H_2O_2 exposure than control cells. In contrast, these H_2O_2 induced sEVs showed a significant lower miRNA expression compared to control. More concretely, 218 out of 384 sEV miRNAs were detected by the array. However, only 2 out of 218 sEV miRNAs were significantly lower in sEVs released from treated cells ($p < 0.05$) hsa-miR-302a (FC = 1.159) and hsa-miR-122 (FC = 1.576) than in control sEVs (Fig. 5B,D).

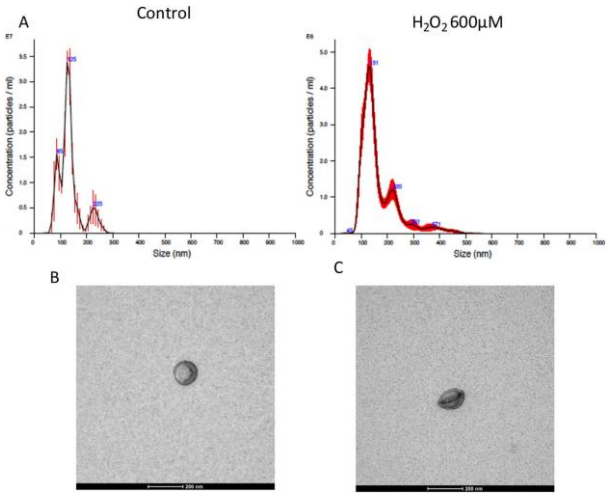

Figure 2. Characterization of sEVs released by ARPE-19 cells. Size-distribution analysis and sEVs number were performed by Nanoparticle Tracking Analysis. (**A**) EVs released by ARPE-19 cells control (**B**) and ARPE-19 cells treated by 600 µM H_2O_2 (**C**) were detected by electron microscopy.

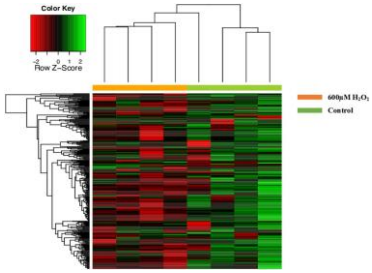

Figure 3. Heatmap of miRNA expression profile from array assay of ARPE-19 cells. After 24 h of 600 µM H_2O_2 the miRNA expression profile was analyzed, using an array for microRNA. Hierarchical unsupervised clustering was performed with the expressed miRNAs in ARPE-19 cells. Each column represents an individual cell sample. Orange columns are ARPE-19 cells treat with 600 µM H_2O_2 and green columns ARPE-19 cell controls. Control sample (n = 4) and 600 µM H_2O_2 sample (n = 4). The overexpressed miRNAs are shown in green and under-expressed miRNAs in red. Expression values are calculated with respect to the reference genes of the array assay.

Microarray validation. Among the miRNAs differently expressed in ARPE-19 cells, seven out of 59 presented a significant fold-change. In order to validate this finding, qRT-PCR was performed by using independent RNA samples. We selected three out of seven significant miRNAs (those with the highest differences observed):

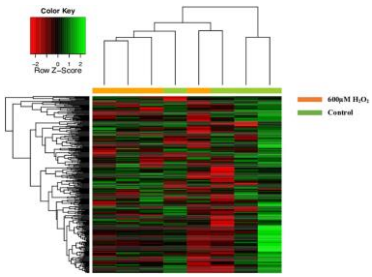

Figure 4. Heatmap of miRNA expression profile from array assay of the sEVs released by ARPE-19 cells. After 24 h of 600 µM H_2O_2, the miRNA expression profile of sEVs was analyzed, using an array of microRNA. Hierarchical unsupervised clustering was performed with the expressed miRNAs in ARPE-19-released sEVs. Each column represents an individual cell sample. Orange columns are sEVs released by ARPE-19 cells treat with 600 µM H_2O_2 and green columns are sEVs released by ARPE-19 control cells. Control sample (n = 4) and 600 µM H_2O_2 sample (n = 4). Overexpressed miRNAs (green) and under-expressed miRNAs (red). The expression values are calculated with respect to the reference genes of the array.

miRNA	FC	P_value	miRNA	FC	P_value
hsa-miR-139-3p	0,71	0,00065	**hsa-miR-371-5p**	0,95	0,02665
hsa-miR-192	0,74	0,00129	**hsa-miR-92a**	0,70	0,02672
hsa-miR-22	0,73	0,00646	**hsa-miR-361-5p**	0,79	0,02674
hsa-miR-15b	0,73	0,00657	**hsa-miR-521**	1,35	0,02850
hsa-let-7c	0,82	0,00661	**hsa-miR-30c**	0,78	0,02935
hsa-let-7b	0,77	0,00670	**hsa-miR-335**	0,85	0,03051
hsa-miR-221	0,66	0,00723	**hsa-miR-28-5p**	0,94	0,03170
hsa-miR-323-5p	0,79	0,01131	**hsa-let-7g**	0,84	0,03204
hsa-miR-15a	0,67	0,01139	**hsa-miR-29c**	0,82	0,03218
hsa-miR-18b	0,70	0,01164	**hsa-miR-488**	0,98	0,03271
hsa-miR-151-3p	0,78	0,01193	**hsa-miR-532-3p**	0,86	0,03316
hsa-miR-183	0,80	0,01214	**hsa-miR-338-5p**	1,11	0,03332
hsa-miR-518b	0,76	0,01364	**hsa-miR-125a-5p**	0,82	0,03352
hsa-miR-10a	0,78	0,01407	**hsa-miR-499-3p**	0,72	0,03376
hsa-miR-23a	0,79	0,01456	**hsa-miR-29a**	0,72	0,03509
hsa-miR-151-5p	0,85	0,01492	**hsa-miR-20b**	0,81	0,03536
hsa-miR-224	0,78	0,01537	**hsa-miR-148a**	0,90	0,03727
hsa-miR-186	0,52	0,01561	**hsa-miR-548b-5p**	1,91	0,03849
hsa-let-7f	0,86	0,01619	**hsa-miR-218**	1,00	0,04031
hsa-miR-27a	0,80	0,01739	**hsa-miR-505**	0,65	0,04090
hsa-miR-148b	0,66	0,01813	**hsa-miR-205**	2,29	0,04350
hsa-miR-25	0,83	0,01956	**hsa-miR-17**	0,78	0,04392
hsa-miR-98	1,00	0,01966	**hsa-miR-324-5p**	0,73	0,04490
hsa-miR-106a	0,71	0,02016	**hsa-miR-320c**	0,82	0,04523
hsa-let-7a	1,06	0,02102	**hsa-miR-99a**	0,84	0,04595
hsa-miR-300	0,89	0,02126	**hsa-miR-302c**	2,55	0,04598
hsa-miR-18a	0,70	0,02210	**hsa-miR-30b**	0,85	0,04622
hsa-miR-515-3p	0,89	0,02262	**hsa-miR-28-3p**	0,83	0,04717
hsa-miR-27b	0,78	0,02454	**hsa-miR-99**	0,77	0,04962
hsa-miR-518d-3p	1,06	0,02537			

Table 1. miRNAs significantly regulated in ARPE-19 cells under oxidative stress. The miRNAs are ranged according to the P-value.

A

miRNA name	FC	P_value	Control mean	Treated mean
Let-7a	1,056	0,021	1,153	0,097
Hsa-miR-518d-3p	1,056	0,025	1,202	0,146
Hsa-miR-521	1,348	0,028	1,459	0,315
Hsa-miR-338-5p	1,108	0,033	1,258	0,149
Hsa-miR-548b-5p	1,908	0,038	2,08	0,176
Hsa-miR-205	2,287	0,043	2,618	0,331
Hsa-miR-302c	2,55	0,046	2,697	0,145

B

miRNA name	FC	P_value	Control mean	Treated mean
Hsa-miR-302a	1,159	0,020	1,251	0,092
Hsa-miR-122	1,576	0,049	1,581	0,005

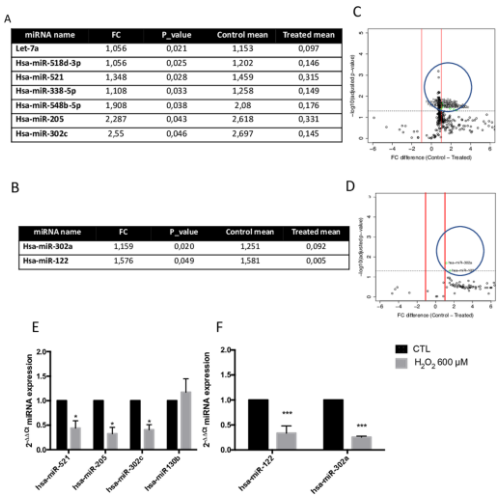

Figure 5. miRNAs significantly regulated in ARPE-19 cells. Cell miRNAs (**A**) and sEV miRNA (**B**) up-regulated in ARPE-19 cells with fold change (FC) > 1. Volcano plot of miRNA expression profile. The X axis represent the miRNA expression level and the Y axis represents p-value (T-student Test). The red lines indicate FC ± 1 P < 0.05 (**C**,**D**). Relative expression of the selected Cell miRNAs (**E**) and sEV miRNAs (**F**) with FC > 1 (control vs 600 µM H_2O_2). miRNA expression was quantified by qRT-PCR and calculate using the $2^{-\Delta\Delta Ct}$. The p-value was calculated by Two-way ANOVA. Results are expressed as mean ± SEM of n = 3–4. *p-value < 0.05 vs Control and ***p-value < 0.001.

hsa-miR-205-5p, hsa-miR-521, and hsa-miR-302c; plus a miRNA that was unchanged: hsa-miR-130b, as a control. The outcome confirmed the results obtained, hsa-miR-205-5p, hsa-miR-521 and hsa-miR-302c were down-regulated by 600 µM H_2O_2 compared to control (Fig. 5E).

The same procedure, qRT-PCR, was performed using the two sEV miRNAs which expression had changed: hsa-miR-302a and hsa-miR-122. As expected, miRNAs were under-expressed in sEVs released from ARPE-19 cells treated with 600 µM H_2O_2 (Fig. 5F).

Pathway analysis and prediction of miRNA targets regulated by oxidative stress. Subsequently, the role of the under-expressed miRNAs in treated ARPE-19 cells and in sEVs from treated cells (seven in cells and two in sEVs), was analysed. For that reason, two independent *"in silico"* analysis were performed in order to determine potential biological processes related to oxidative stress induction. The analysis of the KEGG pathway, regulated by Let-7a, miR-518d-3p, miR-521, miR-338-5p, miR-548b-5p, miR-205, and miR-302c, shows a large number of pathways involving these miRNAs. Among them, cell cycle, adherent junction, p53 signalling pathway, and HIF-1 signalling pathway are the most relevant (Fig. 6A). Both sEV miRNAs, miR-302a and miR-122, are involved in different pathways, such as TGF-beta signalling pathway, FoxO signalling pathway, and cell cycle (Fig. 7A).

Potential targets of miRNAs. In order to identify biological functions of the validated miRNAs and to select their putative targets, two programs were handled: DIANA TOOLS mirPath and Target Scan Human. The outcome on sEV miRNA and Cell miRNA related pathways are not completely equivalent. Most of the significantly involved KEGG are related to cancer or cell cycle pathways (Figs. 6B and 7B).

Discussion

The study of circulating miRNAs on AMD has been addressed to find biological markers which might help implementing an early diagnosis for the disease, or to find new therapeutic strategies[18]. Although neovascular processes and oxidative stress are well known characters involved on AMD, the origin of the disease is far from being completely understood. Several studies were focused in identifying neovascularization-related miRNAs or oxidative

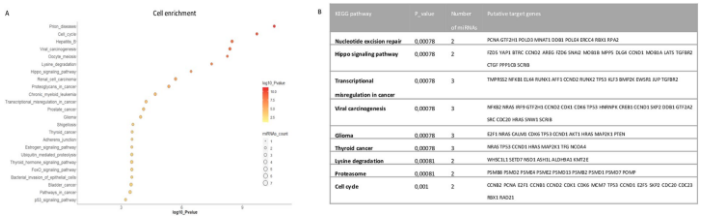

Figure 6. Cell miRNA related pathways after H_2O_2 exposure in ARPE-19 cells. Graphic representation of cellular pathways (Y) and $\log_{10}$ P-value (X), circle size represents the number of involved miRNAs up to 7 deregulated miRNAs. (**A**) KEGG pathways regulated and putative target genes (**B**).

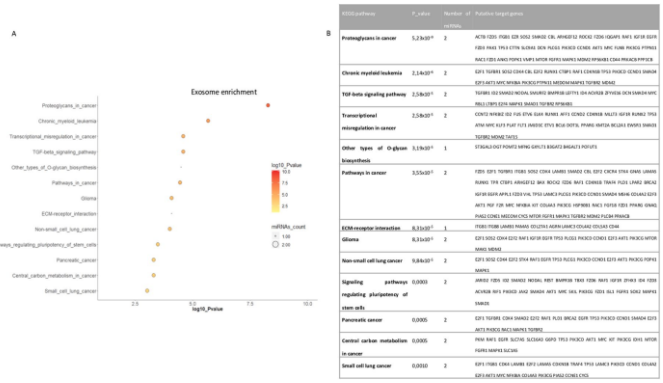

Figure 7. sEVmiRNA related pathways after H_2O_2 exposure in ARPE-19 cells (**A**) Graphic representation of cell pathways (Y) and $\log_{10}$ P-value (X), circle size represents the number of involved miRNAs up to 2 deregulated miRNAs. (**A**) KEGG pathways regulated and putative target genes (**B**).

stress-related ones[23–26]. On this line, the use of RPE cell cultures, as ARPE-19 under oxidative challenges (eg. H_2O_2, rotenone or EtOH), results useful to study the RPE response to oxidative stimuli[27–29].

As mentioned earlier, 600 µM was the highest H_2O_2 concentration used which increased ROS levels without generating early apoptosis (800 µM H_2O_2 exposure significantly increased early apoptosis). Other authors have used different H_2O_2 ranges (200-600 µM) and some differences can be found in terms of cell viability (XTT or MTT), apoptosis and ROS production[7,27,30]. Plausibly, the differences on time exposure (12–24 h) or cell confluence level could explain these discrepancies.

Fitting with previous data, pro-oxidant challenge resulted on significant high sEVs release from ARPE-19 cells. It is well documented that EtOH or high glucose conditions resulted in the same response increasing sEVs release from ARPE-19 cells[28,31].

Extracellular or circulating miRNAs can be included on sEVs, associated to lipoproteins or proteins[13]. In this respect, we have just focused on miRNAs contained as sEVs cargo (sEV miRNA). In spite of the fact that in sEVs only 218 out of 384 miRNAs could be detected, only two sEV miRNAs were significantly high in control released sEVs than in sEVs from treated cells. The hsa-miR-302a and hsa-miR-122 have already been seen in sEVs confirming our results[32–35].

miRNA	Reference
hsa-miR-139-3p	Szemraj *et al.* and Ertekin *et al.*[17,52]
hsa-miR-192	Grassmann *et al.* and Ertekin *et al.*[24,52,53]
hsa-let-7c	Ren *et al.* and Szemraj *et al.*[17,19]
hsa-miR-18b	Ren *et al.* and Wang *et al.*[19,54]
hsa-miR-183	Karali *et al.*, Loscher *et al.* and Xiang *et al.*[55–57]
hsa-miR-23a	Li *et al.*, Lin *et al.*, Romano *et al.*, Szemraj *et al.* and Zhou *et al.*[7,16,17,47,58]
hsa-miR-27a	Ren *et al.*; Romano *et al.*; Szemraj *et al.*[16,17,19]
hsa-miR-25	Ren *et al.* and Zhang *et al.*[19,59]
hsa-miR-106a	Ertekin *et al.*[52]
hsa-let-7a	Ertekin *et al.* and SanGiovanni *et al.*[52,60]
hsa-miR-27b	Ertekin *et al.* and Howell *et al.*[30,52]
hsa-miR-518d-3p	Dinç *et al.*[27]
hsa-miR-92a	Dinç *et al.*, Howell *et al.*, Desjarlais *et al.* and Walz *et al.*[27,30,61,62]
hsa-miR-361-5p	Grassmann *et al.* and Szemraj *et al.*[17,24]
hsa-miR-335	Ertekin *et al.* and Grassmann *et al.*[24,52]
hsa-miR-30c	Ren *et al.*[19]
hsa-miR-28-5p	Ren *et al.*[19]
hsa-miR-29a	Ertekin *et al.*, Howell *et al.*, Walz *et al.*, Zhang *et al.* and Zhang *et al.* (2)[30,52,62–64]
hsa-miR-205	Ménard *et al.*[4]
hsa-miR-17	Ertekin *et al.*, Barber *et al.* and Tian *et al.*[5,18,52]
hsa-miR-324-5p	Ertekin *et al.*[52]
hsa-miR-302c	Howell *et al.*[30]
hsa-miR-30b	Dinç *et al.*, Romano *et al.*, Mazzeo *et al.* and Haque *et al.*[16,27,65,66]
hsa-miR-28-3p	Howell *et al.*[30]

Table 2. Relevant miRNAs identified on eye disorders.

When comparing the two sEV miRNAs, hsa-miR-302a and hsa-miR-122, to those miRNAs on ARPE-19 cells (Cell miRNA), no matches could be found. Surprisingly, the sEV miRNA hsa-miR-302a and the Cell miRNA hsa-miR-302c belong to the miR 302/367 *La-related protein 7* (*LARP7*) intragenic cluster. This includes hsa-miR-367, hsa-miR-302d, hsa-miR-302a, hsa-miR-302c, and hsa-miR-302b. This cluster is involved in several processes coordinating proliferation, differentiation, pluripotency maintenance, and cell reprogramming[36]. Moreover, the cluster, regulates TGF pathway, PI3K–AKT and BMP cell signaling[37–39]. Additionally, hsa-miR-302a acts as a tumor suppressor[40] and repressor of cell division, and more concretely, VEGFA is one of the direct targets for this miRNA[41]. In addition, hsa-miR-122 has been related to VEGFC[42]. Interestingly, low hsa-miR-302a/hsa-miR-122 expression levels are inversely related to VEGF levels in hepatocellular carcinoma, promoting vascular changes[43,44]. In addition, miR-122 seems to have a role against oxidative stress, since the use of pre-miR-122 protects from H_2O_2 induced oxidative stress[45], targeting the mitochondrial ribosomal protein S11[46].

Recent data from other groups indicate how diverse oxidative insults -EtOH or high glucose, and now H_2O_2 - lead to increased sEVs release from ARPE-19 cells[28,31]. Furthermore, those oxidative-induced sEVs were capable of promoting neovascular processes in endothelial cell cultures, whereas control-released sEVs inhibited this phenomenon[28,31]. In view of these findings, we hypothesize that sEVs hsa-miR-122 and hsa-miR-302a decreased levels could play a role on angiogenesis involving oxidative stress related pathways.

Several reports on AMD or experimental AMD, have reported significant changes on miRNAs (see Table 2). Among them, hsa-miR-23a is present in five reports[7,16,17,42,47]. This miRNA seems to be downregulated in both AMD patients and H_2O_2-treated ARPE-19 cells. In fact, H_2O_2 induced-apoptotic cell death is significantly observed in ARPE-19 cells after hsa-miR-23a inhibition[7]. Fitting with this, we found significant expression differences on hsa-miR-23a after H_2O_2 exposure (FC = 0.79). Table 2 summarizes those Cell miRNAs matching with previous reports on AMD or AMD experimental models. Besides, there are reports that locate the sEVS-miRNAs in eye tissue. MiR-302 expression was observed already in RPE cells by Li and collaborators, playing an important role in the RPE differentiation[48]. Other authors observed a miR-122 differential expression on canine retinas[49], in aqueous humor[50] and are related in fact with diabetic retinopathy[51]. In agreement with others, up/down regulated miRNAs are related to several and different cell signaling pathways. After seeing the results in both sEV miRNA and Cell miRNAs related pathways, cancer related pathways are commonly involved in many of the deregulated miRNAs. More research must be performed on these generic pathways to determine the concrete role of these cell signaling routes.

As a conclusion, H_2O_2 significantly increased sEVs release from ARPE-19 cells compared to control cells. Paradoxically, the miRNA sEVs cargo (hsa-miR-302a and hsa-miR-122) resulted in significantly lower in H_2O_2-induced sEVs compared to control. Since hsa-miR-302a and hsa-miR-122 regulates vasculogenic targets, these results support those on ARPE-19 cells indicating that oxidative-induced sEVs promote angiogenesis[28,31].

Material and Methods

Cell culture. Arising retinal pigment epithelium (ARPE-19) human cell line was obtained from American Type Culture Collection (ATCC, Barcelona, Spain) at passage 19. ARPE-19 cells were cultured in Dulbecco's modified Eagle's DMEM/F12 (Invitrogen, Carlsbad, CA, USA), as previously described[21]. Cells were used until passage 30. Cells were cultured to 80–90% confluence at a starting density of 1×10^6 cells/cm^2 in different plates depending on the technique. After 2 days, the cells were treated for 24 h with 600 µM H_2O_2 (Scharlau, Senmenat, Spain), using filtered media with 1% of Fetal Bovine Serum, exosome-depleted (FBS; Thermo Fisher Scientific, Gibco, USA). Cells and supernatant were collected and preserved for future experiments.

Determination of intracellular ROS. Intracellular ROS levels were measured using dihydroethidium, (DHE; Thermo Fisher Scientific, Waltham, MA, USA), which is a superoxide indicator. This molecule has a blue fluorescence, but, when oxidized to ethidium, it stains DNA in red. ARPE-19 cells were seeded at 6×10^3 cells/well in a 96 well plate. Cells were rinsed with PBS (phosphate-buffered saline) twice and incubated with 5 µM of DHE during 30 min at 37 °C and 5% CO_2. ROS levels were measured by a fluorescence multiplate reader (Victor X5; Perkin Elmer) excited at 518 nm and read at 605 nm.

Apoptosis detection. Number of dead cells by apoptosis or necrosis was measured by flow cytometry using the FITC Annexin V Apoptosis detection Kit (Immunostep, Salamanca, Spain) that can discriminate live cells from those in early apoptosis, late apoptosis, or necrosis. A total of 10,000 cells per condition were analysed using the FACS Verse (Beccton Dikinson, New Jersey, USA). Four populations are detected: unmarked Annexin (−)/Propidium Iodide (−) are live cells; double marked Annexin (+)/Propidium Iodide (+) represent apoptotic cells; simple marked Annexin (+)/Propidium Iodide (−) are early apoptotic cells; and simple marked Annexin (−)/Propidium Iodide (+) are necrotic cells.

sEVs isolation and size distribution. sEVs isolation was performed by successive ultracentrifugation as previously reported[21]. The sEVs pellet was stored at 4 °C until further processing in PBS solution. For microarray assay, sEVs were isolated using ExoQuick-TC (Systems Biosciences, Mountain View, CA, USA) following the manufacturer's instructions. sEVs identity was confirmed by the nanoparticle tracking system NanoSight NS300 following manufacturer's protocols (Malvern Instruments, Malvern, UK).

Electron microscopy. sEVs pellets were resuspended in PBS and ultracentrifuged at 120.000 × g for 70 min at 4 °C. After that, approximately 10 µg of the samples were resuspended in PBS on parafilm. The sample was fixed by depositing a drop of 2% Paraformaldehyde on the parafilm and placing the grid (Mesh with Formvar) on top of the drop. Negative staining was performed with 2% uranyl acetate. Photomicrographs were obtained using the transmission electron microscope FEI Tecnai G2 Spirit (FEI Europe, Eindhoven, Netherlands) using a digital camera Morada (Olympus Soft Image Solutions GmbH, Münster, Germany). EVs were identified under the microscope solely based on size and morphology.

RNA isolation and miRNA expression analysis. To perform microarray analysis, ARPE-19 cells from 4 separate cultures were exposed to control and H_2O_2 600 µM treatment for 24 h. Total RNA was extracted using SeraMir Kit (System Biosciences, Mountain View, CA, USA) according to manufacturer's instructions. Therefore, four microarrays were performed for each condition: control, ARPE-19 cells exposed to H_2O_2 600 µM, sEVs released by control cells and sEVs released by ARPE-19 cells exposed to H_2O_2 600 µM.

Total RNA quantity and quality (260/280 absorbance ratio) were assessed using NanoDrop 2000 (Thermo Fisher Scientific, Waltham, MA, USA). Total RNA was reversely transcribed (cDNA synthesis) using PeqSTAR 96 Universal Gradient (PeqLAb, Erlangen, Germany) under the following conditions: 60 °C/5 min, RT/2 min, 42 °C/30 min, 95 °C/10 min and 15 °C/hold. Real-time quantitative PCR (qPCR) was performed using 384 well SeraMir Profiler using RT-PCR QuantStudio™ 3 y 4 system (Thermo Fisher Scientific, Waltham, MA, USA) with the appropriate temperature cycles 50 °C/2 min, 95 °C/10 min, 40 ciclos; 95 °C/15 s, 6 °C/1 min. The miRNA expression values were calculated using three endogenous controls: RNU43, RNU1Q and RNU6. The expression was calculated according to the $2^{-\Delta\Delta Ct}$ method.

Array analysis. We analyzed miRNA expression differences between ARPE-19 control cells and ARPE-19 treated with H_2O_2. Moreover, differences in miRNA expression between EVs released by ARPE-19 cells treated and EVs released by ARPE-19 control cells were also studied. Differences were analyzed using a t-test study from *genefilter* package from R Bioconductor. *P-values* were adjusted by the Benjamini-Hochberg method. MiRNAs that presented an adjusted p-value < 0.05 were considered statistically significant. Significantly modified miRNAs from different samples were represented in a hierarchical clustering heatmap representation. Heatmaps were performed using *heatmap.3* package from R Bioconductor.

Analysis of miRNA target genes. *In silico* analysis of the pathways in which the miRNAs regulated by H_2O_2 were involved using DIANA TOOLS mirPath v.3 algorithm (http://snf-515788.vm.okeanos.grnet.gr/). Moreover, we carry out an analyse of the putative miRNAs target using TargetScanHuman (http://www.targetscan.org/vert_72/).

Quantitative real-time PCR validation. Quantitative real time PCR (qRT-PCR) was used to validate the miRNA expression profile of the selected miRNAs in an independent sample set. The RNA was isolated from ARPE-19 cells by miRNeasy Mini Kit (Qiagen, Hilden, Germany) according to the manufacturer's instructions.

100–300 ng of RNA were retro transcribed using TaqMan MicroRNA Reverse Transcription Kit (Thermo Fisher Scientific, Waltham, MA, USA) using specific TaqMan RT primers and the thermocycler PeqSTAR 96 Universal Gradient (PeqLAB, Erlangen, Germany), the cycles used were 16 °C/30 min, 42 °C/30 min, 85 °C/5 min and 4 °C/infinity. Quantitative real time PCR was performed using TaqMan™ microRNA Assays (Thermo Fisher Scientific, Waltham, MA, USA) with TaqMan Gene Expression master Mix (Thermo Fisher Scientific, Waltham, MA, USA) and RT-PCR Roche 234 LighterCycler 480 with the appropriate temperature cycles (50 °C/2 min, 95 °C/10 min, 40 cycles: 95 °C/15 s and 60 °C/1 min). Normalisation was performed with RNU6B snoRNA and RNU43 snoRNA. Relative expression was calculated as $2^{-\Delta\Delta C_T}$.

Statistical analysis. The results of each experiment are presented as mean ± SEM. Statistical significance was determined using t-test and 2-way-ANOVA.

Data availability

The datasets generated during and/or analysed during the current study are available from the corresponding author on reasonable request.

Received: 12 March 2019; Accepted: 14 November 2019;
Published online: 29 November 2019

References

1. Kumar, S., Vijayan, M., Bhatti, J. S. & Reddy, P. H. MicroRNAs as Peripheral Biomarkers in Aging and Age-Related Diseases. *Prog. Mol. Biol. Transl. Sci.* **146**, 47–94 (2017).
2. Bhaskaran, M. & Mohan, M. MicroRNAs: history, biogenesis, and their evolving role in animal development and disease. *Vet. Pathol.* **51**, 759–774 (2014).
3. Elbay, A., Ercan, Ç., Akbaş, F., Bulut, H. & Ozdemir, H. Three new circulating microRNAs may be associated with wet age-related macular degeneration. *Scand. J. Clin. Lab. Invest.* **79**, 1–7 (2019).
4. Ménard, C. *et al.* MicroRNA signatures in vitreous humour and plasma of patients with exudative AMD. *Oncotarget* **7**, 19171–19184 (2016).
5. Tian, B. *et al.* miR-17-3p Exacerbates Oxidative Damage in Human Retinal Pigment Epithelial Cells. *PLoS One* **11**, e0160887 (2016).
6. Yoon, C. *et al.* Delivery of miR-155 to retinal pigment epithelial cells mediated by Burkitt's lymphoma exosomes. *Tumor Biol.* **37**, 313–321 (2016).
7. Lin, H. *et al.* Effect of miR-23 on Oxidant-Induced Injury in Human Retinal Pigment Epithelial. *Cells. Investig. Opthalmology Vis. Sci.* **52**, 6308 (2011).
8. He, J.-F., Du, Y., Jiang, B.-L. & He, J.-F. Increased microRNA-155 and decreased microRNA-146a may promote ocular inflammation and proliferation in Graves' ophthalmopathy. *Med. Sci. Monit.* **20**, 639–643 (2014).
9. Turturici, G., Tinnirello, R., Sconzo, G. & Geraci, F. Extracellular membrane vesicles as a mechanism of cell-to-cell communication: advantages and disadvantages. *Am. J. Physiol. Cell Physiol.* **306**, C621–C633 (2014).
10. Yang, X., Weng, Z., Mendrick, D. L. & Shi, Q. Circulating extracellular vesicles as a potential source of new biomarkers of drug-induced liver injury. *Toxicol. Lett.* **225**, 401–406 (2014).
11. Février, B. & Raposo, G. Exosomes: Endosomal-derived vesicles shipping extracellular messages. *Curr. Opin. Cell Biol.* **16**, 415–421 (2004).
12. Théry, C. *et al.* Minimal information for studies of extracellular vesicles 2018 (MISEV2018): a position statement of the International Society for Extracellular Vesicles and update of the MISEV2014 guidelines. *J. Extracell. vesicles* **7**, 1535750 (2018).
13. Creemers, E. E., Tijsen, A. J. & Pinto, Y. M. Circulating MicroRNAs. *Circ. Res.* **110**, 483–495 (2012).
14. Biasutto, L., Chiechi, A., Couch, R., Liotta, L. A. & Espina, V. Retinal pigment epithelium (RPE) exosomes contain signaling phosphoproteins affected by oxidative stress. *Exp. Cell Res.* **319**, 2113–2123 (2013).
15. Wang, S., Koster, K. M., He, Y. & Zhou, Q. miRNAs as potential therapeutic targets for age-related macular degeneration. *Future Med. Chem.* **4**, 277–287 (2012).
16. Romano, G. L. *et al.* Retinal and Circulating miRNAs in Age-Related Macular Degeneration: An *In vivo* Animal and Human Study. *Front. Pharmacol.* **8**, 168 (2017).
17. Szemraj, M. *et al.* Serum MicroRNAs as Potential Biomarkers of AMD. *Med. Sci. Monit.* **21**, 2734–2742 (2015).
18. Berber, P., Grassmann, F., Kiel, C. & Weber, B. H. F. An Eye on Age-Related Macular Degeneration: The Role of MicroRNAs in Disease Pathology. *Mol. Diagnosis Ther.* **21**, 31–43 (2017).
19. Ren, C. *et al.* Circulating miRNAs as potential biomarkers of age-related macular degeneration. *Cell. Physiol. Biochem.* **41**, 1413–1423 (2017).
20. Kim, J. M. *et al.* Responses of Types 1 and 2 Neovascularization in Age-Related Macular Degeneration to Anti-Vascular Endothelial Growth Factor Treatment: Optical Coherence Tomography Angiography Analysis. *Semin. Ophthalmol.* **34**, 168–176 (2019).
21. Strauss, O. The Retinal Pigment Epithelium in Visual Function. *Physiol. Rev.* **85**, 845–881 (2005).
22. Hernández-Zimbrón, L. F. *et al.* Age-Related Macular Degeneration: New Paradigms for Treatment and Management of AMD. *Oxid. Med. Cell. Longev.* **2018**, 8374647 (2018).
23. Shen, J. *et al.* MicroRNAs Regulate Ocular Neovascularization. *Mol. Ther.* **16**, 1208–1216 (2008).
24. Grassmann, F. *et al.* A circulating MicroRNA profile is associated with late- stage neovascular age-related macular degeneration. *PLoS One* **9**, 1–8 (2014).
25. Magenta, A., Greco, S., Gaetano, C. & Martelli, F. Oxidative Stress and MicroRNAs in Vascular Diseases. *Int. J. Mol. Sci.* **14**, 17319–17346 (2013).
26. Baker, J. R. *et al.* Oxidative stress dependent microRNA-34a activation via PI3Kα reduces the expression of sirtuin-1 and sirtuin-6 in epithelial cells. *Sci. Rep.* **6**, 35871 (2016).
27. Dinç, E., Ayaz, L. & Kurt, A. H. Effects of Bevacizumab, Ranibizumab, and Aflibercept on MicroRNA Expression in a Retinal Pigment Epithelium Cell Culture Model of Oxidative Stress. *J. Ocul. Pharmacol. Ther.* **34**, 1–8 (2018).
28. Atienzar-Aroca, S. *et al.* Oxidative stress in retinal pigment epithelium cells increases exosome secretion and promotes angiogenesis in endothelial cells. *J. Cell. Mol. Med.* **20**, 1457–1466 (2016).
29. Ayaz, L. & Dinç, E. Evaluation of microRNA responses in ARPE-19 cells against the oxidative stress. *Cutan. Ocul. Toxicol.* **37**, 121–126 (2018).
30. Howell, J. C. *et al.* Global microRNA expression profiling: curcumin (diferuloylmethane) alters oxidative stress-responsive microRNAs in human ARPE-19 cells. *Mol. Vis.* **19**, 544–560 (2013).
31. Maisto, R. *et al.* ARPE-19-derived VEGF-containing exosomes promote neovascularization in HUVEC: the role of the melanocortin receptor 5 has been built and requires approval. *Cell Cycle* **18**, 413–424 (2019).

32. Bukong, T. N., Momen-Heravi, F., Kodys, K., Bala, S. & Szabo, G. Exosomes from hepatitis C infected patients transmit HCV infection and contain replication competent viral RNA in complex with Ago2-miR122-HSP90. *PLoS Pathog.* **10**, e1004424 (2014).
33. Mittelbrunn, M. *et al.* Unidirectional transfer of microRNA-loaded exosomes from T cells to antigen-presenting cells. *Nat. Commun.* **2**, 282 (2011).
34. van Balkom, B. W. M., Eisele, A. S., Pegtel, D. M., Bervoets, S. & Verhaar, M. C. Quantitative and qualitative analysis of small RNAs in human endothelial cells and exosomes provides insights into localized RNA processing, degradation and sorting. *J. Extracell. vesicles* **4**, 26760 (2015).
35. Jiao, X. *et al.* Serum and exosomal miR-122 and miR-199a as a biomarker to predict therapeutic efficacy of hepatitis C patients. *J. Med. Virol.* **89**, 1597–1605 (2017).
36. Gao, Z., Zhu, X. & Dou, Y. The miR-302/367 cluster: a comprehensive update on its evolution and functions. *Open Biol.* **5**, 150138 (2015).
37. Kuo, C.-H., Deng, J. H., Deng, Q. & Ying, S.-Y. A novel role of miR-302/367 in reprogramming. *Biochem. Biophys. Res. Commun.* **417**, 11–16 (2012).
38. Barroso-del Jesus, A., Lucena-Aguilar, G. & Menendez, P. The miR-302-367 cluster as a potential stemness regulator in ESCs. *Cell Cycle* **8**, 394–398 (2009).
39. Lipchina, I., Studer, L. & Betel, D. The expanding role of miR-302–367 in pluripotency and reprogramming. *Cell Cycle* **11**, 1517–1523 (2012).
40. Chen, W., Zhuang, X., Qi, R. & Qiao, T. MiR-302a-5p suppresses cell proliferation and invasion in non-small cell lung carcinoma by targeting ITGA6. *Am. J. Transl. Res.* **11**, 4348–4357 (2019).
41. Qin, C. *et al.* MicroRNA-302a inhibits cell proliferation and invasion, and induces cell apoptosis in hepatocellular carcinoma by directly targeting VEGFA. *Mol. Med. Rep.* **16**, 6360–6367 (2017).
42. Li, C. *et al.* Chronic inflammation contributes to the development of hepatocellular carcinoma by decreasing miR-122 levels. *Oncotarget* **7**, 17021–17034 (2016).
43. Qin, C. *et al.* MicroRNA-302a inhibits cell proliferation and invasion, and induces cell apoptosis in hepatocellular carcinoma by directly targeting VEGFA. *Mol. Med. Rep.* **16**, 6360–6367 (2017).
44. Wang, Y. *et al.* MiR-122 targets VEGFC in bladder cancer to inhibit tumor growth and angiogenesis. *Am. J. Transl. Res.* **8**, 3056–3066 (2016).
45. Bai, J. *et al.* DNA Methylation of miR-122 Aggravates Oxidative Stress in Colitis Targeting SELENBP1 Partially by p65NF- κ B Signaling. *Oxid. Med. Cell. Longev.* **2019**, 1–14 (2019).
46. Song, L. *et al.* MicroRNA-122 is involved in oxidative stress in isoniazid-induced liver injury in mice. *Genet. Mol. Res.* **14**, 13258–13265 (2015).
47. Zhou, Q. *et al.* Regulation of angiogenesis and choroidal neovascularization by members of microRNA-23~27~24 clusters. *Proc. Natl. Acad. Sci. USA* **108**, 8287–8292 (2011).
48. Li, W.-B. *et al.* Development of Retinal Pigment Epithelium from Human Parthenogenetic Embryonic Stem Cells and MicroRNA Signature. *Investig. Opthalmology Vis. Sci.* **53**, 5334–5343 (2012).
49. Genini, S., Guziewicz, K. E., Beltran, W. A. & Aguirre, G. D. Altered miRNA expression in canine retinas during normal development and in models of retinal degeneration. *BMC Genomics* **15**, 172 (2014).
50. Drewry, M. D. *et al.* Differentially expressed microRNAs in the aqueous humor of patients with exfoliation glaucoma or primary open-angle glaucoma. *Hum. Mol. Genet.* **27**, 1263–1275 (2018).
51. Pastukh, N., Meerson, A., Kalish, D., Jabaly, H. & Blum, A. Serum miR-122 levels correlate with diabetic retinopathy. *Clin. Exp. Med.* **19**, 255–260 (2019).
52. Ertekin, S. *et al.* Evaluation of circulating miRNAs in wet age-related macular degeneration. *Mol. Vis.* **20**, 1057–1066 (2014).
53. Wu, J. *et al.* Protective effects of methane-rich saline on diabetic retinopathy via anti-inflammation in a streptozotocin-induced diabetic rat model. *Biochem. Biophys. Res. Commun.* **466**, 155–161 (2015).
54. Wang, H.-C. *et al.* Profiling the microRNA Expression in Human iPS and iPS-derived Retinal Pigment Epithelium. *Cancer Inform.* **13**, 25–35 (2014).
55. Karali, M. *et al.* High-resolution analysis of the human retina miRNome reveals isomiR variations and novel microRNAs. *Nucleic Acids Res.* **44**, 1525–1540 (2016).
56. Loscher, C. J. *et al.* Altered retinal microRNA expression profile in a mouse model of retinitis pigmentosa. *Genome Biol.* **8**, R248 (2007).
57. Xiang, L. *et al.* miR-183/96 plays a pivotal regulatory role in mouse photoreceptor maturation and maintenance. *Proc. Natl. Acad. Sci.* **114**, 6376–6381 (2017).
58. Li, Ddan *et al.* Inhibition of the oxidative stress-induced miR-23a protects the human retinal pigment epithelium (RPE) cells from apoptosis through the upregulation of glutaminase and glutamine uptake. *Mol. Biol. Rep.* **43**, 1079–1087 (2016).
59. Zhang, J. *et al.* miR-25 Mediates Retinal Degeneration Via Inhibiting ITGAV and PEDF in Rat. *Curr. Mol. Med.* **17**, 359–374 (2017).
60. SanGiovanni, J. P., SanGiovanni, P. M., Sapieha, P. & De Guire, V. miRNAs, single nucleotide polymorphisms (SNPs) and age-related macular degeneration (AMD). *Clin. Chem. Lab. Med.* **55**, 763–775 (2017).
61. Desjarlais, M. *et al.* MicroRNA expression profile in retina and choroid in oxygen-induced retinopathy model. *PLoS One* **14**, e0218282 (2019).
62. Walz, J. M. *et al.* Impact of angiogenic activation and inhibition on miRNA profiles of human retinal endothelial cells. *Exp. Eye Res.* **181**, 98–104 (2019).
63. Zhang, Y. *et al.* Regulation of Matrix Metalloproteinase-2 Secretion from Scleral Fibroblasts and Retinal Pigment Epithelial Cells by miR-29a. *Biomed. Res. Int.* **2017**, 1–7 (2017).
64. Zhang, Y. *et al.* miR-29a regulates the proliferation and differentiation of retinal progenitors by targeting Rbm8a. *Oncotarget* **8**, 31993–32008 (2017).
65. Mazzeo, A. *et al.* Functional analysis of miR-21-3p, miR-30b-5p and miR-150-5p shuttled by extracellular vesicles from diabetic subjects reveals their association with diabetic retinopathy. *Exp. Eye Res.* **184**, 56–63 (2019).
66. Haque, R. *et al.* MicroRNA-30b-Mediated Regulation of Catalase Expression in Human ARPE-19 Cells. *PLoS One* **7**, e42542 (2012).

Acknowledgements

The present project was supported by internal funds from Universidad Católica de Valencia San Vicente Mártir (2018-128-001), Centro de Investigación Traslacional San Alberto Magno de la UCV (2019-128-001), and Conselleria de Educación, Investigación, Cultura y Deporte; Generalitat Valenciana (PROMETEO/2016/094). Oltra M and Vidal-Gil L, PhD training program fellowship UCV (EDUCV-PRE-2016-005 and EDUCV-PRE-2015-006 Personal Investigador en Formación UCV, respectively).

Author contributions

M.O. Cell cultures and sEVs isolation, flow citometry, miRNA extraction and quantification, qPCR, validation. L.V.G. Cell cultures and sEVs isolation, electronic microscopy. R.M. Cell cultures and sEVs isolation. S.S.O. Statistical analysis. F.J.R. MS revision and interpretation of results. J.S.P. Corresponding author and discussion. J.M.B. supervision and MS writing.

Competing interests

The authors declare no competing interests.

Additional information

Correspondence and requests for materials should be addressed to J.S.-P.

Reprints and permissions information is available at www.nature.com/reprints.

Publisher's note Springer Nature remains neutral with regard to jurisdictional claims in published maps and institutional affiliations.

Open Access This article is licensed under a Creative Commons Attribution 4.0 International License, which permits use, sharing, adaptation, distribution and reproduction in any medium or format, as long as you give appropriate credit to the original author(s) and the source, provide a link to the Creative Commons license, and indicate if changes were made. The images or other third party material in this article are included in the article's Creative Commons license, unless indicated otherwise in a credit line to the material. If material is not included in the article's Creative Commons license and your intended use is not permitted by statutory regulation or exceeds the permitted use, you will need to obtain permission directly from the copyright holder. To view a copy of this license, visit http://creativecommons.org/licenses/by/4.0/.

© The Author(s) 2019